

Distribution, drivers, and impacts of compound marine heatwave and low net primary productivity extreme events in the ocean

Inaugural dissertation
of the Faculty of Science, University of Bern
presented by

Natacha Le Grix de la Salle

from France

Supervisors of the doctoral thesis:

Prof. Thomas Frölicher

Climate and Environmental Physics
University of Bern, Bern

Prof. Jakob Zscheischler

Helmholtz Centre for Environmental Research
UFZ, Leipzig, Germany

This work is licensed under a [Creative Commons Attribution 4.0 International License](https://creativecommons.org/licenses/by/4.0/)

Distribution, drivers, and impacts of compound marine heatwave and low net primary productivity extreme events in the ocean

Inaugural dissertation
of the Faculty of Science, University of Bern
presented by

Natacha Le Grix de la Salle

from France

Supervisors of the doctoral thesis:

Prof. Thomas Frölicher

Climate and Environmental Physics
University of Bern, Bern

Prof. Jakob Zscheischler

Helmholtz Centre for Environmental Research
UFZ, Leipzig, Germany

Accepted by the Faculty of Science.

Bern, 10.07.2023

The Dean: Prof. Dr. Marco Herwegh

Thesis overview and summary

Ocean extreme events can severely impact marine organisms and ecosystems. Of particular concern are multivariate compound events, namely when conditions are simultaneously extreme for multiple ocean ecosystem stressors. In 2013-2015, for example, an extensive marine heatwave (MHW), known as the ‘Blob’, co-occurred locally with extremely low net primary productivity (NPPX) and negatively impacted marine life in the northeastern Pacific. Yet, little is known about the distribution, drivers, and impacts of such multivariate compound MHW-NPPX events.

The introduction of this thesis (Chapter 1) motivates the study of compound MHW-NPPX events by first giving an overview of how sea surface temperature (SST) and net primary production (NPP) are changing under climate change, with repercussions on climate and marine ecosystems. Long-term changes in SST and NPP are associated with a rise in extremely high SST and low NPP events, which may co-occur during compound MHW-NPPX events and drive severe impacts on marine ecosystems.

The Methods section (Chapter 2) then introduces the tools used in this thesis to study these potentially harmful compound MHW-NPPX events. We specifically use a combination of satellite-derived SST, chlorophyll concentration, and NPP observations, and large ensemble simulations by two Earth system models and by one global marine fish model.

Chapter 3, published in *Biogeosciences* (Le Grix et al., 2021), characterizes the distributions of MHW-NPPX events over the satellite period using satellite-based SST and chlorophyll concentration as a proxy for NPP. From 1998 to 2018, we find compound events to be frequent in the low latitudes, especially in the center of the equatorial Pacific, in the Arabian Sea and along the borders of the subtropical gyres. In contrast, compound events are rare in the high latitudes, where MHWs rarely co-occur with NPPX events. The frequency of compound MHW-NPPX events also varies across seasons, with most events occurring in spring in the mid-latitudes and in summer in the high latitudes. At the interannual time scale, large-scale modes of climate variability seem to modulate the frequency of compound events. For example, in the eastern equatorial Pacific, compound event likelihood is multiplied by a factor of 4 during El Niño events. Climate modes are associated with particular ocean conditions, which can favor or prevent the occurrence of compound MHW-NPPX events. Surface warming and reduced upwelling of nutrient-rich waters in the eastern equatorial Pacific during El Niño events may, for instance, contribute to driving compound MHW-NPPX events (Le Grix et al., 2022).

Earth system models (ESMs) can help identify the exact drivers of compound MHW-NPPX events. In Chapter 4, also published in *Biogeosciences* (Le Grix et al., 2022), we use large ensemble simulations by two ESMs: the GFDL ESM2M and the CESM2. Their representation of compound MHW-NPPX events is evaluated against satellite-derived observations. Both models correctly simulate frequent compound MHW-NPPX events in the low latitudes. There, MHWs are associated with nutrient limitation on phytoplankton growth and a relative increase in phytoplankton loss (e.g., grazing) compared to phytoplankton production, which drive low phytoplankton NPP and result in frequent compound MHW-NPPX events. In the high latitudes, however, models disagree on the likelihood and drivers of compound MHW-NPPX events. There,

improved understanding of the factors controlling phytoplankton NPP is key to improving model representation of NPPX events and, ultimately, of compound MHW-NPPX events.

Lastly, in Chapter 5 (Le Grix et al., 2023 (submitted)), we evaluate the actual threat posed by compound MHW-NPPX events on marine ecosystems using a global marine fish model, the DBEM, forced by a large ensemble simulation from an ESM, the GFDL ESM2M. We first identify events of extremely low biomass of pelagic fish, and then look back at the ocean conditions that may have driven these events. We find that MHWs and NPPX events are both drivers of extreme impacts on pelagic fish biomass in the equatorial Atlantic, the central and eastern equatorial Pacific, in the northern part of the Indian Ocean and in the northeastern Pacific. There, pelagic marine ecosystems may be particularly vulnerable to compound MHW-NPPX events. We also identify regions where impacts may be caused by ocean conditions other than compound MHW-NPPX events, and by ocean conditions that do not necessarily correspond to a compound extreme event. Moderate anomalies in one ocean ecosystem stressor were found to never drive extreme impacts on pelagic fish. In contrast, over 78% of the global ocean, a combination of anomalies in multiple ocean ecosystem stressors is necessary to experience extreme impacts. Overall, Chapter 5 highlights the key role of ocean compound events in driving extreme impacts on marine ecosystems.

The Discussion (Chapter 6) summarizes our results and puts them into the larger perspective of ocean and compound event research. Overall, this thesis provides a first understanding of the distribution, drivers, and impacts of compound MHW-NPPX events. We highlight the need to improve their representation in ESMs, to further study their impacts, and to extend compound event research to other types of oceanic compound events. We also inform potential strategies to predict, prevent and moderate compound MHW-NPPX events impacts on marine ecosystems.

Bibliography

- Le Grix, N., Zscheischler, J., Laufkötter, C., Rousseaux, C. S., & Frölicher, T. L., 2021. Compound high-temperature and low-chlorophyll extremes in the ocean over the satellite period, *Biogeosciences*, 18(6), 2119–2137.
- Le Grix, N., Zscheischler, J., Rodgers, K. B., Yamaguchi, R., & Frölicher, T. L., 2022. Hotspots and drivers of compound marine heatwaves and low net primary production extremes, *Biogeosciences*, 19(24), 5807–5835.
- Le Grix, N., Cheung, W., Reygondeau, G., Zscheischler, J., & Frölicher, T. L., 2023 (submitted). Extreme and compound ocean events are key drivers of projected low pelagic fish biomass.

Contents

Thesis overview and summary	3
1 Introduction	9
1.1 Ocean temperature and net primary productivity under climate change . . .	9
1.2 Ocean extreme events accompany changes in ocean temperature and net primary productivity	12
1.3 Compound extreme events combine ocean extreme events across time and space	15
1.4 Impacts of compound extreme events on marine ecosystems	17
1.5 Knowledge gaps prior to this thesis	19
1.6 Aims and outline of this thesis	20
2 Methods	31
2.1 Observations	31
2.1.1 Sea surface temperature	31
2.1.2 Surface chlorophyll concentration	32
2.1.3 Net primary productivity	32
2.2 Models	35
2.2.1 Earth system models	35
2.2.2 Global marine fish models	37
2.2.3 Large ensemble simulations	39
3 Compound high temperature and low chlorophyll extremes in the ocean over the satellite period	47
3.1 Introduction	48
3.2 Methods	50
3.3 Results	52
3.3.1 Marine heatwaves and low-chlorophyll events	52
3.3.2 Compound marine heatwaves and low-chlorophyll events	53
3.3.3 Distribution of marine heatwaves and low-chlorophyll and compound events over time	54
3.3.4 The role of natural internal climate variability	55
3.4 Discussion and conclusion	57

4	Hotspots and drivers of compound marine heatwaves and low net primary production extremes	67
4.1	Introduction	69
4.2	Methods	70
4.3	Results	75
4.3.1	Hotspots of compound MHW-NPPX events in the global ocean	75
4.3.2	Small and large phytoplankton NPP anomalies during compound MHW-NPPX events	76
4.3.3	Drivers of low NPP during compound MHW-NPPX events	77
4.4	Discussion and conclusion	82
5	Extreme and compound ocean events are key drivers of projected low pelagic fish biomass	97
5.1	Introduction	98
5.2	Methods	100
5.3	Results	104
5.3.1	Drivers of low fish biomass events	105
5.3.2	The role of lagged effects in driving low fish biomass events	108
5.3.3	Most influential predictor of low fish biomass events	109
5.3.4	Categorizing the drivers of low fish biomass events into moderate, extreme, univariate, and compound drivers	109
5.4	Discussion and conclusion	112
6	Discussion	127
6.1	Summary and discussion of the main results	127
6.2	Limitations	132
6.2.1	Low confidence in NPP estimates	132
6.2.2	2D perspective	132
6.2.3	Imperfect representation of ocean biogeochemical extremes in ESMs	133
6.2.4	Imperfect representation of the drivers of extreme impact on fish in global marine fish models	134
6.3	Outlook	134
6.3.1	Describe the spatio-temporal structure of compound MHW-NPPX events	134
6.3.2	Further investigate the impacts of compound MHW-NPPX events	134
6.3.3	Implications for the carbon pump	135
6.3.4	Other types of ocean compound events	136
6.3.5	Impact prediction and mitigation	137
6.4	Conclusion	138
Appendix A Simulating compound weather extremes responsible for critical crop failure with stochastic weather generators		147

Acknowledgements	167
Publications	169
Erklärung gemäss Art. 18 PromR Phil.-nat. 2019	171

Chapter 1

Introduction

1.1 Ocean temperature and net primary productivity under climate change

Greenhouse gases emitted by human activities have accumulated in the atmosphere since the industrial revolution, mostly in the form of carbon dioxide (CO_2) and methane (CH_4) (Gulev et al., 2021). Human emissions provide strong radiative forcing, which causes global surface warming at a rate unprecedented since at least the past 2000 years (Gulev et al., 2021). More than 90% of the excess heat is stored in the ocean (Bindoff et al., 2019), while the residual heat contributes to melting land and sea ice and to warming the atmosphere and land surface. The ocean is therefore a strong moderator of global warming.

Sea surface temperature (SST) is a primary indicator of ocean warming. On average, global mean SST has already increased by 0.88°C ($0.68\text{--}1.01^\circ\text{C}$) from 1850–1900 to 2011–2020 (Fox-Kemper et al., 2021). Earth system models simulate an SST increase of about 0.5°C between 1950 and 2005 (in orange on Fig. 1.1) and project further SST increase between 2005 and 2100 of about 0.5°C (in blue on Fig. 1.1) and 2.5°C (in red on Fig. 1.1) under a low and a high emissions scenario, respectively.

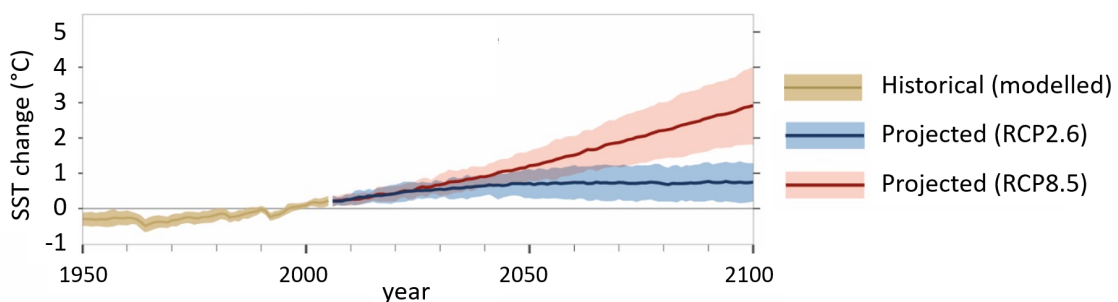


Figure 1.1: Global mean sea surface temperature (SST) change relative to 1986–2005. SST changes are simulated over the historical period (in orange), and projected under a low (in blue) and a high (in red) greenhouse gas emissions scenario by models participating in the fifth phase of the Coupled Model Intercomparison Project (CMIP5). Lines correspond to the multi-model mean. Shadings indicate \pm one multi-model standard deviation. This figure is modified from Figure TS.3 in IPCC, 2019: Technical Summary (Pörtner et al., 2019).

Warming is heterogeneously distributed over the global ocean, with the fastest surface warming occurring in the Indian Ocean and in western boundary currents, and slower warming or even surface cooling occurring in the Southern Ocean and in the subpolar North Atlantic since the 1950s (Fox-Kemper et al., 2021). Disparate ocean warming patterns perturb atmospheric weather

patterns (e.g., Xie (2020)) and may enhance risk from extreme weather events. For instance, ocean warming in Central America, in the tropical Atlantic and in the Indian Ocean has been associated with more intense tropical Atlantic cyclones (Grinsted et al., 2013). Ocean warming rates also vary vertically, as heat is taken up by the surface ocean before being distributed to the deeper ocean (Barnett et al., 2005). Surface waters warm faster than subsurface waters, which increases stratification (Li et al., 2020; Sallée et al., 2021). Stratification hinders the ventilation of surface waters, potentially reducing the uptake of atmospheric heat by the ocean.

Oceans not only take up excess atmospheric heat, they have also taken up about 25% of cumulative CO₂ emissions since 1850 (Friedlingstein et al., 2022; Terhaar et al., 2022). CO₂ uptake begins with atmospheric CO₂ dissolving in ocean surface waters. The driving force governing the exchange of CO₂ across the air–sea interface is the air–sea difference in pCO₂, the CO₂ partial pressure. As long as surface waters pCO₂ remains lower than atmospheric pCO₂, oceans can take up atmospheric CO₂. The transfer of carbon from surface waters to the ocean interior contributes to maintaining surface pCO₂ lower than atmospheric pCO₂ and therefore sustains the ocean carbon uptake. The physical carbon pump refers to the transfer of dissolved inorganic carbon from surface waters to the ocean interior by ocean circulation (Boyd et al., 2019). The biological carbon pump also participates in maintaining surface CO₂ concentration relatively low, by converting CO₂ into organic carbon, and exporting the latter to depth (Volk & Hoffert, 1985; Neuer et al., 2014). Fig. 1.2 illustrates the role of primary productivity in the biological carbon pump.

Primary producers, i.e., mainly phytoplankton in the open ocean, first convert CO₂ into organic matter during photosynthesis (Sarmiento & Gruber, 2006; Williams & Follows, 2011). Photosynthesis requires macronutrients, such as nitrogen and phosphorus, and micronutrients, such as iron (Falkowski, 1994; Coale et al., 1996; Street & Paytan, 2005; Bristow et al., 2017). It is also limited by light availability (Sarmiento & Gruber, 2006), and therefore restricted to the sunlit euphotic layer, where incoming sunlight is, by definition, degraded down to 1% of its surface strength (Lee et al., 2007). Net primary productivity (NPP) accounts for the difference between the gross production of organic matter during photosynthesis and its loss during respiration (Sarmiento & Gruber, 2006). NPP sustains the growth and reproduction of phytoplankton, whose organic matter is then grazed by zooplankton and transferred to larger marine species throughout the marine food web (Pauly & Christensen, 1995). Marine organisms can migrate from the surface ocean, where they mostly feed, to the deeper ocean, resulting in a net export of carbon toward the deep (Vinogradov, 1997; Davison et al., 2013; Boyd et al., 2019). Marine organisms produce and are degraded into particulate organic carbon (POC), which can be exported to the deeper ocean through physical mixing and gravitational settling (Sarmiento & Gruber, 2006). As they sink, particles form aggregates that sink faster and can potentially reach the seafloor, where they are sequestered in the sediments for millions of years. However, most particles never reach the seafloor and are degraded into dissolved organic carbon (DOC). DOC is remineralized by bacteria into dissolved inorganic carbon (DIC) which either accumulates in the ocean interior or is upwelled by ocean circulation to the euphotic layer, where it can again be used by phytoplankton to form organic carbon (Volk & Hoffert, 1985).

Overall, NPP sustains the marine food web and plays a key role in the biological carbon pump by converting inorganic carbon into organic carbon. The future of marine fisheries (Pauly & Christensen, 1995; Chassot et al., 2010; Friedland et al., 2012; Marshak & Link, 2021) and of the carbon cycle on multi-centennial to geological timescales (Sarmiento & Bender, 1994; Bopp et al., 2001) therefore depend on how NPP will change as oceans are getting warmer and more stratified.

Changes in NPP are driven by an interplay of physical and biological processes. Stratification, for instance, reduces the nutrient supply to surface waters (Sarmiento et al., 1998). In turn, nutrient limitation on phytoplankton growth may drive a decrease in phytoplankton NPP (Bopp

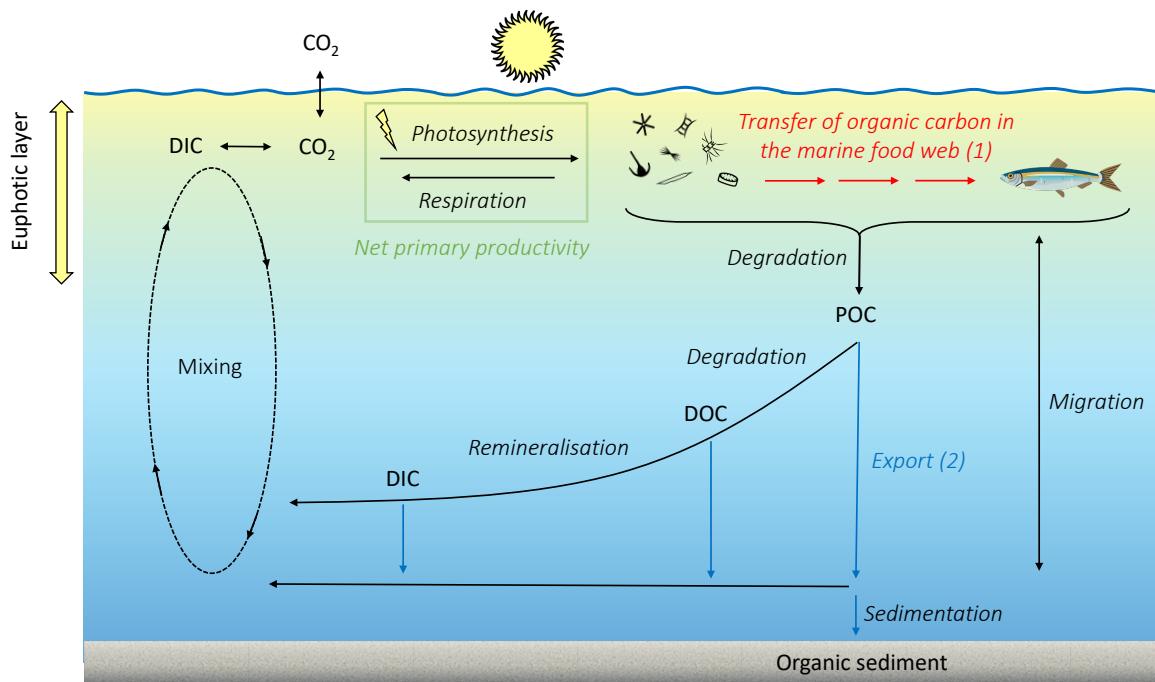


Figure 1.2: Role of net primary productivity (NPP) in the ocean as (1) the base of the marine food web and (2) a key element of the biological carbon pump. NPP is the production of organic carbon from CO₂ through photosynthesis that remains after respiration. NPP by phytoplankton is grazed by larger plankton, which are then eaten by larger marine predators, allowing a transfer of organic carbon in the marine food web. Marine organisms produce particulate organic carbon (POC), which forms aggregates that sink and either reach the bottom of the ocean, where they form sediments, or are degraded into dissolved organic carbon (DOC) and remineralized into dissolved inorganic carbon (DIC). DOC and DIC either accumulate at depth, or are upwelled back to the euphotic layer by circulation processes such as vertical mixing. Note that for simplicity, this schematic only presents a selection of the processes involved in the biological carbon pump.

et al., 2001; Sarmiento et al., 2004; Behrenfeld et al., 2006; Laufkötter et al., 2015; Roxy et al., 2016). However, stratification also maintains phytoplankton within the warm euphotic layer (Sarmiento et al. (1998); Bopp et al. (2001); Fig. 1.2), where enhanced temperature and light availability may counteract nutrient limitation on phytoplankton growth (Steinacher et al., 2010; Laufkötter et al., 2015; Frölicher et al., 2016). Phytoplankton biomass may also be affected by enhanced grazing pressure and by changes in ocean circulation (Laufkötter et al., 2015). Overall, the future of phytoplankton NPP under climate change remains unclear (Steinacher et al., 2010; Bopp et al., 2013; Laufkötter et al., 2015; Kwiatkowski et al., 2020). Previous studies based on satellite-derived and in situ observations suggested a global decline over the past century (Behrenfeld et al., 2006; Boyce et al., 2010). In contrast, Saba et al. (2010) reported a local increase in NPP measured in-situ at two stations in the low latitudes. Disagreement arises from various methodologies and regions under study (Saba et al., 2010; Siegel et al., 2013; Hammond et al., 2020; Pinkerton et al., 2021), and in the past decades, observations remained anyway too limited to detect a robust trend in NPP (Henson et al., 2010; Pinkerton et al., 2021). Earth system models are another way to apprehend changes in NPP. On average, Earth system models project a further decrease in NPP over the 21st century, especially in the nutrient-limited waters of the low to mid latitudes (Bopp et al., 2013; Kwiatkowski et al., 2020). However, individual Earth system models disagree on the magnitude and even sign of NPP changes (Steinacher

et al., 2010; Laufkötter et al., 2015; Kwiatkowski et al., 2020; Tagliabue et al., 2021). Improved representation of NPP in Earth system models is necessary to reduce uncertainties in future marine NPP.

1.2 Ocean extreme events accompany changes in ocean temperature and net primary productivity

Warming and reduced net primary productivity are considered to be two of the major potential stressors of open ocean ecosystems, along with acidification and deoxygenation (Gruber, 2011; Bopp et al., 2013; Doney et al., 2012; Bindoff et al., 2019). However, marine ecosystems are not only threatened by long-term decadal-scale changes in SST (Cheng et al., 2017) and NPP (Boyce et al., 2010; Doney et al., 2012), they are also increasingly exposed to short-term extreme events, such as marine heatwaves (MHWs) (Wernberg et al., 2013; Frölicher & Laufkötter, 2018b; Oliver et al., 2018) and extremely low NPP events (hereafter called ‘NPPX’ events; Whitney (2015); Cavole et al. (2016); Le Grix et al. (2022)).

Extreme events are broadly defined as the normally rare occurrences when a system is far outside the norm (Gruber et al., 2021). Yet their exact definition varies across studies, depending on the scientific question that is to be addressed. In the following, we describe the various criteria that can be used when defining extreme events. Namely, extreme events occur when the stress variable, such as SST or NPP, exceeds a certain threshold, which can be (1) absolute, i.e. set to a particular value, or (2) varying in time or space relative to a climatological baseline. This baseline can be (3) fixed or (4) shifting in time to account for long-term variability in the stress variable. Extreme event definition may also consider (5) seasonal variability in the stress variable, as well as (6) additional criteria such as extreme event duration.

(1) **Absolute thresholds** are recommended when the stress variable is expected to impact marine organisms upon exceedance of a particular value (Gruber et al., 2021). For example, warm-water corals seem to be impacted by temperatures exceeding a certain temperature threshold, e.g. 32°C for *Acropora* in northwestern Australia (Schoepf et al., 2015). One could therefore define MHWs as periods over which temperatures exceed the 32°C absolute threshold. However, even though corals may motivate the use of an absolute temperature threshold, the most common definition of MHWs in recent literature uses a relative threshold (Hobday et al., 2016; Oliver et al., 2021).

(2) **Relative thresholds** vary in time and space. Their use is warranted in situations when marine ecosystems are impacted by extreme deviations of a stress variable outside its normal range of variability (Gruber et al., 2021). Most widely-used relative thresholds are percentile thresholds. For example, MHWs are typically defined as events when the SST anomaly relative to the climatological SST exceeds its local 90th or 99th percentile. The choice of percentile threshold depends on the range of variability that marine ecosystems are expected to be able to cope with. A restrictive (e.g., 99th) percentile threshold allows for identifying truly “extreme” extreme events, which are bound to impact marine ecosystems. The percentile threshold also controls the sample size, e.g., a 90th percentile threshold would sample 10 times as many extreme events as a 99th percentile threshold, and therefore be recommended in situations where short time series limit the statistical relevance of an extreme event analysis.

Relative thresholds are defined locally relative to a climatological baseline. This baseline may be (3) fixed or (4) shifting in time (Oliver et al., 2019; Gruber et al., 2021; Burger et al., 2022).

(3) **A fixed baseline** is a fixed reference period over which to assess the distribution of the stress variable when defining extreme events. A fixed baseline is usually stationary or sufficiently short to be considered quasi-stationary. For example, Frölicher et al. (2018) use

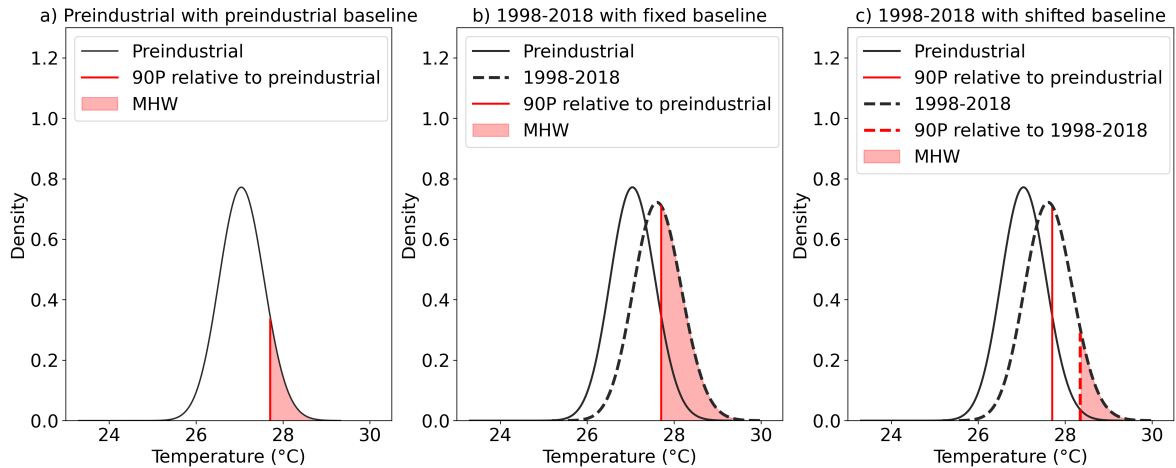


Figure 1.3: Marine heatwaves (MHWs) are defined relative to a climatological baseline that is either fixed or shifting in time. (a) Simulated 5-day mean SST distribution over the preindustrial period at a grid cell in the northern Pacific at $17^{\circ}\text{N} - 90^{\circ}\text{W}$ (black line). The 90th percentile of SST (red line) is used as a threshold for the definition of MHWs, resulting in 10% of MHWs over the preindustrial period (red shading). (b) The 5-day mean SST distribution over 1998-2018 (black dotted line) has shifted toward warmer SST compared to the preindustrial period (black line). MHWs are still defined using the 90th percentile of SST relative to the fixed preindustrial baseline (red line), resulting in an increase in MHW frequency over 1998-2018 compared to the preindustrial period. (c) MHWs are now defined using the 90th percentile of SST relative to the shifted 1998-2018 baseline (red dotted line) to account for the shift in 5-day mean SST distribution, resulting in 10% of MHWs over 1998-2018. On the y-axes, density accounts for the probability density function, which is smoothed using Gaussian kernel density estimation and whose area under the curve is equal to 1. SST time series come from the GDFL ESM2M simulations presented in Chapter 2, section 2.2.1.

multi-centennial preindustrial simulations as a baseline for their definition of MHWs. In Fig. 1.3a, the preindustrial period also serves as baseline over which to assess the distribution of 5-day mean SST at $17^{\circ}\text{N} - 90^{\circ}\text{W}$. MHWs occur when the 5-day mean SST exceeds the 90th percentile of this distribution (in red on Fig. 1.3a). A fixed baseline remains fixed despite any long-term variability in the stress variable. A fixed baseline therefore allows to consider changes in extreme event properties driven by a shift in the variable’s distribution over time (Frölicher et al., 2018; Burger et al., 2022). For example, global mean ocean warming since the preindustrial period has led to increased frequency, duration, spatial extent, and intensity of MHWs (Frölicher et al., 2018; Oliver et al., 2019; Gruber et al., 2021). Simulated 5-day mean SST also increases over 1998-2018 compared to the preindustrial period, which results in more frequent MHWs over 1998-2018 (Fig. 1.3b) than over the cooler preindustrial period (Fig. 1.3a).

(4) In contrast, a **shifting baseline** shifts in time so as to be centered around the period over which to sample extreme events (Fig. 1.3c). Thereby, the use of a shifting baseline accounts for the mean shift in the stress variable, e.g. the warming trend in SST (Oliver et al., 2019; Xu et al., 2022). It also accounts for the change in shape of the distribution. For example, the SST distribution at $17^{\circ}\text{N} - 90^{\circ}\text{W}$ is more tailed towards extreme values over 1998-2018 than over the preindustrial period (Fig. 1.3c compared to Fig. 1.3a), resulting in more intense MHWs. A shifting baseline allows for sampling events that are truly extreme relative to the current distribution of the stress variable.

(5) In addition, **seasonal variability** in the stress variable is sometimes accounted for in the definition of extreme events (Hobday et al., 2016; Gruber et al., 2021). (5a) The stress variable

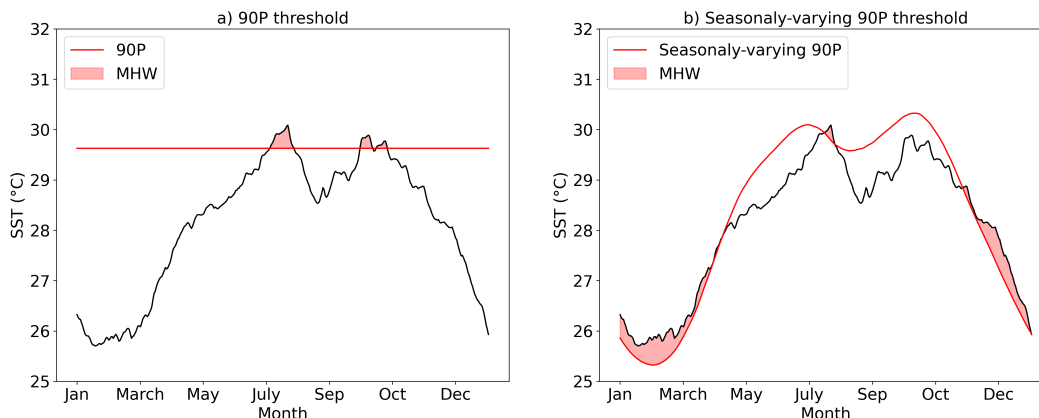


Figure 1.4: Accounting for seasonality in the definition of marine heatwaves (MHWs) affects the sampling of MHWs. (a) MHWs, defined as days when the SST exceeds its 90th percentile, occur in summer. (b) MHWs, defined as days when the SST exceeds its seasonally-varying 90th percentile, can occur in all seasons. The black line indicates the SST time series, the red line the percentile threshold, and the red shading the MHWs identified at a grid cell in the northern Pacific (at 90°W - 17°N). Percentile thresholds are defined relative to the 1998-2018 baseline. SST time series come from the GDFL ESM2M simulations presented in Chapter 2, section 2.2.1.

may be deseasonalized before applying any threshold to sample extreme events (e.g., Le Grix et al. (2021); Gruber et al. (2021); Le Grix et al. (2022)). For example, Le Grix et al. (2022) remove the seasonal cycles of SST and NPP before sampling MHWs and NPPX events. By doing so, MHWs can occur throughout the year and not only in summer, whereas NPPX events are not limited to the low productive seasons. However, this method does not account for enhanced SST variability in summer and NPP variability in spring, which result in higher MHW frequency in summer and NPPX event frequency in spring (Fig. 6 in (Le Grix et al., 2021)). (5b) Another way to account for seasonal variability is to apply a seasonally-varying threshold (Burger et al., 2020, 2022), such as the 90th percentile of SST computed on each calendar day (Fig. 1.4b). A seasonally varying threshold ensures that extreme events are evenly sampled throughout the year (Fig. 1.4b compared to Fig. 1.4a). Burger et al. (2022) thereby define MHWs that have the same probability to occur on each calendar day. The use of a seasonally-varying threshold is warranted in situations where marine ecosystems might be adapted to seasonal variability in the stress variable.

(6) Lastly, **additional conditions** may be applied to the definition of extreme events, such as a minimum duration. For example, Hobday et al. (2018) define MHWs as prolonged events of anomalously warm water, where “prolonged” implies a duration of at least 5 days. Extreme events can also be categorized based on the degree to which the stress variable exceeds the local climatology (Hobday et al., 2018). None of these additional conditions apply in this thesis.

Although extreme events have always existed, they are rare by definition. Long-term changes in ocean conditions under climate change have been associated with a rise in their frequency. The number of MHW days has, for example, doubled between 1982 and 2016 (Frölicher et al., 2018; Oliver et al., 2018) and is projected to increase strongly under continued global warming (Frölicher et al., 2018). Yet impacts from extreme events may be worse than impacts due to long-term climate change only (Cheung & Frölicher, 2020). The rise in ocean extreme events under climate change motivates their study and explains growing interest in their distribution, drivers and impacts (Gruber et al., 2021). Extreme events in the ocean have not been studied as extensively as extreme events on land, which are more directly observed and which can directly impact humans and ecosystems on land (Parmesan et al., 2000; Smith et al., 2021, 2023). Still, ocean extreme events can have severe impacts on marine ecosystems, with repercussions on

human societies. MHWs, for instance, have already impacted many key habitats (Smale et al., 2019), including seagrass meadows (Marba & Duarte, 2010; Thomson et al., 2015), kelp forests (Wernberg et al., 2013; Smale et al., 2019) and coral reefs (Hughes et al., 2018). Changes in the biomass and distribution of marine species further impacted socio-economically important fisheries (Cavole et al., 2016; Cheung & Frölicher, 2020). Given the role of NPP as the base of the marine food web, NPPX events may also impact marine ecosystems (Cavole et al., 2016; Le Grix et al., 2022).

1.3 Compound extreme events combine ocean extreme events across time and space

When combined across time and space, MHWs and NPPX events may have synergistic effects driving severe impacts on marine ecosystems. “Compound events” refer to potentially harmful situations where more than one ecosystem driver is outside the norm simultaneously, in close spatial proximity, or temporal succession (Leonard et al., 2014; Zscheischler et al., 2018). Zscheischler et al. (2020) differentiate between four types of compound events: (1) the “multivariate”, where multiple events co-occur and may lead to an impact; (2) the “preconditioned”, where a precondition aggravates the impact of an event; (3) the “temporally compounding”, where a succession of events may lead to an impact; and (4) the “spatially compounding”, where events in multiple connected locations cause an aggregated impact.

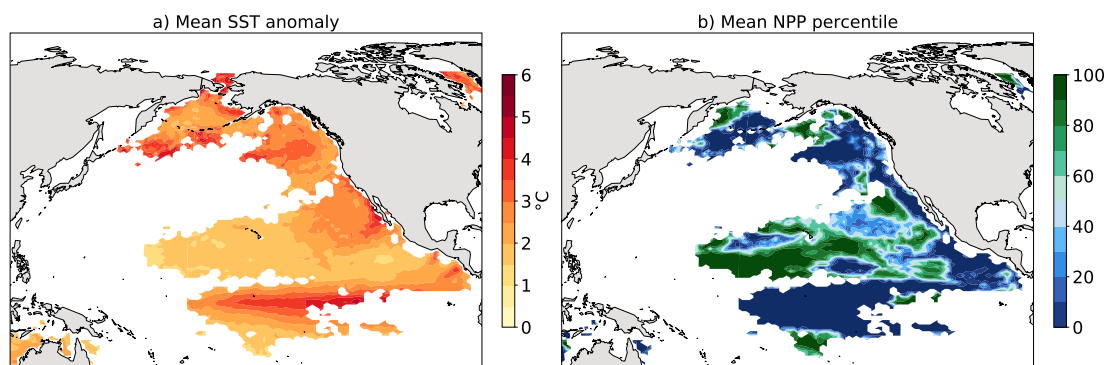


Figure 1.5: The 2013-2015 ‘Blob’ in the northeastern Pacific, a compound marine heatwave (MHW) and low NPP (NPPX) event. (a) Mean sea surface temperature (SST) anomaly during the Blob, relative to the climatological seasonal cycle of SST. (b) Mean net primary productivity (NPP) percentile during the Blob, relative to the climatological seasonal cycle of NPP. Dark blue areas indicate regions where NPP was extremely low during the Blob compared to normal conditions. The Blob’s extent is taken from Laufkötter et al. (2020) and corresponds to a spatiotemporally continuous area with SST anomalies above their 99.5 percentile.

Although early research on compound events mostly focused on land (Zscheischler et al., 2013; Leonard et al., 2014; Ridder et al., 2020), compound events also occur in the ocean. The ‘Blob’, for instance, refers to an extensive marine heatwave in the northeastern Pacific which lasted from 2013 to 2015 and was associated with intense surface warming of 2 to 3°C on average (Fig. 1.5a). It coincided with anomalously low oxygen, low pH, and large anomalies in phytoplankton NPP (Whitney, 2015; Le Grix et al., 2021; Gruber et al., 2021; Mogen et al., 2022; Wyatt et al., 2022; Le Grix et al., 2022). NPP anomalies were particularly negative along the western coast of America and in the eastern equatorial Atlantic (in dark blue on Fig. 1.5b). Ocean compound events such as the Blob constitute compound hazards (Ridder et al., 2020) and, as such, pose a threat for marine ecosystems that warrants further investigation.

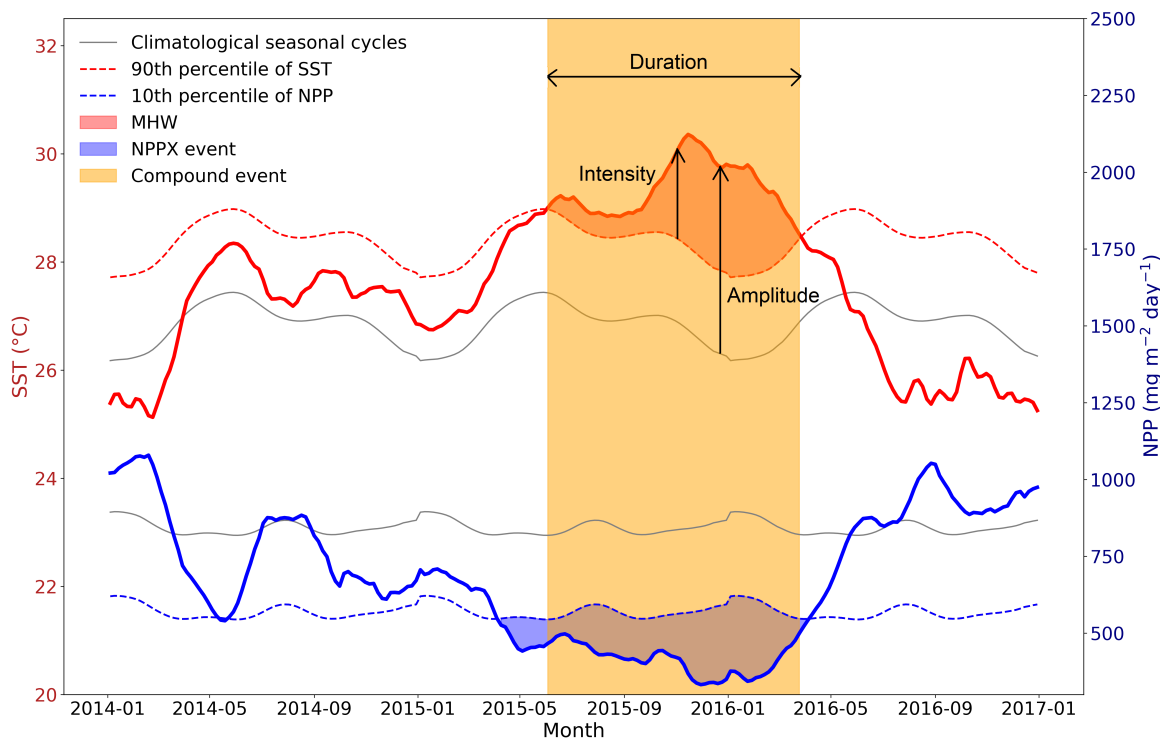


Figure 1.6: Schematic for the definition of compound extreme events. Sea surface temperature (SST, in red) and net primary productivity (NPP, in blue) at a grid cell in the equatorial Pacific (at $155^{\circ}\text{W} - 0.7^{\circ}\text{N}$). A marine heatwave (MHW, red shading) occurs when the SST anomaly relative to its climatological seasonal cycle exceeds its 90th percentile (red dotted line) and an extremely low NPP (NPPX, blue shading) event occurs when the NPP anomaly relative to its climatological seasonal cycle is lower than its 10th percentile (blue dotted line). A compound MHW-NPPX event occurs when a MHW co-occurs with an NPPX event. Figure modified from Fig. A1 in Le Grix et al. (2021).

So far, published studies have mostly focused on the “multivariate” type of ocean compound events. Ocean compound events are usually defined as events when at least two ocean ecosystem drivers are extreme at the same time and space. It is important to note that the original definitions of compound events do not require *extreme* conditions in multiple drivers (Leonard et al., 2014; Zscheischler et al., 2018). The combination of multiple moderate drivers may also drive severe impacts on marine ecosystems and thereby be considered a compound event (van der Wiel et al., 2020). Nevertheless, most studies on ocean compound events have decided to define ocean compound events as the combination of multiple ocean extreme events, such as marine heatwaves with extremely low oxygen (Gruber et al., 2021), with extremely high acidity (Gruber et al., 2021; Burger et al., 2022), or with extremely low NPP (Le Grix et al., 2021, 2022). For example, a compound MHW and NPPX event can be defined as the co-occurrence of extremely high SST and extremely low NPP (Fig. 1.6).

Various metrics are commonly used to characterize compound events (Gruber et al., 2021). The **duration** corresponds to the number of days, months or years that a compound event lasts without interruption (Fig. 1.6). The **intensity** of a univariate extreme event, such as a MHW, is defined as the exceedance of the stress variable over its threshold. For example, the intensity of a MHW would be the SST anomaly relative to the 90th percentile threshold (Fig. 1.6). The **amplitude** is similar to the intensity, with the difference that it is defined as the exceedance of the stress variable over its climatological baseline. The amplitude of a MHW would be the SST

anomaly relative to the climatological seasonal cycle (Fig. 1.6). A compound MHW-NPPX event can be characterized by the intensity or amplitude of both the MHW and NPPX event it combines. The **frequency** of a compound event is the number of compound event days, months or years, divided by the total number of days, months or years in the time series. Under the assumption of independence between MHWs and NPPX events, the expected frequency of compound MHW and NPPX events would be the product of the frequency of MHWs and of NPPX events (Equation 1.1). Finally, the **likelihood multiplication factor** (LMF) of a compound MHW-NPPX event is defined as the ratio of the observed frequency of compound MHW-NPPX events to their expected frequency under the assumption of independence between MHWs and NPPX events (Zscheischler & Seneviratne (2017), Equation 1.2). An LMF of more than 1 indicates that compound events are more frequent than expected.

$$f_{\text{expected}}(\text{MHW-NPPX}) = f(\text{MHW}) * f(\text{NPPX}) \quad (1.1)$$

$$\text{LMF} = \frac{f(\text{MHW-NPPX})}{f_{\text{expected}}(\text{MHW-NPPX})} = \frac{f(\text{MHW-NPPX})}{f(\text{MHW}) * f(\text{NPPX})} \quad (1.2)$$

These metrics are used to identify regions that are particularly exposed to compound extreme events, i.e., where compound extreme events are particularly long, intense, or frequent (Gruber et al., 2021). They can also be used to quantify changes in compound event characteristics under climate change (e.g., Burger et al. (2022)). The incentive to characterize compound events is motivated by their potentially negative impacts on marine ecosystems.

1.4 Impacts of compound extreme events on marine ecosystems

Marine species are sensitive to changes in ocean conditions (e.g., Denman et al. (1996)). For example, reduced nutrient supply limits net primary productivity (NPP), i.e. food supply, with repercussions on the whole marine food web (Field et al., 1998; Sarmiento et al., 2004; Blanchard et al., 2012). Marine species are also adapted to a certain temperature range (Pörtner, 2002), which sustains their metabolism and allows for growth and reproduction. They are sensitive to oxygen levels, which determine their growth and maximum body size (Pauly, 1980). Oxygen demand increases with acidity (Melzner et al., 2009), i.e., $[\text{H}^+]$ concentration, and with temperature (von Bertalanffy, 1951; Pauly & Cheung, 2017), thereby limiting fish growth. Reductions in sea-ice also affect the reproduction, growth and development of polar species (e.g., Barber & Iacozza (2004)). Individual species react differently to changes in these ocean conditions, depending on their habitat preferences, food demand and specificity, and dispersal ability (e.g., Urban et al. (2012, 2013); Cavole et al. (2016)). Diverse responses of individual species to anomalous oceans conditions alter the structure and functioning of marine ecosystems (e.g., Dossena et al. (2012); Puerta et al. (2019)).

Of particular concern are ocean extreme events, which may rapidly push marine ecosystems beyond the limits of their adaptability (Gruber et al., 2021). Marine heatwaves (MHWs) have, for example, been associated with habitat degradation (Wernberg et al., 2013; Thomson et al., 2015), rapid population declines and destabilization of trophic interactions, resulting in reduced ecosystem functioning (Frölicher & Laufkötter, 2018a; Oliver et al., 2019; Smale et al., 2019). Cheung & Frölicher (2020) have shown that impacts from MHWs may be worse than impacts from long-term climate change from 1981 to 2100. However, not all MHWs have devastating impacts (Fredston, A. L. et al. (2023), submitted); they may even be beneficial to certain species such as tunas and orcas (Cavole et al., 2016; Stuhr et al., 6 juil. 2017; Pansch et al., 2018; Saha et al., 2020; Britton et al., 2020).

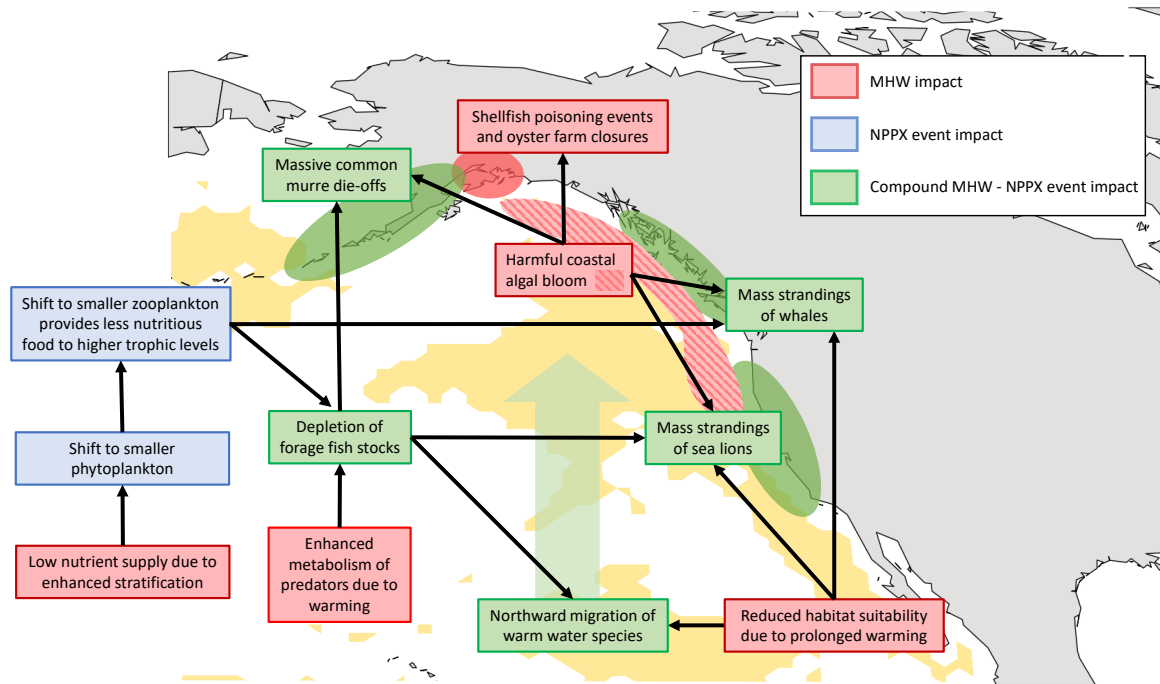


Figure 1.7: Schematic illustrating some of the ecological impacts of the 2013-2015 ‘Blob’, a compound marine heatwave (MHW) and low NPP (NPPX) event, in the northeastern Pacific. The color of the box indicates that an impact is directly or indirectly driven by the MHW (in red), the NPPX event (in blue), or by their compounding effects (in green). The yellow shading on the map indicates the approximate extent of the compound MHW-NPPX event, here defined as the area over which the mean NPP during the 2013-2015 MHW was lower than its climatological mean (i.e., the blue area on Fig. 1.5b).

The response of marine organisms to extreme deviations in one stress variable may also depend on the state of other ocean ecosystem stressors. Indeed, stressors do not act independently, but rather have synergistic or antagonistic effects (Boyd & Brown, 2015). They interact to cause non-linear changes in the performance of marine organisms. Ocean compound events, which combine multiple stressors, may drive severe impacts on marine ecosystems when these stressors act synergistically (Zscheischler & Seneviratne, 2017).

The Blob illustrates the potential threat posed by ocean compound events on marine ecosystems (Fig. 1.7). A lack of nutrients due to enhanced stratification and reduced upwelling (Leising et al., 2015) limited the growth of large phytoplankton in the northeastern Pacific during the Blob (Yang et al., 2018; Wyatt et al., 2022; Arteaga & Rousseaux, 2023), resulting in a shift towards smaller phytoplankton, e.g. cyanobacteria (Peña et al., 2019; Wyatt et al., 2022). This shift in phytoplankton community, associated with overall extremely low phytoplankton productivity (Whitney, 2015; Cavole et al., 2016; Capuzzo et al., 2017; Yang et al., 2018), might have favored certain phytoplankton grazers and led to cascading impacts on marine ecosystems (Cavole et al., 2016; Bindoff et al., 2019; Cheung & Frölicher, 2020). For instance, decreased phytoplankton biomass led to declines in zooplankton populations (Leising et al., 2015), with repercussions on fish and whale species in the northeastern Pacific (Cavole et al., 2016). Extreme warming probably amplified the impacts by further disrupting the marine food web (Frölicher & Laufkötter, 2018a; Oliver et al., 2019; Smale et al., 2019). For example, warm waters are characterized by lipid-poor zooplankton in the northeastern Pacific, and therefore reduced prey energy content for Cassin’s Auklets colonies, which massively died from starvation during the Blob (Jones et al., 2018). Piatt et al. (2020) have shown that the prolonged heatwave also

reduced the fat content and body size of forage fish, while enhancing the metabolism and thus food demand of groundfish, thereby depleting forage fish stock. Poor food supply caused reproductive failure and massive die-offs of common murre (Piatt et al., 2020). The heatwave also triggered harmful algal blooms, which, in combination with changing prey dynamics, struck a blow to marine bird and mammal species (Cavole et al., 2016; Piatt et al., 2020). Mass strandings of sea lions were reported in California, while whales stranded in the western Gulf of Alaska (Cavole et al., 2016). Harmful algal blooms also caused shellfish poisoning events and oyster farm closures in Kachemak Bay, in Alaska (Vandersea et al., 2018). Further impacts from the Blob included northward migration of certain marine species, such as tuna crabs, which were followed northward by their predators, such as tuna or market squid, followed in turn by their respective predators (Cavole et al., 2016). Shifts in species composition toward warm-water species had further repercussions on fisheries (Cavole et al., 2016; Cheung & Frölicher, 2020). Fig. 1.7 summarizes some of the aforementioned impacts of the Blob. Overall, the compound effects of intense surface warming and reduced phytoplankton productivity may explain the severity of some of the Blob's impacts.

Nevertheless, not all compound MHW-NPPX events are necessarily harmful (van der Wiel et al., 2020). Besides, compound moderate events, such as moderately high SST and low NPP, may also impact marine ecosystems. Additional information on how to identify the actual drivers of extreme impacts will be given in section 2.2.2.

1.5 Knowledge gaps prior to this thesis

As we have seen in this introduction, ocean compound MHW-NPPX events are rare by definition, yet they may become more frequent under climate change and cause devastating impacts on marine ecosystems (Gruber et al., 2021). However, little is known about the distribution, drivers and impacts of compound MHW-NPPX events. The Blob, in the northeastern Pacific, is one of the rare documented MHWs during which extremely low NPP has been reported. It remains unclear whether compound MHW-NPPX events occur elsewhere over the global ocean, and at which frequency. Assessing the distribution of compound MHW-NPPX events would help assess where and when they generally occur, which in turn could facilitate the prediction of compound MHW-NPPX events. Previous studies have linked MHW frequency and NPP variability to large-scale modes of climate variability (e.g., Holbrook et al. (2019); Racault et al. (2017)), which may also modulate the frequency of compound MHW-NPPX events and therefore be used to predict their future occurrences.

A necessary step toward prediction is to develop a better mechanistic understanding of the drivers of compound MHW-NPPX events (Gruber et al., 2021). Previous studies have investigated the drivers of MHWs (e.g., Holbrook et al. (2019); Gupta et al. (2020); Oliver et al. (2021); Vogt et al. (2022)) and of phytoplankton variability (e.g., Whitney (2015); Gittings et al. (2018); Long et al. (2021)), separately. However, only a few studies have explored the drivers of NPPX events during MHWs. For example, Wyatt et al. (2022) suggested that nutrient limitation during MHWs generally reduces phytoplankton biomass in the northeastern Pacific transition zone, which could potentially drive extremely low NPP and thus a compound MHW-NPPX event. However, not all warming events are accompanied by NPPX events. For instance, Long et al. (2021) noted an increase in NPP during two recent MHWs in the Northeast Pacific. This could be explained by warm temperatures enhancing phytoplankton growth (e.g., Laufkötter et al. (2015)). Phytoplankton biology is indeed modulated by multiple interacting processes in the ocean, rendering it a complex task to identify the drivers of extremely low NPP, and more specifically, of compound MHW-NPPX events. Understanding the drivers of compound MHW-NPPX events is nonetheless crucial to build the tools for their prediction and ultimately allow for adaptation and ecosystem management (Gruber et al., 2021).

Ecosystem management requires a better understanding of the actual risks posed by compound MHW-NPPX events on marine ecosystems. Compound MHW-NPPX events are, by definition, extremely rare and therefore constitute a hazard for marine ecosystems. Yet risks arise not only from hazards, but from the interactions between hazards, exposure and vulnerability (e.g., Bindoff et al. (2019); Magnan et al. (2021)). Marine ecosystems may not be exposed nor vulnerable to compound MHW-NPPX events. Certain marine species may even benefit from such compound events. For instance, Cavole et al. (2016) reported increased recruitment of rockfish in California and northward expansion of tropical and subtropical copepods during the Blob. These findings highlight the complexity in the relationship between hazards and impacts on marine ecosystems (Zscheischler et al., 2018; van der Wiel et al., 2020). To effectively predict and mitigate future impacts on marine ecosystems, a better understanding of the ocean conditions leading to extreme impacts on marine ecosystems is needed.

1.6 Aims and outline of this thesis

This thesis addresses the aforementioned gaps in our understanding of compound marine heatwave (MHW) and low net primary productivity (NPPX) events in the ocean (section 1.5). The principal objectives of this thesis are: to characterize compound MHW-NPPX events over the satellite period (1st goal), to assess the ability of Earth system models to correctly represent them (2nd goal), before using the Earth system models to identify their physical and biogeochemical drivers (3rd goal), and finally, to evaluate the risk posed by compound MHW-NPPX events for marine ecosystems (4th goal).

To analyze these compound MHW-NPPX events, we employ a combination of satellite-based observations and models, which will be presented in the Methods (Chapter 2).

(1st goal) Satellite-based SST and sea surface chlorophyll concentration (which we use as a proxy for NPP) data from 1998 to 2018 allow us to provide a first characterization of the compound events over the satellite period (Chapter 3). We describe their duration, intensity, and frequency, and identify hotspots of particularly frequent compound events. We also assess their distribution over time. At the interannual time-scale, we investigate the link between the phase of large-scale climate modes of variability and the frequency of compound events, and show that climate modes could be used to predict the occurrence of compound events.

(2nd and 3rd goal) In the second part of this thesis, we identify their physical and biogeochemical drivers using large ensemble simulations by two Earth system models: the GFDL ESM2M and the CESM2 (Chapter 4). First, we evaluate these models against observations based on satellite SST and five different satellite-derived NPP products. Second, we use the comprehensive outputs of the GFDL ESM2M and CESM2 to identify the drivers of compound MHW-NPPX events. Since previous studies have already determined the drivers of MHWs (Holbrook et al., 2019; Gupta et al., 2020; Vogt et al., 2022), we focus our analysis on the drivers of an extreme reduction in NPP during MHWs, which would result in driving compound MHW-NPPX events.

(4th goal) In the third part of this thesis, we take a step back and ask whether compound MHW-NPPX events actually threaten marine ecosystems (Chapter 5). All compound MHW-NPPX events may not impact marine ecosystems. In contrast, marine ecosystems may be vulnerable to other types of compound extreme events, to certain univariate extreme events, or even to compound events with moderate anomalous ocean conditions. In Chapter 5, we specifically identify the drivers of extremely low biomass of pelagic fish in a global marine fish model, the DBEM, forced by a large ensemble simulation from an Earth system model, the GFDL ESM2M. We first identify events of extremely low fish biomass and then look back at the ocean conditions that may have driven these events. This backward “impact-driven” analysis allows to identify unexpected drivers of low fish biomass. We determine whether these drivers

correspond to extreme events, compound events, or compound extreme events, and show that compound MHW-NPPX events pose a significant threat to pelagic ecosystems, especially in the low latitudes.

The Discussion of this thesis (Chapter 6) summarizes our results, states their caveats, and puts them into the wider perspective of compound event research in the ocean. A final outlook discusses the way our thesis can orient both future research on compound events and strategies to mitigate their impacts on marine ecosystems.

Lastly, the Appendix (A) of this thesis includes a paper co-written as part of a group project, which started during the first training school on *Statistical Modelling of Compound Events*. The training school, organized by the COST Action DAMOCLES, took place at the Lake Como School of Advanced Studies in Fall 2019. There, I participated in a group project to which I dedicated some time and energy during the first months of my PhD, although it was unrelated to the study of compound MHW-NPPX events. The outcome is a paper published in *Earth System Dynamics*, which discusses the use of stochastic weather generators based on atmospheric circulation analogues, to simulate compound extreme events responsible for crop failure (Pfleiderer et al., 2021).

Bibliography

- Arteaga, L. A. & Rousseaux, C. S., 2023. Impact of Pacific Ocean heatwaves on phytoplankton community composition, *Communications Biology*, 6(1), 1–13.
- Barber, D. G. & Iacozza, J., 2004. Historical Analysis of Sea Ice Conditions in M'Clintock Channel and the Gulf of Boothia, Nunavut: Implications for Ringed Seal and Polar Bear Habitat, *Arctic*, 57(1), 1–14.
- Barnett, T. P., Pierce, D. W., AchutaRao, K. M., Gleckler, P. J., Santer, B. D., Gregory, J. M., & Washington, W. M., 2005. Penetration of Human-Induced Warming into the World's Oceans, *Science*, 309(5732), 284–287.
- Behrenfeld, M. J., O'Malley, R. T., Siegel, D. A., McClain, C. R., Sarmiento, J. L., Feldman, G. C., Milligan, A. J., Falkowski, P. G., Letelier, R. M., & Boss, E. S., 2006. Climate-driven trends in contemporary ocean productivity, *Nature*, 444(7120), 752–755.
- Bindoff, N., Cheung, W., Kairo, J., Arístegui, J., Guinder, V., Hallberg, R., Hilmi, N., Jiao, N., Karim, M., Levin, L., O'Donoghue, S., Cuicapusa, S. P., Rinkevich, B., Suga, T., Tagliabue, A., & Williamson, P., 2019. Changing ocean, marine ecosystems, and dependent communities, in *IPCC Special Report on the Ocean, Cryosphere in a Changing Climate*, eds Pörtner, H.-O., Roberts, D., Masson-Delmotte, V., Zhai, P., Tignor, M., Poloczanska, E., Mintenbeck, K., Alegría, A., Nicolai, M., Okem, A., Petzold, J., Rama, B., & Weyer, N., Cambridge University Press.
- Blanchard, J. L., Jennings, S., Holmes, R., Harle, J., Merino, G., Allen, J. I., Holt, J., Dulvy, N. K., & Barange, M., 2012. Potential consequences of climate change for primary production and fish production in large marine ecosystems, *Philosophical Transactions of the Royal Society B: Biological Sciences*, 367(1605), 2979–2989.
- Bopp, L., Monfray, P., Aumont, O., Dufresne, J.-L., Le Treut, H., Madec, G., Terray, L., & Orr, J. C., 2001. Potential impact of climate change on marine export production, *Global Biogeochemical Cycles*, 15(1), 81–99.
- Bopp, L., Resplandy, L., Orr, J. C., Doney, S. C., Dunne, J. P., Gehlen, M., Halloran, P., Heinze, C., Ilyina, T., Séférian, R., Tjiputra, J., & Vichi, M., 2013. Multiple stressors of ocean ecosystems in the 21st century: Projections with CMIP5 models, *Biogeosciences*, 10(10), 6225–6245.
- Boyce, D. G., Lewis, M. R., & Worm, B., 2010. Global phytoplankton decline over the past century, *Nature*, 466(7306), 591–596.
- Boyd, P. W. & Brown, C. J., 2015. Modes of interactions between environmental drivers, marine biota, *Frontiers in Marine Science*, 2, 9.
- Boyd, P. W., Claustre, H., Levy, M., Siegel, D. A., & Weber, T., 2019. Multi-faceted particle pumps drive carbon sequestration in the ocean, *Nature*, 568(7752), 327–335.
- Bristow, L. A., Mohr, W., Ahmerkamp, S., & Kuypers, M. M. M., 2017. Nutrients that limit growth in the ocean, *Current biology: CB*, 27(11), R474–R478.
- Britton, D., Schmid, M., Noisette, F., Havenhand, J. N., Paine, E. R., McGraw, C. M., Reville, A. T., Virtue, P., Nichols, P. D., Mundy, C. N., & Hurd, C. L., 2020. Adjustments in fatty acid composition is a mechanism that can explain resilience to marine heatwaves and future ocean conditions in the habitat-forming seaweed *Phyllospora comosa* (Labillardière) C. Agardh, *Global Change Biology*, 26(6), 3512–3524.
- Burger, F. A., John, J. G., & Frölicher, T. L., 2020. Increase in ocean acidity variability, extremes under increasing atmospheric CO₂, *Biogeosciences*, 17(18), 4633–4662.
- Burger, F. A., Terhaar, J., & Frölicher, T. L., 2022. Compound marine heatwaves and ocean acidity extremes, *Nature Communications*, 13(1), 4722.
- Capuzzo, E., Lynam, C., Barry, J., Stephens, D., Forster, R., Greenwood, N., McQuatters-Gollop, A., Silva, T., van Leeuwen, S., & Engelhard, G., 2017. A decline in primary production in the North Sea over twenty-five years, associated with reductions in zooplankton abundance and fish stock recruitment, *Global Change Biology*, 24.
- Cavole, L., Demko, A., Diner, R., Giddings, A., Koester, I., Pagniello, C., Paulsen, M.-L., Ramírez-Valdez, A., Schwenck, S., Zill, M., & Franks, P., 2016. Biological impacts of the 2013–2015 warm-water anomaly in the northeast pacific: Winners, losers, and the future, *Oceanography (Washington D.C.)*, 29.
- Chassot, E., Bonhommeau, S., Dulvy, N. K., Mélin, F., Watson, R., Gascuel, D., & Le Pape, O., 2010. Global marine primary production constrains fisheries catches, *Ecology Letters*, 13(4), 495–505.

- Cheng, L., Trenberth, K. E., Fasullo, J., Boyer, T., Abraham, J., & Zhu, J., 2017. Improved estimates of ocean heat content from 1960 to 2015, *Science Advances*, 3(3).
- Cheung, W. W. L. & Frölicher, T. L., 2020. Marine heatwaves exacerbate climate change impacts for fisheries in the northeast Pacific, *Scientific Reports*, 10(1), 6678.
- Coale, K. H., Johnson, K. S., Fitzwater, S. E., Gordon, R. M., Tanner, S., Chavez, F. P., Ferioli, L., Sakamoto, C., Rogers, P., Millero, F., Steinberg, P., Nightingale, P., Cooper, D., Cochlan, W. P., Landry, M. R., Constantinou, J., Rollwagen, G., Trasvina, A., & Kudela, R., 1996. A massive phytoplankton bloom induced by an ecosystem-scale iron fertilization experiment in the equatorial Pacific Ocean, *Nature*, 383(6600), 495–501.
- Davison, P., Checkley, D., Koslow, J., & Barlow, J., 2013. Carbon export mediated by mesopelagic fishes in the northeast Pacific Ocean, *Progress in Oceanography*, 116, 14–30.
- Denman, K., Hofmann, E., Marchant, H., Abbott, M., Bates, T., Calvert, S., Fasham, M., Jahnke, R., Kempe, S., Lara, R., Laws, C., Liss, P., Michaels, A., Pedersen, T., Pena, M., Platt, T., Sharp, J.H., Thomas, D., Scoy, K., & Watson, A., 1996. Chapter 10: Marine biotic responses to Environmental change and feedbacks to climate, pp. 483–516.
- Doney, S. C., Ruckelshaus, M., Emmett Duffy, J., Barry, J. P., Chan, F., English, C. A., Galindo, H. M., Grebmeier, J. M., Hollowed, A. B., Knowlton, N., Polovina, J., Rabalais, N. N., Sydeman, W. J., & Talley, L. D., 2012. Climate change impacts on marine ecosystems, *Annual Review of Marine Science*, 4(1), 11–37.
- Dossena, M., Yvon-Durocher, G., Grey, J., Montoya, J. M., Perkins, D. M., Trimmer, M., & Woodward, G., 2012. Warming alters community size structure and ecosystem functioning, *Proceedings of the Royal Society B: Biological Sciences*, 279(1740), 3011–3019.
- Falkowski, P. G., 1994. The role of phytoplankton photosynthesis in global biogeochemical cycles, *Photosynthesis Research*, 39(3), 235–258.
- Field, C. B., Behrenfeld, M. J., Randerson, J. T., & Falkowski, P., 1998. Primary Production of the Biosphere: Integrating Terrestrial and Oceanic Components, *Science*, 281(5374), 237–240.
- Fox-Kemper, B., Hewitt, H., Xiao, C., Aalgeirsdóttir, G., Drijfhout, S., Edwards, T., Golledge, N., Hemer, M., Kopp, R., Krinner, G., Mix, A., Notz, D., Nowicki, S., Nurhati, I., Ruiz, L., Sallée, J.-B., Slangen, A., & Yu, Y., 2021. Ocean, cryosphere and sea level change., in *Climate Change 2021: The Physical Science Basis. Contribution of Working Group I to the Sixth Assessment Report of the Intergovernmental Panel on Climate Change*, pp. 1211–1362, eds Masson-Delmotte, V., Zhai, P., Pirani, A., Connors, S., Péan, C., Berger, S., Caud, N., Chen, Y., Goldfarb, L., Gomis, M., Huang, M., Leitzell, K., Lonnoy, E., Matthews, J., Maycock, T., Waterfield, T., Yeleki, O., Yu, R., & Zhou, B., Cambridge University Press.
- Fredston, A. L., Cheung, W. W. L., Frölicher, T. L., Kitchel, Z., A. A. Maureaud, J. T. Thorson, A. Auber, B. Mérigot, J. Palacios-Abrantes, Lourdes D. Palomares, L. Pecuchet, N. Shackell, & M. L. Pinsky, 2023. Marine heatwaves have not emerged as a dominant driver of ecological change., *Nature (in review)*.
- Friedland, K. D., Stock, C., Drinkwater, K. F., Link, J. S., Leaf, R. T., Shank, B. V., Rose, J. M., Pilskaln, C. H., & Fogarty, M. J., 2012. Pathways between Primary Production and Fisheries Yields of Large Marine Ecosystems, *PLOS ONE*, 7(1), e28945.
- Friedlingstein, P., O’Sullivan, M., Jones, M. W., Andrew, R. M., Gregor, L., Hauck, J., Le Quéré, C., Luijckx, I. T., Olsen, A., Peters, G. P., Peters, W., Pongratz, J., Schwingshackl, C., Sitch, S., Canadell, J. G., Ciais, P., Jackson, R. B., Alin, S. R., Alkama, R., Arneeth, A., Arora, V. K., Bates, N. R., Becker, M., Bellouin, N., Bittig, H. C., Bopp, L., Chevallier, F., Chini, L. P., Cronin, M., Evans, W., Falk, S., Feely, R. A., Gasser, T., Gehlen, M., Gkritzalis, T., Gloege, L., Grassi, G., Gruber, N., Gürses, Ö., Harris, I., Hefner, M., Houghton, R. A., Hurtt, G. C., Iida, Y., Ilyina, T., Jain, A. K., Jersild, A., Kadono, K., Kato, E., Kennedy, D., Klein Goldewijk, K., Knauer, J., Korsbakken, J. I., Landschützer, P., Lefèvre, N., Lindsay, K., Liu, J., Liu, Z., Marland, G., Mayot, N., McGrath, M. J., Metzl, N., Monacchi, N. M., Munro, D. R., Nakaoka, S.-I., Niwa, Y., O’Brien, K., Ono, T., Palmer, P. I., Pan, N., Pierrot, D., Pockock, K., Poulter, B., Resplandy, L., Robertson, E., Rödenbeck, C., Rodriguez, C., Rosan, T. M., Schwinger, J., Séférian, R., Shutler, J. D., Skjelvan, I., Steinhoff, T., Sun, Q., Sutton, A. J., Sweeney, C., Takao, S., Tanhua, T., Tans, P. P., Tian, X., Tian, H., Tilbrook, B., Tsujino, H., Tubiello, F., van der Werf, G. R., Walker, A. P., Wanninkhof, R., Whitehead, C., Willstrand Wranne, A., Wright, R., Yuan, W., Yue, C., Yue, X., Zaehle, S., Zeng, J., & Zheng, B., 2022. Global Carbon Budget 2022, *Earth System Science Data*, 14(11), 4811–4900.
- Frölicher, T. L. & Laufkötter, C., 2018a. Emerging risks from marine heat waves, *Nature Communications*, 9(1), 650.

- Frölicher, T. L. & Laufkötter, C., 2018b. Emerging risks from marine heat waves, *Nature Communications*, 9(1), 650.
- Frölicher, T. L., Rodgers, K. B., Stock, C. A., & Cheung, W. W. L., 2016. Sources of uncertainties in 21st century projections of potential ocean ecosystem stressors, *Global Biogeochemical Cycles*, 30(8), 1224–1243.
- Frölicher, T. L., Fischer, E. M., & Gruber, N., 2018. Marine heatwaves under global warming, *Nature*, 560(7718), 360–364.
- Gittings, J., Raitsoo, D., Krokos, G., & Hoteit, I., 2018. Impacts of warming on phytoplankton abundance, phenology in a typical tropical marine ecosystem, *Scientific Reports*, 8.
- Grinsted, A., Moore, J. C., & Jevrejeva, S., 2013. Projected Atlantic hurricane surge threat from rising temperatures, *Proceedings of the National Academy of Sciences*, 110(14), 5369–5373.
- Gruber, N., 2011. Warming up, turning sour, losing breath: Ocean biogeochemistry under global change, *Philosophical Transactions of the Royal Society A: Mathematical, Physical, Engineering Sciences*, 369(1943), 1980–1996.
- Gruber, N., Boyd, P. W., Frölicher, T. L., & Vogt, M., 2021. Biogeochemical extremes and compound events in the ocean, *Nature*, 600(7889), 395–407.
- Gulev, S., Thorne, P., Ahn, J., Dentener, F., Domingues, C., Gerland, S., Gong, D., Kaufman, D., Nnamchi, H., Quaas, J., Rivera, J., Sathyendranath, S., Smith, S., Trewin, B., von Schuckmann, K., & Vose, R., 2021. Changing state of the climate system., in *Climate Change 2021: The Physical Science Basis. Contribution of Working Group I to the Sixth Assessment Report of the Intergovernmental Panel on Climate Change*, pp. 287–422, eds Masson-Delmotte, V., Zhai, P., Pirani, A., Connors, S., Péan, C., Berger, S., Caud, N., Chen, Y., Goldfarb, L., Gomis, M., Huang, M., Leitzell, K., Lonnoy, E., Matthews, J., Maycock, T., Waterfield, T., Yelekçi, O., Yu, R., & Zhou, B., Cambridge University Press.
- Gupta, A., Thomsen, M., Benthuisen, J., Hobday, A., Oliver, E., Alexander, L., Burrows, M., Donat, M., Feng, M., Holbrook, N., Perkins-Kirkpatrick, S., Moore, P., Rodrigues, R., Scannell, H., Taschetto, A., Ummenhofer, C., Wernberg, T., & Smale, D., 2020. Drivers and impacts of the most extreme marine heatwave events, *Scientific Reports*, 10.
- Hammond, M. L., Beaulieu, C., Henson, S. A., & Sahu, S. K., 2020. Regional surface chlorophyll trends and uncertainties in the global ocean, *Scientific Reports*, 10(1), 1–9.
- Henson, S. A., Sarmiento, J. L., Dunne, J. P., Bopp, L., Lima, I., Doney, S. C., John, J., & Beaulieu, C., 2010. Detection of anthropogenic climate change in satellite records of ocean chlorophyll and productivity, *Biogeosciences*, 7(2), 621–640.
- Hobday, A. J., Alexander, L. V., Perkins, S. E., Smale, D. A., Straub, S. C., Oliver, E. C., Benthuisen, J. A., Burrows, M. T., Donat, M. G., Feng, M., Holbrook, N. J., Moore, P. J., Scannell, H. A., Sen Gupta, A., & Wernberg, T., 2016. A hierarchical approach to defining marine heatwaves, *Progress in Oceanography*, 141, 227–238.
- Hobday, A. J., Oliver, E. C. J., Gupta, A. S., Benthuisen, J. A., Burrows, M. T., Donat, M. G., Holbrook, N. J., Moore, P. J., Thomsen, M. S., Wernberg, T., & Smale, D. A., 2018. Categorizing and naming marine heatwaves, *Oceanography*, 31.
- Holbrook, N. J., Scannell, H. A., Gupta, A. S., Benthuisen, J. A., Feng, M., Oliver, E. C. J., Alexander, L. V., Burrows, M. T., Donat, M. G., Hobday, A. J., Moore, P. J., Perkins-Kirkpatrick, S. E., Smale, D. A., Thomas, S. C. S., & Thomas, W., 2019. A global assessment of marine heatwaves and their drivers, *Nature Communications*, 10(1), 2624.
- Hughes, T. P., Kerry, J. T., Baird, A. H., Connolly, S. R., Dietzel, A., Eakin, C. M., Heron, S. F., Hoey, A. S., Hoogenboom, M. O., Liu, G., McWilliam, M. J., Pears, R. J., Pratchett, M. S., Skirving, W. J., Stella, J. S., & Torda, G., 2018. Global warming transforms coral reef assemblages, *Nature*, 556(7702), 492–496.
- Jones, T., Parrish, J. K., Peterson, W. T., Bjorkstedt, E. P., Bond, N. A., Ballance, L. T., Bowes, V., Hipfner, J. M., Burgess, H. K., Dolliver, J. E., Lindquist, K., Lindsey, J., Nevins, H. M., Robertson, R. R., Roletto, J., Wilson, L., Joyce, T., & Harvey, J., 2018. Massive mortality of a planktivorous seabird in response to a marine heatwave, *Geophysical Research Letters*, 45(7), 3193–3202.

- Kwiatkowski, L., Torres, O., Bopp, L., Aumont, O., Chamberlain, M., Christian, J. R., Dunne, J. P., Gehlen, M., Ilyina, T., John, J. G., Lenton, A., Li, H., Lovenduski, N. S., Orr, J. C., Palmieri, J., Santana-Falcón, Y., Schwinger, J., Séférian, R., Stock, C. A., Tagliabue, A., Takano, Y., Tjiputra, J., Toyama, K., Tsujino, H., Watanabe, M., Yamamoto, A., Yool, A., & Ziehn, T., 2020. Twenty-first century ocean warming, acidification, deoxygenation, and upper-ocean nutrient and primary production decline from CMIP6 model projections, *Biogeosciences*, 17(13), 3439–3470.
- Laufkötter, C., Vogt, M., Gruber, N., Aita-Noguchi, M., Aumont, O., Bopp, L., Buitenhuis, E., Doney, S. C., Dunne, J., Hashioka, T., Hauck, J., Hirata, T., John, J., Le Quéré, C., Lima, I. D., Nakano, H., Seferian, R., Totterdell, I., Vichi, M., & Völker, C., 2015. Drivers and uncertainties of future global marine primary production in marine ecosystem models, *Biogeosciences*, 12(23), 6955–6984.
- Laufkötter, C., Zscheischler, J., & Frölicher, T. L., 2020. High-impact marine heatwaves attributable to human-induced global warming, *Science (New York, N.Y.)*, 369(6511), 1621–1625.
- Le Grix, N., Zscheischler, J., Laufkötter, C., Rousseaux, C. S., & Frölicher, T. L., 2021. Compound high-temperature and low-chlorophyll extremes in the ocean over the satellite period, *Biogeosciences*, 18(6), 2119–2137.
- Le Grix, N., Zscheischler, J., Rodgers, K. B., Yamaguchi, R., & Frölicher, T. L., 2022. Hotspots and drivers of compound marine heatwaves and low net primary production extremes, *Biogeosciences*, 19(24), 5807–5835.
- Lee, Z., Weidemann, A., Kindle, J., Arnone, R., Carder, K. L., & Davis, C., 2007. Euphotic zone depth: Its derivation and implication to ocean-color remote sensing, *Journal of Geophysical Research: Oceans*, 112(C3).
- Leising, A., Schroeder, I., Bograd, S., Abell, J., Durazo, R., Gaxiola-Castro, G., CICESE, Bjorkstedt, E., Field, J., Sakuma, K., Robertson, R., Goericke, R., Peterson, W., Brodeur, R., Barceló, C., Auth, T., Daly, E., Suryan, R., Gladics, A., & Warzybok, P., 2015. State of the California Current 2014–15: Impacts of the warm-water “Blob”, *CalCOFI Report*, 56, 31–68.
- Leonard, M., Westra, S., Phatak, A., Lambert, M., van den Hurk, B., McInnes, K., Risbey, J., Schuster, S., Jakob, D., & Stafford-Smith, M., 2014. A compound event framework for understanding extreme impacts, *WIREs Climate Change*, 5(1), 113–128.
- Li, G., Cheng, L., Zhu, J., Trenberth, K. E., Mann, M. E., & Abraham, J. P., 2020. Increasing ocean stratification over the past half-century, *Nature Climate Change*, 10(12), 1116–1123.
- Long, J. S., Fassbender, A. J., & Estapa, M. L., 2021. Depth-resolved net primary production in the northeast pacific ocean: A comparison of satellite, profiling float estimates in the context of two marine heatwaves, *Geophysical Research Letters*, 48(19), e2021GL093462.
- Magnan, A. K., Pörtner, H.-O., Duvat, V. K. E., Garschagen, M., Guinder, V. A., Zommers, Z., Hoegh-Guldberg, O., & Gattuso, J.-P., 2021. Estimating the global risk of anthropogenic climate change, *Nature Climate Change*, 11(10), 879–885.
- Marba, N. & Duarte, C. M., 2010. Mediterranean warming triggers seagrass (*Posidonia oceanica*) shoot mortality, *Global Change Biology*, 16(8), 2366–2375.
- Marshak, A. R. & Link, J. S., 2021. Primary production ultimately limits fisheries economic performance, *Scientific Reports*, 11(1), 12154.
- Melzner, F., Gutowska, M. A., Langenbuch, M., Dupont, S., Lucassen, M., Thorndyke, M. C., Bleich, M., & Pörtner, H.-O., 2009. Physiological basis for high CO₂ tolerance in marine ectothermic animals: Pre-adaptation through lifestyle and ontogeny?, *Biogeosciences*, 6(10), 2313–2331.
- Mogen, S. C., Lovenduski, N. S., Dallmann, A. R., Gregor, L., Sutton, A. J., Bograd, S. J., Quiros, N. C., Di Lorenzo, E., Hazen, E. L., Jacox, M. G., Buil, M. P., & Yeager, S., 2022. Ocean biogeochemical signatures of the north pacific blob, *Geophysical Research Letters*, 49(9), e2021GL096938.
- Neuer, S., Iversen, M., & Fischer, G., 2014. The Ocean’s Biological Carbon Pump as Part of the Global Carbon Cycle., *Limnology and Oceanography e-Lectures*, 4(4), 1–51.
- Oliver, E., Burrows, M., Donat, M., Gupta, A., Alexander, L., Perkins-Kirkpatrick, S., Benthuisen, J., Hobday, A., Holbrook, N., Moore, P., Thomsen, M., Wernberg, T., & Smale, D., 2019. Projected marine heatwaves in the 21st century and the potential for ecological impact, *Frontiers in Marine Science*, 6, 734.
- Oliver, E. C., Benthuisen, J. A., Darmaraki, S., Donat, M. G., Hobday, A. J., Holbrook, N. J., Schlegel, R. W., & Gupta, A. S., 2021. Marine heatwaves, *Annual Review of Marine Science*, 13(1).

- Oliver, E. C. J., Donat, M. G., Burrows, M. T., Moore, P. J., Smale, D. A., Alexander, L. V., Benthuisen, J. A., Feng, M., Sen Gupta, A., Hobday, A. J., Holbrook, N. J., Perkins-Kirkpatrick, S. E., Scannell, H. A., Straub, S. C., & Wernberg, T., 2018. Longer and more frequent marine heatwaves over the past century, *Nature Communications*, 9(1), 1324.
- Pansch, C., Scotti, M., Barboza, F. R., Al-Janabi, B., Brakel, J., Briski, E., Bucholz, B., Franz, M., Ito, M., Paiva, F., Saha, M., Sawall, Y., Weinberger, F., & Wahl, M., 2018. Heat waves and their significance for a temperate benthic community: A near-natural experimental approach, *Global Change Biology*, 24(9), 4357–4367.
- Parnesan, C., Root, T. L., & Willig, M. R., 2000. Impacts of Extreme Weather and Climate on Terrestrial Biota, *Bulletin of the American Meteorological Society*, 81(3), 443–450.
- Pauly, D., 1980. On the interrelationships between natural mortality, growth parameters, and mean environmental temperature in 175 fish stocks, *ICES Journal of Marine Science*, 39(2), 175–192.
- Pauly, D. & Cheung, W., 2017. Sound physiological knowledge and principles in modeling shrinking of fishes under climate change, *Global Change Biology*, 24.
- Pauly, D. & Christensen, V., 1995. Primary production required to sustain global fisheries, *Nature*, 374(6519), 255–257.
- Peña, M. A., Nemcek, N., & Robert, M., 2019. Phytoplankton responses to the 2014–2016 warming anomaly in the northeast subarctic Pacific Ocean, *Limnology and Oceanography*, 64(2), 515–525.
- Pfleiderer, P., Jézéquel, A., Legrand, J., Legrix, N., Markantonis, I., Vignotto, E., & Yiou, P., 2021. Simulating compound weather extremes responsible for critical crop failure with stochastic weather generators, *Earth System Dynamics*, 12(1), 103–120.
- Piatt, J. F., Parrish, J. K., Renner, H. M., Schoen, S. K., Jones, T. T., Arimitsu, M. L., Kuletz, K. J., Bodenstein, B., García-Reyes, M., Duerr, R. S., Corcoran, R. M., Kaler, R. S. A., McChesney, G. J., Golightly, R. T., Coletti, H. A., Suryan, R. M., Burgess, H. K., Lindsey, J., Lindquist, K., Warzybok, P. M., Jahncke, J., Roletto, J., & Sydeman, W. J., 2020. Extreme mortality and reproductive failure of common murrets resulting from the northeast Pacific marine heatwave of 2014–2016, *PLOS ONE*, 15(1), e0226087.
- Pinkerton, M. H., Boyd, P. W., Deppeler, S., Hayward, A., Höfer, J., & Moreau, S., 2021. Evidence for the Impact of Climate Change on Primary Producers in the Southern Ocean, *Frontiers in Ecology and Evolution*, 9.
- Pörtner, H. O., 2002. Climate variations and the physiological basis of temperature dependent biogeography: Systemic to molecular hierarchy of thermal tolerance in animals, *Comparative Biochemistry and Physiology. Part A, Molecular & Integrative Physiology*, 132(4), 739–761.
- Puerta, P., Ciannelli, L., Rykaczewski, R. R., Opiekun, M., & Litzow, M. A., 2019. Do Gulf of Alaska fish and crustacean populations show synchronous non-stationary responses to climate?, *Progress in Oceanography*, 175, 161–170.
- Pörtner, H.-O., Roberts, D., Masson-Delmotte, V., Zhai, P., Tignor, M., Poloczanska, E., Mintenbeck, K., Alegría, A., Nicolai, M., Okem, A., Petzold, J., Rama, B., & Weyer, N., 2019. Technical summary, in *In: IPCC Special Report on the Ocean and Cryosphere in a Changing Climate*, Cambridge University Press.
- Racault, M.-F., Sathyendranath, S., Brewin, R. J. W., Raitsos, D. E., Jackson, T., & Platt, T., 2017. Impact of el niño variability on oceanic phytoplankton, *Frontiers in Marine Science*, 4, 133.
- Ridder, N., Pitman, A., Westra, S., Ukkola, A., Do, H., Bador, M., Hirsch, A., Evans, J., Luca, A. D., & Zscheischler, J., 2020. Global hotspots for the occurrence of compound events, *Nature Communications*, 11, 5956.
- Roxy, M. K., Modi, A., Murtugudde, R., Valsala, V., Panickal, S., Prasanna Kumar, S., Ravichandran, M., Vichi, M., & Lévy, M., 2016. A reduction in marine primary productivity driven by rapid warming over the tropical Indian Ocean, *Geophysical Research Letters*, 43(2), 826–833.
- Saba, V. S., Friedrichs, M. A. M., Carr, M.-E., Antoine, D., Armstrong, R. A., Asanuma, I., Aumont, O., Bates, N. R., Behrenfeld, M. J., Bennington, V., Bopp, L., Bruggeman, J., Buitenhuis, E. T., Church, M. J., Ciotti, A. M., Doney, S. C., Dowell, M., Dunne, J., Dutkiewicz, S., Gregg, W., Hoepffner, N., Hyde, K. J. W., Ishizaka, J., Kameda, T., Karl, D. M., Lima, I., Lomas, M. W., Marra, J., McKinley, G. A., Mélin, F., Moore, J. K., Morel, A., O'Reilly, J., Salihoglu, B., Scardi, M., Smyth, T. J., Tang, S., Tjiputra, J., Uitz, J., Vichi, M., Waters, K., Westberry, T. K., & Yool, A., 2010. Challenges of modeling depth-integrated marine primary productivity over multiple decades: A case study at BATS and HOT: MODELING MARINE PRIMARY PRODUCTIVITY, *Global Biogeochemical Cycles*, 24(3).

- Saha, M., Barboza, F. R., Somerfield, P. J., Al-Janabi, B., Beck, M., Brakel, J., Ito, M., Pansch, C., Nascimento-Schulze, J. C., Jakobsson Thor, S., Weinberger, F., & Sawall, Y., 2020. Response of foundation macrophytes to near-natural simulated marine heatwaves, *Global Change Biology*, 26(2), 417–430.
- Sallée, J.-B., Pellichero, V., Akhoudas, C., Pauthenet, E., Vignes, L., Schmidtko, S., Garabato, A. N., Sutherland, P., & Kuusela, M., 2021. Summertime increases in upper-ocean stratification and mixed-layer depth, *Nature*, 591(7851), 592–598.
- Sarmiento, J. L. & Bender, M., 1994. Carbon biogeochemistry and climate change, *Photosynthesis Research*, 39(3), 209–234.
- Sarmiento, J. L. & Gruber, N., 2006. *Ocean Biogeochemical Dynamics*, Princeton University Press.
- Sarmiento, J. L., Hughes, T. M. C., Stouffer, R. J., & Manabe, S., 1998. Simulated response of the ocean carbon cycle to anthropogenic climate warming, *Nature*, 393(6682), 245–249.
- Sarmiento, J. L., Gruber, N., Brzezinski, M. A., & Dunne, J. P., 2004. High-latitude controls of thermocline nutrients and low latitude biological productivity, *Nature*, 427(6969), 56–60.
- Schoepf, V., Stat, M., Falter, J., & McCulloch, M., 2015. Limits to the thermal tolerance of corals adapted to a highly fluctuating, naturally extreme temperature environment, *Scientific Reports*, 5, 17639.
- Siegel, D., Behrenfeld, M., Maritorea, S., McClain, C., Antoine, D., Bailey, S., Bontempi, P., Boss, E., Dierssen, H., Doney, S., Eplee, R., Evans, R., Feldman, G., Fields, E., Franz, B., Kuring, N., Mengelt, C., Nelson, N., Patt, F., Robinson, W., Sarmiento, J., Swan, C., Werdell, P., Westberry, T., Wilding, J., & Yoder, J., 2013. Regional to global assessments of phytoplankton dynamics from the SeaWiFS mission, *Remote Sensing of Environment*, 135, 77–91.
- Smale, D. A., Wernberg, T., Oliver, E. C. J., Thomsen, M., Harvey, B. P., Straub, S. C., Burrows, M. T., Alexander, L. V., Benthuyssen, J. A., Donat, M. G., Feng, M., Hobday, A. J., Holbrook, N. J., Perkins-Kirkpatrick, S. E., Scannell, H. A., Sen Gupta, A., Payne, B. L., & Moore, P. J., 2019. Marine heatwaves threaten global biodiversity and the provision of ecosystem services, *Nature Climate Change*, 9(4), 306–312.
- Smith, K. E., Burrows, M. T., Hobday, A. J., Sen Gupta, A., Moore, P. J., Thomsen, M., Wernberg, T., & Smale, D. A., 2021. Socioeconomic impacts of marine heatwaves: Global issues and opportunities, *Science*, 374(6566), eabj3593.
- Smith, K. E., Burrows, M. T., Hobday, A. J., King, N. G., Moore, P. J., Sen Gupta, A., Thomsen, M. S., Wernberg, T., & Smale, D. A., 2023. Biological Impacts of Marine Heatwaves, *Annual Review of Marine Science*, 15(1), null.
- Steinacher, M., Joos, F., Frölicher, T., Bopp, L., Cadule, P., Cocco, V., Doney, S., Gehlen, M., Lindsay, K., Moore, J., Schneider, B., & Segschneider, J., 2010. Projected 21st century decrease in marine productivity: A multi-model analysis, *Biogeosciences*, 7, 979–1005.
- Street, J. H. & Paytan, A., 2005. Iron, phytoplankton growth, and the carbon cycle, *Metal Ions in Biological Systems*, 43, 153–193.
- Stuhr, M., Reymond, C. E., Rieder, V., Hallock, P., Rahnenführer, J., Westphal, H., & Kucera, M., 6 juil. 2017. Reef calcifiers are adapted to episodic heat stress but vulnerable to sustained warming, *PLOS ONE*, 12(7), e0179753.
- Tagliabue, A., Kwiatkowski, L., Bopp, L., Butenschön, M., Cheung, W., Lengaigne, M., & Vialard, J., 2021. Persistent uncertainties in ocean net primary production climate change projections at regional scales raise challenges for assessing impacts on ecosystem services, *Frontiers in Climate*, 3.
- Terhaar, J., Frölicher, T. L., & Joos, F., 2022. Observation-constrained estimates of the global ocean carbon sink from Earth system models, *Biogeosciences*, 19(18), 4431–4457.
- Thomson, J. A., Burkholder, D. A., Heithaus, M. R., Fourqurean, J. W., Fraser, M. W., Statton, J., & Kendrick, G. A., 2015. Extreme temperatures, foundation species, and abrupt ecosystem change: An example from an iconic seagrass ecosystem, *Global Change Biology*, 21(4), 1463–1474.
- Urban, M. C., Tewksbury, J. J., & Sheldon, K. S., 2012. On a collision course: Competition and dispersal differences create no-analogue communities and cause extinctions during climate change, *Proceedings of the Royal Society B: Biological Sciences*, 279(1735), 2072–2080.

- Urban, M. C., Zarnetske, P. L., & Skelly, D. K., 2013. Moving forward: Dispersal and species interactions determine biotic responses to climate change, *Annals of the New York Academy of Sciences*, 1297, 44–60.
- van der Wiel, K., Selten, F. M., Bintanja, R., Blackport, R., & Screen, J. A., 2020. Ensemble climate-impact modelling: Extreme impacts from moderate meteorological conditions, *Environmental Research Letters*, 15(3), 034050.
- Vandersea, M. W., Kibler, S. R., Tester, P. A., Holderied, K., Hondolero, D. E., Powell, K., Baird, S., Doroff, A., Dugan, D., & Litaker, R. W., 2018. Environmental factors influencing the distribution and abundance of *Alexandrium catenella* in Kachemak bay and lower cook inlet, Alaska, *Harmful Algae*, 77, 81–92.
- Vinogradov, M. E., 1997. Some Problems of Vertical Distribution of Meso- and Macroplankton in the Ocean, in *Advances in Marine Biology*, vol. 32 of The Biogeography of the Oceans, pp. 1–92, eds Blaxter, J. H. S., Southward, A. J., Gebruk, A. V., Southward, E. C., & Tyler, P. A., Academic Press.
- Vogt, L., Burger, F. A., Griffies, S. M., & Frölicher, T. L., 2022. Local drivers of marine heatwaves: A global analysis with an earth system model, *Frontiers in Climate*, 4.
- Volk, T. & Hoffert, M. I., 1985. Ocean Carbon Pumps: Analysis of Relative Strengths and Efficiencies in Ocean-Driven Atmospheric CO₂ Changes, in *The Carbon Cycle and Atmospheric CO₂: Natural Variations Archean to Present*, pp. 99–110, American Geophysical Union (AGU).
- von Bertalanffy, L., 1951. *Theoretische Biologie: Stoffwechsel, Wachstum. Zweiter Band*, A. Francke.
- Wernberg, T., Smale, D., Thomsen, M., Langlois, T., de Bettignies, T., Bennett, S., & Rousseaux, C., 2013. An extreme climatic event alters marine ecosystem structure in a global biodiversity hotspot, *Nature Climate Change*, 3, 78–82.
- Whitney, F. A., 2015. Anomalous winter winds decrease 2014 transition zone productivity in the NE Pacific, *Geophysical Research Letters*, 42(2), 428–431.
- Williams, R. G. & Follows, M. J., 2011. *Ocean Dynamics and the Carbon Cycle: Principles and Mechanisms*, Cambridge University Press, Cambridge.
- Wyatt, A., Resplandy, L., & Marchetti, A., 2022. Ecosystem impacts of marine heat waves in the Northeast Pacific, *EGUsphere Discussions*, 2022, 1–24.
- Xie, S.-P., 2020. Ocean Warming Pattern Effect On Global And Regional Climate Change, *AGU Advances*, 1(1), e2019AV000130.
- Xu, T., Newman, M., Capotondi, A., Stevenson, S., Di Lorenzo, E., & Alexander, M. A., 2022. An increase in marine heatwaves without significant changes in surface ocean temperature variability, *Nature Communications*, 13(1), 7396.
- Yang, B., Emerson, S. R., & Peña, M. A., 2018. The effect of the 2013–2016 high temperature anomaly in the subarctic Northeast Pacific (the “Blob”) on net community production, *Biogeosciences*, 15(21), 6747–6759.
- Zscheischler, J. & Seneviratne, S. I., 2017. Dependence of drivers affects risks associated with compound events, *Science Advances*, 3(6), e1700263.
- Zscheischler, J., Mahecha, M. D., Harmeling, S., & Reichstein, M., 2013. Detection and attribution of large spatiotemporal extreme events in Earth observation data, *Ecological Informatics*, 15, 66–73.
- Zscheischler, J., Westra, S., van den Hurk, B. J. J. M., Seneviratne, S. I., Ward, P. J., Pitman, A., AghaKouchak, A., Bresch, D. N., Leonard, M., Wahl, T., & Zhang, X., 2018. Future climate risk from compound events, *Nature Climate Change*, 8(6), 469–477.
- Zscheischler, J., Martius, O., Westra, S., Bevacqua, E., Raymond, C., Horton, R. M., van den Hurk, B., AghaKouchak, A., Jézéquel, A., Mahecha, M. D., Maraun, D., Ramos, A. M., Ridder, N. N., Thiery, W., & Vignotto, E., 2020. A typology of compound weather and climate events, *Nature Reviews Earth & Environment*, 1(7), 333–347.

F

Chapter 2

Methods

In this thesis, we use a combination of satellite-based observations and numerical models to analyse compound MHW-NPPX events. Satellite observations are limited to the ocean surface. Although satellite passes cover the global ocean surface at only a few days interval, there remain gaps, which must be interpolated. Cloud cover or sea ice also prevent direct scanning of the ocean surface and cause observational biases. Nevertheless, biases can be corrected using in situ data, and once satellite-based observations skillfully estimate ocean variables, they allow fairly accurate sampling of surface compound events. In contrast, models are not limited in space and time. They provide large datasets from which to statistically analyse rare compound MHW-NPPX events. However, models are an incomplete representation of reality which must be evaluated against observations. Over regions where they are consistent with observations, Earth system models are useful tools to gain understanding on the physical and biogeochemical drivers of compound events, whereas marine fish models allow for estimating their impacts on marine species. Observations and models are therefore complementary. The following chapter presents the satellite-derived observations, Earth system models and global marine fish model used in this thesis to analyse compound MHW-NPPX events.

2.1 Observations

2.1.1 Sea surface temperature

For sea-surface temperature (SST), we use a blended SST dataset developed by the National Oceanic and Atmospheric Administration (NOAA) (Reynolds et al., 2007; Banzon et al., 2016). In situ and satellite observations were combined using Optimal Interpolation at daily resolution and on a 0.25° spatial grid to form an SST analysis, i.e., a spatially complete field. The main input of this Optimum Interpolation SST (OISST) analysis product is infrared satellite data from the Advanced Very High Resolution Radiometer with temporal coverage beginning in late 1981 to the present. Infrared data are limited by the spatial width of the satellite swath. Any gaps are filled in by interpolation so as to produce a consistent long-term record. Note that this is a smoothed product, which may underestimate the intensity and duration of MHWs (Schlegel et al., 2019). Nevertheless, these satellite-derived temperature data have been validated extensively (Reynolds et al., 2007; Huang et al., 2020; Banzon et al., 2016) and used for many recent marine heatwave analyses (e.g. Hobday et al. (2016); Oliver et al. (2018); Frölicher et al. (2018); Laufkötter et al. (2020)). Clouds, dust plumes and volcanic aerosols, especially following the Mt Pinatubo and El Chichón eruptions, also induce satellite biases, which are corrected using in situ data from ships and buoys (Banzon et al., 2016).

2.1.2 Surface chlorophyll concentration

Chlorophyll is a pigment enabling primary producers to convert solar energy into organic matter through photosynthesis. The more chlorophyll in the surface open ocean, the higher net primary productivity by phytoplankton generally is (Behrenfeld & Falkowski, 1997). In Chapter 3, we use surface chlorophyll concentration as a proxy for net primary productivity in the upper ocean.

Surface chlorophyll concentration can be estimated by satellite observations, thanks to empirical relationships between ocean colour and in situ measurements of chlorophyll concentration. Ocean colour is assessed by satellite reflectance measurements at wavelengths spanning the 440-670 nm range. The difference and ratio of the reflectances at various wavelengths within that 440-670 nm range is then used by algorithms to estimate the chlorophyll concentration (Hu et al., 2019; O’Reilly & Werdell, 2019). Satellite ocean color measurements started in 1998 with the Sea-viewing Wide Field-of-view Sensor (SeaWiFS; launched in 1997, O’Reilly et al. (1998)), followed by the Moderate Resolution Imaging Spectroradiometer (MODIS)-Aqua (launched in 2002, Hu et al. (2012, 2019)) and the Visible Infrared Imaging Radiometer Suite (VIIRS; launched in 2011, Wang & Son (2016)). These satellite missions provided an unprecedented record of surface chlorophyll concentrations in the ocean. However, spatial coverage is sparse at the daily scale, notably due to clouds. Here, we rather use chlorophyll concentrations derived by a biogeochemical model which assimilates these SeaWiFS-MODIS-VIIRS data.

The NASA Ocean Biogeochemical Model (NOBM.R2020.1 version) (Gregg & Rousseaux, 2017) is a comprehensive ocean biogeochemical model, coupled to a global ocean circulation and radiative model (Gregg & Casey, 2007). The model spans latitudes 84°S to 72°N at 1.25° longitude by 2/3° latitude spatial resolution. It only resolves open ocean areas where depth exceeds 200m. The NOBM includes four phytoplankton groups: diatoms, chlorophytes, cyanobacteria, and coccolithophores. Total chlorophyll is the sum of all phytoplankton groups’ chlorophyll.

SeaWiFS-MODIS-VIIRS data are assimilated daily into the NOBM, by combining model outputs and satellite data to produce an “analysis”, or best state estimate. Heavier weighting towards the model is enforced where satellite data tend to perform poorly compared to in situ data (Gregg, 2008), e.g., under clouds or sea-ice. The resulting analysis is then used to reinitialize the model for the next simulation day. Temporal coverage extends from 1998 to 2018 at a daily resolution, without the gaps that are intrinsic to satellite data due to clouds and high solar zenith angles. More details on the NOBM product and its limitations are provided in Chapter 3.

2.1.3 Net primary productivity

NPP measurements in the ocean were initially based on radioactive carbon (C^{14}) (Nielsen, 1952) or geochemical tracer distributions (Jenkins & Goldman, 1985; Williams, P.J.L. & Robertson, J.I., 1989). Although numerous, these discrete NPP measurements undersampled spatial and temporal NPP variability (Bidigare et al., 1992). Satellite-based estimates of chlorophyll concentration (section 2.1.2) offered opportunities to develop satellite-based model estimates of NPP over the global ocean. Yet, attempts to quantitatively relate NPP to chlorophyll concentration (e.g., Bidigare et al. (1992); Antoine & Morel (1996)) revealed that, although NPP tends to increase with increasing chlorophyll, chlorophyll variability alone is insufficient to explain the complete NPP variability over time and space (Behrenfeld & Falkowski, 1997). Indeed, chlorophyll simply controls the light-harvesting capacity of photosynthetic organisms. Photosynthesis, however, also depends on light availability and on photosynthetic efficiency, i.e., the carbon fixation rate per chlorophyll unit.

Behrenfeld & Falkowski (1997) used a dataset of ^{14}C -based NPP measurements to determine the variables which, in addition to surface chlorophyll concentrations, were responsible for observed

variability in NPP. Their study led to the first version of the Vertically Generalized Production Model (VGPM), which estimates NPP from satellite-based chlorophyll data. Vertically-integrated NPP is expressed as a function of surface chlorophyll concentration (Chl), photosynthetic efficiency ($P_{\text{opt}}^{\text{B}}$), photosynthetic active radiation (PAR), euphotic layer depth (Z_{eu}) and day length (DL) (Behrenfeld & Falkowski, 1997; Behrenfeld et al., 2001).

$$\mathbf{VGPM} : \text{NPP} = \text{Chl} \cdot P_{\text{opt}}^{\text{B}} \cdot \text{DL} \cdot f(\text{PAR}) \cdot Z_{\text{eu}} \quad (2.1)$$

Z_{eu} is estimated from surface chlorophyll concentrations using the Morel & Berthon (1989) CASE I model, which is based on empirical relationships between surface chlorophyll concentration, vertically-integrated chlorophyll concentration and Z_{eu} . Errors in NPP estimates by the VGPM mainly come from errors in chlorophyll estimates by satellites and uncertainties in the photosynthetic efficiency. Behrenfeld & Falkowski (1997) state that photosynthesis efficiency mainly depends on temperature, which controls the Calvin cycle enzymatic activity performing photosynthesis. In this first version of the VGPM model, which we refer to as Standard-VGPM, photosynthetic efficiency is described as a polynomial function of SST, conveniently available from satellite observations. A subsequent version of the VGPM, the Eppley-VGPM, expresses photosynthetic efficiency as an exponential function of temperature (Eppley, 1972), resulting in weaker spatial gradients in NPP estimates (Le Grix et al., 2022). For example, NPP gradients along the subtropical gyres are weaker in Eppley-VGPM compared to Standard-VGPM (Fig. 2.1b,c). The continuous increase in photosynthetic efficiency with temperature is justified in Eppley-VGPM by warm temperatures generally coinciding with elevated light conditions, and thus with less light limitation.

The temperature-dependent representations of photosynthetic efficiency in Standard-VGPM and Eppley-VGPM neglect physiological adjustments by phytoplankton to changes in nutrient levels and in light quantity and spectral quality (Falkowski, 1980; Falkowski & LaRoche, 1991; Falkowski, 1994; Geider et al., 1996, 1997; MacIntyre et al., 2002). Accurate representation of photosynthetic efficiency is challenging and key to improving the performance of Standard-VGPM and Eppley-VGPM.

Carbon-based models offer an alternative approach to calculating NPP. Phytoplankton carbon biomass estimates can be derived from particulate backscattering coefficients (bbp). In conjunction with satellite-based estimates of the chlorophyll concentration, the Carbon-based Production Model (CbPM; Behrenfeld et al. (2005); Westberry et al. (2008)) is able to infer the chlorophyll to carbon biomass ratio (Chl:C), and thus to account for varying pigment level in phytoplankton in response to changes in light and nutrient levels. NPP is expressed as the product of carbon biomass (C) and growth (μ), where growth is a function of Chl:C and of the median light level in the mixed layer (I_{ML}).

$$\mathbf{CbPM} : \text{NPP} = C \cdot \mu, \text{ where } \mu = f(\text{Chl} : C, I_{\text{ML}}) \quad (2.2)$$

The CbPM distinguishes between the changes in Chl driven by changes in biomass, and the changes in Chl driven by physiology, i.e., by adjustments in the Chl:C ratio (Westberry et al., 2008). This is a significant improvement from Standard-VGPM and Eppley-VGPM, which assign all changes in Chl to a change in biomass then translated into a change in NPP.

Recent advances in the understanding of ocean color properties and phytoplankton physiology led to the development of the Carbon, Absorption, and Fluorescence Euphotic-resolving (CAFE) model (Silsbe et al., 2016), which also derives NPP from satellite observations. The CAFE model expresses NPP as the product of energy absorption (Q_{PAR}) and the efficiency (ϕ) by which absorbed energy is converted into carbon biomass:

$$\mathbf{CAFE} : \text{NPP} = Q_{\text{PAR}} \cdot \phi \quad (2.3)$$

Silsbe et al. (2016) found highest similarity between in-situ NPP measurements and NPP estimates by the CAFE model, compared to other satellite-derived NPP models.

Lastly, we also consider NPP estimates by the NOBM (presented in section 2.1.2) in this thesis. The NOBM calculates NPP as an integrated function of μ , Chl and the carbon to chlorophyll ratio (C:Chl) over depth (Rousseaux & Gregg, 2014). Satellite-based chlorophyll estimates are assimilated into the NOBM (section 2.1.2).

$$\text{NOBM} : \text{NPP} = \int \mu \cdot \text{Chl} \cdot (\text{C} : \text{Chl}) dz \quad (2.4)$$

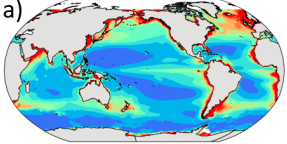
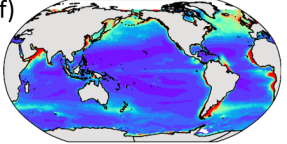
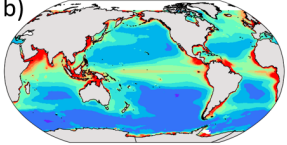
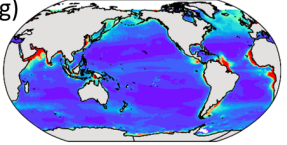
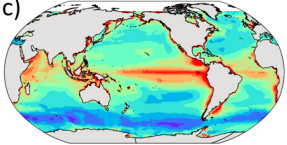
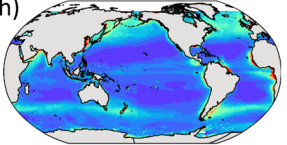
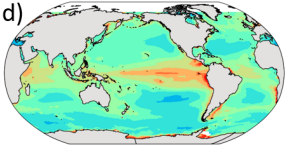
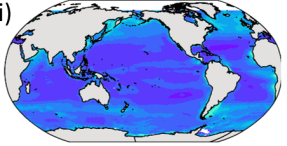
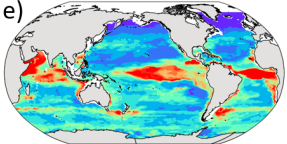
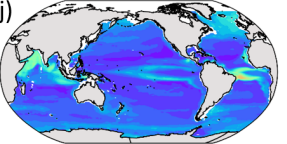
Model	Based on	Global mean NPP	Mean NPP (mg C day ⁻¹ m ⁻²)	NPP standard deviation (mg C day ⁻¹ m ⁻²)
Standard-VGPM¹	Chl, SST, PAR	50 Pg C year ⁻¹	a) 	f) 
Eppley-VGPM^{1,2}	Chl, SST, PAR	52 Pg C year ⁻¹	b) 	g) 
CbPM^{3,4}	Chl, C, PAR	66 Pg C year ⁻¹	c) 	h) 
CAFE⁵	Chl, C, SST, PAR, Absorption at 443 nm	62 Pg C year ⁻¹	d) 	i) 
NOBM^{6,7}	Coupled Circulation-Radiative-Biogeochemical model forced by reanalyses data and assimilating Chl	47 Pg C year ⁻¹	e) 	j) 

Figure 2.1: Main characteristics of the satellite-derived NPP estimates included in this thesis. Model deriving the estimates and associated literature (¹ Behrenfeld & Falkowski (1997); ² Eppley (1972); ³ Behrenfeld et al. (2005); ⁴ Westberry et al. (2008); ⁵ Silsbe et al. (2016); ⁶ Gregg (2008); ⁷ Gregg & Rousseaux (2014)); Data upon which the model is based; Global mean net primary productivity (Pg C m⁻² year⁻¹) over 1998-2018; Mean net primary productivity (mg C m⁻² day⁻¹) over 1998-2018 in Standard-VGPM (a), Eppley-VGPM (b), CbPM (c), CAFE (d), and NOBM (e); Standard deviation of the net primary productivity (mg C m⁻² day⁻¹) over 1998-2018 in Standard-VGPM (f), Eppley-VGPM (g), CbPM (h), CAFE (i), and NOBM (j).

Fig. 2.1 summarizes the main characteristics of all observation-based models included in this thesis. Models differ in their formulation of NPP and in their satellite-based input data, resulting in different NPP estimates. Models considering varying Chl:C ratios (CbPM, CAFE) account for phytoplankton adaptative strategies to low light levels, and thereby obtain higher global oceanic NPP than models with fixed Chl:C ratio (66 and 62 Pg C year⁻¹ in CbPM and CAFE, against 50, 52 and 47 Pg C year⁻¹ in Standard-VGPM, Eppley-VGPM, and NOBM).

Although all models agree with generally low NPP in the subtropical gyres and high NPP in the eastern boundary upwelling systems, absolute values and spatial gradients differ across models (Fig. 2.1a-e). In particular, compared to other models, CbPM and CAFE suggest relatively higher NPP in the oligotrophic subtropical gyres (Fig. 2.1c,d). There, chlorophyll variability can be dominated by photoacclimation, i.e., by adjustments of the Chl:C ratio in response to changes in light levels (Behrenfeld et al., 2005; Silsbe et al., 2016), which Standard-VGPM, Eppley-VGPM and NOBM fail to represent. Lastly, models also represent divergent NPP variability over time, e.g., at the seasonal time-scale (Silsbe et al., 2016).

In this thesis, we include all five observation-based models. The diversity of models allows for distinguishing between regions where results are especially robust across models, and regions where models disagree. High or low agreement is associated with a gain or loss in confidence in our results. Temporal resolution is 5-day mean for the NOBM and 8-day mean for all other models. We focus on the 1998-2018 period, when NPP estimates are available for all models.

2.2 Models

The following section presents two Earth system models and one global marine fish model, which we used to characterize compound extreme events in the ocean, identify their physical and biogeochemical drivers, and verify their impacts on marine ecosystems at the global scale.

2.2.1 Earth system models

Earth system models (ESMs) aim to simulate all climate-relevant aspects of the Earth system. Contrary to global climate models, which represent atmospheric and oceanic processes, ESMs additionally include representations of the global carbon cycle, dynamic vegetation, atmospheric chemistry, ocean biogeochemistry, and sometimes continental ice sheets. ESMs are composed by a set of equations, solved on a three-dimensional grid which can extend from the upper atmosphere to the bottom of the oceans. An efficient infrastructure distributes the representation of each climate component into model components for the atmosphere, ocean physics and biogeochemistry, land, and sometimes land ice and sea ice (Fig. 2.2). A coupler handles fluxes between these components (Fig. 2.2), such as air-sea heat and moisture fluxes, aerosol deposit on sea-ice, and the emission of biogenic compounds by forests on land to the atmosphere.

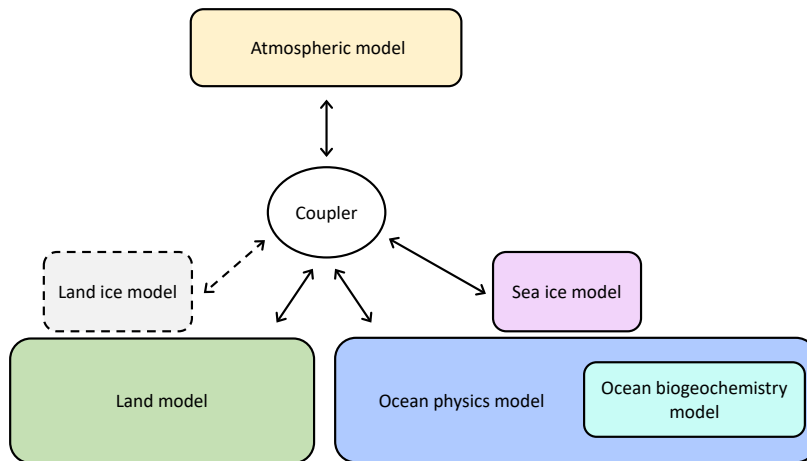


Figure 2.2: Schematic representation of the usual components of an ESM and their interactions through a coupler. Dashed contours indicate model components that are usually not included.

In this thesis, we use two ESMs: the GFDL ESM2M (Dunne et al., 2012, 2013), for which we participated in running an ensemble of simulations, and the CESM2 (Danabasoglu et al., 2020), whose model outputs were kindly provided by Dr. Keith Rodgers. Chapter 4 will review the similarities, differences, and caveats of these two ESMs in details. Here, we give a brief description of their main characteristics, with a focus on the ocean physics and biogeochemistry components (Fig. 2.3).

	GFDL ESM2M	CESM2
Ocean physics	<p>MOM4p1¹</p> <ul style="list-style-type: none"> Nominal 1° horizontal resolution and two northern poles z* vertical coordinate, 50 vertical levels, ~ 10m cell height in the upper ocean Icebergs produced by the land model are treated as Lagrangian particles, with trajectories determined by atmospheric and oceanic drag 	<p>POP2⁷</p> <ul style="list-style-type: none"> Nominal 1° resolution, with uniform spacing of 1.125° in the zonal direction and varying meridional resolution. 60 vertical levels. 10m cell height in the upper ocean <p>WW3⁸</p> <ul style="list-style-type: none"> Special model for surface waves
Ocean biogeochemistry	<p>TOPAZv2²</p> <ul style="list-style-type: none"> 3 phytoplankton groups: small, large, and diazotrophs Growth limited by nutrients, light, and temperature Nitrogen fixation by diazotrophs Flexible N:P:Fe stoichiometry Biogenic CaCO₃ and Si formation Phytoplankton loss by implicit zooplankton grazing Ballasting by mineral dust, biogenic CaCO₃ and Si 	<p>MARBL⁹</p> <ul style="list-style-type: none"> Flexible number of phytoplankton and zooplankton types Growth limited by nutrients, light, and temperature Nitrogen fixation by diazotrophs Flexible N:P:Fe stoichiometry Biogenic CaCO₃ and Si formation Phytoplankton loss by aggregation, mortality and zooplankton grazing Ballasting by biogenic CaCO₃ and Si
Sea ice	<p>Winton et al., (2000)³</p> <ul style="list-style-type: none"> Sea ice thermodynamics 3-layer model (snow, upper ice, lower ice), mass fluxes between layers 5 ice thickness classes MOM4p1 grid 	<p>CICE5¹⁰</p> <ul style="list-style-type: none"> Sea ice thermodynamics 3-layer snow 8-layer sea-ice, mass fluxes between layers POP2grid
Atmosphere	<p>AM2⁴</p> <ul style="list-style-type: none"> 2°x2.5° horizontal resolution, 24 vertical pressure levels, increased resolution near surface. Prescribed aerosols 	<p>CAM6¹¹/WACCM6¹²</p> <ul style="list-style-type: none"> 0.9° latitude × 1.25° longitude, with 32 vertical levels. Limited (CAM6) or comprehensive (WACCM6) representation of chemistry <p>MAM4¹³</p> <ul style="list-style-type: none"> Special model for aerosols Emissions-driven aerosols
Land	<p>LM3.0⁵</p> <ul style="list-style-type: none"> 5 vegetation types 5 vegetation carbon pools Two soil pools (fast and slow overturning) Fire parametrization as function of drought index and biomass above ground Iceberg model derived from Martin et al. (2010)⁶ Excess land snow on land in LM3.0 supplies icebergs to the ocean 	<p>CLM5¹⁴</p> <ul style="list-style-type: none"> 18 vegetation types 7 vegetation carbon pools 25-layer soil, 2 alternate soil decomposition models (fast and slow overturning) Fire parametrization as function of temperature, relative humidity, soil moisture, biomass above ground and human activities <p>MOSART¹⁵</p> <ul style="list-style-type: none"> Special model for river runoff
Land ice	<p><i>Represented by the land model</i></p>	<p>CISM2¹⁶</p> <ul style="list-style-type: none"> Dynamic ice sheet model Calving of floating ice

Figure 2.3: The GFDL ESM2M and CESM2 model components. This is a non-exhaustive list of the models' main characteristics, with a focus on their divergences. *References:* ¹Griffies (2012); ²Dunne et al. (2013); ³Winton (2000); ⁴Anderson et al. (2004); ⁵Shevliakova et al. (2009); ⁶Martin & Adcroft (2010); ⁷Smith & Gent (2010) ⁸Tolman (2009); ⁹Long et al. (2021); ¹⁰Hunke et al. (2017); ¹¹Danabasoglu et al. (2020); ¹²Lin & Rood (1997); ¹³Gottelman et al. (2019); ¹⁴Lawrence et al. (2019); ¹⁵Li et al. (2013); ¹⁶Lipscomb et al. (2019).

The GFDL ESM2M is a fully coupled carbon-climate ESM developed at NOAA’s Geophysical Fluid Dynamics Laboratory (GFDL) (Dunne et al., 2012, 2013). It couples an atmospheric circulation model to an oceanic circulation model, and includes representations of land, sea-ice, and iceberg dynamics, as well as interactive biogeochemistry. The atmospheric model AM2 (Anderson et al., 2004) has a horizontal resolution of 2° latitude x 2.5° longitude, and 24 vertical levels. The horizontal resolution of the ocean model MOM4p1 (Griffies, 2012) is nominally 1° latitude x 1° longitude with increasing meridional resolution of up to $1/3^\circ$ towards the equator, and 50 depth levels. Phytoplankton is represented in GFDL ESM2M by the biogeochemical module “Tracers of Ocean Phytoplankton with Allometric Zooplankton version 2.0” (TOPAZv2; Dunne et al. (2013)), consisting of 30 tracers including three phytoplankton groups (small and large phytoplankton, diazotrophs) and heterotrophic biomass. TOPAZv2 only implicitly simulates zooplankton activity. The GFDL ESM2M does not include a proper land-ice component; land-ice is represented in the land component and exchanged with the ocean model through iceberg production.

The Community Earth System Model version 2 (CESM2, Danabasoglu et al. (2020)) is also a fully coupled ESM. It couples an atmospheric model with comprehensive chemistry to ocean, land, sea-ice, land-ice, river, and ocean wave models. The horizontal resolution of the atmospheric model CAM6 (Danabasoglu et al., 2020) is 0.9° latitude x 1.25° longitude, with 32 vertical levels. The horizontal resolution of the ocean model POP2 (Smith & Gent, 2010) is approximately 1° , with uniform spacing of 1.125° in the zonal direction and significantly varying spacing in the meridional direction, with the finest resolution of about 0.25° at the Equator. The ocean model has 60 vertical levels. The “Marine Biogeochemistry Library” (MARBL; Long et al. (2021)) is the biogeochemical component of CESM2, which simulates marine ecosystem interactions and the coupled cycles of carbon, nitrogen, phosphorus, iron, silicon, and oxygen. This prognostic ocean biogeochemistry model includes a flexible number of phytoplankton types. In the simulations we use in Chapter 4, NPP is produced by three phytoplankton types: small phytoplankton, diatoms (i.e., large phytoplankton) and diazotrophs.

Fig. 2.3 summarizes the main characteristics of the GFDL ESM2M and CESM2 components. More details on their ocean biogeochemistry component will be given in Chapter 4, where we fully describe the models’ representation of phytoplankton production.

2.2.2 Global marine fish models

As was demonstrated in the introduction, compound extreme events constitute hazards potentially driving harmful impacts on marine ecosystems. Understanding the risks posed by extreme events is key to implementing strategies to predict and moderate impacts on marine ecosystems. Risk arises, however, not only from hazards, but from the interactions between hazards, vulnerability and exposure. Marine ecosystems may not be exposed nor vulnerable to compound MHW-NPPX extreme events. In contrast, they may be impacted by other types of extreme events, or by moderate ocean conditions. Global marine fish models are a valuable tool to investigate this complex relationship between ocean conditions and impacts on marine ecosystems (Cheung & Frölicher, 2020; van der Wiel et al., 2020; Cheung et al., 2021). Marine fish models simulate the response of marine species to changes in environmental conditions and/or to fisheries effort. Contrary to observations, which are limited in space and time, fish models can be applied at the global scale and they can sample a greater number of compound events, allowing for a statistically relevant impact assessment. Fish models also allow for distinguishing between environmental and non-environmental drivers (e.g., fisheries) of impacts. In Chapter 5, we use the Dynamic Bioclimatic Envelope Model (DBEM, Cheung et al. (2008, 2009, 2016)) to identify the environmental drivers of extreme impacts on pelagic fish biomass.

The DBEM uses an algorithm by Close et al. (2006) to estimate the distribution of 326

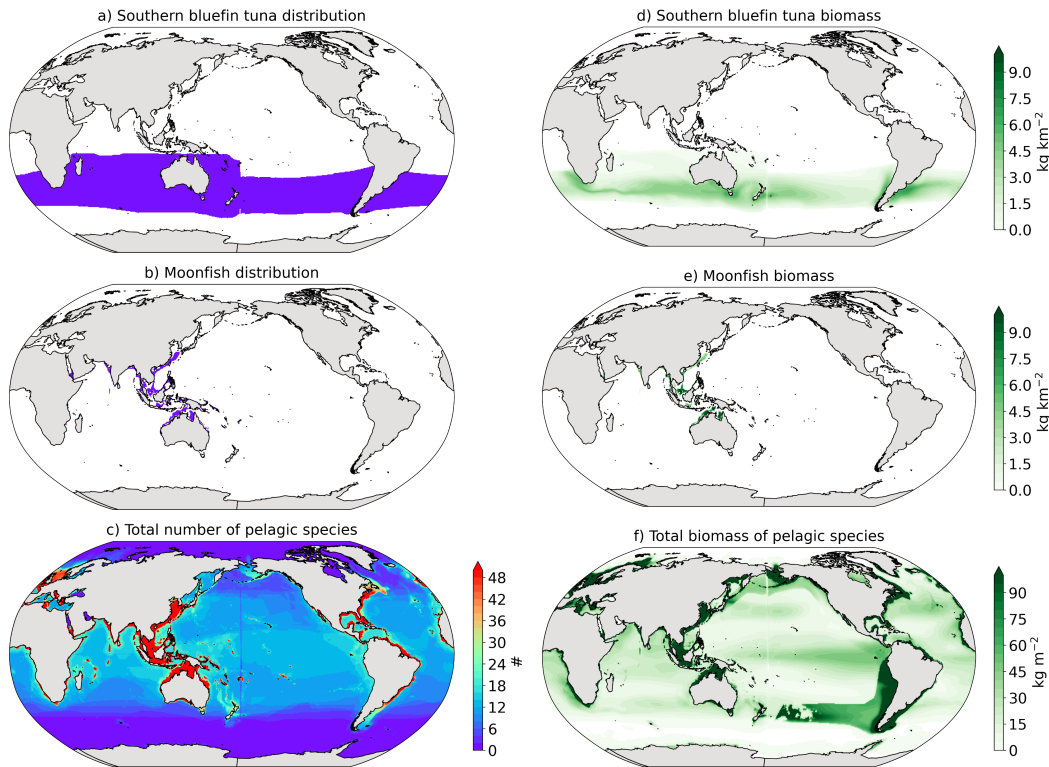


Figure 2.4: Distribution and biomass of pelagic fish species in the DBEM. Distribution of the (a) Southern bluefin tuna and (b) Moonfish. (c) Total number of pelagic fish species. Biomass (kg m^{-2}) of the (d) Southern bluefin tuna, (e) Moonfish, and (f) of all pelagic fish species.

pelagic fish species as well as 602 demersal fish species. This algorithm is based on the species' maximum and minimum depth limits, northern and southern latitudinal range limits, habitat type and known occurrence boundaries. Habitat types include seamounts, estuaries, inshore, offshore, continental shelves, continental slopes and the abyss. These input parameters are mainly provided by two online databases: FishBase (www.fishbase.org) and SeaLifeBase (www.sealifebase.org). The resulting distribution is shown in Fig. 2.4 for two pelagic fish species. The Southern bluefin tuna is distributed between 30°S and 60°S in the Atlantic and Pacific Oceans and between 10°S and 60°S in the Indian Ocean (Fig. 2.4a), whereas the Moonfish is distributed along the coasts of the tropical Indian and western Pacific Oceans (Fig. 2.4b). Overall, many pelagic fish species are distributed along the coasts and few in the high latitudes (Fig. 2.4c). Once the DBEM has determined the species' distribution, it identifies the species' preferred environmental conditions by overlaying environmental data from 1980 to 2000 with maps of the species' distribution.

The DBEM simulates the species' physiological response to changes in environmental conditions using an algorithm derived from von Bertalanffy (1951). Anabolism and catabolism mainly depend on temperature and oxygen levels. They can also depend on acidity when sensitivity to H^+ is activated in the DBEM (note that it is not activated in the simulations we use in Chapter 5). The natural mortality rate of a species is predicted from Pauly (1980). The DBEM then models population growth using a size-based population model. Population growth is limited by the species' carrying capacity, i.e. its maximum relative abundance per grid cell, which depends on habitat suitability. When environmental conditions deviate from a species' environmental preferences, habitat suitability decreases, resulting in a decrease in carrying capacity. An advection-diffusion-reaction model (Cheung et al., 2008) simulates larval dispersal by ocean currents. The DBEM also simulates adult migration, which is assumed to follow the

calculated gradient of habitat suitability. Thus, changes in ocean conditions are translated by the DBEM into changes in species' physiology, population growth and migration, and, hence, relative abundance in each grid cell. Biomass is calculated as the product of the population mean body weight and its relative abundance in each grid cell. For example, the Southern bluefin tuna is most abundant off the eastern coast of South America, where its biomass exceeds 5 kg m^{-2} (Fig. 2.4d).

The DBEM projects annual changes in fish biomass on a $0.5^\circ \times 0.5^\circ$ horizontal grid. Further details on the DBEM and its caveats are presented in Chapter 5, where we use DBEM simulations forced by environmental data from the GFDL ESM2M over 1951-2000. Environmental data include annual mean ocean temperature, oxygen, salinity, NPP, sea-ice extent and advection. Demersal species are forced by bottom ocean variables and pelagic species by surface ocean variables. In Chapter 5, we specifically link surface ocean conditions to their impacts on the total biomass of all pelagic species (Fig. 2.4f).

2.2.3 Large ensemble simulations

Extreme events are, by definition, extremely rare. Yet the large sample size mandated by the study of compound extreme events is even larger than that required for the study of extreme events with single variables (Deser et al., 2020; Burger et al., 2022; Zscheischler & Lehner, 2022). Large ensemble simulations (LES, Frölicher et al. (2009); Deser et al. (2020)), which we use in Chapters 4 and 5, provide the necessary large datasets from which to sample and analyze rare events (e.g., (Poschod et al., 2020; Maher et al., 2021; Bevacqua et al., 2023; Le Grix et al., 2021)).

LES are produced with a single climate model, under a particular historical or future forcing scenario. Different perturbations are applied to the initial conditions of each ensemble member in order to create diverging climate trajectories. For example, we use in subsequent chapters a 30-member LES produced by an Earth system model, the GFDL ESM2M. This LES was started from a quasi-equilibrated 500-year-long preindustrial control simulation, where atmospheric CO_2 concentrations are set to 286 ppm (Burger et al., 2020). We generated an ensemble of 30 members by slightly perturbing the temperature on the order of $10^{-5} \text{ }^\circ\text{C}$ for ten ensemble members at a grid cell at the surface of the Weddell Sea, for ten members at the surface of the North Atlantic, and for ten members in the deep North Pacific (Burger et al., 2022; Le Grix et al., 2022). These 30 simulations were forced with prescribed historical concentrations of atmospheric CO_2 and non- CO_2 radiative-forcing agents from 1861 to 2005, and then by a high-emission no-mitigation scenario (RCP8.5; RCP: Representative Concentration Pathway) from 2006 to 2100 (Riahi et al., 2011) (Fig. 2.5a). Under non-stationary conditions, relatively short time series need to be analyzed to obtain a picture of quasi-stationary conditions. For example, Le Grix et al. (2022) focuses on the recent 1998-2018 period over which observation-derived NPP estimates are available (Fig. 2.5b). In this context, LES allow for sampling enough compound extreme events for their analysis to be statistically relevant, despite short time series.

Single-member simulations from multiple climate models, such as the multi-model ensembles from the Coupled Model Intercomparison Project (CMIP), also offer large sample size. However, they do not allow for distinguishing between internal climate variability, as simulated by a climate model, and structural differences across models (Schlunegger et al., 2020; Bevacqua et al., 2023). In contrast, a single model LES produces multiple simulations based on the same model's physics. These ensemble members evolve from slightly different initial conditions due to internal climate variability only (Maher et al., 2021; Bevacqua et al., 2023). For example, the 30 ensemble members on Fig. 2.5 capture natural variability in annual global mean NPP, as illustrated by the ensemble spread. The larger the LES, the better it captures natural variability. In Chapter 4, we compare the representation of compound MHW-NPPX events in LES produced

by two ESMs: the GFDL ESM2M and the CESM2. Before comparing the two LES, we filtered out natural variability by averaging our results over all ensemble members of each LES (e.g., black line on Fig. 2.5). Thereby, differences between the ensemble mean results of each LES only account for structural differences between GFDL ESM2M and CESM2. This method allows for identifying similarities and divergences in how ESMs simulate compound events.

Finally, LES can also be used as input for impact models, resulting in large ensembles of impact data (e.g., van der Wiel et al. (2020); Chapter 5). This method is referred to as “ensemble climate-impact modelling”. In the context of extreme and compound event research, ensemble climate-impact modelling can follow two approaches. The “forward modelling” approach samples extreme or compound events in the climate data and quantifies their impact as simulated in the output of the impact model. This method requires prior knowledge of potentially harmful extreme or compound events. In Chapter 5, we rather employ a backward “impact-driven” approach (Zscheischler et al., 2014a,b; Ben-Ari et al., 2018; van der Wiel et al., 2020; Vogel et al., 2021)), which starts by sampling rare high-impact events in the large ensembles of impact data and then looks back into the climate data at the environmental conditions potentially causing these high-impact events. This impact-driven approach allows for the discovery of unexpected drivers of extreme impact (van der Wiel et al., 2020). Both approaches are further discussed in Chapter 5.

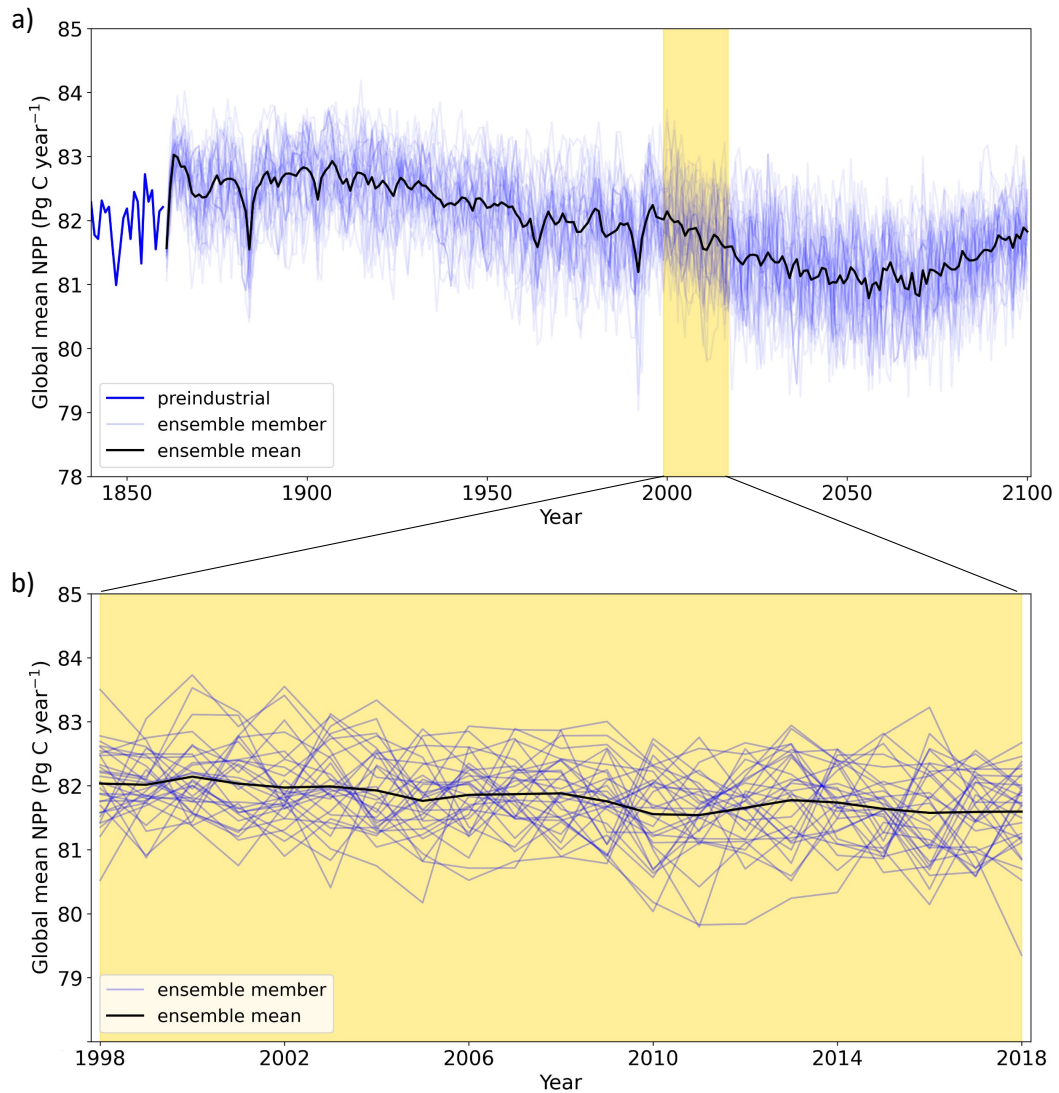


Figure 2.5: Annual mean net primary productivity integrated over the global ocean (Pg C year⁻¹) simulated by a GFDL ESM2M 30-member LES. (a) The LES is started from a preindustrial simulation (dark blue line), which provides the initial conditions. Initial conditions on January 1, 1861 are perturbed so as to generate 30 different simulations, i.e., a 30-member LES (light blue lines), forced by historical CO₂ concentrations from 1861 to 2005 and by RCP8.5 from 2006 to 2100. (b) Focus on the 1998-2018 period under study in Le Grix et al. (2021, 2022). The black line indicates the ensemble mean.

Bibliography

- Anderson, J. L., Balaji, V., Broccoli, A. J., Cooke, W. F., Delworth, T. L., Dixon, K. W., Donner, L. J., Dunne, K. A., Freidenreich, S. M., Garner, S. T., Gudgel, R. G., Gordon, C. T., Held, I. M., Hemler, R. S., Horowitz, L. W., Klein, S. A., Knutson, T. R., Kushner, P. J., Langenhost, A. R., Lau, N.-C., Liang, Z., Malyshev, S. L., Milly, P. C. D., Nath, M. J., Ploshay, J. J., Ramaswamy, V., Schwarzkopf, M. D., Shevliakova, E., Sirutis, J. J., Soden, B. J., Stern, W. F., Thompson, L. A., Wilson, R. J., Wittenberg, A. T., & Wyman, B. L., 2004. The new GFDL global atmosphere and land model AM2-LM2: Evaluation with prescribed SST simulations, *Journal of Climate*, 17(24), 4641–4673.
- Antoine, D. & Morel, A., 1996. Oceanic primary production: 1. Adaptation of a spectral light-photosynthesis model in view of application to satellite chlorophyll observations, *Global Biogeochemical Cycles*, 10(1), 43–55.
- Banzon, V., Smith, T. M., Chin, T. M., Liu, C., & Hankins, W., 2016. A long-term record of blended satellite and in situ sea-surface temperature for climate monitoring and modeling, environmental studies, *Earth System Science Data*, 8(1), 165–176.
- Behrenfeld, M. J. & Falkowski, P. G., 1997. Photosynthetic rates derived from satellite-based chlorophyll concentration, *Limnology, Oceanography*, 42, 1–20.
- Behrenfeld, M. J., Randerson, J. T., McClain, C. R., Feldman, G. C., Los, S. O., Tucker, C. J., Falkowski, P. G., Field, C. B., Frouin, R., Esaias, W. E., Kolber, D. D., & Pollack, N. H., 2001. Biospheric Primary Production During an ENSO Transition, *Science (New York, N.Y.)*, 291(5513), 2594.
- Behrenfeld, M. J., Boss, E., Siegel, D. A., & Shea, D. M., 2005. Carbon-based ocean productivity, phytoplankton physiology from space, *Global Biogeochemical Cycles*, 19(1).
- Ben-Ari, T., Boé, J., Ciais, P., Lecerf, R., Van der Velde, M., & Makowski, D., 2018. Causes and implications of the unforeseen 2016 extreme yield loss in the breadbasket of France, *Nature Communications*, 9(1), 1627.
- Bevacqua, E., Suarez-Gutierrez, L., Jézéquel, A., Lehner, F., Vrac, M., Yiou, P., & Zscheischler, J., 2023. Advancing research on compound weather and climate events via large ensemble model simulations, *Nature Communications*, 14(1), 2145.
- Bidigare, R., Prézélin, B., & Smith, R., 1992. Bio-Optical Models and the Problems of Scaling, pp. 175–212.
- Burger, F. A., John, J. G., & Frölicher, T. L., 2020. Increase in ocean acidity variability, extremes under increasing atmospheric CO₂, *Biogeosciences*, 17(18), 4633–4662.
- Burger, F. A., Terhaar, J., & Frölicher, T. L., 2022. Compound marine heatwaves and ocean acidity extremes, *Nature Communications*, 13(1), 4722.
- Cheung, W., Lam, V., & Pauly, D., 2008. Dynamic bioclimate envelope model to predict climate-induced changes in distribution of marine fishes and invertebrates, *Modelling Present and Climate-shifted Distributions of Marine Fishes and Invertebrates*, 16, 5–50.
- Cheung, W. W., Lam, V. W., Sarmiento, J. L., Kearney, K., Watson, R., & Pauly, D., 2009. Projecting global marine biodiversity impacts under climate change scenarios, *Fish and Fisheries*, 10(3), 235–251.
- Cheung, W. W. L. & Frölicher, T. L., 2020. Marine heatwaves exacerbate climate change impacts for fisheries in the northeast Pacific, *Scientific Reports*, 10(1), 6678.
- Cheung, W. W. L., Jones, M. C., Reygondeau, G., Stock, C. A., Lam, V. W. Y., & Frölicher, T. L., 2016. Structural uncertainty in projecting global fisheries catches under climate change, *Ecological Modelling*, 325, 57–66.
- Cheung, W. W. L., Frölicher, T. L., Lam, V. W. Y., Oyinlola, M. A., Reygondeau, G., Sumaila, U. R., Tai, T. C., Teh, L. C. L., & Wabnitz, C. C. C., 2021. Marine high temperature extremes amplify the impacts of climate change on fish and fisheries, *Science Advances*, 7(40), eabh0895.
- Close, C., Cheung, W., Hodgson, S., Lam, V., Watson, R., & Pauly, D., 2006. *Distribution Ranges of Commercial Fishes and Invertebrates*, vol. 14.
- Danabasoglu, G., Lamarque, J.-F., Bacmeister, J., Bailey, D. A., DuVivier, A. K., Edwards, J., Emmons, L. K., Fasullo, J., Garcia, R., Gettelman, A., Hannay, C., Holland, M. M., Large, W. G., Lauritzen, P. H., Lawrence, D. M., Lenaerts, J. T. M., Lindsay, K., Lipscomb, W. H., Mills, M. J., Neale, R., Oleson, K. W., Otto-Bliesner, B., Phillips, A. S., Sacks, W., Tilmes, S., van Kampenhout, L., Vertenstein, M., Bertini, A., Dennis, J., Deser, C., Fischer, C., Fox-Kemper, B., Kay, J. E., Kinnison, D., Kushner, P. J., Larson, V. E., Long, M. C., Mickelson, S., Moore, J. K., Nienhouse, E., Polvani, L., Rasch, P. J., & Strand, W. G., 2020. The community earth system model version 2 (CESM2), *Journal of Advances in Modeling Earth Systems*, 12(2), e2019MS001916.

- Deser, C., Lehner, F., Rodgers, K., Ault, T., Delworth, T., DiNezio, P., Fiore, A., Frankignoul, C., Fyfe, J., Horton, D., Kay, J., Knutti, R., Lovenduski, N., Marotzke, J., McKinnon, K., Minobe, S., Randerson, J., Screen, J., Simpson, I., & Ting, M., 2020. Insights from Earth system model initial-condition large ensembles and future prospects, *Nature Climate Change*, 10, 277–286.
- Dunne, J. P., John, J. G., Adcroft, A. J., Griffies, S. M., Hallberg, R. W., Shevliakova, E., Stouffer, R. J., Cooke, W., Dunne, K. A., Harrison, M. J., Krasting, J. P., Malyshev, S. L., Milly, P. C. D., Philipps, P. J., Sentman, L. T., Samuels, B. L., Spelman, M. J., Winton, M., Wittenberg, A. T., & Zadeh, N., 2012. GFDL's ESM2 global coupled Climate–Carbon earth system models. Part I: Physical formulation, baseline simulation characteristics, *Journal of Climate*, 25(19), 6646–6665.
- Dunne, J. P., John, J. G., Shevliakova, E., Stouffer, R. J., Krasting, J. P., Malyshev, S. L., Milly, P. C. D., Sentman, L. T., Adcroft, A. J., Cooke, W., Dunne, K. A., Griffies, S. M., Hallberg, R. W., Harrison, M. J., Levy, H., Wittenberg, A. T., Phillips, P. J., & Zadeh, N., 2013. GFDL's ESM2 global coupled Climate–Carbon earth system models. Part II: Carbon system formulation, baseline simulation characteristics, *Journal of Climate*, 26(7), 2247–2267.
- Eppley, R. W., 1972. Temperature, phytoplankton growth in the sea, *Fish. bull.*, 70(4), 1063–1085.
- Falkowski, P. G., 1980. Light-Shade Adaptation in Marine Phytoplankton, in *Primary Productivity in the Sea*, Environmental Science Research, pp. 99–119, ed. Falkowski, P. G., Springer US, Boston, MA.
- Falkowski, P. G., 1994. The role of phytoplankton photosynthesis in global biogeochemical cycles, *Photosynthesis Research*, 39(3), 235–258.
- Falkowski, P. G. & LaRoche, J., 1991. Acclimation to Spectral Irradiance in Algae, *Journal of Phycology*, 27(1), 8–14.
- Frölicher, T. L., Joos, F., Plattner, G.-K., Steinacher, M., & Doney, S. C., 2009. Natural variability and anthropogenic trends in oceanic oxygen in a coupled carbon cycle–climate model ensemble, *Global Biogeochemical Cycles*, 23(1).
- Frölicher, T. L., Fischer, E. M., & Gruber, N., 2018. Marine heatwaves under global warming, *Nature*, 560(7718), 360–364.
- Geider, R., Macintyre, H., & Kana, T., 1997. Dynamic model of phytoplankton growth and acclimation: Responses of the balanced growth rate and the chlorophyll a:carbon ratio to light, nutrient-limitation and temperature, *Marine Ecology Progress Series*, 148, 187–200.
- Geider, R. J., MacIntyre, H. L., & Kana, T. M., 1996. A dynamic model of photoadaptation in phytoplankton, *Limnology and Oceanography*, 41(1), 1–15.
- Gottelman, A., Mills, M. J., Kinnison, D. E., Garcia, R. R., Smith, A. K., Marsh, D. R., Tilmes, S., Vitt, F., Bardeen, C. G., McInerny, J., Liu, H.-L., Solomon, S. C., Polvani, L. M., Emmons, L. K., Lamarque, J.-F., Richter, J. H., Glanville, A. S., Bacmeister, J. T., Phillips, A. S., Neale, R. B., Simpson, I. R., DuVivier, A. K., Hodzic, A., & Randel, W. J., 2019. The Whole Atmosphere Community Climate Model Version 6 (WACCM6), *Journal of Geophysical Research: Atmospheres*, 124(23), 12380–12403.
- Gregg, W. & Rousseaux, C., 2017. NASA Ocean Biogeochemical Model assimilating satellite chlorophyll data global daily VR2017.
- Gregg, W. W., 2008. Assimilation of SeaWiFS ocean chlorophyll data into a three-dimensional global ocean model, *Journal of Marine Systems*, 69(3), 205–225.
- Gregg, W. W. & Casey, N. W., 2007. Sampling biases in MODIS and SeaWiFS ocean chlorophyll data, *Remote Sensing of Environment*, 111(1), 25–35.
- Gregg, W. W. & Rousseaux, C. S., 2014. Decadal trends in global pelagic ocean chlorophyll: A new assessment integrating multiple satellites, in situ data, and models, *Journal of Geophysical Research: Oceans*, 119(9), 5921–5933.
- Griffies, S., 2012. Elements of the modular ocean model (MOM), pp. 1–633.
- Hobday, A. J., Alexander, L. V., Perkins, S. E., Smale, D. A., Straub, S. C., Oliver, E. C., Benthuisen, J. A., Burrows, M. T., Donat, M. G., Feng, M., Holbrook, N. J., Moore, P. J., Scannell, H. A., Sen Gupta, A., & Wernberg, T., 2016. A hierarchical approach to defining marine heatwaves, *Progress in Oceanography*, 141, 227–238.

- Hu, C., Lee, Z., & Franz, B., 2012. Chlorophyll algorithms for oligotrophic oceans: A novel approach based on three-band reflectance difference, *Journal of Geophysical Research: Oceans*, 117(C1).
- Hu, C., Feng, L., Lee, Z., Franz, B. A., Bailey, S. W., Werdell, P. J., & Proctor, C. W., 2019. Improving Satellite Global Chlorophyll a Data Products Through Algorithm Refinement and Data Recovery, *Journal of Geophysical Research: Oceans*, 124(3), 1524–1543.
- Huang, B., C. Liu, V. B., Freeman, E., Graham, G., W. Hankins, T. S., & Zhang, H.-M., 2020. Improvements of the daily optimum sea surface temperature (DOISST) - version 2.1.
- Hunke, E., Lipscomb, W., Jones, P., Turner, A., Jeffery, N., & Elliott, S., 2017. CICE, The Los Alamos Sea Ice Model, Tech. Rep. CICE; 005315WKSTN00, Los Alamos National Lab. (LANL), Los Alamos, NM (United States).
- Jenkins, W. J. & Goldman, J. C., 1985. Seasonal oxygen cycling and primary production in the Sargasso Sea, *Journal of Marine Research*, 43(2), 465–491.
- Laufkötter, C., Zscheischler, J., & Frölicher, T. L., 2020. High-impact marine heatwaves attributable to human-induced global warming, *Science (New York, N.Y.)*, 369(6511), 1621–1625.
- Lawrence, D. M., Fisher, R. A., Koven, C. D., Oleson, K. W., Swenson, S. C., Bonan, G., Collier, N., Ghimire, B., van Kampenhout, L., Kennedy, D., Kluzek, E., Lawrence, P. J., Li, F., Li, H., Lombardozzi, D., Riley, W. J., Sacks, W. J., Shi, M., Vertenstein, M., Wieder, W. R., Xu, C., Ali, A. A., Badger, A. M., Bisht, G., van den Broeke, M., Brunke, M. A., Burns, S. P., Buzan, J., Clark, M., Craig, A., Dahlin, K., Drewniak, B., Fisher, J. B., Flanner, M., Fox, A. M., Gentine, P., Hoffman, F., Keppel-Aleks, G., Knox, R., Kumar, S., Lenaerts, J., Leung, L. R., Lipscomb, W. H., Lu, Y., Pandey, A., Pelletier, J. D., Perket, J., Randerson, J. T., Ricciuto, D. M., Sanderson, B. M., Slater, A., Subin, Z. M., Tang, J., Thomas, R. Q., Val Martin, M., & Zeng, X., 2019. The Community Land Model Version 5: Description of New Features, Benchmarking, and Impact of Forcing Uncertainty, *Journal of Advances in Modeling Earth Systems*, 11(12), 4245–4287.
- Le Grix, N., Zscheischler, J., Laufkötter, C., Rousseaux, C. S., & Frölicher, T. L., 2021. Compound high-temperature and low-chlorophyll extremes in the ocean over the satellite period, *Biogeosciences*, 18(6), 2119–2137.
- Le Grix, N., Zscheischler, J., Rodgers, K. B., Yamaguchi, R., & Frölicher, T. L., 2022. Hotspots and drivers of compound marine heatwaves and low net primary production extremes, *Biogeosciences*, 19(24), 5807–5835.
- Li, H., Wigmosta, M. S., Wu, H., Huang, M., Ke, Y., Coleman, A. M., & Leung, L. R., 2013. A Physically Based Runoff Routing Model for Land Surface and Earth System Models, *Journal of Hydrometeorology*, 14(3), 808–828.
- Lin, S.-J. & Rood, R. B., 1997. An explicit flux-form semi-lagrangian shallow-water model on the sphere, *Quarterly Journal of the Royal Meteorological Society*, 123(544), 2477–2498.
- Lipscomb, W. H., Price, S. F., Hoffman, M. J., Leguy, G. R., Bennett, A. R., Bradley, S. L., Evans, K. J., Fyke, J. G., Kennedy, J. H., Perego, M., Ranken, D. M., Sacks, W. J., Salinger, A. G., Vargo, L. J., & Worley, P. H., 2019. Description and evaluation of the Community Ice Sheet Model (CISM) v2.1, *Geoscientific Model Development*, 12(1), 387–424.
- Long, M. C., Moore, J. K., Lindsay, K., Levy, M., Doney, S. C., Luo, J. Y., Krumhardt, K. M., Letscher, R. T., Grover, M., & Sylvester, Z. T., 2021. Simulations with the marine biogeochemistry library (MARBL), *Journal of Advances in Modeling Earth Systems*, 13(12), e2021MS002647.
- MacIntyre, H. L., Kana, T. M., Anning, T., & Geider, R. J., 2002. Photoacclimation of Photosynthesis Irradiance Response Curves and Photosynthetic Pigments in Microalgae and Cyanobacteria, *Journal of Phycology*, 38(1), 17–38.
- Maher, N., Milinski, S., & Ludwig, R., 2021. Large ensemble climate model simulations: Introduction, overview, and future prospects for utilising multiple types of large ensemble, *Earth System Dynamics*, 12(2), 401–418.
- Martin, T. & Adcroft, A., 2010. Parameterizing the fresh-water flux from land ice to ocean with interactive icebergs in a coupled climate model, *Ocean Modelling*, 34(3), 111–124.
- Morel, A. & Berthon, J.-F., 1989. Surface pigments, algal biomass profiles, and potential production of the euphotic layer: Relationships reinvestigated in view of remote-sensing applications, *Limnology and Oceanography*, 34(8), 1545–1562.

- Nielsen, E. S., 1952. The Use of Radio-active Carbon (C14) for Measuring Organic Production in the Sea, *ICES Journal of Marine Science*, 18(2), 117–140.
- Oliver, E. C. J., Donat, M. G., Burrows, M. T., Moore, P. J., Smale, D. A., Alexander, L. V., Benthuyssen, J. A., Feng, M., Sen Gupta, A., Hobday, A. J., Holbrook, N. J., Perkins-Kirkpatrick, S. E., Scannell, H. A., Straub, S. C., & Wernberg, T., 2018. Longer and more frequent marine heatwaves over the past century, *Nature Communications*, 9(1), 1324.
- O'Reilly, J. E. & Werdell, P. J., 2019. Chlorophyll algorithms for ocean color sensors - oc4, oc5 oc6, *Remote Sensing of Environment*, 229, 32–47.
- O'Reilly, J. E., Maritorea, S., Mitchell, B. G., Siegel, D. A., Carder, K. L., Garver, S. A., Kahru, M., & McClain, C., 1998. Ocean color chlorophyll algorithms for SeaWiFS, *Journal of Geophysical Research: Oceans*, 103(C11), 24937–24953.
- Pauly, D., 1980. On the interrelationships between natural mortality, growth parameters, and mean environmental temperature in 175 fish stocks, *ICES Journal of Marine Science*, 39(2), 175–192.
- Poschod, B., Zscheischler, J., Sillmann, J., Wood, R. R., & Ludwig, R., 2020. Climate change effects on hydrometeorological compound events over southern Norway, *Weather and Climate Extremes*, 28, 100253.
- Reynolds, R. W., Smith, T. M., Liu, C., Chelton, D. B., Casey, K. S., & Schlax, M. G., 2007. Daily high-resolution-blended analyses for sea surface temperature, *Journal of Climate*, 20(22), 5473–5496.
- Riahi, K., Rao, S., Krey, V., Cho, C., Chirkov, V., Fischer, G., Kindermann, G., Nakicenovic, N., & Rafaj, P., 2011. RCP 8.5—A scenario of comparatively high greenhouse gas emissions, *Climatic Change*, 109, 33–57.
- Rousseaux, C. S. & Gregg, W. W., 2014. Interannual variation in phytoplankton primary production at A global scale, *Remote Sensing*, 6(1), 1–19.
- Schlegel, R. W., Oliver, E. C. J., Hobday, A. J., & Smit, A. J., 2019. Detecting Marine Heatwaves With Sub-Optimal Data, *Frontiers in Marine Science*, 6.
- Schlunegger, S., Rodgers, K. B., Sarmiento, J. L., Ilyina, T., Dunne, J. P., Takano, Y., Christian, J. R., Long, M. C., Frölicher, T. L., & Slater, R., 2020. Time of emergence and large ensemble intercomparison for ocean biogeochemical trends, *Global biogeochemical cycles*, 34(8), e2019GB006453.
- Shevliakova, E., Pacala, S. W., Malyshev, S., Hurtt, G. C., Milly, P. C. D., Caspersen, J. P., Sentman, L. T., Fisk, J. P., Wirth, C., & Crevoisier, C., 2009. Carbon cycling under 300 years of land use change: Importance of the secondary vegetation sink, *Global Biogeochemical Cycles*, 23(2).
- Silsbe, G. M., Behrenfeld, M. J., Halsey, K. H., Milligan, A. J., & Westberry, T. K., 2016. The CAFE model: A net production model for global ocean phytoplankton, *Global Biogeochemical Cycles*, 30(12), 1756–1777.
- Smith, R. & Gent, P., 2010. The parallel ocean program (POP) reference manual, *Los Alamos Unclassified Report LA-UR-02-2484*.
- Tolman, H., 2009. User manual and system documentation of WAVEWATCH III version 3.14, *Analysis*, 166.
- van der Wiel, K., Selten, F. M., Bintanja, R., Blackport, R., & Screen, J. A., 2020. Ensemble climate-impact modelling: Extreme impacts from moderate meteorological conditions, *Environmental Research Letters*, 15(3), 034050.
- Vogel, J., Rivoire, P., Deidda, C., Rahimi, L., Sauter, C. A., Tschumi, E., van der Wiel, K., Zhang, T., & Zscheischler, J., 2021. Identifying meteorological drivers of extreme impacts: An application to simulated crop yields, *Earth System Dynamics*, 12(1), 151–172.
- von Bertalanffy, L., 1951. *Theoretische Biologie: Stoffwechsel, Wachstum. Zweiter Band*, A. Francke.
- Wang, M. & Son, S., 2016. VIIRS-derived chlorophyll-a using the ocean color index method, *Remote Sensing of Environment*, 182, 141–149.
- Westberry, T., Behrenfeld, M. J., Siegel, D. A., & Boss, E., 2008. Carbon-based primary productivity modeling with vertically resolved photoacclimation, *Global Biogeochemical Cycles*, 22(2).
- Williams, P.J.L. & Robertson, J.I., 1989. A serious inhibition problem from a niskin sampler during plankton productivity studies, *Limnology and Oceanography*, 34(7), 1300–1305.

- Winton, M., 2000. A Reformulated Three-Layer Sea Ice Model, *Journal of Atmospheric and Oceanic Technology*, 17(4), 525–531.
- Zscheischler, J. & Lehner, F., 2022. Attributing compound events to anthropogenic climate change, *Bulletin of the American Meteorological Society*, 103(3), E936 – E953.
- Zscheischler, J., Michalak, A. M., Schwalm, C., Mahecha, M. D., Huntzinger, D. N., Reichstein, M., Berthier, G., Ciais, P., Cook, R. B., El-Masri, B., Huang, M., Ito, A., Jain, A., King, A., Lei, H., Lu, C., Mao, J., Peng, S., Poulter, B., Ricciuto, D., Shi, X., Tao, B., Tian, H., Viovy, N., Wang, W., Wei, Y., Yang, J., & Zeng, N., 2014a. Impact of large-scale climate extremes on biospheric carbon fluxes: An intercomparison based on MsTMIP data, *Global Biogeochemical Cycles*, 28(6), 585–600.
- Zscheischler, J., Reichstein, M., von Buttlar, J., Mu, M., Randerson, J. T., & Mahecha, M. D., 2014b. Carbon cycle extremes during the 21st century in CMIP5 models: Future evolution and attribution to climatic drivers, *Geophysical Research Letters*, 41(24), 8853–8861.

Chapter 3

Compound high temperature and low chlorophyll extremes in the ocean over the satellite period

Natacha Le Grix, Jakob Zscheischler, Charlotte Laufkötter, Cecile S. Rousseaux, and Thomas L. Frölicher

Published in *Biogeosciences*, Volume 18, 2119-2137, 2021. This chapter includes an Appendix and Bibliography

Biogeosciences, 18, 2119–2137, 2021
https://doi.org/10.5194/bg-18-2119-2021
© Author(s) 2021. This work is distributed under
the Creative Commons Attribution 4.0 License.



Compound high-temperature and low-chlorophyll extremes in the ocean over the satellite period

Natacha Le Grix^{1,2}, Jakob Zscheischler^{1,2,3}, Charlotte Laufkötter^{1,2}, Cecile S. Rousseaux^{4,5}, and Thomas L. Frölicher^{1,2}

¹Climate and Environmental Physics, Physics Institute, University of Bern, Bern, Switzerland

²Oeschger Centre for Climate Change Research, University of Bern, Bern, Switzerland

³Department of Computational Hydrosystems, Helmholtz Centre for Environmental Research – UFZ, Leipzig, Germany

⁴Global Modeling and Assimilation Office, NASA Goddard Space Flight Center, Greenbelt, USA

⁵Universities Space Research Association, Columbia, USA

Correspondence: Natacha Le Grix (natacha.legrix@climate.unibe.ch)

Received: 6 November 2020 – Discussion started: 14 November 2020

Revised: 25 January 2021 – Accepted: 9 February 2021 – Published: 24 March 2021

Abstract. Extreme events in the ocean severely impact marine organisms and ecosystems. Of particular concern are compound events, i.e., when conditions are extreme for multiple potential ocean ecosystem stressors such as temperature and chlorophyll. Yet, little is known about the occurrence, intensity, and duration of such compound high-temperature (a.k.a. marine heatwaves – MHWs) and low-chlorophyll (LChl) extreme events, whether their distributions have changed in the past decades, and what the potential drivers are. Here we use satellite-based sea surface temperature and chlorophyll concentration estimates to provide a first assessment of such compound extreme events. We reveal hotspots of compound MHW and LChl events in the equatorial Pacific, along the boundaries of the subtropical gyres, in the northern Indian Ocean, and around Antarctica. In these regions, compound events that typically last 1 week occur 3 to 7 times more often than expected under the assumption of independence between MHWs and LChl events. The occurrence of compound MHW and LChl events varies on seasonal to interannual timescales. At the seasonal timescale, most compound events occur in summer in both hemispheres. At the interannual timescale, the frequency of compound MHW and LChl events is strongly modulated by large-scale modes of natural climate variability such as the El Niño–Southern Oscillation, whose positive phase is associated with increased compound event occurrence in the eastern equatorial Pacific and in the Indian Ocean by a factor of up to 4. Our results provide a first understanding of

where, when, and why compound MHW and LChl events occur. Further studies are needed to identify the exact physical and biological drivers of these potentially harmful events in the ocean and their evolution under global warming.

1 Introduction

Over the last few decades, extreme events in the ocean, such as marine heatwaves (MHWs), have occurred in all ocean basins (Fig. 1a) (Frölicher and Laufkötter, 2018; Hobday et al., 2016; Laufkötter et al., 2020). Alongside the long-term warming of the global ocean (Cheng et al., 2017), the number of MHW days has doubled between 1982 and 2016 (Frölicher et al., 2018; Oliver et al., 2018) and is projected to increase strongly under continued global warming (Frölicher et al., 2018). MHWs have already negatively impacted many key habitats (Smale et al., 2019), including seagrass meadows (Marba and Duarte, 2010; Thomson et al., 2015), kelp forests (Wernberg et al., 2013; Smale et al., 2019), and coral reefs (Hughes et al., 2018b). Changes in extreme conditions are also expected in the concentration of phytoplankton, which regulate key biogeochemical processes such as ocean carbon uptake and export and form the base of the aquatic food web, but so far less is known about extremes in the abundance of these species.

An emerging concern is compound events, i.e., situations where more than one ocean ecosystem driver is outside the

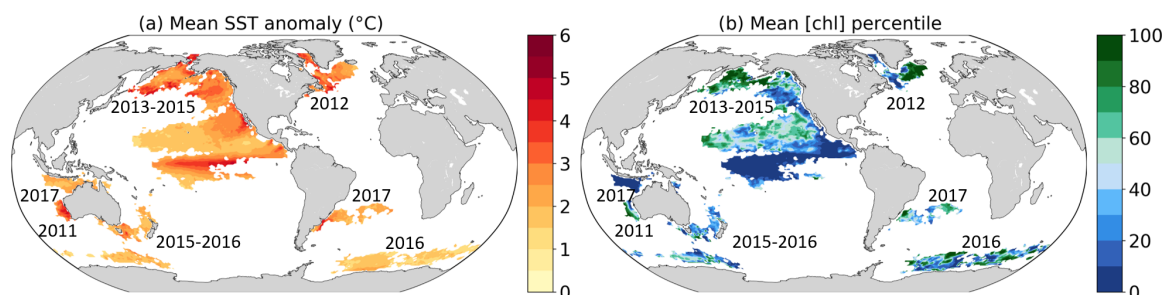


Figure 1. Recent (a) prominent large-scale marine heatwaves (MHWs) for which impacts have been documented and (b) associated changes in surface chlorophyll concentrations ([chl]). We use sea surface temperature (SST) and [chl] deseasonalized anomalies. MHWs are defined when SST anomalies exceed their percentile 99.5 locally, and numbers indicate the years of the MHW occurrences. (a) SST anomaly averaged over the MHW duration. (b) Percentile associated with the mean [chl] anomaly averaged over the duration of the MHW, compared to the local empirical distribution of [chl] daily anomalies from 1998 to 2018. The MHW extent is taken from Laufkötter et al. (2020) and corresponds to a spatiotemporally continuous area where each grid cell exhibits daily temperature anomalies above percentile 99.5.

norm simultaneously, in close spatial proximity or temporal succession (Leonard et al., 2014; Zscheischler et al., 2018). Major climate-related disasters often result from the compounding effect of multiple drivers and/or hazards. Such situations might arise, for example, when the drivers of one hazard (e.g., elevated temperature causing a marine heatwave) also cause other relevant changes, such as decreased nutrient concentrations caused by increased thermal stratification and reduced supply of nutrient-rich subsurface water to the surface. Compound events can severely impact marine ecosystems, especially when the hazards act synergistically. While MHWs may enhance mortality of some marine organisms, low productivity also threatens marine ecosystems that rely on phytoplankton as the base of their food web (Cavole et al., 2016). In recent years, interest in compound events has evolved into a rapidly growing research field (Zscheischler et al., 2020). However, most studies so far focus on compound events over land (Ridder et al., 2020). Few have addressed compound events in the ocean (Collins et al., 2019).

This lack of knowledge is of concern as MHWs often coincide with large anomalies in surface chlorophyll concentrations (Fig. 1). One of the most prominent examples of a compound event is “the Blob” in the northeast Pacific. Between 2013 and 2015, the northeast Pacific experienced the most intense and longest-lasting MHW ever recorded, with maximum surface temperature anomalies of more than 5 °C (Fig. 1a) lasting for more than 350 d (Di Lorenzo and Mantua, 2016; Laufkötter et al., 2020). At its initiation, the MHW coincided with large negative anomalies in phytoplankton production along the California Current ($\sim 28\text{--}48^\circ\text{N}$) because of below-average strength in coastal upwelling, resulting in low chlorophyll levels throughout spring and summer (Leising et al., 2015). Later in 2014–2015, high temperature and low chlorophyll concentrations were observed further south in the eastern equatorial Pacific. The compound high-temperature and low-chlorophyll and low-nutrient event had severe consequences for marine life (Cavole et al.,

2016). Ecosystem impacts included low primary productivity (Whitney, 2015), extreme mortality and reproductive failure of sea birds (Jones et al., 2018; Piatt et al., 2020), mass strandings of whales in the western Gulf of Alaska and of sea lions in California, and changes in species distribution in favor of warm-water species (Cavole et al., 2016; Cheung and Frölicher, 2020). These changes in biomass and species distribution further impacted socio-economically important fisheries (Cheung and Frölicher, 2020). Another example of a compound high-temperature and low-chlorophyll event is the southwestern Atlantic 2013/14 MHW (not shown in Fig. 1). This unprecedented MHW was associated with very low surface chlorophyll *a* levels (Rodrigues et al., 2019). However, not all MHWs coincided with low-chlorophyll events in the past (Fig. 1). During the Blob, for example, chlorophyll anomalies were positive in some locations (e.g., Bering Sea), exceeding on average the 80th percentile of their distribution, whereas along the northwestern coast of North America and in the equatorial Pacific, chlorophyll anomalies fell on average below their 5th percentile.

Previous studies have identified drivers of MHWs (e.g., Holbrook et al., 2019) and of chlorophyll variability (Boyce et al., 2010; McClain, 2009; Wilson and Adamec, 2002) separately, but it is currently unknown what the underlying drivers of compound MHW and low-chlorophyll (LChl) events are (Frölicher, 2019). Global warming is the dominant driver of long-term changes in MHW frequency (Frölicher et al., 2018; Oliver, 2019). Yet, natural variability of the climate system also creates situations that favor the occurrence of extreme events. Recent MHWs have been linked to various large-scale modes of climate variability (Holbrook et al., 2019). These climate modes favor or suppress the occurrence of MHWs by modulating the local conditions. Bond et al. (2015) attributed the development of the Blob to an unusually strong and persistent weather pattern, featuring sea level pressure much higher than normal over the Gulf of Alaska. These sea level pres-

sure anomalies resulted from the strengthened Victoria Mode of variability in the northeast Pacific, which was forced by the atmosphere through the North Pacific Oscillation (Tseng et al., 2017). Reduced circulation in the North Pacific Subtropical Gyre suppressed the heat loss from the ocean to the atmosphere and caused relatively weak cold advection in the upper ocean (Leising et al., 2015). The resulting warming in the northeast Pacific is thought to have acted as a precursor to the development of the 2015/16 El Niño (Di Lorenzo and Mantua, 2016), which further enhanced the Blob (Tseng et al., 2017). Oceanic and atmospheric teleconnections associated with large-scale climate modes can also modulate the occurrence of MHWs in distant regions. For example, the extraordinary 2010–2011 La Niña remotely strengthened and shifted the poleward-flowing Leeuwin Current along the western coast of Australia to the south. As a result the southwestern coast of Australia experienced anomalous warm waters in 2011 (Feng et al., 2013). Climate variability may also cause low-productivity events, since large-scale climate modes affect nutrient concentrations and primary production of phytoplankton (Behrenfeld et al., 2001, 2006; Racault et al., 2017; Rousseaux and Gregg, 2014) at the surface via, for example, changes in mixed-layer depth and upwelling strength. Therefore, climate modes are potentially modulating the occurrence of compound MHW and LChl events and may be used to predict such events.

In this study, we provide a first characterization of compound MHW and LChl events using satellite-based observations. We first quantify the intensity and duration over time and space of MHWs and LChl events separately, before identifying hotspots and characterizing the temporal distribution of compound MHW and LChl events over the past decades. Finally, we investigate the modulation of their frequency by large-scale modes of climate variability.

2 Methods

2.1 Observation-based data

To identify and characterize compound MHW and LChl events, we use satellite-derived sea surface temperature (SST) and chlorophyll concentration data. For SST, we use NOAA's daily Optimum Interpolation SST (OISST) analysis product with a spatial grid resolution of 0.25° (Banzon et al., 2016; Reynolds et al., 2007). This dataset provides a daily global record of surface ocean temperature observations obtained from satellites, ships, buoys, and Argo floats on a regular grid. Its main input is infrared satellite data from the Advanced Very High Resolution Radiometer with temporal coverage beginning in late 1981 to the present. Any large-scale satellite biases relative to in situ data from ships and buoys are corrected, and any gaps are filled in by interpolation. For chlorophyll, satellite data derived from ocean color cannot be used because the coverage is too poor at the daily

scale, notably due to clouds. Instead, we use outputs from the NASA Ocean Biogeochemical Model (NOBM.R2020.1 version) (Gregg and Rousseaux, 2017), which provides assimilated daily data for mean chlorophyll concentration within the mixed layer. This comprehensive ocean biogeochemical model, coupled to a global ocean circulation and radiative model (Gregg and Casey, 2007), assimilates satellite ocean chlorophyll data from the Sea-viewing Wide Field-of-view Sensor (SeaWiFs), the Moderate Resolution Imaging Spectroradiometer (MODIS) Aqua, and the Visible Infrared Imaging Radiometer Suite (VIIRS). The model spans the domain from 84° S to 72° N in increments of 1.25° longitude by $2/3^\circ$ latitude, including only open-ocean areas where bottom depth exceeds 200 m. Temporal coverage extends from 1998 to 2018. NOBM takes care of differences between sensors and also provides complete coverage at a daily resolution, without the gaps that are intrinsic to satellite data due to clouds and high solar zenith angles. Its chlorophyll outputs have been validated against the NASA satellite products (Gregg and Rousseaux, 2014). The annual median chlorophyll is similar when computed using the satellite products or the NOBM products, although in the high latitudes, areas of high chlorophyll in the satellite products are reduced in the assimilation data. According to Gregg and Rousseaux (2014), these are artifacts of satellites sampling only the warmer, more sunlit months while the assimilation model produces information for all days of the year. In the North Indian Ocean, high chlorophyll due to seasonal aerosol obscuration in the satellite product is also reduced when assimilated. Trends in global mean chlorophyll are similar from 1998 to 2012 in both the satellite and assimilation products.

Prior to any analysis, the SST dataset is regridded onto the lower-resolution chlorophyll dataset for the period from 1998 until 2018 so that the length of the SST dataset corresponds to the length of the chlorophyll dataset. As chlorophyll concentration is close to or equal to zero during winter in the polar regions when solar radiation is near zero, we removed all days during which a particular grid cell receives no solar radiation, thereby focusing on the growing season. The daily shortwave radiation data were obtained from the Modern-Era Retrospective analysis for Research and Applications version 2 (Gelaro et al., 2017).

2.2 Analysis

2.2.1 Definition of extreme and compound extreme events

We first computed anomalies by subtracting the mean daily seasonal cycle from the SST and chlorophyll data. MHWs and LChl events may therefore occur in any season, if solar radiation is non-zero. The mean seasonal cycle has been smoothed using a 30 d running mean to remove noise on a daily scale associated with the 21-year data record. We also

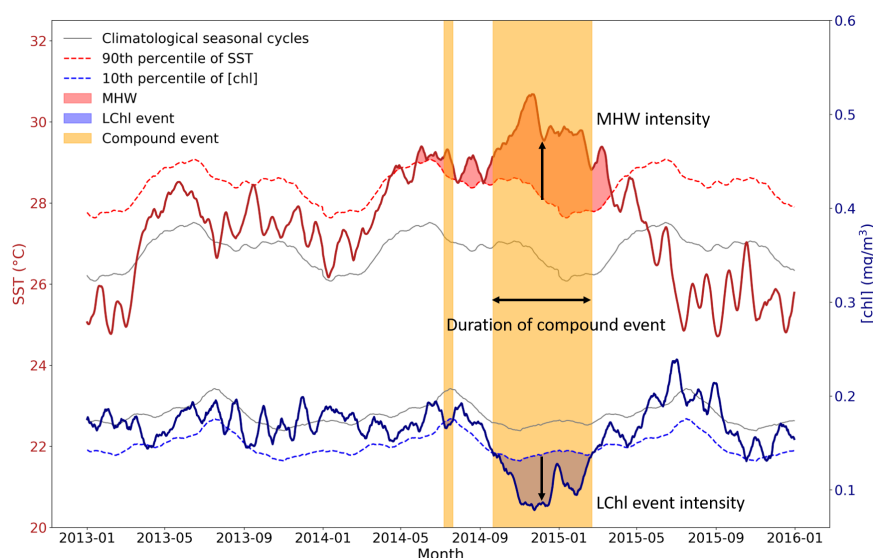


Figure 2. Schematic figure illustrating the definition of MHWs, LChl events, and compound MHW and LChl events. Time series of SST and chlorophyll concentration are extracted from 2013 to 2015 at 0° N and 155° E and smoothed with a 14 d running mean for illustrative purposes. A MHW occurs (red shaded area) when the SST (bold red line) exceeds its 90th percentile (dashed red line). A LChl event (blue shaded area) occurs when the surface chlorophyll concentration (bold blue line) is below its 10th percentile (dashed blue line). Yellow bands indicate the occurrence of compound MHW and LChl events.

used 7 and 14 d running means for smoothing, but the main results are not sensitive to this choice.

Figure 2 illustrates our definition of univariate and compound extreme events. Time series of SST and chlorophyll concentration are smoothed with a 14 d running mean to obtain a better visualization of extreme events; for comparison, Fig. A1 shows results with no smoothing. We define MHWs (i.e., hot temperature extremes) as events when the daily SST anomaly exceeds its local 90th percentile (Fig. A2a). Following this definition, MHWs can be as short as 1 d and extend over only one grid cell. Respectively, we define low-chlorophyll (LChl) events as days when the anomaly in the chlorophyll concentration is below its local 10th percentile (Fig. A2b). Here, we do not apply a duration threshold as has been done for example in Hobday et al. (2016) for MHWs. Duration thresholds are rather arbitrary as it is unknown which thresholds are most impact-relevant in particular for LChl events and compound events. Our definition without a duration threshold is consistent with the usage in the IPCC SROCC report (Collins et al., 2019). We have chosen to focus here on rather moderate extremes, as defined with the 90th and the 10th percentiles, because they provide sufficiently large sample sizes for robust statistical assessments over the current chlorophyll record extending from 1998 to 2018.

Compound MHW and LChl events are defined when both extreme hot temperatures and low-chlorophyll conditions co-occur in time and space (yellow bands in Fig. 2). For simplicity we refer to them as “compound events”. If

MHWs and LChl events were independent, we would expect compound events to occur at a frequency (f) equal to the product of their univariate frequencies at each grid cell, that is $10\% \cdot 10\% = 1\%$. The likelihood multiplication factor (LMF) of compound events is defined as the ratio of the observed frequency of events to their expected frequency under the assumption of independence (Zscheischler and Seneviratne, 2017).

$$\begin{aligned} \text{LMF} &= \frac{f(\text{Compound MHW and LChl event})}{f(\text{MHW}) \cdot f(\text{LChl event})} \\ &= \frac{\text{Compound MHW and LChl event frequency (\%)}}{1\%} \quad (1) \end{aligned}$$

Since the latter equals 1% in our case, compound event frequency (in percent) and the LMF are equivalent. Thus, compound events occur particularly often at grid cells where their frequency exceeds 1% of all days.

2.2.2 Metrics for characterizing univariate extremes and compound extremes

We compute the duration, intensity, and frequency of extreme events. The duration of a univariate and compound extreme event corresponds to the number of days the event lasted without interruption (Fig. 2). Figure A3 shows that the duration of MHWs, LChl events, and compound events is exponentially distributed. For this reason, we present the 90th percentile of the duration distribution in maps. The intensity of a MHW is defined as its mean SST exceedance anomaly over

Table 1. Large-scale modes of climate variability used in this study and which potentially modulate the occurrence of compound marine heatwave and low-chlorophyll events.

Climate mode	Climate mode index	Acronym
El Niño–Southern Oscillation	Niño-3.4 index	ENSO
El Niño Modoki	El Niño Modoki Index	EMI
Pacific Decadal Oscillation	Pacific Decadal Oscillation index	PDO
North Pacific Gyre Oscillation	North Pacific Gyre Oscillation index	NPGO
Indian Ocean Dipole	Dipole Mode Index	DMI
North Atlantic Oscillation	North Atlantic Oscillation Index	NAO
Antarctic Oscillation	Antarctic Oscillation index	AAO

the duration of the event (Fig. 2). It corresponds to the difference between the mean SST anomaly over all MHW days of an event and the 90th percentile of SST anomalies. The intensity of a LChl event is defined as its mean chlorophyll exceedance anomaly, which corresponds to the difference between the mean chlorophyll anomaly over the duration of the event and the 10th percentile of chlorophyll anomalies. The intensity of a compound event is characterized by both the mean SST exceedance anomaly and the mean chlorophyll exceedance anomaly over the duration of the event in a bivariate plane. Finally, the frequency of an event is the number of event days over the total number of days, expressed as a percentage.

2.2.3 Attributing extreme and compound extreme occurrence to large-scale modes of climate variability

Large-scale modes of interannual to decadal climate variability may strongly modify the occurrence of MHWs, LChl events, and compound events. Holbrook et al. (2019) established an analytical framework to identify regions where statistically significant relationships exist between surface MHW occurrence and large-scale climate modes. Following the approach by Holbrook et al. (2019) for MHWs, we compute the frequency of MHWs, LChl events, and compound events during both positive and negative phases of the most relevant large-scale climate modes. These climate modes are the El Niño–Southern Oscillation (ENSO), the El Niño Modoki, the Pacific Decadal Oscillation (PDO), the North Pacific Gyre Oscillation (NPGO), the Indian Ocean Dipole, the North Atlantic Oscillation (NAO), and the Antarctic Oscillation (AAO) (Table 1). In Appendix B, we briefly describe the individual modes and where we obtained the necessary data. In total we consider the impact of 14 different climate phases (positive and negative phases of seven climate modes) on the frequency of univariate extreme and compound extreme events.

For each climate mode, we define positive, negative, and neutral phases based on their index values. We consider all days associated with the 50% lowest absolute values of the climate index to be in a neutral phase. Days associated with

its most positive or negative values are respectively in a positive or negative phase. To estimate whether a climate mode has a discernible effect on local univariate and compound extreme events, we compare at each grid cell the frequency of extreme event days over the positive and negative phases to their frequency over the neutral phase. To ensure these frequency changes are statistically significant, we shuffle the temporal order of each climate index and recompute the frequency change in extreme event days 1000 times for each grid point. If the observed frequency increase/decrease during a particular climate phase is higher/lower than 95% of the shuffled cases, we consider the association of that climate phase with a change frequency of extreme events significant at that grid point ($\alpha = 0.1$). We then also report significant associations for those climate modes that lead to the largest increase in extreme events for each location.

3 Results

We first assess the intensity and duration of MHWs and low-chlorophyll events separately (Sect. 3.1), before we analyze spatial and temporal distribution of compound extreme events (Sect. 3.2 and 3.3) and their drivers (Sect. 3.4).

3.1 Marine heatwaves and low-chlorophyll events

The strongest MHWs with mean temperatures of up to 2°C above the 90th percentile are observed in high latitudes in regions with high temperature variability (Oliver et al., 2018; Holbrook et al., 2019; Deser et al., 2010), such as the western boundary currents and the Agulhas Current and Return Current, but also in the eastern equatorial Pacific (Fig. 3a). Less intense MHWs (< 0.3°C) occur in the western part of the subtropical gyres, the northern Indian Ocean, and south of 45° S. The mean intensity pattern of low-chlorophyll events broadly resembles the MHW intensity map but with distinct differences (Fig. 3b). The most intense (up to -0.2 mg m^{-3}) LChl events are located at high latitudes, especially in the seasonally varying sea ice region of the Southern Ocean, the North Atlantic, and the North Pacific. LChl events are also intense in the equatorial Ocean, but

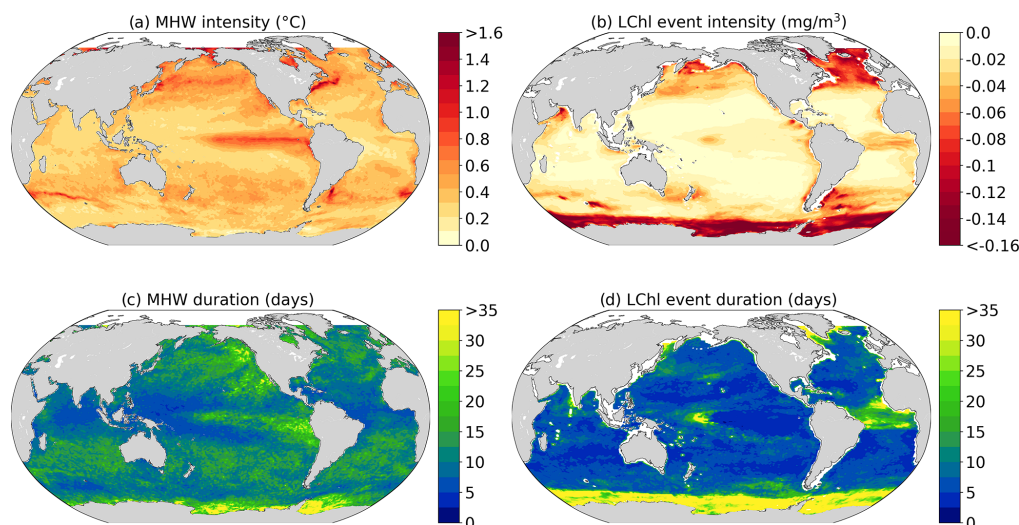


Figure 3. Observed marine heatwave and low-chlorophyll extreme event characteristics averaged over the 1998–2018 period. **(a, b)** Mean intensity of MHWs ($^{\circ}\text{C}$) and LChl events (mg m^{-3}). **(c, d)** The 90th percentile of the duration of MHWs and LChl events in days.

in contrast to MHWs, the mean intensity is not as pronounced in the eastern equatorial Pacific. Less intense chlorophyll extremes ($< -0.02 \text{ mg m}^{-3}$) are generally found in the tropics and mid-latitudes, similar to MHWs.

The spatial distribution of the 90th percentile of MHW and LChl event durations is shown in Fig. 3c and d. Particularly long MHWs ($> 20 \text{ d}$) occur in the eastern equatorial Pacific, where prolonged El Niño conditions may sustain positive SST anomalies for a few months and occasionally for up to 2 years (Fig. 3c). Long MHWs ($> 30 \text{ d}$) are also observed in the seasonally varying sea ice region of the Southern Ocean and the northeastern Pacific. Short MHWs ($< 5 \text{ d}$) are found in the western part of the subtropical gyres, where the intensity of MHWs is also weak. Similar to MHWs, long LChl events are observed in high latitudes, in particular in the Southern Ocean around Antarctica, where 10 % of events last longer than a month. Maximum durations are found in the Weddell Sea, where LChl events last up to 130 d. When excluding the Southern Ocean, MHW and LChl events have rather opposite duration patterns over most of the global ocean. In contrast to MHWs, low-chlorophyll extremes last longest in the equatorial Atlantic and in the center of the equatorial Pacific, where El Niño oscillations may lead to zonal shifts of warm surface waters and high variability in phytoplankton growth conditions (Fig. 3d).

3.2 Compound marine heatwaves and low-chlorophyll events

MHWs and LChl events often occur simultaneously. Indeed, the frequency of compound MHW and LChl events exceeds 1 % in most of the global ocean (over 80 % of the area), indicating that MHWs and LChl co-occur more often than if

variations in SST and chlorophyll anomalies were independent (Fig. 4a). Globally, the average frequency of compound event days is 1.65 %. Compound events are especially frequent ($> 2 \%$ of all days) in the equatorial Pacific, along the boundaries of the subtropical gyres, in the Arabian Sea, and around Antarctica. On the contrary, compound events occur on less than 1 % of days in the North Atlantic and in the North Pacific, in the Indian Ocean south of 15° S , and in the Southern Ocean between 40 and 60° S .

Hotspots of compound MHW and LChl events are typically located in regions where SST and chlorophyll anomalies are strongly negatively correlated (Fig. 4c), indicating that the overall dependence between SST and chlorophyll is not fundamentally different from the dependence in the tails of the distributions. The highest frequencies of compound event days ($> 6 \%$ of all days) occur at grid points for which this correlation coefficient is especially negative ($r < -0.5$; Fig. 4d). The most frequent events ($> 7 \%$ of all days) occur in the center of the equatorial Pacific. Here, the negative correlation between SST and chlorophyll anomalies is much lower than -0.5 (Fig. 4c). Grid points with positive correlations between SST and chlorophyll anomalies ($r > 0.2$) tend to have low frequencies of compound event days ($< 1 \%$ of all days). Overall, there is a strong relationship ($r = -0.74$) between the occurrence of compound events and the correlation coefficient between SST and chlorophyll anomalies (Fig. 4d).

The frequency pattern of compound MHW and LChl events shown in Fig. 4a also resembles to some extent the observed temperature and chlorophyll concentrations during the most recent prominent large-scale marine heatwaves (Fig. 1). Chlorophyll concentrations were exceptionally low in the eastern equatorial Pacific during the 2013–2015 north-

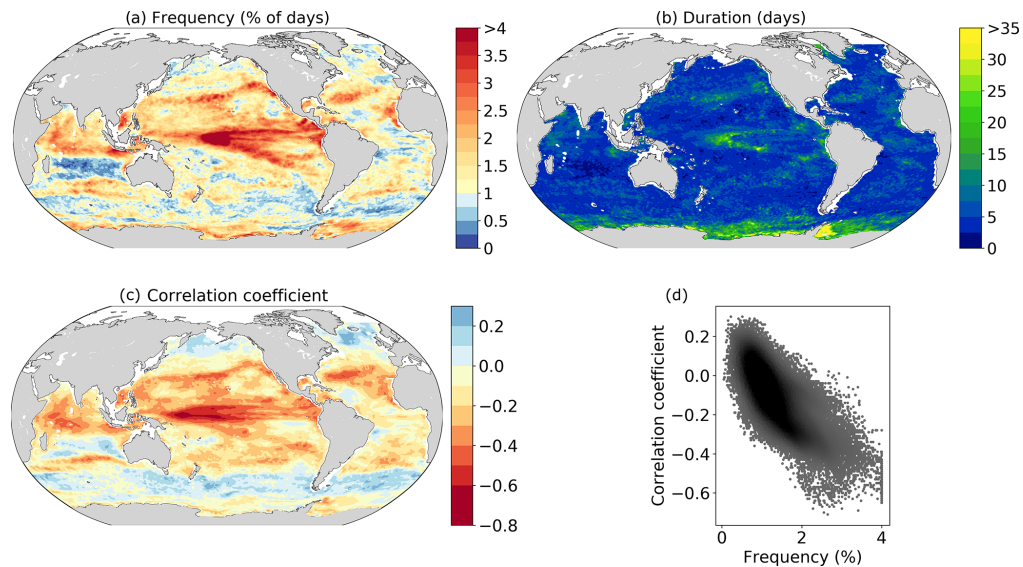


Figure 4. Occurrence of compound marine heatwave and low-chlorophyll events and its relationship to the correlation coefficient between SST and chlorophyll anomalies over the 1998–2018 period. **(a)** Frequency of compound MHW and LChl event days (%). Here, the frequency is equivalent to the likelihood multiplication factor. **(b)** The 90th percentile of the duration of compound events. **(c)** Linear correlation coefficient between SST and chlorophyll anomalies. **(d)** Scatter plot of this correlation coefficient against the frequency of compound event days over the global ocean.

east Pacific MHW and in the Indonesian Sea during the 2017 MHW. These are regions where the compound event frequencies are very high (Fig. 4a). Chlorophyll concentrations were normal or high during the 2012 northwest Atlantic MHW and during the 2016 MHW in the Southern Ocean, regions where the compound event frequency is also low. There are exceptions however, such as in the northern subtropical Pacific gyre where chlorophyll concentrations were locally high during the 2013–2015 MHW, even though compound MHW and LChl events are relatively frequent (> 1.8 % of all days) there.

Next, we assess the duration of compound events (Fig. 4b). The longest compound events (> 15 d) occur in regions of the longest MHWs or LChl events, i.e., in the center of the equatorial Pacific and in the seasonally varying sea ice region of the Southern Ocean (Fig. 4b). In the Weddell Sea, 10 % of compound events last longer than a month. Long compound events (where 10 % of events last longer than 10 d) also occur along the boundaries of the subtropical gyres in the North Pacific and in the Arabian Sea. The shortest compound events occur in the western part of the subtropical gyres and, in general, in the extra-tropics.

Assessing the intensity of compound events is not as straightforward as assessing their frequency or duration, since they involve two variables. Figure 5 illustrates the joint 90th–10th percentile threshold exceedance anomalies of SST and chlorophyll anomalies averaged over all compound events at a grid point. These joint exceedance anomalies are generally low over most of the low-latitude to mid-latitude

ocean (green colors in Fig. 5). High exceedance anomalies are reached in regions exhibiting the most intense MHWs and LChl events (see Fig. 3a and b). Specifically, compound events with particularly warm SST (yellow and light pink colors in Fig. 5) occur in the eastern equatorial Pacific, while compound events with particularly low chlorophyll (purple colors in Fig. 5) occur in the seasonally varying sea ice region of the Southern Ocean, in parts of the North Atlantic, and in the equatorial Atlantic. Intense compound events characterized by both extremely warm SST and low chlorophyll concentration (pink colors) occur at high northern latitudes; in eastern boundary upwelling regions such as the Canary, Humboldt, and California upwelling systems; in the western boundary currents of the Atlantic; and in the center of the equatorial Pacific.

3.3 Distribution of marine heatwaves and low-chlorophyll and compound events over time

Next, we assess occurrences of MHWs and LChl and compound events on seasonal to inter-annual timescales.

3.3.1 Seasonal timescale

The seasonal occurrences of extreme events strongly vary with latitude. MHWs occur all year long at low latitudes and mid-latitudes (Fig. 6a). In high latitudes, MHWs mostly occur in summer, especially in the Southern Ocean where, on average, more than 14% of austral summer days are affected by a MHW, while there are almost no MHW days in austral

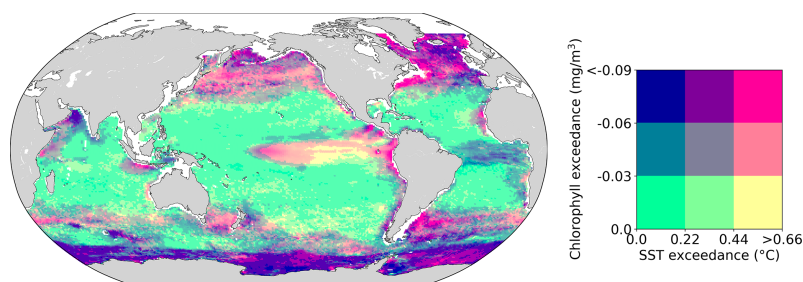


Figure 5. Intensity of compound marine heatwaves and low-chlorophyll events over the 1998–2018 period. Mean exceedance anomalies above the 90th and 10th percentile thresholds of SST ($^{\circ}\text{C}$) and chlorophyll (mg m^{-3}) anomalies, respectively, during compound events.

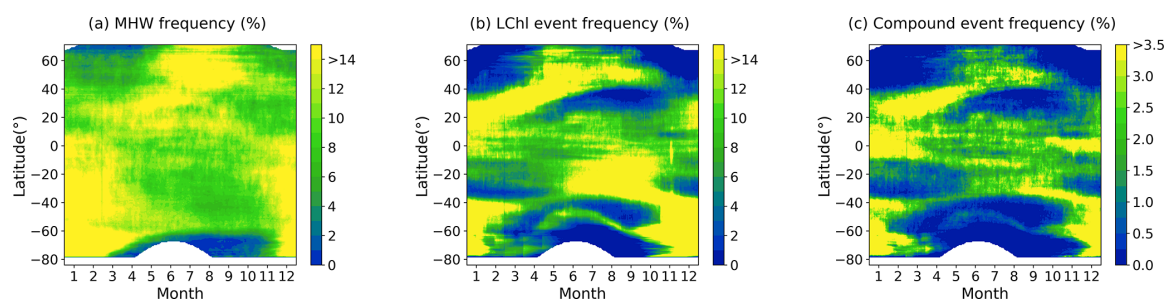


Figure 6. Seasonal cycle of MHWs, LChl events, and compound events over the 1998–2018 period. Frequency of (a) MHW, (b) LChl, and (c) compound event days (%) as a function of latitude and day of the year.

winter and spring south of 55°S . The temporal distribution over the year of LChl events is more heterogeneous across latitudes (Fig. 6b). While these events occur throughout the year along the Equator (about 10% of days correspond to a LChl event), they seem to follow the onset of the spring bloom in mid-latitudes. This onset varies over the spring, resulting in higher chlorophyll variability in spring, which may explain why LChl events occur more frequently in this season. In high latitudes, LChl events mostly occur in summer, especially in the Southern Ocean. As a result of the temporal distributions in MHW and LChl occurrences, compound events predominantly follow the distribution of LChl events over the year (Fig. 6c). At low latitudes, compound events occur at a similar frequency throughout the year. They mostly occur in spring at mid-latitudes and in summer at high latitudes, with especially high frequency ($> 3\%$ of days) in the Southern Ocean in austral summer.

3.3.2 Interannual timescale

The occurrence of extreme events also varies at the interannual timescale from 1998 to 2018 (Fig. 7). In 1998, 2010, and 2015–2016, the frequency of MHW days exceeded 15% on average over the global ocean (Fig. 7a and Oliver et al., 2018). The mean frequency of MHWs is positively correlated with time series of the El Niño 3.4 index ($r = 0.54$). As indicated by the red bands, these years were all characterized by strong El Niño events. These years were also char-

acterized by longer MHWs, especially in 2015 when MHWs lasted more than 30 d on average (not shown). In contrast, the occurrence probability and duration of MHWs is reduced during La Niña events (blue bands in Fig. 7a). LChl events also vary over the years, but to a smaller extent than MHWs. The frequency of LChl days strongly increased during the 2015–2016 El Niño event to up to 15% on average over the global ocean, but other strong El Niño events had almost no impact on the frequency of LChl events (Fig. 7b), also exemplified by the low correlation coefficient of $r = 0.23$ between LChl events and the El Niño 3.4 index. Most of the interannual distribution of compound events seems to be explained by the interannual distribution of MHWs, as LChl events are relatively uniformly distributed over the years. Compound events occurred most frequently ($> 2.5\%$ of all days) in the global ocean in 1998 and 2015–2016 (Fig. 7c), years which are characterized by strong El Niño events. Their frequency is more positively correlated with El Niño 3.4 ($r = 0.42$) than the frequency of LChl events but slightly less than the frequency of MHWs.

3.4 The role of natural internal climate variability

To improve our understanding of when and where compound MHW and LChl events occur, we identify the large-scale modes of internal climate variability that are associated with compound events locally. We compute the frequency of compound event days during the positive and negative phases

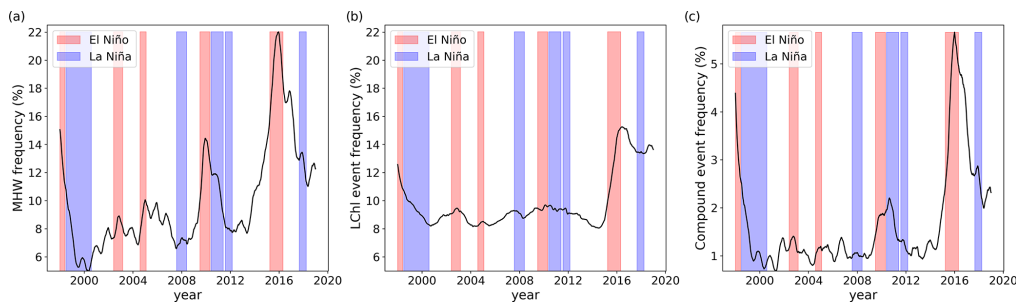


Figure 7. Global mean frequency of MHWs (a), LChl events (b), and compound events (c) over time. Daily time series are smoothed with a 1-year running mean to highlight interannual variability. Red and blue shading indicates the occurrence of El Niño and La Niña events, respectively. These events occur when the El Niño 3.4 index exceeds 0.4 or is lower than -0.4 , respectively, for at least 6 months. Note the different y-axis scales.

of seven different climate modes (see Methods). Figure 8 presents the frequency change in compound event days during these climate modes compared to their frequency over all days in a neutral phase from 1998 to 2018.

Overall, the relationship between compound event occurrence and climate modes is rather complex, but there are clear patterns emerging that are consistent with the well-known SST or atmospheric pressure patterns during these modes. The positive phase of ENSO (i.e., El Niño events) is associated with increased frequency of compound events in the central and eastern equatorial Pacific ($> 300\%$) (Fig. 8a). In 2015, an El Niño event was indeed associated with a compound MHW and LChl event (Fig. 1); chlorophyll anomalies reached extremely low values as the warming extended southward into the eastern equatorial Pacific due to the enhancement of the Blob by El Niño (Tseng et al., 2017). El Niño events are also associated with increased frequency of compound events in the Indian Ocean ($> 300\%$), the Pacific sector of the Southern Ocean, and the California Current system, whereas they suppress compound events in the western Pacific (-100%) and in the mid-latitudes (Fig. 8a). On the contrary, the negative phase of ENSO (i.e., La Niña events) is associated with higher frequency in the western Pacific ($> 300\%$) and in the Southern Ocean from 30 to 50° S ($> 300\%$) and with fewer compound events in the eastern equatorial Pacific and in the Indian Ocean (Fig. 8b). During the positive and negative phases of EMI (Fig. 8c and d), the pattern of compound event frequency broadly resembles the pattern during positive and negative ENSO phases. However, compound events in the eastern equatorial Pacific and the Indian Ocean are less affected by EMI than by ENSO. The positive phase of PDO is associated with increased frequency of compound events in the eastern equatorial Pacific, in the northeastern Pacific, and in the Indian Ocean, and vice versa during the negative phase of PDO (Fig. 8e and f). Although the ENSO and PDO patterns are very similar in the Pacific – PDO is often described as the long-lived El Niño-like climate pattern in the Pacific (Zhang et al., 1997) – they differ in the

Southern Ocean where PDO phases are associated with less frequent compound events than ENSO phases (Fig. 8a, b, e and f). NPGO is another leading mode of climate variability in the Pacific; its positive phase is associated with suppressed compound event occurrence in the northern Pacific gyre and reduced occurrence in the southern Pacific gyre while its negative phase is associated with increased occurrence of compound events in the subtropical Pacific (Fig. 8g and h). Note that ENSO, EMI, PDO, and NPGO are all correlated, their definition being based on climate variability in the Pacific Ocean. The positive phase of the Indian Ocean Dipole (i.e., DMI+) is associated with higher frequency ($> 75\%$) in the Arabian Sea and reduced frequency ($< -75\%$) around the Maritime Continent (Fig. 8i). The positive phase of NAO is associated with increased frequency of compound events in the North Atlantic mid-latitudes and in the northeastern Pacific, while it suppresses compound events in the North Atlantic high and low latitudes (Fig. 8k). Finally, the positive phase of AAO is associated with higher frequency of compound events ($> 75\%$) in parts of the Southern Ocean, of the eastern Pacific, and of the eastern Indian Ocean (Fig. 8m).

In general, the positive and negative phases of each climate mode are associated with opposite changes in the frequency of compound events. However, Fig. 8a, c, e, g, i, k, and m are not exactly complementary to Fig. 8b, d, f, h, j, l, and n, which partly reflects that the modes themselves are not perfectly complementary; e.g., there are asymmetries in the spatial structure, amplitude, duration, and time evolution of El Niño and La Niña (An and Jin, 2004; Dommenges et al., 2013; Okumura and Deser, 2010).

The climate mode associated with the largest frequency increase in compound event days varies over the global ocean (Fig. 9). ENSO seems to be the main modulator of compound events in the eastern equatorial Pacific and in the northwestern part of the Indian Ocean, where El Niño events are associated with the highest frequency of compound event days from 1998 to 2018. The positive phase of PDO is associated with the greatest occurrence of compound events in some

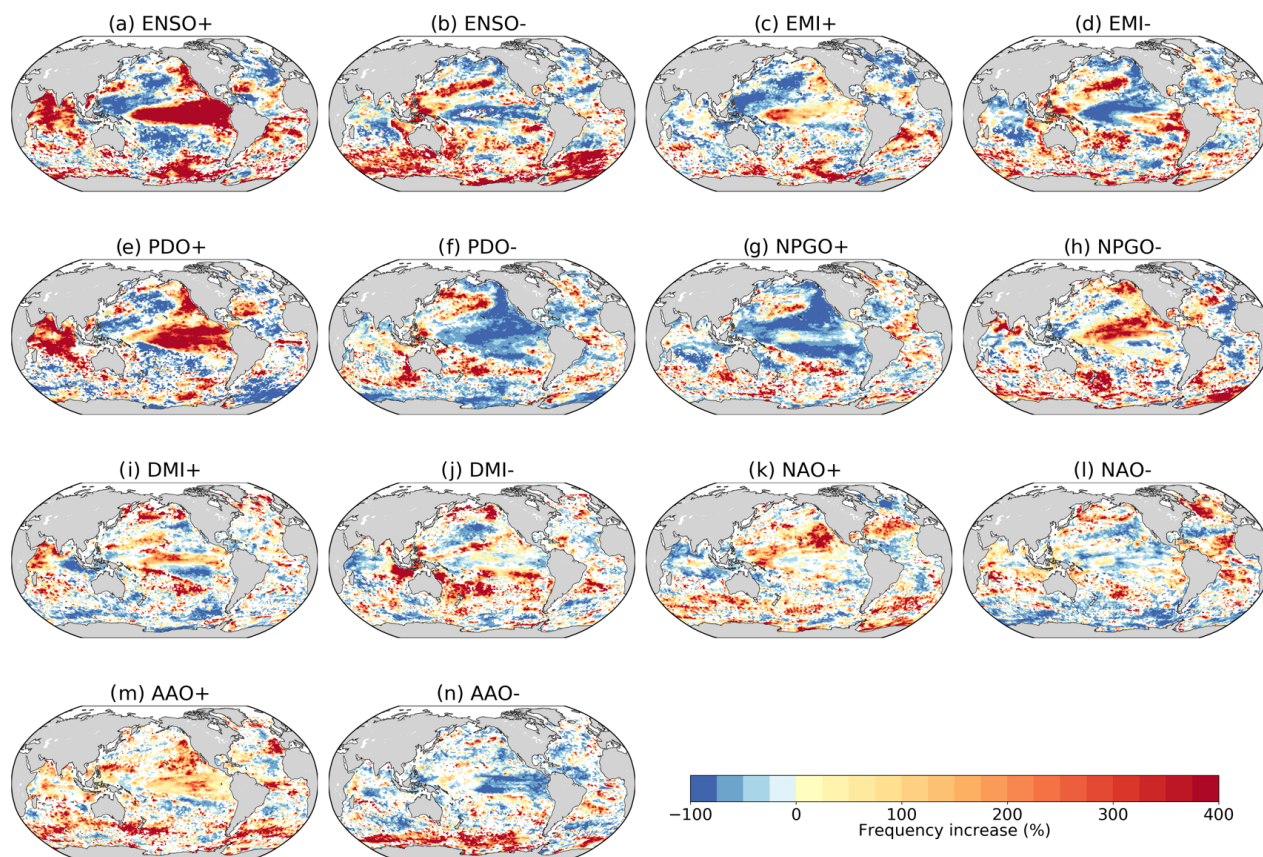


Figure 8. Frequency change in compound event days during positive and negative phases of several climate modes compared to their frequency over the neutral phase (in percent). Analyzed climate modes are (a, b) El Niño Southern Oscillation, (c, d) El Niño Modoki, (e, f) Pacific Decadal Oscillation, (g, h) North Pacific Gyre Oscillation, (i, j) Indian Ocean Dipole using its Dipole Mode Index, (k, l) North Atlantic Oscillation, and (m, n) Antarctic Oscillation. Grids cells where this frequency change is not statistically relevant remain white.

parts of the Indian Ocean and of the tropical and northeastern Pacific. The negative phase of NPGO is associated with the largest frequency of compound events in some parts of the North Pacific gyre. The Indian Ocean Dipole is the climate mode associated with the highest occurrence of compound events around Indonesia and in parts of the subtropical Pacific. NAO is associated with their highest occurrence in the eastern equatorial Atlantic, in the Gulf Stream region, and in some parts of the northeastern Pacific. Finally, AAO is associated with the highest frequency of compound events in some parts of the Southern Ocean. Figure 9 is patchy in many areas, presumably due to the relatively short 1998–2018 time period over which the sampling of compound events is limited. The climate modes associated with the largest frequency increase in MHW days and in LChl event days, separately, are provided in the Appendix for reference (Fig. A4).

4 Discussion and conclusion

In this study, we provide a first assessment of compound marine heatwave and low-chlorophyll extreme events in the global ocean over the 1998–2018 period. We show that hotspots of compound MHW and LChl events can be found in the equatorial Pacific, along the boundaries of the subtropical gyres, and in the Arabian Sea. These correspond to regions where the sea surface temperature and chlorophyll anomalies are predominantly negatively correlated and also to regions where most of the warm-water corals are located and where coral-bleaching events have often occurred in the recent past (Hughes et al., 2018a). Furthermore, we show that compound events mostly occur in summer in the high latitudes and throughout the year in the low latitudes to mid-latitudes and that different large-scale modes of climate variability are associated with compound MHW and LChl events.

Our identified global pattern of compound event frequency in Fig. 4a also corresponds to some extent with the re-

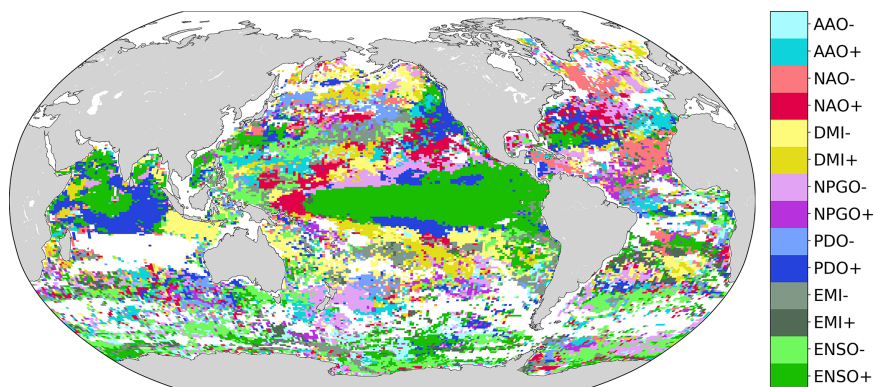


Figure 9. Phases of large-scale climate modes associated with the highest frequency of compound event days from 1998 to 2018. Regions for which the base frequency over the whole 1998–2018 period is $< 1\%$ are marked white.

sults of Hayashida et al. (2020), who concluded that the general response of chlorophyll to MHWs at specific sites depends on the background surface nutrient concentration. They showed that during MHWs, shallower mixed-layer depth and lower nitrate concentration exacerbate nutrient stress (Behrenfeld et al., 2006; Racault et al., 2017), resulting in lower chlorophyll concentration in nutrient-limited surface waters, whereas the relief of light limitation during MHWs leads to higher chlorophyll concentrations in nutrient-rich surface waters. The eastern equatorial Pacific is an exception, where, for example during El Niño events, the reduction in the upwelling of cold and nutrient-rich subsurface waters leads to lower chlorophyll concentration (Hayashida et al., 2020; Racault et al., 2017). The decrease in chlorophyll concentration may be exacerbated by a potential increase in grazing pressure in warmer waters in these eutrophic waters (Laufkötter et al., 2015). In contrast to the Hayashida et al. (2020) study, which investigates the general response of chlorophyll to MHWs at specific sites regardless of whether the chlorophyll concentration is extreme or not, our analysis identifies regions at the global scale where both temperature and chlorophyll are extreme at the same time. Despite this difference, we also identify elevated compound event frequency in the nutrient-limited surface waters of the low latitudes and in the eastern equatorial Pacific and low compound event frequency in the nutrient-rich surface waters of the Southern Ocean (Fig. 4a). The eastern equatorial Pacific behaves like a nutrient-limited region even though it is nutrient-rich. There are exceptions, however, between our results and Hayashida et al. (2020). Compound events are relatively frequent in the North Pacific, North Atlantic, and around Antarctica even though the background nutrient concentration is relatively high in these regions. There, phytoplankton growth may be limited by other key nutrients (e.g., iron around Antarctica), and increased phytoplankton grazing may lead to low chlorophyll during marine heatwaves. In addition, the frequency of compound events in the

tropical Indian Ocean is relatively low even though the surface nutrient concentrations are low there. This calls for additional process-oriented studies to identify the exact physical and biogeochemical processes driving compound high-temperature and low-chlorophyll events.

While there is a growing understanding of how the occurrence of MHWs changes under several modes of internal climate variability (Holbrook et al., 2019), the modulation of LChl events and in particular of compound MHW and LChl event frequency is barely understood. We assessed changes in the frequency of compound events during the positive and negative phases of several climate modes. Even though statistical relationships do not necessarily indicate causal links, these changes help predict the occurrence of compound events as a function of the oceanic region and the state of a climate mode. For example, compound event frequency is increased by up to 300% in the Pacific and Indian oceans during El Niño events. We can therefore expect frequent compound events in these regions during upcoming El Niño events. The relationships we demonstrate between climate drivers and compound events resemble the relationships between climate drivers and MHWs shown in Holbrook et al. (2019) in the equatorial Pacific, in the Indian Ocean, and in the northern Atlantic. Therefore, the state of the different large-scale climate modes can potentially be used to predict the occurrence of both MHWs and compound MHW and LChl events in these regions. However, this is not the case in other regions (e.g., in the western Pacific), where the occurrence pattern of MHWs and compound MHW and LChl events differ for the different large-scale modes of climate variability. This indicates again that other processes (see above) may affect chlorophyll concentrations in these regions, that MHWs are mostly modulated by climate modes that we omitted in our study (e.g., the Interdecadal Pacific Oscillation in parts of the Pacific Ocean) because our shorter period of analysis does not capture their variability, or that some climate modes would be dominant if we used a longer

period of analysis such as in Holbrook et al. (2019). Given that compound events are strongly associated with several large-scale modes of climate variability, skillful multi-annual forecasts of the state of these climate modes may be used as an early warning system for the occurrence of compound events and may therefore provide critical information for fishery management and adaptation interventions to reduce risks and impacts on marine organisms and ecosystems during such events (Holbrook et al., 2020).

Even though we consider our results robust, two potential uncertainties need to be discussed. First, our quantitative results are sensitive to the particular assumptions that need to be made during the statistical analysis (e.g., threshold value, fixed vs. moving baseline; Burger et al., 2020; Oliver et al., 2021). We chose to use the 90th and 10th percentile thresholds to have a relatively large number of compound events given the length of the satellite record for chlorophyll. Choosing different thresholds led to qualitatively similar results. In addition, we use a fixed baseline climatology (i.e., the entire 1998–2018 satellite record). Therefore, any long-term changes in sea surface temperature and chlorophyll affect the frequency of compound events over time. Because there is a gradual increase in mean sea surface temperature (SST), MHWs generally occur more often towards the end of the satellite record (Fig. 7a; Frölicher et al., 2018; Oliver et al., 2018; Laufkötter et al., 2020). This is not the case for LChl events, as the long-term trend in mean chlorophyll concentrations is close to zero (Hammond et al., 2020; Rousseaux and Gregg, 2014). Consequently, a fixed baseline might not affect the occurrence of LChl events, but it might favor an increase in the occurrence of compound MHW and LChl events over the satellite period along with the increase in mean SST.

Second, whereas the satellite-derived temperature data have been validated extensively (Banzon et al., 2016; Huang et al., 2021; Reynolds et al., 2007) and used for many recent marine heatwave analyses (e.g., Hobday et al., 2016; Oliver et al., 2018; Frölicher et al., 2018; Laufkötter et al., 2020), the satellite-derived chlorophyll estimates have not been extensively used to analyze extreme events. High solar zenith angles, clouds, aerosols, and interorbital gaps can lead to a bias in the chlorophyll (and temperature) data (Gregg et al., 2009). Furthermore, the data have to be merged over several weeks or even months to achieve true global representation. By assimilating satellite ocean color in the NASA Ocean Biogeochemical Model, we reduced some of these biases. Nevertheless, we note that our results need to be taken with caution, especially near the coasts and at high latitudes, where the chlorophyll estimates remain uncertain.

Impacts of compound MHW and LChl events on marine organisms and ecosystems may be more severe than the impacts from MHWs and LChl events individually. Even though little is known about the impacts of compound MHW and LChl events, many studies have documented the mostly strong negative effects of MHWs alone. It is assumed that

marine species are particularly vulnerable to MHWs in the low latitudes, since these species already live at the upper thermal edge of their habitat (Smale et al., 2019). MHWs in the low latitudes also have critical impacts on foundation species such as corals, seagrass, and kelp (Smale et al., 2019). In the high latitudes, where biological production is often light-limited (McClain, 2009), MHWs may be beneficial for some species as long as MHWs are not very abrupt, prolonged, or compounded with other stressors over time (Cavole et al., 2016; Walsh et al., 2018). On the other hand, low chlorophyll, when indicating lower net primary production, results in lower food supply in all oceanic regions with harmful effects on marine biology. While chlorophyll is not always correlated with phytoplankton biomass or net primary production, particularly in subtropical regions (Barbireux et al., 2018), it is still commonly used as a proxy for phytoplankton biomass or net primary production (e.g., Behrenfeld et al., 2005; Henson et al., 2010). We therefore assume that LChl events often exacerbate the impacts from MHWs. In addition, phytoplankton includes a diverse range of different species that may respond differently to MHWs. For example, both the phytoplankton and zooplankton community composition have changed from larger species to smaller species during the northeast Pacific 2013–2015 MHW (Cavole et al., 2016), resulting in less energy available for the food web. While some species benefited from the compound MHW and LChl event (e.g., rockfish, subtropical copepods, tuna, and orcas), the mortality of many other species substantially increased (subarctic copepods, crabs and mussels, sea birds, seals, sea lions, and whales). More research is needed to understand the effects of exceptional warming events combined with LChl levels, as marine ecosystems could suffer severe damage.

Earth system models project further surface warming and decreasing primary production in nutrient-limited waters of the low latitudes to mid-latitudes during the 21st century (Bopp et al., 2013; Kwiatkowski et al., 2020). Given these projected long-term trends, we can expect more frequent compound events and increasing pressure on marine organisms and ecosystems over the next decades in these regions. We therefore encourage future work aimed at assessing the vulnerability, adaptability, and resilience of marine ecosystems to these compound events.

Our results provide a first characterization of where and when compound MHW and LChl events might occur and how these events are associated with large-scale modes of internal climate variability. Additional observationally based and modeling studies are needed to identify the exact physical and biological drivers of such compound events in the ocean, their evolution with climate change, and their impacts on marine ecosystems.

Appendix A: Additional figures

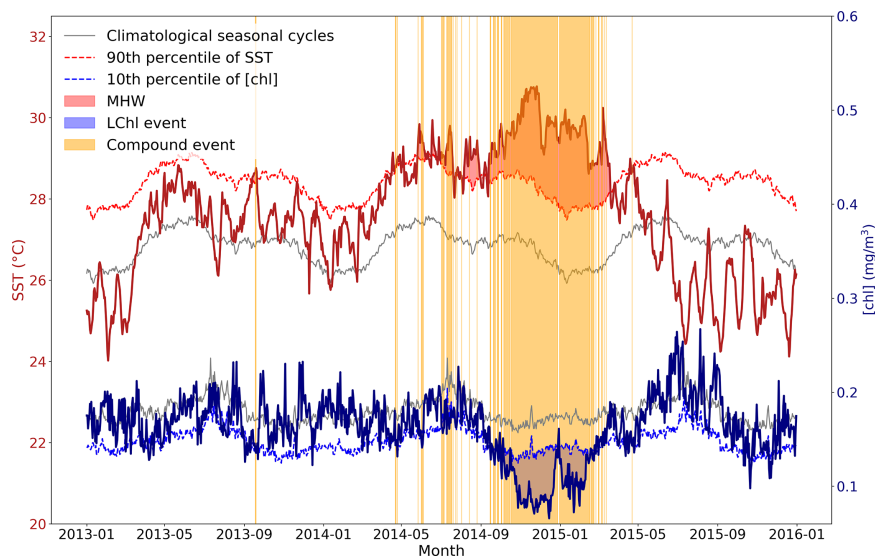


Figure A1. Schematic figure illustrating the definition of MHWs, LChl events, and compound MHW and LChl events. Time series of SST and chlorophyll concentration are extracted from 2013 to 2015 at 0° N and 155° E. A MHW occurs (red shaded area) when the SST (bold red line) exceeds its 90th percentile (dashed red line). A LChl event (blue shaded area) occurs when the surface chlorophyll concentration (bold blue line) is below its 10th percentile (dashed blue line). Yellow bands indicate the occurrence of compound MHW and LChl events.

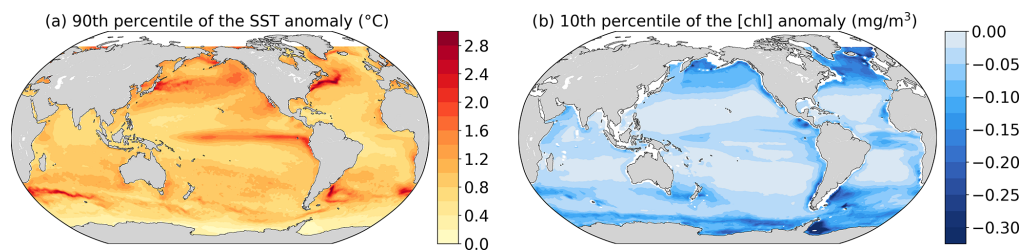


Figure A2. (a) The 90th percentile of SST anomalies ($^{\circ}$ C) and (b) 10th percentile of chlorophyll anomalies (mg m^{-3}) from 1998 to 2010 at each grid cell.

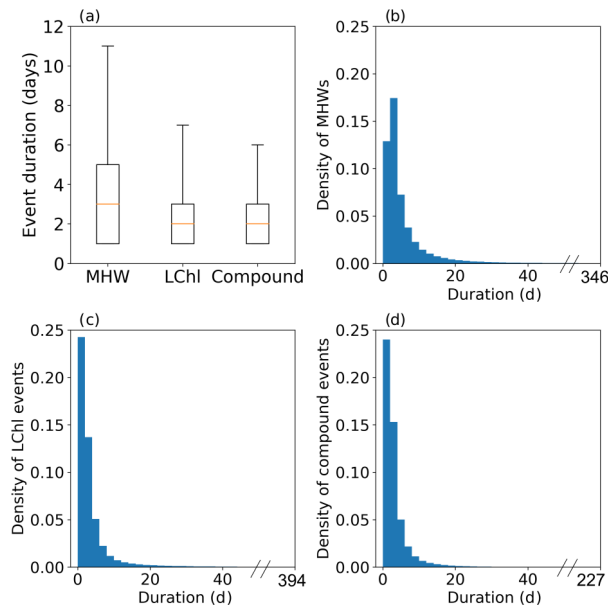


Figure A3. Distribution of the duration of all MHWs (a, b), LChl events (a, c), and compound events (a, d) sampled over the global ocean from 1998 to 2018. In (a), the box extends from the lower to upper quartiles, with a line at the median. The bottom and upper whiskers correspond to the 10th and 90th percentiles of the duration, respectively. Density plots (b–d) show the probability density function (PDF) for 2 d wide bars. The longest MHW lasted 346 d, the longest LChl event 394 d, and the longest compound event 227 d.

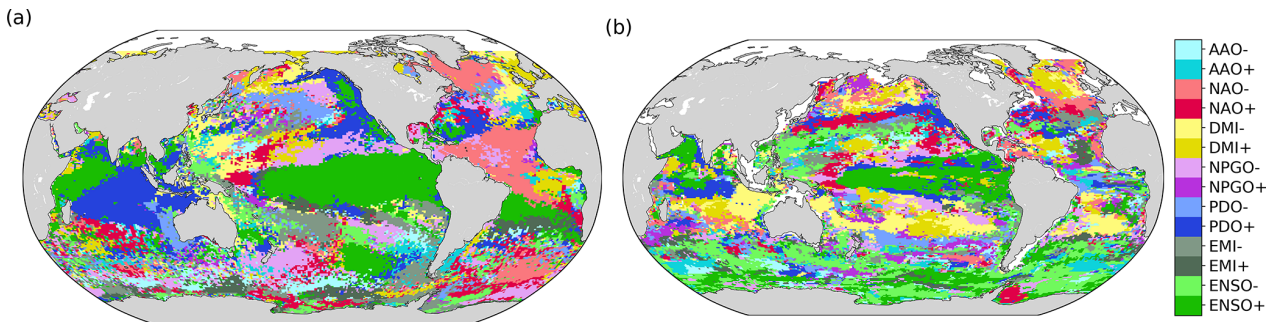


Figure A4. Phases of large-scale climate modes associated with the highest frequency of MHW days (a) and low-chlorophyll event days (b). Regions for which none of the climate modes reach a significant change of the frequency (see Methods) are marked grey.

Appendix B: Climate indices

- The Niño-3.4 index indicates the state of ENSO and corresponds to the area-averaged SST anomaly in the equatorial central Pacific from 5° S–5° N and 170–120° W, relative to the mean SST over this area (https://psl.noaa.gov/gcos_wgsp/Timeseries/Nino34/, last access: March 2021).
- The El Niño Modoki is equivalent to the central Pacific ENSO. It is estimated using the El Niño Modoki Index (EMI), which is based on the difference between SST anomalies in the central equatorial Pacific and the averaged eastern and western Pacific SST anomalies (http://www.jamstec.go.jp/frsgc/research/d1/iod/modoki_home.html.en, last access: March 2021).
- The PDO index is obtained by linearly regressing monthly SST anomalies upon the leading principal component of SST anomalies in the North Pacific Ocean poleward of 20° N (<http://research.jisao.washington.edu/pdo/PDO.latest>, last access: March 2021).
- The NPGO index is based on the second mode of sea surface height variability in the northeast Pacific and it accurately describes the climate pattern south of 40° N (<http://www.o3d.org/npgo/npgo.php>, last access: March 2021).
- The Dipole Mode Index (DMI) measures the strength of the Indian Ocean Dipole. It is based on the difference between SST anomalies in the western equatorial Indian Ocean (50–70° E and 10° S–10° N) and in the southeastern equatorial Indian Ocean (90–110° E and 10° S–0° N) (http://www.jamstec.go.jp/frsgc/research/d1/iod/e/iod/dipole_mode_index.html, last access: March 2021).
- The NAO index is constructed by projecting the daily 500 mb height anomalies over the Northern Hemisphere onto the loading pattern of the North Atlantic Oscillation. The latter oscillation of atmospheric pressure anomalies consists of a north–south dipole with one center located over Greenland and the other center of opposite sign over the North Atlantic between 35 and 40° N (<https://www.cpc.ncep.noaa.gov/products/precip/CWlink/pna/nao.shtml>, last access: March 2021).
- Finally, the AAO index is constructed by projecting daily 700 mb height anomalies poleward of 20° S onto the loading pattern of the Antarctic Oscillation (https://www.cpc.ncep.noaa.gov/products/precip/CWlink/daily_ao_index/aao/monthly.ao.index.b79.current.ascii.table, last access: March 2021).

Data availability. The satellite SST data are available under <https://www.ncdc.noaa.gov/oisst/data-access> (last access: March 2021) (Banzon et al., 2016; Reynolds et al., 2007). The chlorophyll data assimilated by the NASA Ocean Biogeochemical Model are publicly available from 1998 to 2015 under https://disc.gsfc.nasa.gov/datasets/NOBM_DAY_R2017/summary (last access: March 2021) (Gregg and Rousseaux, 2017). Cécile Rousseaux provided a pre-release of the chlorophyll data from 2016 to 2018, and these data are available upon request. The figures and analysis are available under the following link on ZENODO: <https://doi.org/10.5281/zenodo.4542015> (Le Grix, 2021).

Author contributions. NLG, JZ, and TLF designed the study, with substantial input from CL. NLG performed the analysis and wrote the initial draft of the paper. CSR provided the chlorophyll dataset. All authors discussed the analysis and results and contributed to the writing of the paper.

Competing interests. The authors declare that they have no conflict of interest.

Disclaimer. The work reflects only the authors' view; the European Commission and their executive agency are not responsible for any use that may be made of the information the work contains.

Special issue statement. This article is part of the special issue "Understanding compound weather and climate events and related impacts (BG/ESD/HESS/NHESS inter-journal SI)". It is not associated with a conference.

Acknowledgements. The authors acknowledge the European COST Action DAMOCLES (CA17109).

Financial support. Natacha Le Grix is funded by the Alfred Bretscher Fund. This research has been supported by the Swiss National Science Foundation (nos. PP00P2_170687, 174124, 179876), the European Union's Horizon 2020 research and innovation program under grant agreement no. 820989 (project COMFORT, "Our common future ocean in the Earth system – quantifying coupled cycles of carbon, oxygen, and nutrients for determining and achieving safe operating spaces with respect to tipping points") and grant agreement no. 862923 (project AtlantECO, "Atlantic Ecosystems Assessment, Forecasting & Sustainability"), and the Helmholtz Initiative and Networking Fund (Young Investigator Group COMPOUNDX, grant agreement VH-NG-1537).

Review statement. This paper was edited by Julia Uitz and reviewed by Monique Messié and one anonymous referee.

References

- An, S.-I. and Jin, F.-F.: Nonlinearity and Asymmetry of ENSO, *J. Climate*, 17, 2399–2412, [https://doi.org/10.1175/1520-0442\(2004\)017<2399:NAAOE>2.0.CO;2](https://doi.org/10.1175/1520-0442(2004)017<2399:NAAOE>2.0.CO;2), 2004.
- Banzon, V., Smith, T. M., Chin, T. M., Liu, C., and Hankins, W.: A long-term record of blended satellite and in situ sea-surface temperature for climate monitoring, modeling and environmental studies, *Earth Syst. Sci. Data*, 8, 165–176, <https://doi.org/10.5194/essd-8-165-2016>, 2016.
- Barbieux, M., Uitz, J., Bricaud, A., Organelli, E., Poteau, A., Schmechtig, C., Gentili, B., Obolensky, G., Leymarie, E., Penkerç'h, C., D'Ortenzio, F., and Claustre, H.: Assessing the Variability in the Relationship Between the Particulate Backscattering Coefficient and the Chlorophyll a Concentration From a Global Biogeochemical-Argo Database, *J. Geophys. Res.-Oceans*, 123, 1229–1250, <https://doi.org/10.1002/2017JC013030>, 2018.
- Behrenfeld, M. J., Randerson, J. T., McClain, C. R., Feldman, G. C., Los, S. O., Tucker, C. J., Falkowski, P. G., Field, C. B., Frouin, R., Esaias, W. E., Kolber, D. D., and Pollack, N. H.: Biospheric Primary Production During an ENSO Transition, *Science*, 291, 2594, <https://doi.org/10.1126/science.1055071>, 2001.
- Behrenfeld, M. J., Boss, E., Siegel, D. A., and Shea, D. M.: Carbon-based ocean productivity and phytoplankton physiology from space, *Global Biogeochem. Cy.*, 19, GB1006, <https://doi.org/10.1029/2004GB002299>, 2005.
- Behrenfeld, M. J., O'Malley, R. T., Siegel, D. A., McClain, C. R., Sarmiento, J. L., Feldman, G. C., Milligan, A. J., Falkowski, P. G., Letelier, R. M., and Boss, E. S.: Climate-driven trends in contemporary ocean productivity, *Nature*, 444, 752–755, <https://doi.org/10.1038/nature05317>, 2006.
- Bond, N. A., Cronin, M. F., Freeland, H., and Mantua, N.: Causes and impacts of the 2014 warm anomaly in the NE Pacific, *Geophys. Res. Lett.*, 42, 3414–3420, <https://doi.org/10.1002/2015GL063306>, 2015.
- Bopp, L., Resplandy, L., Orr, J. C., Doney, S. C., Dunne, J. P., Gehlen, M., Halloran, P., Heinze, C., Ilyina, T., Séférian, R., Tjiputra, J., and Vichi, M.: Multiple stressors of ocean ecosystems in the 21st century: projections with CMIP5 models, *Biogeosciences*, 10, 6225–6245, <https://doi.org/10.5194/bg-10-6225-2013>, 2013.
- Boyce, D. G., Lewis, M. R., and Worm, B.: Global phytoplankton decline over the past century, *Nature*, 466, 591–596, <https://doi.org/10.1038/nature09268>, 2010.
- Burger, F. A., John, J. G., and Frölicher, T. L.: Increase in ocean acidity variability and extremes under increasing atmospheric CO₂, *Biogeosciences*, 17, 4633–4662, <https://doi.org/10.5194/bg-17-4633-2020>, 2020.
- Cavole, L., Demko, A., Diner, R., Giddings, A., Koester, I., Pagniello, C., Paulsen, M.-L., Ramírez-Valdez, A., Schwenck, S., Zill, M., and Franks, P.: Biological Impacts of the 2013–2015 Warm-Water Anomaly in the Northeast Pacific: Winners, Losers, and the Future, *Oceanography*, 29, 273–285, <https://doi.org/10.5670/oceanog.2016.32>, 2016.
- Cheng, L., Trenberth, K. E., Fasullo, J., Boyer, T., Abraham, J., and Zhu, J.: Improved estimates of ocean heat content from 1960 to 2015, *Sci. Adv.*, 3, E1601545, <https://doi.org/10.1126/sciadv.1601545>, 2017.

N. Le Grix et al.: Compound high-temperature and low-chlorophyll extremes in the ocean

2135

- Cheung, W. W. L. and Frölicher, T. L.: Marine heatwaves exacerbate climate change impacts for fisheries in the northeast Pacific, *Scient. Rep.*, 10, 6678, <https://doi.org/10.1038/s41598-020-63650-z>, 2020.
- Collins, M., Sutherland, M., Bouwer, L., Cheong, S.-M., Frölicher, T., Combes, H. J. D., Roxy, M. K., Losada, I., McInnes, K., Ratter, B., Rivera-Arriaga, E., Susanto, R., Swingedouw, D., and Tibig, L.: Extremes, Abrupt Changes and Managing Risk, in: IPCC Special Report on the Ocean and Cryosphere in a Changing Climate, IPCC, in press, 2019.
- Deser, C., Alexander, M., Xie, S.-P., and Phillips, A.: Sea Surface Temperature Variability: Patterns and Mechanisms, *Annu. Rev. Mar. Sci.*, 2, 115–143, <https://doi.org/10.1146/annurev-marine-120408-151453>, 2010.
- Di Lorenzo, E. and Mantua, N.: Multi-year persistence of the 2014/15 North Pacific marine heatwave, *Nat. Clim. Change*, 6, 1042–1047, <https://doi.org/10.1038/nclimate3082>, 2016.
- Dommenget, D., Bayr, T., and Frauen, C.: Analysis of the non-linearity in the pattern and time evolution of El Niño southern oscillation, *Clim. Dynam.*, 40, 2825–2847, <https://doi.org/10.1007/s00382-012-1475-0>, 2013.
- Feng, M., McPhaden, M. J., Xie, S.-P., and Hafner, J.: La Niña forces unprecedented Leeuwin Current warming in 2011, *Scient. Rep.*, 3, 1277, <https://doi.org/10.1038/srep01277>, 2013.
- Frölicher, T. L.: Chapter 5 – Extreme climatic events in the ocean, in: *Predicting Future Oceans*, edited by: Cisneros-Montemayor, A. M., Cheung, W. W., and Ota, Y., Elsevier, 53–60, <https://doi.org/10.1016/B978-0-12-817945-1.00005-8>, 2019.
- Frölicher, T. L. and Laufkötter, C.: Emerging risks from marine heat waves, *Nat. Commun.*, 9, 650, <https://doi.org/10.1038/s41467-018-03163-6>, 2018.
- Frölicher, T. L., Fischer, E. M., and Gruber, N.: Marine heatwaves under global warming, *Nature*, 560, 360–364, <https://doi.org/10.1038/s41586-018-0383-9>, 2018.
- Gelaro, R., McCarty, W., Suárez, M. J., Todling, R., Molod, A., Takacs, L., Randall, C. A., Darnenov, A., Bosilovich, M. G., Reichle, R., Wargan, K., Coy, L., Cullather, R., Draper, C., Akella, S., Buchard, V., Conaty, A., Silva, A. M., Gu, W., Kim, G., Koster, R., Lucchesi, R., Merkova, D., Nielsen, J. E., Partyka, G., Pawson, S., Putman, W., Rienecker, M., Schubert, S. D., Sienkiewicz, M., and Zhao, B.: The Modern-Era Retrospective Analysis for Research and Applications, Version 2 (MERRA-2), *J. Climate*, 30, 5419–5454, <https://doi.org/10.1175/JCLI-D-16-0758.1>, 2017.
- Gregg, W. and Rousseaux, C. (Eds.): NASA Ocean Biogeochemical Model assimilating satellite chlorophyll data global daily VR2017, Goddard Earth Sciences Data and Information Services Center GES DISC, Greenbelt, MD, USA, <https://doi.org/10.5067/PT6TXZKSHBW9>, 2017.
- Gregg, W., Casey, N., O'Reilly, J., and Esaias, W.: An empirical approach to ocean color data: Reducing bias and the need for post-launch radiometric re-calibration, *Remote Sens. Environ.*, 113, 1598–1612, <https://doi.org/10.1016/j.rse.2009.03.005>, 2009.
- Gregg, W. W. and Casey, N. W.: Sampling biases in MODIS and SeaWiFS ocean chlorophyll data, *Remote Sens. Environ.*, 111, 25–35, <https://doi.org/10.1016/j.rse.2007.03.008>, 2007.
- Gregg, W. W. and Rousseaux, C. S.: Decadal trends in global pelagic ocean chlorophyll: A new assessment integrating multiple satellites, in situ data, and models, *J. Geophys. Res.-Oceans*, 119, 5921–5933, <https://doi.org/10.1002/2014JC010158>, 2014.
- Hammond, M. L., Beaulieu, C., Henson, S. A., and Sahu, S. K.: Regional surface chlorophyll trends and uncertainties in the global ocean, *Scient. Rep.*, 10, 15273, <https://doi.org/10.1038/s41598-020-72073-9>, 2020.
- Hayashida, H., Matear, R. J., and Strutton, P. G.: Background nutrient concentration determines phytoplankton bloom response to marine heatwaves, *Global Change Biol.*, 26, 4800–4811, <https://doi.org/10.1111/gcb.15255>, 2020.
- Henson, S. A., Sarmiento, J. L., Dunne, J. P., Bopp, L., Lima, I., Doney, S. C., John, J., and Beaulieu, C.: Detection of anthropogenic climate change in satellite records of ocean chlorophyll and productivity, *Biogeosciences*, 7, 621–640, <https://doi.org/10.5194/bg-7-621-2010>, 2010.
- Hobday, A. J., Alexander, L. V., Perkins, S. E., Smale, D. A., Straub, S. C., Oliver, E. C., Benthuisen, J. A., Burrows, M. T., Donat, M. G., Feng, M., Holbrook, N. J., Moore, P. J., Scannell, H. A., Sen Gupta, A., and Wernberg, T.: A hierarchical approach to defining marine heatwaves, *Prog. Oceanogr.*, 141, 227–238, <https://doi.org/10.1016/j.pocean.2015.12.014>, 2016.
- Holbrook, N. J., Scannell, H. A., Gupta, A. S., Benthuisen, J. A., Feng, M., Oliver, E. C. J., Alexander, L. V., Burrows, M. T., Donat, M. G., Hobday, A. J., Moore, P. J., Perkins-Kirkpatrick, S. E., Smale, D. A., Thomas, S. C. S., and Thomas, W.: A global assessment of marine heatwaves and their drivers, *Nat. Commun.*, 10, 2624, <https://doi.org/10.1038/s41467-019-10206-z>, 2019.
- Holbrook, N. J., Sen Gupta, A., Oliver, E. C. J., Hobday, A. J., Benthuisen, J. A., Scannell, H. A., Smale, D. A., and Wernberg, T.: Keeping pace with marine heatwaves, *Nat. Rev. Earth Environ.*, 1, 482–493, <https://doi.org/10.1038/s43017-020-0068-4>, 2020.
- Huang, B. C., Liu, V. B., Freeman, E., Graham, G. W., Hankins, T. S., and Zhang, H.-M.: Improvements of the Daily Optimum Sea Surface Temperature (DOISST) – Version 2.1, *J. Climate*, 34, 2923–2939, <https://doi.org/10.1175/JTECH-D-19-0177.1>, 2021.
- Hughes, T. P., Anderson, K. D., Connolly, S. R., Heron, S. F., Kerry, J. T., Lough, J. M., Baird, A. H., Baum, J. K., Berumen, M. L., Bridge, T. C., Claar, D. C., Eakin, C. M., Gilmour, J. P., Graham, N. A. J., Harrison, H., Hobbs, J.-P. A., Hoey, A. S., Hoogenboom, M., Lowe, R. J., McCulloch, M. T., Pandolfi, J. M., Pratchett, M., Schoepf, V., Torda, G., and Wilson, S. K.: Spatial and temporal patterns of mass bleaching of corals in the Anthropocene, *Science*, 359, 80–83, <https://doi.org/10.1126/science.aan8048>, 2018a.
- Hughes, T. P., Kerry, J. T., Baird, A. H., Connolly, S. R., Dietzel, A., Eakin, C. M., Heron, S. F., Hoey, A. S., Hoogenboom, M. O., Liu, G., McWilliam, M. J., Pears, R. J., Pratchett, M. S., Skirving, W. J., Stella, J. S., and Torda, G.: Global warming transforms coral reef assemblages, *Nature*, 556, 492–496, <https://doi.org/10.1038/s41586-018-0041-2>, 2018b.
- Jones, T., Parrish, J. K., Peterson, W. T., Bjorkstedt, E. P., Bond, N. A., Ballance, L. T., Bowes, V., Hipfner, J. M., Burgess, H. K., Dolliver, J. E., Lindquist, K., Lindsey, J., Nevins, H. M., Robertson, R. R., Roletto, J., Wilson, L., Joyce, T., and Harvey, J.: Massive Mortality of a Planktivorous Seabird in Response to a Marine Heatwave, *Geophys. Res. Lett.*, 45, 3193–3202, <https://doi.org/10.1002/2017GL076164>, 2018.
- Kwiatkowski, L., Torres, O., Bopp, L., Aumont, O., Chamberlain, M., Christian, J. R., Dunne, J. P., Gehlen, M., Ilyina, T., John,

- J. G., Lenton, A., Li, H., Lovenduski, N. S., Orr, J. C., Palmieri, J., Santana-Falcón, Y., Schwinger, J., Séférian, R., Stock, C. A., Tagliabue, A., Takano, Y., Tjiputra, J., Toyama, K., Tsujino, H., Watanabe, M., Yamamoto, A., Yool, A., and Ziehn, T.: Twenty-first century ocean warming, acidification, deoxygenation, and upper-ocean nutrient and primary production decline from CMIP6 model projections, *Biogeosciences*, 17, 3439–3470, <https://doi.org/10.5194/bg-17-3439-2020>, 2020.
- Laufkötter, C., Vogt, M., Gruber, N., Aita-Noguchi, M., Aumont, O., Bopp, L., Buitenhuis, E., Doney, S. C., Dunne, J., Hashioka, T., Hauck, J., Hirata, T., John, J., Le Quééré, C., Lima, I. D., Nakano, H., Seferian, R., Totterdell, I., Vichi, M., and Völker, C.: Drivers and uncertainties of future global marine primary production in marine ecosystem models, *Biogeosciences*, 12, 6955–6984, <https://doi.org/10.5194/bg-12-6955-2015>, 2015.
- Laufkötter, C., Zscheischler, J., and Frölicher, T. L.: High-impact marine heatwaves attributable to human-induced global warming, *Science*, 369, 1621–1625, <https://doi.org/10.1126/science.aba0690>, 2020.
- Le Grix, N.: Data used for creating the figures in “Compound high temperature and low chlorophyll extremes in the ocean over the satellite period” (Version 1) [Data set], Zenodo, <https://doi.org/10.5281/zenodo.4542015>, 2021.
- Leising, A., Schroeder, I., Bograd, S., Abell, J., Durazo, R., Gaxiola-Castro, G., CICESE, Bjorkstedt, E., Field, J., Sakuma, K., Robertson, R., Goericke, R., Peterson, W., Brodeur, R., Barceló, C., Auth, T., Daly, E., Suryan, R., Gladics, A., and Warzybok, P.: State of the California Current 2014–15: Impacts of the warm-water “Blob”, *CalCOFI Report* 56, 31–68, available at: <http://calcofi.org/publications/calcofireports/v56/Vol56-SOTCC.web.31-69.pdf> (last access: March 2021), 2015.
- Leonard, M., Westra, S., Phatak, A., Lambert, M., van den Hurk, B., McInnes, K., Risbey, J., Schuster, S., Jakob, D., and Stafford-Smith, M.: A compound event framework for understanding extreme impacts, *WIREs Clim. Change*, 5, 113–128, <https://doi.org/10.1002/wcc.252>, 2014.
- Marba, N. and Duarte, C. M.: Mediterranean warming triggers seagrass (*Posidonia oceanica*) shoot mortality, *Global Change Biol.*, 16, 2366–2375, <https://doi.org/10.1111/j.1365-2486.2009.02130.x>, 2010.
- McClain, C. R.: A Decade of Satellite Ocean Color Observations, *Annu. Rev. Mar. Sci.*, 1, 19–42, <https://doi.org/10.1146/annurev.marine.010908.163650>, 2009.
- Okumura, Y. and Deser, C.: Asymmetry in the Duration of El Niño and La Niña, *J. Climate*, 23, 5826–5843, <https://doi.org/10.1175/2010JCLI3592.1>, 2010.
- Oliver, E. C., Benthuyesen, J. A., Darmaraki, S., Donat, M. G., Hobday, A. J., Holbrook, N. J., Schlegel, R. W., and Gupta, A. S.: Marine Heatwaves, *Annu. Rev. Mar. Sci.*, 13, 313–342, <https://doi.org/10.1146/annurev-marine-032720-095144>, 2021.
- Oliver, E. C. J.: Mean warming not variability drives marine heatwave trends, *Clim. Dynam.*, 53, 1653–1659, <https://doi.org/10.1007/s00382-019-04707-2>, 2019.
- Oliver, E. C. J., Donat, M. G., Burrows, M. T., Moore, P. J., Smale, D. A., Alexander, L. V., Benthuyesen, J. A., Feng, M., Sen Gupta, A., Hobday, A. J., Holbrook, N. J., Perkins-Kirkpatrick, S. E., Scannell, H. A., Straub, S. C., and Wernberg, T.: Longer and more frequent marine heatwaves over the past century, *Nat. Commun.*, 9, 1324, <https://doi.org/10.1038/s41467-018-03732-9>, 2018.
- Piatt, J. F., Parrish, J. K., Renner, H. M., Schoen, S. K., Jones, T., Arimitsu, M. L., Kuletz, K. J., Bodenstern, B. L., García-Reyes, M., Duerr, R. S., Corcoran, R. M., Kaler, R. S. A., McChesney, G. J., Golightly, R. T., Coletti, H. A., Suryan, R. M., Burgess, H. K., Lindsey, J., Lindquist, K., Warzybok, P. M., Jahnce, J., Rolletto, J., and Sydeman, W. J.: Extreme mortality and reproductive failure of common murrelets resulting from the northeast Pacific marine heatwave of 2014–2016, *PLoS ONE*, 15, e0226087, <https://doi.org/10.1371/journal.pone.0226087>, 2020.
- Racault, M.-F., Sathyendranath, S., Brewin, R. J. W., Raitos, D. E., Jackson, T., and Platt, T.: Impact of El Niño Variability on Oceanic Phytoplankton, *Front. Mar. Sci.*, 4, 133, <https://doi.org/10.3389/fmars.2017.00133>, 2017.
- Reynolds, R. W., Smith, T. M., Liu, C., Chelton, D. B., Casey, K. S., and Schlax, M. G.: Daily High-Resolution-Blended Analyses for Sea Surface Temperature, *J. Climate*, 20, 5473–5496, <https://doi.org/10.1175/2007JCLI1824.1>, 2007.
- Ridder, N., Pitman, A., Westra, S., Ukkola, A., Do, H., Bador, M., Hirsch, A., Evans, J., Luca, A. D., and Zscheischler, J.: Global hotspots for the occurrence of compound events, *Nat. Commun.*, 11, 5956, <https://doi.org/10.1038/s41467-020-19639-3>, 2020.
- Rodrigues, R. R., Taschetto, A. S., Sen Gupta, A., and Foltz, G. R.: Common cause for severe droughts in South America and marine heatwaves in the South Atlantic, *Nat. Geosci.*, 12, 620–626, <https://doi.org/10.1038/s41561-019-0393-8>, 2019.
- Rousseaux, C. and Gregg, W.: Interannual Variation in Phytoplankton Primary Production at A Global Scale, *Remote Sens.*, 6, 1–19, <https://doi.org/10.3390/rs6010001>, 2014.
- Smale, D. A., Wernberg, T., Oliver, E. C. J., Thomsen, M., Harvey, B. P., Straub, S. C., Burrows, M. T., Alexander, L. V., Benthuyesen, J. A., Donat, M. G., Feng, M., Hobday, A. J., Holbrook, N. J., Perkins-Kirkpatrick, S. E., Scannell, H. A., Sen Gupta, A., Payne, B. L., and Moore, P. J.: Marine heatwaves threaten global biodiversity and the provision of ecosystem services, *Nat. Clim. Change*, 9, 306–312, <https://doi.org/10.1038/s41558-019-0412-1>, 2019.
- Thomson, J. A., Burkholder, D. A., Heithaus, M. R., Fourqurean, J. W., Fraser, M. W., Statton, J., and Kendrick, G. A.: Extreme temperatures, foundation species, and abrupt ecosystem change: an example from an iconic seagrass ecosystem, *Global Change Biol.*, 21, 1463–1474, <https://doi.org/10.1111/gcb.12694>, 2015.
- Tseng, Y.-H., Ding, R., and Huang, X.-M.: The warm Blob in the northeast Pacific – the bridge leading to the 2015/16 El Niño, *Environ. Res. Lett.*, 12, 054019, <https://doi.org/10.1088/1748-9326/aa67c3>, 2017.
- Walsh, J., Thoman, R., Bhatt, U., Bieniek, P., Brettschneider, B., Brubaker, M., Danielson, S., Lader, R., Fetterer, F., Holderied, K., Iken, K., Mahoney, A., McCammon, M., and Partain, J.: The High Latitude Marine Heat Wave of 2016 and Its Impacts on Alaska, *B. Am. Meteorol. Soc.*, 99, S39–S43, <https://doi.org/10.1175/BAMS-D-17-0105.1>, 2018.
- Wernberg, T., Smale, D., Tuya, F., Thomsen, M., Langlois, T., de Bettignies, T., Bennett, S., and Rousseaux, C.: An extreme climatic event alters marine ecosystem structure in a global biodiversity hotspot, *Nat. Clim. Change*, 3, 78–82, <https://doi.org/10.1038/nclimate1627>, 2013.

N. Le Grix et al.: Compound high-temperature and low-chlorophyll extremes in the ocean

2137

- Whitney, F. A.: Anomalous winter winds decrease 2014 transition zone productivity in the NE Pacific, *Geophys. Res. Lett.*, 42, 428–431, <https://doi.org/10.1002/2014GL062634>, 2015.
- Wilson, C. and Adamec, D.: A global view of biophysical coupling from SeaWiFS and TOPEX satellite data, 1997–2001, *Geophys. Res. Lett.*, 29, 98-1–98-4, <https://doi.org/10.1029/2001GL014063>, 2002.
- Zhang, Y., Wallace, J. M., and Battisti, D. S.: ENSO-like Interdecadal Variability: 1900–93, *J. Climate*, 10, 1004–1020, [https://doi.org/10.1175/1520-0442\(1997\)010<1004:ELIV>2.0.CO;2](https://doi.org/10.1175/1520-0442(1997)010<1004:ELIV>2.0.CO;2), 1997.
- Zscheischler, J. and Seneviratne, S. I.: Dependence of drivers affects risks associated with compound events, *Sci. Adv.*, 3, e1700263, <https://doi.org/10.1126/sciadv.1700263>, 2017.
- Zscheischler, J., Westra, S., van den Hurk, B. J. J. M., Seneviratne, S. I., Ward, P. J., Pitman, A., AghaKouchak, A., Bresch, D. N., Leonard, M., Wahl, T., and Zhang, X.: Future climate risk from compound events, *Nat. Clim. Change*, 8, 469–477, <https://doi.org/10.1038/s41558-018-0156-3>, 2018.
- Zscheischler, J., Martius, O., Westra, S., Bevacqua, E. R. C., Horton, R. M., van den Hurk, B., AghaKouchak, A., Jézéquel, A., Mahecha, M. D., Maraun, D., Ramos, A. M., Ridder, N., Thiery, W., and Vignotto, E.: A typology of compound weather and climate events, *Nat. Rev. Earth Environ.*, 1, 333–347, <https://doi.org/10.1038/s43017-020-0060-z>, 2020.

Chapter 4

Hotspots and drivers of compound marine heatwaves and low net primary production extremes

Natacha Le Grix, Jakob Zscheischler, Keith B. Rodgers, Ryohei Yamaguchi, and Thomas L. Frölicher

Published in *Biogeosciences*, Volume 19, 5807-5835, 2022. This chapter includes an Appendix and Bibliography

Biogeosciences, 19, 5807–5835, 2022
https://doi.org/10.5194/bg-19-5807-2022
© Author(s) 2022. This work is distributed under
the Creative Commons Attribution 4.0 License.



Hotspots and drivers of compound marine heatwaves and low net primary production extremes

Natacha Le Grix^{1,2}, Jakob Zscheischler^{1,2,3}, Keith B. Rodgers^{4,5}, Ryohei Yamaguchi^{4,5,6}, and Thomas L. Frölicher^{1,2}

¹Climate and Environmental Physics, Physics Institute, University of Bern, Bern, Switzerland

²Oeschger Centre for Climate Change Research, University of Bern, Bern, Switzerland

³Department of Computational Hydrosystems, Helmholtz Centre for Environmental Research – UFZ, Leipzig, Germany

⁴Center for Climate Physics, Institute for Basic Science, Busan, South Korea

⁵Pusan National University, Busan, South Korea

⁶Research Institute for Global Change, Japan Agency for Marine-Earth Science and Technology, Yokosuka, Japan

Correspondence: Natacha Le Grix (natacha.legrix@unibe.ch)

Received: 7 June 2022 – Discussion started: 20 June 2022

Revised: 10 November 2022 – Accepted: 15 November 2022 – Published: 16 December 2022

Abstract. Extreme events can severely impact marine organisms and ecosystems. Of particular concern are multivariate compound events, namely when conditions are simultaneously extreme for multiple ocean ecosystem stressors. In 2013–2015 for example, an extensive marine heatwave (MHW), known as the Blob, co-occurred locally with extremely low net primary productivity (NPPX) and negatively impacted marine life in the northeast Pacific. Yet, little is known about the characteristics and drivers of such multivariate compound MHW–NPPX events. Using five different satellite-derived net primary productivity (NPP) estimates and large-ensemble-simulation output of two widely used and comprehensive Earth system models, the Geophysical Fluid Dynamics Laboratory (GFDL) ESM2M-LE and Community Earth System Model version 2 (CESM2-LE), we assess the present-day distribution of compound MHW–NPPX events and investigate their potential drivers on the global scale. The satellite-based estimates and both models reveal hotspots of frequent compound events in the center of the equatorial Pacific and in the subtropical Indian Ocean, where their occurrence is at least 3 times higher (more than 10 d yr^{-1}) than if MHWs (temperature above the seasonally varying 90th-percentile threshold) and NPPX events (NPP below the seasonally varying 10th-percentile threshold) were to occur independently. However, the models show disparities in the northern high latitudes, where compound events are rare in the satellite-based estimates and GFDL ESM2M-LE (less than 3 d yr^{-1}) but relatively frequent in CESM2-LE.

In the Southern Ocean south of 60° S , low agreement between the observation-based estimates makes it difficult to determine which of the two models better simulates MHW–NPPX events. The frequency patterns can be explained by the drivers of compound events, which vary among the two models and phytoplankton types. In the low latitudes, MHWs are associated with enhanced nutrient limitation on phytoplankton growth, which results in frequent compound MHW–NPPX events in both models. In the high latitudes, NPPX events in GFDL ESM2M-LE are driven by enhanced light limitation, which rarely co-occurs with MHWs, resulting in rare compound events. In contrast, in CESM2-LE, NPPX events in the high latitudes are driven by reduced nutrient supply that often co-occurs with MHWs, moderates phytoplankton growth, and causes biomass to decrease. Compound MHW–NPPX events are associated with a relative shift towards larger phytoplankton in most regions, except in the eastern equatorial Pacific in both models, as well as in the northern high latitudes and between 35 and 50° S in CESM2-LE, where the models suggest a shift towards smaller phytoplankton, with potential repercussions on marine ecosystems. Overall, our analysis reveals that the likelihood of compound MHW–NPPX events is contingent on model representation of the factors limiting phytoplankton production. This identifies an important need for improved process understanding in Earth system models used for predicting and projecting compound MHW–NPPX events and their impacts.

1 Introduction

Warming and reduced primary productivity of organic matter by marine phytoplankton are considered to be two of the major potential stressors of open-ocean ecosystems, along with acidification and deoxygenation (Gruber, 2011; Bopp et al., 2013; Bindoff et al., 2019). Not only are marine ecosystems threatened by long-term decadal-scale changes in sea surface temperature (SST) (Cheng et al., 2017) and net primary productivity (NPP) (Boyce et al., 2010; Doney et al., 2012), they are also increasingly impacted by short-term extreme events, such as marine heatwaves (MHWs) (Wernberg et al., 2013; Frölicher and Laufkötter, 2018; Oliver et al., 2018) and extremely low NPP events (hereafter called “NPPX” events; Whitney, 2015; Cavole et al., 2016). An emerging concern is the occurrence of multivariate compound events, namely situations when multiple ecosystem stressors deviate from normal conditions simultaneously, in close spatial proximity or temporal succession (Leonard et al., 2014; Zscheischler et al., 2018, 2020). Together they may severely impact marine ecosystems (Boyd and Brown, 2015; Gruber et al., 2021). To date, the majority of studies have focused on compound events over land (e.g., Ridder et al., 2020; Zscheischler et al., 2020), with only a relatively small number of studies having addressed compound events in the ocean (Gruber et al., 2021; Shi et al., 2021; Le Grix et al., 2021; Mogen et al., 2022; Burger et al., 2022).

The combination of MHW and NPPX may cause severe impacts on marine organisms and ecosystems (Boyd and Brown, 2015; Le Grix et al., 2021). The “Blob” in the northeast Pacific stands as an example of such an impactful compound event. Between 2013 and 2015, the northeast Pacific experienced the most intense and longest-lasting MHW ever recorded, with maximum SST anomalies of more than 5 °C lasting for more than 350 d (Di Lorenzo and Mantua, 2016; Laufkötter et al., 2020). Along with anomalously low oxygen and high $[H^+]$ concentrations, the Blob coincided with large negative anomalies in phytoplankton NPP (Whitney, 2015; Gruber et al., 2021; Mogen et al., 2022), and it had severe impacts on marine life (Cavole et al., 2016), including extreme mortality and reproductive failure of sea birds (Jones et al., 2018; Piatt et al., 2020) and mass stranding of whales in the western Gulf of Alaska and of sea lions in California, not to mention shifts in species distribution towards warm-water species (Cavole et al., 2016; Cheung and Frölicher, 2020). Although not all compound MHW and NPPX events may lead to extreme consequences for marine organisms and ecosystems, they should at the very least be considered compound hazards (Ridder et al., 2022) and, as such, pose a threat that warrants further investigation.

In a previous study, Le Grix et al. (2021) characterized compound high-SST and low-chlorophyll events, with low chlorophyll assumed as a proxy for low phytoplankton biomass. Using satellite-derived chlorophyll and SST observations, they found hotspots of frequent compound events

in the equatorial Pacific, in the Indian Ocean, and along the borders of the subtropical gyres. In these regions, more than 10 compound-event days occurs per year. This is 3 to 7 times more often than expected under the assumption of independence between high-SST and low-chlorophyll events. The authors also showed that compound-event occurrence is strongly modulated over interannual timescales by large-scale modes of climate variability. An example is the El Niño–Southern Oscillation, whose positive phase is associated with increased occurrence of compound events in the eastern equatorial Pacific. Although the state of climate modes provides valuable information regarding the likelihood of compound events occurring, much remains to be learned regarding local physical and biological drivers of such compound events. Enhanced mechanistic understanding of these potentially harmful events in the ocean is crucial for building and improving the tools for their prediction and ultimately for adaptation and ecosystem management (Gruber et al., 2021).

Previous studies have investigated the drivers of MHWs, which can act on various spatial and temporal scales (e.g., Holbrook et al., 2019; Gupta et al., 2020; Oliver et al., 2021; Vogt et al., 2022). MHWs can be triggered through local processes affecting the temperature budget of the mixed layer such as air–sea heat fluxes, local vertical mixing, or advection (Gupta et al., 2020; Vogt et al., 2022), while MHWs can also be caused remotely through atmospheric or oceanic teleconnection processes (Bond et al., 2015; Holbrook et al., 2019). A number of studies have investigated phytoplankton variability using data derived from satellite ocean color (Boyce et al., 2010; Whitney, 2015; Gittings et al., 2018; J. S. Long et al., 2021). However, only a few studies have explored the drivers of NPPX events during MHWs. For example, Whitney (2015) shows that in winter 2013/14 during the Blob, anomalous winds weakened nutrient transport to the northeastern Pacific transition zone and decreased phytoplankton NPP, resulting in the lowest chlorophyll concentrations ever measured using satellite observations. Wyatt et al. (2022) suggest that nutrient limitation during MHWs generally reduces the biomass of small and large phytoplankton in the northeast Pacific transition zone. However, not all warming events are accompanied by NPPX events. For instance, J. S. Long et al. (2021) noted an increase in NPP during two recent MHWs in the northeast Pacific. Even though high SST may be associated with nutrient limitation on phytoplankton growth and with enhanced phytoplankton grazing, it also directly enhances phytoplankton growth (Laufkötter et al., 2015). Phytoplankton biology is indeed modulated by multiple interacting processes in the ocean, rendering it a complex task to identify drivers of any extreme change in NPP. As data derived from satellite observations can be sparse, biased, or uncertain (Behrenfeld et al., 2005; J. S. Long et al., 2021) and limited to recent decades, multiple simulations from Earth system models that include a biological component in the

ocean appear to be a useful tool to improve our lack of understanding of NPP variability and extremes.

Extreme events are rare by definition, and compound extreme events occur even less frequently. Understanding compound MHW–NPPX events from a statistical point of view requires therefore large datasets from which to sample numerous combinations of extremely high SST and extremely low NPP. Over our period of interest (i.e., satellite period 1998–2018) both extremes rarely co-occur together. In this context, large-ensemble simulations (LES) with climate models (Frölicher et al., 2009; Deser et al., 2020) provide an invaluable tool for advancing our understanding of compound events. LES are created with a single climate model under a particular historical or future radiative-forcing scenario by applying perturbations to the initial conditions of each member in order to create diverging climate trajectories. LES provide the necessary large datasets from which to infer the uncertainty in the likelihood of compound events. Here, we use LES from two global coupled climate Earth system models, the Geophysical Fluid Dynamics Laboratory (GFDL) ESM2M and Community Earth System Model version 2 (CESM2), to investigate compound MHW–NPPX events.

The principal objectives of our study are to identify hotspots of compound MHW–NPPX events, to assess the fidelity of both Earth system models in simulating MHW–NPPX events, and to gain mechanistic insights into processes driving these compound events, to thereby enhance our capacity to better project the occurrence of such events into the future. We focus on the satellite period (1998–2018) over which we have satellite-based data of NPP.

2 Methods

2.1 Observation-based data

We use SST data from NOAA's daily high-resolution Optimum Interpolation SST (OISST) analysis product with a horizontal resolution of 0.25° latitude \times 0.25° longitude (Reynolds et al., 2007; Banzon et al., 2016). This observation-based data product provides a high-quality daily global record of surface ocean temperature obtained from satellites, ships, buoys, and Argo floats on a regular grid. Its main input is infrared satellite data from the Advanced Very High Resolution Radiometer with high temporal–spatial coverage spanning late 1981 to the present. Any large-scale satellite biases relative to in situ data from ships and buoys are corrected, and any gaps are filled in by interpolation.

We use five different satellite-based estimates of NPP. The first is calculated by the NASA Ocean Biogeochemical Model (NOBM) (Gregg and Rousseaux, 2017; Gregg and Casey, 2007), a comprehensive ocean biogeochemical model coupled to a global ocean circulation and radiative model, which assimilates satellite ocean color data

from the Sea-viewing Wide Field-of-view Sensor (SeaWiFS), the Moderate Resolution Imaging Spectroradiometer (MODIS) aboard Aqua, and the Visible Infrared Imaging Radiometer Suite (VIIRS) to constrain NPP estimates over the mixed layer. The four other NPP datasets are based on the Vertically Generalized Production Model (VGPM) (Behrenfeld et al., 2005), which estimates NPP within the euphotic layer from chlorophyll or phytoplankton carbon concentrations, available light, and a temperature-dependent description of photosynthetic efficiency. The four versions of this model are Standard VGPM, Eppley-VGPM, CbPM-VGPM, and CAFE-VGPM (<http://sites.science.oregonstate.edu/ocean.productivity/index.php>, last access: 30 November 2021). The only difference between Standard VGPM (Behrenfeld and Falkowski, 1997) and Eppley-VGPM is the temperature-dependent description of photosynthetic efficiencies: Standard VGPM uses a polynomial function of temperature, while Eppley-VGPM uses the exponential function described by Eppley (1972). Instead of deriving phytoplankton biomass from surface chlorophyll, the Carbon-based Production Model (CbPM; Behrenfeld et al., 2005; Westberry et al., 2008) estimates phytoplankton carbon concentrations using coefficients of particulate scattering. And finally, CAFE-VGPM refers to the Carbon, Absorption, and Fluorescence Euphotic-resolving (CAFE) model (Silsbe et al., 2016), which calculates NPP as the product of energy absorption and the efficiency by which absorbed energy is converted into carbon biomass. VGPM-based models also use SeaWiFS, MODIS, or VIIRS data. Figure B1a–j in the Appendix provide the temporal mean and standard deviation of each observation-based NPP product. We chose to include all five observation-based NPP products as NPP estimates by models assimilating satellite data are still uncertain and highly sensitive to their respective model configurations (e.g., Behrenfeld et al., 2005; J. S. Long et al., 2021).

The SST and all satellite-derived NPP data used in this study are regridded to the coarser NOBM grid resolution of 1.25° longitude by $2/3^\circ$ latitude for the period 1998 to 2018 before the analysis. The NOBM-based NPP product has a 5 d resolution, whereas the four VGPM-based NPP products have an 8 d resolution. From daily SST, we computed and used the 5 d mean SST when working with the 5 d mean NOBM-based NPP products and the 8 d mean SST when working with VGPM-based NPP. As NPP is close to or equal to zero during winter in the polar regions when solar radiation is near zero, we follow the approach of Le Grix et al. (2021) and remove all days during which a particular grid cell receives no solar radiation, thereby focusing on the growing season. The daily shortwave radiation data were obtained from the Modern-Era Retrospective analysis for Research and Applications version 2 (Gelaro et al., 2017).

2.2 Model descriptions and large-ensemble simulations

We use two global fully coupled Earth system models (ESMs): GFDL's ESM2M and CESM2. ESM2M is a fully coupled carbon–climate ESM developed at NOAA's Geophysical Fluid Dynamics Laboratory (GFDL) (Dunne et al., 2012, 2013). It couples an atmospheric circulation model to an oceanic circulation model and includes representations of land, sea ice, and iceberg dynamics, as well as interactive biogeochemistry. The atmospheric model AM2 (The GFDL Global Atmospheric Model Development Team, 2004) has a horizontal resolution of 2° latitude \times 2.5° longitude and 24 vertical levels. The horizontal resolution of the ocean model MOM4p1 (Griffies, 2012) is nominally 1° latitude \times 1° longitude with increasing meridional resolution of up to $1/3^\circ$ towards the Equator, with 50 depth levels. Phytoplankton is represented in ESM2M by the biogeochemical module “Tracers of Ocean Phytoplankton with Alometric Zooplankton version 2.0” (TOPAZv2; Dunne et al., 2013), consisting of 30 tracers including three phytoplankton groups (small and large phytoplankton, diazotrophs) and heterotrophic biomass (see Sect. 2.4 for further details). TOPAZv2 only implicitly simulates zooplankton activity. The large-ensemble simulation ESM2M-LE was started from a quasi-equilibrated 500-year-long preindustrial control simulation, where atmospheric CO_2 concentrations are set to 286 ppm (Burger et al., 2020). We generated an ensemble of 15 members by slightly perturbing the temperature on the order of 10^{-5}°C for five ensemble members at a grid cell at the surface of the Weddell Sea, for five members at the surface of the North Atlantic and for five members in the deep North Pacific (Burger et al., 2022). These 15 simulations were forced with prescribed historical concentrations of atmospheric CO_2 and non- CO_2 radiative-forcing agents from 1861 to 2005 and then by following a high-emission no-mitigation scenario (RCP8.5; RCP: Representative Concentration Pathway) from 2006 to 2100 (Riahi et al., 2011).

The Community Earth System Model version 2 (CESM2; Danabasoglu et al., 2020) is also a fully coupled ESM. It couples an atmospheric model with comprehensive chemistry to ocean, land, sea-ice, land-ice, river, and ocean wave models. The horizontal resolution of the atmospheric model CAM6 (Danabasoglu et al., 2020) is 0.9° latitude \times 1.25° longitude, with 32 vertical levels. The horizontal resolution of the ocean model POP2 (Smith and Gent, 2010) is approximately 1° , with uniform spacing of 1.125° in the zonal direction and varying significantly in the meridional direction, with the finest resolution of $\sim 0.25^\circ$ at the Equator. The ocean model has 60 vertical levels. The “Marine Biogeochemistry Library” (MARBL; M. C. Long et al., 2021) is the biogeochemical component of CESM2, which includes three phytoplankton types: small phytoplankton, diatoms (i.e., large phytoplankton), and diazotrophs. It is a prognostic ocean biogeochemistry model that simulates marine-ecosystem interactions and the coupled cycles of carbon, nitrogen, phos-

phorus, iron, silicon, and oxygen. We use nine members of a 100-member large-ensemble simulation (CESM2-LE; Rodgers et al., 2021) in this study, for which all necessary 5 d mean data for the analysis were available. All members differ by their starting day, sampled at 20-year intervals from a preindustrial control simulation (Rodgers et al., 2021). Historical simulations were run from 1850 to 2014, forced by prescribed atmospheric CO_2 concentrations and non- CO_2 radiative-forcing agents. Projections from 2015 to 2100 follow the SSP3-7.0 (SSP: Shared Socioeconomic Pathway) scenario (Eyring et al., 2016).

Aside from differences in their physical ocean and atmosphere modules, ESM2M and CESM2 differ in their ocean biogeochemical module and how the latter computes phytoplankton growth and decay (see Appendix A for a detailed description and comparison). For example in ESM2M, TOPAZv2 uses an Eppley function of temperature to represent the dependence of phytoplankton growth on temperature, whereas in CESM2, MARBL uses a power function following a Q_{10} model (Sherman et al., 2016), resulting in weaker dependence of phytoplankton growth on temperature in CESM2. Although both models represent the nutrient limitation on phytoplankton growth according to Michaelis–Menten kinetics, MARBL uses lower half-saturation constants for each nutrient than TOPAZv2. In addition to these differences, ESM2M-LE is forced by RCP8.5 after 2006, whereas CESM2-LE is forced by SSP3-7.0 after 2015. However, the different forcings applied do not impact our results, as the total radiative forcing of the two scenarios differ very little before the year 2018 (Riahi et al., 2017), which is the end point of our analysis period.

For both ESM2M-LE and CESM2-LE, we select the historical period spanning from 1998 to 2018, over which we can compare the simulations to available satellite-derived observations of SST and NPP. Outputs are saved at a 5 d mean resolution. They include SST, NPP, and all variables from which we analyze the drivers of NPP – phytoplankton biomass, growth, and loss terms (i.e., grazing of phytoplankton by zooplankton in ESM2M, grazing, mortality, and aggregation in CESM2) – as well as the temperature, light, and nutrient limitations on phytoplankton growth. These variables are saved at a 10 m vertical resolution. We integrate the phytoplankton NPP, biomass, and loss terms over the upper 100 m layer of the ocean and compute biomass-weighted averages of phytoplankton growth and of its limitation terms by multiplying these variables with the biomass at each depth level, computing the vertical mean over the top 100 m and dividing by the vertical mean biomass. Similarly to for the observation-based products, we focus on the growing season by removing all calendar days receiving no solar radiation (Gelaro et al., 2017).

2.3 Definition of compound MHW–NPPX events

We subtract from each time series its mean seasonal cycle, which we smoothed to remove noise associated with the relatively short time series. For the observations, the smoothed seasonal cycle was obtained using a 30 d running average, and for ESM2M-LE and CESM2-LE, it was identified using their respective ensemble mean seasonal cycle. As we work with de-seasonalized anomalies, compound events can occur throughout the year. At each grid cell, an MHW occurs when the SST anomaly exceeds its local 90th percentile. An NPPX event occurs when the NPP anomaly is lower than its 10th percentile. There are pros and cons to using a relative threshold compared to using an absolute threshold. Certain marine species might only be negatively impacted by MHWs and NPPX events once an absolute SST or NPP threshold is reached. Still, given our limited knowledge of marine-ecosystem response to extremes, especially to NPPX events, we decided to align with the common definition of MHWs in recent literature; i.e., we define extreme events relative to the seasonal cycle (Hobday et al., 2016). Thereby, we identify MHWs and NPPX events that would potentially impact all marine ecosystems vulnerable to extreme deviations from the seasonally varying climatology.

A multivariate compound MHW–NPPX event occurs when MHW and NPPX conditions are satisfied at the same time and location. Following this definition where no duration threshold is applied, extreme events can be as short as one time step, which here is a 5 d mean.

We use a relatively low threshold to define MHWs and NPPX events so as to capture enough compound MHW–NPPX events in the relatively short 1998–2018 time period over which NPP observations are available. Due to their definition, univariate extreme events have the same frequency over the global ocean. At each grid cell, 10 % of all time steps are MHWs and 10 % are NPPX events. This implies that under the assumption of independence between MHW and NPPX events, the frequency of compound MHW–NPPX events would be 1 % over the global ocean. Compound MHW–NPPX events can be considered unexpectedly frequent or infrequent over all regions where their frequency is not equal to 1 %, which indicates potential dependences between the drivers of MHWs and NPPX events. In our case, the frequency of compound events is equivalent to the likelihood multiplication factor, i.e., a measure of how many times more frequent compound events are compared to their expected frequency under the assumption of independence (Zscheischler and Seneviratne, 2017; Le Grix et al., 2021; Woolway et al., 2021; Burger et al., 2022).

2.4 Model evaluation

The Taylor diagrams presented in Fig. 1 provide a summary of the relative skill with which the models simulate the mean of and variability in SST and NPP as well as the extreme

event magnitude (i.e., mean SST and NPP anomalies during extreme events relative to their climatological mean values) and duration of MHWs and NPPX events. The simulated patterns of the mean state of SST by ESM2M-LE and CESM2-LE are very similar to that computed from the observation-based SST ($r > 0.99$ and normalized SD ~ 1 , red point and cross in Fig. 1a). CESM2-LE is slightly better than ESM2M-LE at simulating the pattern of temporal variability in SST ($r = 0.8$ for ESM2M-LE and $r = 0.9$ for CESM2-LE, Fig. 1b). The globally integrated NPP is 74 Pg C yr^{-1} in ESM2M-LE and 43 Pg C yr^{-1} in CESM2-LE, compared to 53 Pg C yr^{-1} on average (range of 46 to 62 Pg C yr^{-1}) in the observation-based estimates (Fig. B1). ESM2M-LE substantially overestimates NPP, especially in the low latitudes where the simulated NPP exceeds $1000 \text{ mg C m}^{-2} \text{ d}^{-1}$ compared to the observation-based estimate of about 400– $800 \text{ mg C m}^{-2} \text{ d}^{-1}$. Despite these differences, ESM2M-LE and CESM2-LE succeed in representing the NPP mean spatial pattern of higher values in the low latitudes and lower values in the subtropical gyres and in the Southern Ocean. These results are summarized in Fig. 1a, where the different observation-based NPP products are as dispersed as ESM2M-LE and CESM2-LE themselves, indicating that the models are approximately within the range of the observations. The NPP temporal variability simulated by the two models is also similar to that estimated by the observation-based products (Figs. 1b and B1, right column), although the models underestimate the spatial heterogeneity in the NPP temporal variability pattern (normalized SD < 0.25).

The MHW magnitudes identified from the satellite-based observations are similar to those simulated by ESM2M-LE and CESM2-LE (Figs. 1c and B2a–c). However, both models simulate MHWs that last longer than those in the observations (Fig. B2d–f), especially in the eastern equatorial Pacific. This is a common bias across all current global Earth system models (Frölicher et al., 2018), irrespective of their vertical and horizontal resolution (Pilo et al., 2019). The spatial pattern of MHW duration is reasonably well simulated in both models (Fig. 1d). In contrast, the models differ in their representation of NPPX events (Figs. 1c–d and B3). The observation-based mean NPPX magnitude is most intense ($< 250 \text{ mg C m}^{-2} \text{ d}^{-1}$) in the tropical Atlantic Ocean and in the northern high latitudes, whereas the magnitude is most intense in ESM2M-LE in the equatorial Pacific and in the Indian Ocean and in CESM2-LE in the northern high latitudes and in the Southern Ocean. Given the low agreement between the observation-based NPP products (Fig. 1c), it is difficult to assess how well ESM2M-LE and CESM2-LE simulate the magnitude of NPPX events and which of the two models is more realistic. We also compare the 90th percentile of the duration of NPPX events (Fig. 1d) to highlight differences between the observations and the models even though their observed and simulated median duration is close to 5 d over the global ocean due to the predominance of short NPPX events. In the observations, NPPX events reach

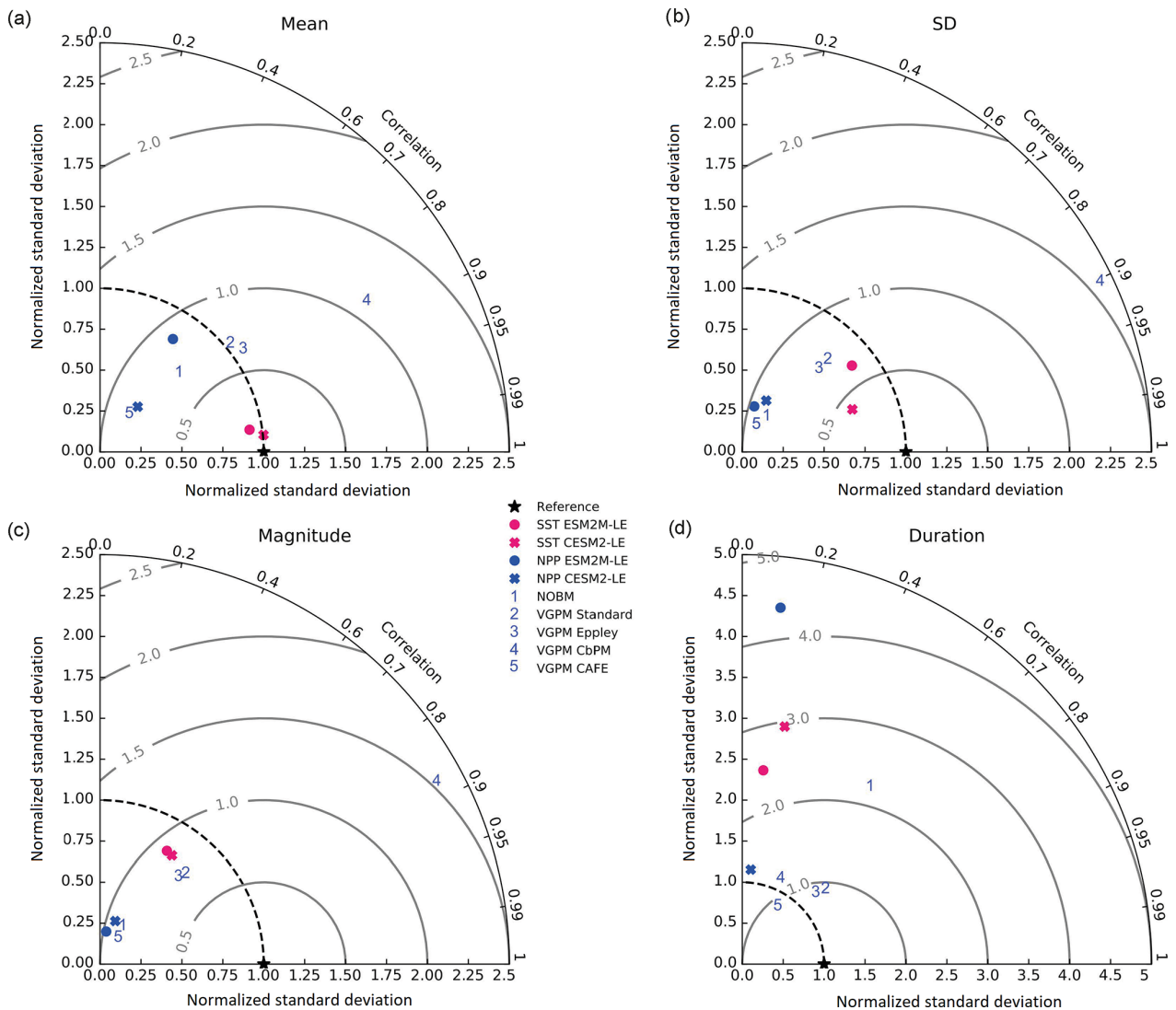


Figure 1. Comparative assessment of the simulated mean and extreme states of SST and NPP and an observed reference. These Taylor diagrams compare the spatial pattern of the climatological mean state (a) and standard deviation (b) of 5 d mean SST and NPP, as well as of the magnitude (c) and 90th percentile of the duration (d) of MHWs and NPPX events, simulated by each model to that of a reference. The reference is calculated from the observation-based SST estimate or from the mean of the five different observation-based NPP estimates, and it is indicated by a star on the diagrams. A circle; a triangle; and the numbers 1, 2, 3, 4, and 5 represent ESM2M-LE, CESM2, NOBM, Standard VGPM, Eppley-VGPM, CbPM-VGPM, and CAFE-VGPM, respectively. The Pearson correlation coefficient, which quantifies similarity between the simulated pattern and the reference, is indicated by the azimuthal angle; the centered RMSE in the simulated field is proportional to the distance from the star on the x axis; and the standard deviation of the simulated pattern is indicated by the radial distance from the origin. All statistics are normalized by the standard deviation of the reference.

their longest durations (> 70 d) in the central equatorial Pacific (Fig. B3d). The spatial patterns simulated by the models for the NPPX event duration differ from that of the observed reference ($r < 0.2$ for ESM2M-LE and for CESM2-LE, Fig. 1d). In ESM2M-LE, the longest events (> 90 d) occur within the subtropical gyres, where NPP anomalies do not vary much over time (Fig. B3e, normalized and centered RMSE = 4.3 in Fig. 1d). Longer NPPX durations in

ESM2M-LE compared to observations might arise from an overestimation of durations in the non-eddy ocean models, which might fail to capture short-lived extremes associated with mesoscale and submesoscale processes. However, it might also be explained by an underestimation of durations in the observations due to gaps in satellite observations. In contrast, in CESM2-LE, events are of short duration over

most of the global ocean and slightly longer (> 30 d) in the high latitudes and in the eastern equatorial Pacific (Fig. B3f).

Overall, ESM2M-LE and CESM2-LE represent the mean state of and variability in SST reasonably well. Their representation of NPP diverges from observations, yet the reference for NPP observation in Fig. 1 is computed as the mean of five observation-based NPP products which themselves disagree (Fig. B1), although the spatial pattern of the mean state of and variability in NPP is broadly similar across products. Considering that both ESM2M-LE and CESM2-LE capture this spatial pattern, they appear suited to investigating the likelihood and drivers of compound MHW–NPPX events over the global ocean. However, divergent magnitudes and durations of NPPX events in ESM2M-LE and CESM2-LE hint at different drivers for NPPX events in the two models. Different processes might thus drive NPPX in association with an MHW and result in a compound MHW–NPPX event in ESM2M-LE and CESM2-LE.

2.5 Driver decomposition of compound MHW–NPPX events

We investigate the drivers of compound MHW–NPPX events and more specifically the drivers of extreme reductions in NPP during MHWs. Both ESM2M and CESM2 contain an ecological module distinguishing between three different phytoplankton types (small, large, and diazotrophs), for which specific constants and limitation terms are used to compute NPP. Total net phytoplankton production is simply the sum of NPP over all three phytoplankton types. Thus, during a low-NPP event, although the total phytoplankton NPP is extremely low, not all types may have contributed to that anomaly. We ignore the diazotrophs in this study as their contribution to total NPP (1.5 % in ESM2M-LE and 3 % in CESM2-LE on average) and to the total NPP anomaly during compound MHW–NPPX events (< 0.1 % in ESM2M-LE and CESM2-LE) is negligible. Thus, in each model, total NPP is approximated as the sum of small- and large-phytoplankton NPP.

For each phytoplankton type i , NPP is the product of its growth rate μ and its biomass n :

$$\text{NPP}_i = \mu_i n_i. \quad (1)$$

Therefore, any anomaly in NPP, dNPP, can be decomposed as

$$\text{dNPP}_i = n_i \text{d}\mu_i + \mu_i \text{d}n_i. \quad (2)$$

If dNPP stands for the mean NPP anomaly during compound events relative to the climatological mean state of the seasonal cycle, we can assess the contributions of the mean growth anomaly, $\text{d}\mu$, and of the mean biomass anomaly, $\text{d}n$, during compound events to dNPP.

TOPAZv2 and MARBL define μ in the same way:

$$\mu_i = \mu_{\max_i} T_f L_{\text{lim}_i} N_{\text{lim}_i}, \quad (3)$$

where T_f is a function of the temperature, L_{lim} is the light limitation, and the nutrient limitation N_{lim} is computed using Liebig's law of the minimum. More details are provided in Appendix A. Both N_{lim} and L_{lim} are between 0 and 1, where 1 means they do not limit phytoplankton growth and 0 means they fully suppress growth. Figure B4 in the Appendix presents the climatological mean states of T_f , L_{lim} , and N_{lim} .

$\text{d}\mu$ can be decomposed into the contributions of a change in T_f , L_{lim} , and N_{lim} during compound events.

$$\begin{aligned} \text{d}\mu_i = \mu_{\max_i} & (N_{\text{lim}_i} L_{\text{lim}_i} \text{d}T_f + N_{\text{lim}_i} T_f \text{d}L_{\text{lim}_i} \\ & + T_f L_{\text{lim}_i} \text{d}N_{\text{lim}_i}) \end{aligned} \quad (4)$$

This decomposition enables us to assess the drivers of a change in phytoplankton growth during compound events. Drivers of a change in phytoplankton biomass n are less trivial as n depends on NPP itself. In TOPAZv2 and MARBL, n is considered a tracer whose time derivative is defined as follows:

$$\partial_t n_i = \text{NPP}_i - \text{Loss}_i + \text{Circ}_i, \quad (5)$$

where NPP and Loss are the biological production and decay of phytoplankton, respectively, and Circ corresponds to the physical advection and mixing of phytoplankton by ocean circulation. The model equations only hold at the time and vertical resolution of model computations, i.e., at 2 h and 10 m resolution. Here we use 5 d mean output and data averaged over the top 100 m layer. Therefore, Eq. (5) becomes

$$\partial_t n_i = \text{NPP}_i - \text{Loss}_i + \text{Circ}_i + \text{Errors}_i. \quad (6)$$

Given that we do not have the necessary output to compute the circulation term, we cannot assess how small Errors is, and therefore we cannot neglect it.

Over time, biomass changes build up a biomass anomaly $\text{d}n$ that might be sufficient to drive or contribute to driving extremely low dNPP. In this study, we intend to explain the contribution of $\text{d}n$ to dNPP during compound MHW–NPPX events using Eq. (6). A positive or negative biomass anomaly during a compound event may be explained by an overall increase or decrease in biomass over time, until the largest biomass anomaly reached during the compound event. Therefore, we integrate $\partial_t n$, NPP, and Loss over all periods over which $\text{d}n$ builds up, i.e., over which n changes from its climatological mean value (at t_0 , $n_i(t_0) = 0$) to its maximum absolute anomaly relative to the climatology reached during a compound event (at t_{\max} , $n_i(t_{\max}) = n_{i\max}$). Δn refers to the integrated biomass change between t_0 and t_{\max} , which corresponds to the largest biomass anomaly reached during a compound event. Note that Δn is not exactly equivalent to $\text{d}n$. Δn is a tool to understand the buildup

of the largest biomass anomaly reached during a compound event, whereas dn is the mean biomass anomaly over all compound-event days.

$$\Delta n_i = \int_{t_0}^{t_{\max}} \partial_t n_i dt = \int_{t_0}^{t_{\max}} (\text{NPP}_i - \text{Loss}_i) dt + \int_{t_0}^{t_{\max}} (\text{Circ}_i + \text{Errors}_i) dt \quad (7)$$

$$\Delta n_i = \int_{t_0}^{t_{\max}} \partial_t n_i dt = \int_{t_0}^{t_{\max}} (\text{NPP}_i - \text{Loss}_i) dt + \text{Residual}_i \quad (8)$$

The term $\int_{t_0}^{t_{\max}} (\text{NPP}_i - \text{Loss}_i) dt$ accounts for the contribution of biological processes to Δn , whereas Residual includes both the contribution of ocean circulation to Δn and all errors inherent to the decomposition using 5 d mean and vertically integrated output. Results are averaged over all compound events. In theory, this method could enable us to apprehend the contribution of biological processes to dn . However, errors in the decomposition might be substantial and result in a poor estimation of that contribution. Further work with more highly temporally and spatially resolved model output is needed to fully decompose the biomass changes during compound MHW–NPPX events into its drivers.

Details on the computation of phytoplankton loss are provided in Sect. A1.5 for TOPAZv2 and Sect. A2.5 for MARBL, and Fig. B5 presents the climatological mean states of NPP, Loss, n , and μ .

3 Results

3.1 Hotspots of compound MHW–NPPX events in the global ocean

Figure 2 shows the present-day distribution of compound MHW–NPPX events. Under the assumption of independence between MHW and NPPX events, the expected frequency of compound MHW–NPPX events is 1 % of time intervals or 3.65 d yr^{-1} over the global ocean (Sect. 2.3). However, observation-based estimates show strong regional deviations from this expected frequency (Fig. 2a). Most compound events occur in the low latitudes, with hotspots of especially high frequency in the center of the equatorial Pacific, in the subtropical Indian Ocean, and around Antarctica. In these regions, compound MHW–NPPX events occur more than 3 times more frequently ($> 3 \%$ or $> 10 \text{ d yr}^{-1}$) than would be expected if univariate extremes were independent. Compound MHW–NPPX events are also relatively frequent (about 2 % or 7 d yr^{-1}) in the low to middle latitudes between 10 and 45° . In contrast, compound events are rare (about 0.5 % or 2 d yr^{-1}) in the high northern latitudes

north of 45° N and between 45 and 60° S in the Southern Ocean. However, these estimates correspond to the mean of the results obtained from five observation-based NPP products, which disagree particularly in the high southern latitudes and somewhat in the low latitudes (Figs. 2d and B6). Around Antarctica, the frequency computed using NOBM's NPP is much lower on average (0.5 %) than those computed using VGPM-based NPP products ($> 4 \%$). Sea ice and clouds create gaps in the satellite ocean color data that are potentially more extended in time and space around Antarctica than over the rest of the global ocean. Sparse satellite data coverage implies that in NOBM, fewer ocean color observations are available to constrain NPP estimates, whereas in VGPM-based models, gaps are filled by interpolation with data points that might be too distant in space and time to yield a realistic estimate of NPP (Rousseaux and Gregg, 2014; http://orca.science.oregonstate.edu/gap_fill.php, last access: 21 October 2021). For this reason, we have lower confidence in the NOBM and VGPM-based NPP products around Antarctica than elsewhere. In the low to middle latitudes, the frequency computed using Standard VGPM is higher than that of all other observation-based estimates (Fig. 2d). Standard VGPM is the only model that uses a polynomial function to describe the temperature dependence of photosynthesis. Therefore, extremely hot surface waters in the warm low to middle latitudes have a weaker positive effect on photosynthesis and thus on NPP in Standard VGPM than in the other observation-based products. It may thereby be easier for high SST to co-occur with low NPP, resulting in higher frequency of compound MHW–NPPX events in Standard VGPM in the low to middle latitudes.

Next, we compare the simulated frequency of compound MHW–NPPX events in ESM2M-LE (Fig. 2b) and CESM2-LE (Fig. 2c) to the observation-based frequency (Fig. 2a, d). Overall, the simulated frequency pattern is similar in the two models and mostly within the uncertainty range of the observational products (e.g., areas with no stippling in Fig. 2b and c, corresponding to 84 % of the global ocean in ESM2M-LE and to 82 % in CESM2-LE). The models correctly simulate frequent compound MHW–NPPX events in the equatorial Pacific ($> 4 \%$ or $> 14 \text{ d yr}^{-1}$) and relatively frequent compound events in the low to middle latitudes between 10 and 45° (2 % or 7 d yr^{-1} ; Fig. 2a–c). ESM2M-LE simulates too frequent compound events in the southern tropical Atlantic, in the center of the equatorial Pacific, and in the northern part of the Indian Ocean. CESM2-LE simulates too frequent compound events in the western equatorial Pacific and in the northern part of the Indian Ocean. In spite of there being relatively few dissimilarities between models and observations in the low and middle latitudes, they strongly disagree in the high latitudes. ESM2M-LE slightly outperforms CESM2-LE, especially in the northern high latitudes, where it simulates rare compound events consistent with the observation-based estimates, whereas CESM2-LE simulates too frequent compound events ($> 1 \%$). Around Antarctica,

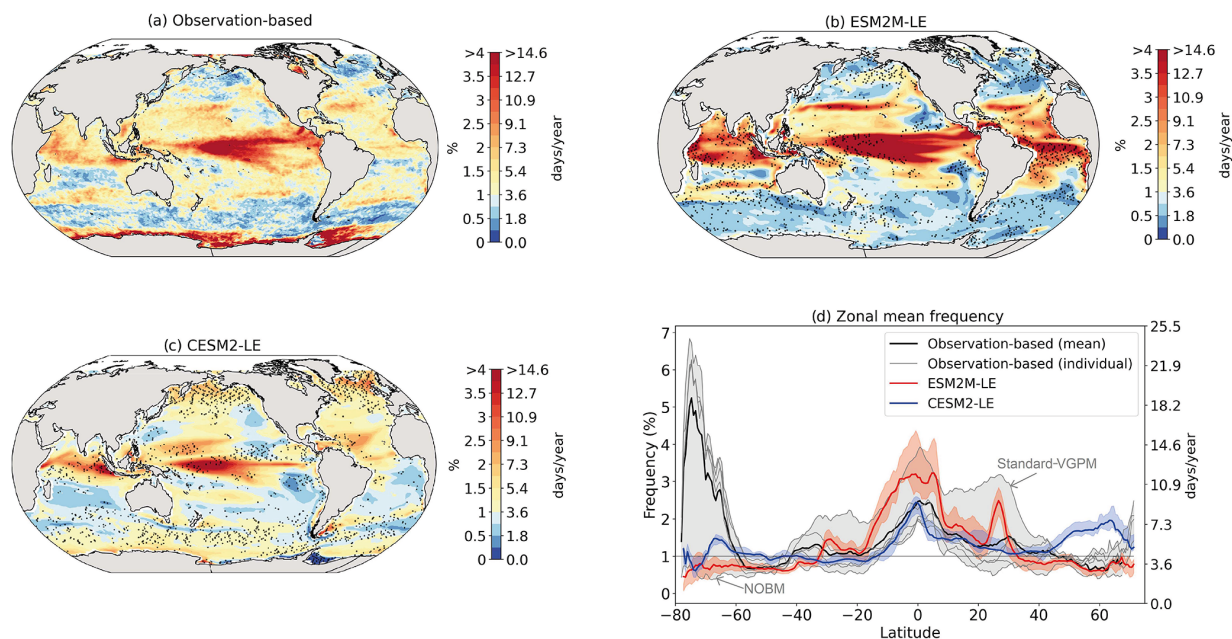


Figure 2. Frequency of compound MHW–NPPX events in (a) observation-based estimates and as simulated by (b) ESM2M-LE and (c) CESM2-LE. Observations correspond to the mean of the results obtained with five satellite-based estimates of NPP, namely NOBM, Standard VGPM, Eppley-VGPM, CbPM-VGPM, and CAFE-VGPM. (d) Zonal mean frequency of compound MHW–NPPX events. The gray-, red-, and blue-shaded areas in (d) indicate the range of the observation-based estimates, of the ESM2M-LE members, and of the CESM2-LE members, respectively. Stippling in (b) and (c) corresponds to regions where the frequency simulated by ESM2M-LE and CESM2-LE is outside the range of the observation-based estimates, i.e., higher or lower than all five observation-based estimates.

neither ESM2M-LE nor CESM2-LE simulates the very frequent compound MHW–NPPX events shown in the observations. However, low agreement between the five observation-based estimates (their frequency being as low as 0.5 % and as high as 6.5 % on average at 75° S, in Fig. 2d) makes it difficult to determine which of the two models better simulates compound events in this regions.

3.2 Small- and large-phytoplankton NPP anomalies during compound MHW–NPPX events

Next, we assess which phytoplankton type is responsible for NPPX during compound MHW–NPPX events. In both models, total NPP is approximately equal to the sum of small- and large-phytoplankton NPP (Sect. 2.5), whose respective mean anomalies (relative to the mean seasonal cycle) during compound MHW–NPPX events are presented in Fig. 3a–d.

The decrease in small-phytoplankton NPP dominates the overall decrease in NPP during compound MHW–NPPX events in both models, although the models differ in the magnitude and spatial pattern of anomalies in small and large phytoplankton. The decrease in small-phytoplankton NPP accounts for 79 % and 70 % of the total NPPX anomalies in the global ocean during MHW–NPPX events in ESM2M-LE and CESM2-LE, respectively (Fig. 3a, c). Especially pronounced is the dominance of small-phytoplankton NPP

decreases in the low to middle latitudes and the Southern Ocean in both models. This implies a shift in the phytoplankton community composition from small phytoplankton towards more large phytoplankton during MHW–NPPX events in these regions, with potential repercussions for marine community structure. In both models, decreases in large-phytoplankton NPP dominate the NPP decrease during MHW–NPPX events in the eastern equatorial Pacific. Large-phytoplankton NPP also decreases during MHW–NPPX events in the northern high latitudes. In CESM2-LE, the decline in large-phytoplankton NPP even dominates the response in the northern high latitudes as small-phytoplankton NPP increases, resulting in an assemblage shift towards smaller phytoplankton there. In addition, the decline in large-phytoplankton NPP also dominates along the southern boundaries of the subtropical gyres in the Southern Hemisphere in CESM2-LE. Overall, these patterns resemble well the climatological mean state pattern of small- and large-phytoplankton NPP (Figs. 3a–d and B5a–d). Small-phytoplankton anomalies during MHW–NPPX events dominate in regions where the climatological mean state of small-phytoplankton NPP generally dominates, whereas large-phytoplankton NPP anomalies play an important role during MHW–NPPX events where the climatological mean state of large-phytoplankton NPP generally dominates.

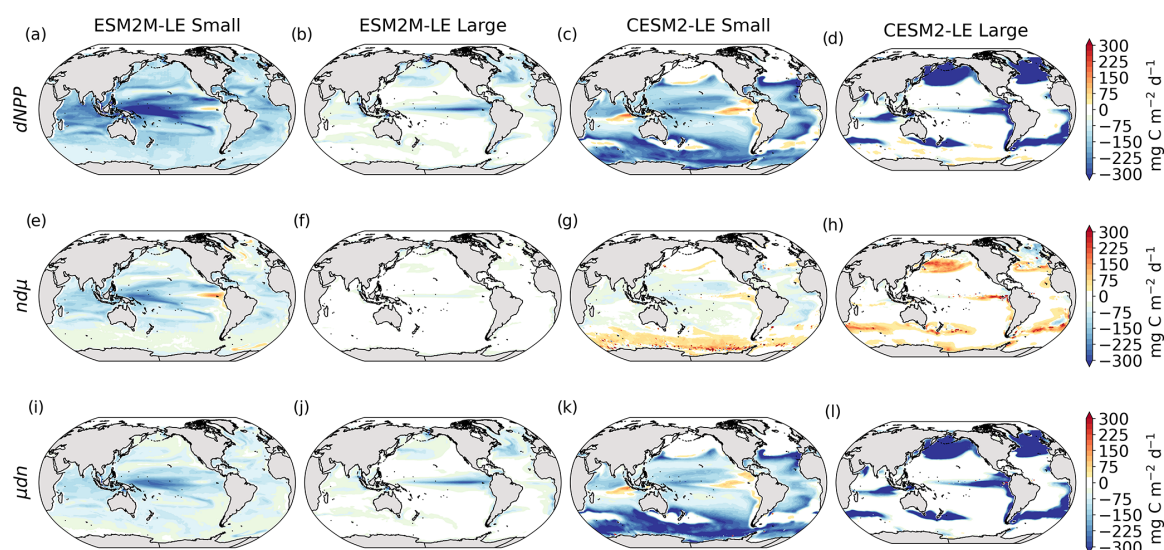


Figure 3. Small- and large-phytoplankton NPP anomalies, dNPP, relative to the climatological seasonal cycle ($\text{mg C m}^{-2} \text{d}^{-1}$) during compound MHW–NPPX events in ESM2M-LE (a, b) and in CESM2-LE (c, d) and contributions of the growth rate $nd\mu$ (e–h) and of the biomass anomaly μdn (i–l) to these NPP anomalies. Contours on panels (a)–(d) indicate the climatological mean state of small and large NPP averaged over 1998–2018 (see also Fig. B5a–d); labels have been omitted.

3.3 Drivers of low NPP during compound MHW–NPPX events

To understand the drivers of NPPX during compound MHW–NPPX events, we decompose the NPP anomaly dNPP of each phytoplankton type into the contributions of its growth rate anomaly $d\mu$ (Fig. 3e–h) and of its biomass anomaly dn (Fig. 3i–l) (see Eq. 2 in Sect. 2.5). One must note, however, that these variables are not independent and that the biomass anomaly may result from changes in the growth rate itself. The decomposition amounts to 104 % and 105 % of the global dNPP of small and large phytoplankton, respectively, in ESM2M-LE and to 104 % and 99 % of the global dNPP of small and large phytoplankton, respectively, in CESM2-LE (Fig. B7). Our decomposition method is therefore well suited to investigating the drivers of extreme reductions in NPP during MHW–NPPX events.

Globally, the growth rate anomaly $d\mu$ barely contributes to the large-phytoplankton dNPP in ESM2M-LE (28 %, Fig. 3b, f) and to the small- and large-phytoplankton dNPP in CESM2-LE (−12 % and −14 %, respectively; Fig. 3c, d, g, h). A large part of the extreme reduction in NPP during MHWs is in fact driven by a negative biomass anomaly dn in both models and for both phytoplankton types. However, the growth rate anomaly explains about half (51 %) of the global small-phytoplankton dNPP in ESM2M-LE (Fig. 3a, e) and can regionally be even more dominant. In ESM2M-LE, the contribution of $d\mu$ (i.e., $nd\mu$) is most negative in the low latitudes for small phytoplankton (Fig. 3e), especially in the western equatorial Pacific. In CESM2-LE, the contribution

of $d\mu$ is slightly negative in the low latitudes (Fig. 3g), and positive (i.e., it counteracts the negative dNPP) in the high latitudes and eastern equatorial Pacific for small and large phytoplankton (Fig. 3g, h). In other words, an increase in the growth rate increases small- and large-phytoplankton NPP in these regions in CESM2-LE. However, the large decreases in dn overcompensate for this increase in the growth rate and lead to an overall decrease in NPP for small phytoplankton in the low to middle latitudes and in the high southern latitudes (Fig. 3k) and for large phytoplankton in the eastern equatorial Pacific, in the high northern latitudes, and at around 40° S (Fig. 3l).

Increases in small- or large-phytoplankton NPP moderate the negative dNPP during MHW–NPPX events. In ESM2M-LE, small-phytoplankton NPP locally increases in the eastern equatorial Pacific as a result of increased small-phytoplankton growth (Fig. 3e). In CESM2-LE, the increase in small-phytoplankton NPP in the northern high latitudes and the increase in large-phytoplankton NPP in the southern high latitudes are driven by both an increase in growth and an increase in biomass (Fig. 3g, h, k, l).

3.3.1 Phytoplankton growth rate anomaly during compound MHW–NPPX events

Before explaining the changes in phytoplankton biomass, we look into the drivers of changes in phytoplankton growth rates because they contribute to reducing NPP either directly or indirectly by affecting phytoplankton biomass. Figure 4 shows the spatial pattern of the mean growth rate anomaly $d\mu$ during compound events for small and large phytoplankton in

each model, as well as the contributions of temperature, light and nutrient limitations to $d\mu$, as described in Sect. 2.5.

In ESM2M-LE, the drivers of $d\mu$ are similar during compound events for small and large phytoplankton. The negative growth rate anomaly in the low to middle latitudes (Fig. 4a, b) is associated with increased nutrient limitation (-0.10 d^{-1} on average between 40° S and 35° N ; Fig. 4m, n), i.e., reduced mixing of nutrient-rich waters from the deeper ocean to the upper 100 m. In the high latitudes, the negative growth rate anomaly is mainly associated with increased light limitation (-0.05 d^{-1} on average south of 40° S and north of 35° N ; Fig. 4i, j). Even though the light limitation depends on a number of factors other than the light supply, such as temperature, nutrient levels, mixed-layer depth, or the carbon-to-chlorophyll ratio in phytoplankton, increased light limitation is here a direct result of reduced light supply by -13 W m^{-2} on average (Fig. B8a). High-latitude MHWs are, however, mainly driven by enhanced shortwave radiation in summer (Vogt et al., 2022). Enhanced shortwave radiation seems incompatible with reduced light levels, hence the low compound MHW–NPPX event frequency in the high latitudes in ESM2M-LE. Therefore, for MHWs to co-occur with reduced light levels, they must be driven by drivers other than radiative heating, such as vertical mixing or advective processes. These drivers might be compatible with clouds or extended sea-ice cover and thus with light limitation. In addition, high temperatures during MHWs also raise energy demand on phytoplankton and directly enhance the light limitation (see the role of T_f in Sect. A1.3 and A2.3). High temperatures during MHWs somewhat moderate the negative growth rate anomalies by their positive effect on the growth rate for both large and small phytoplankton, especially in the low latitudes (Fig. 4e, f). In the eastern equatorial Pacific, this positive effect of the temperature is able to overcompensate for the negative effect of nutrient limitation on the growth rate of small phytoplankton (Fig. 4e), resulting in increased small-phytoplankton growth and a shift towards small phytoplankton during MHW–NPPX events (Fig. 3a, b).

In CESM2-LE, $d\mu$ is negative in the low latitudes (Fig. 4c, d) for both small and large phytoplankton. The growth of small phytoplankton is mainly reduced by increased nutrient limitation (-0.05 d^{-1} on average between 15° S and 20° N ; Fig. 4o, p), whereas the growth of large phytoplankton is mainly reduced by light limitation in the low latitudes (-0.03 d^{-1} on average between 20° S and 20° N ; Fig. 4l). Divergent responses of the nutrient limitation to changes in nutrient levels during compound MHW–NPPX events for small and large phytoplankton can be explained by smaller half-saturation constants in small phytoplankton, which, given the formulation of the nutrient limitation in MARBL (Sect. A2.2), would result in a stronger decrease in N_{lim} given a certain decrease in nutrient levels. In the high latitudes, increased light levels by 7 W m^{-2} on average reduce light limitation (Fig. B8b), which ultimately enhances small- and large-phytoplankton growth. High temperature

anomalies contribute positively to the growth rate of small and large phytoplankton, especially in the eastern equatorial Pacific for small phytoplankton ($> 0.09 \text{ d}^{-1}$; Fig. 4g), resulting in a shift towards large phytoplankton during MHW–NPPX events there (Fig. 3c, d).

In both models, nutrient limitation on phytoplankton growth is especially strong during MHW–NPPX events compared to simple NPPX events (not shown here). Stronger nutrient limitation all over the ocean counteracts the positive temperature effect on phytoplankton growth associated with MHWs. Overall, the models agree that phytoplankton growth is enhanced by high temperatures and reduced by low nutrient levels during MHW–NPPX events. However, the models disagree on the strength of the nutrient limitation, especially in the low latitudes and the eastern equatorial Pacific, potentially due to a stronger reduction in nutrient levels in ESM2M-LE compared to CESM2-LE. Background nutrient limitation is also higher in ESM2M-LE compared to CESM2-LE (Fig. B4i–l) and therefore more sensitive to changes in nutrient levels (see the formulation of N_{lim} in Sect. A1.2 and A2.2). Lastly, the models disagree on their representation of the light limitation changes during MHW–NPPX events, especially in the high latitudes. This model divergence may arise from a number of factors involved in the calculation of L_{lim} , such as different light harvest coefficients in TOPAZv2 (Sect. A1.3) and MARBL (Sect. A2.3), but most importantly, divergent representation of the coupling between radiative fluxes, ocean temperature, and phytoplankton growth in the two models results in different light levels during MHW–NPPX events.

3.3.2 Phytoplankton biomass anomaly during compound MHW–NPPX events

Next, we investigate the drivers of the mean phytoplankton biomass anomaly dn during compound MHW–NPPX events (Fig. 5a–d), which contributes to driving dNPP. The spatial pattern of dn resembles the spatial pattern of dNPP (Fig. 3a–d); their Pearson's correlation coefficients are 0.4 and 0.9 for small and large phytoplankton, respectively, in ESM2M and 0.8 and 0.9 for small and large phytoplankton, respectively, in CESM2. In ESM2M-LE, the negative dn is rather uniform across latitudes for small phytoplankton (Fig. 5a) but shows a distinct spatial pattern for large phytoplankton with stronger declines in the eastern equatorial Pacific and in the high northern latitudes (Fig. 5b). In CESM2-LE, low NPP is driven by a decrease in small-phytoplankton biomass in the southern high latitudes and partly in the low latitudes (Fig. 5c) and by a decrease in large-phytoplankton biomass along the Equator, in the northern high latitudes, and in the southern boundary of the subtropical gyres of the Southern Hemisphere (Fig. 5d).

We are further interested in the buildup of this biomass anomaly dn over time. Δn is the integrated biomass change over the period over which biomass anomalies build up

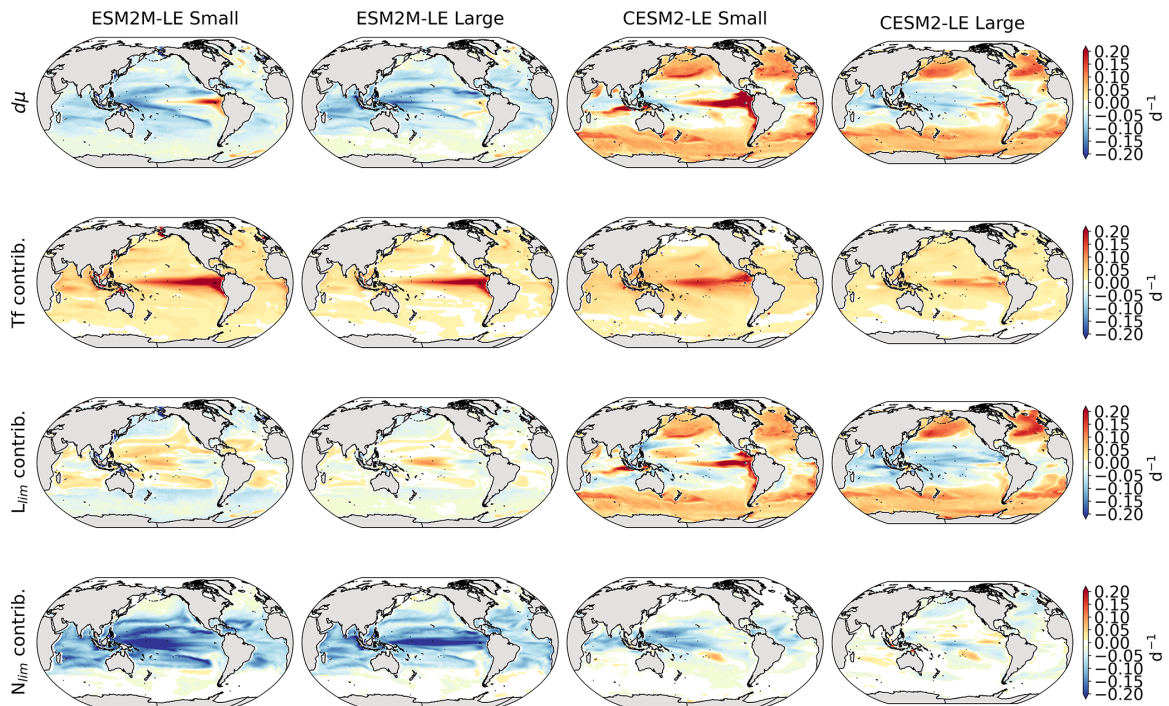


Figure 4. Growth rate anomaly $d\mu$ (d^{-1}) of small and large phytoplankton during compound MHW–NPPX events in ESM2M-LE (a, b) and in CESM2-LE (c, d) and contributions of a change in the temperature function T_f (e–h), in the light limitation L_{lim} (i–l), and in the nutrient limitation N_{lim} (m–p) to this growth rate anomaly. The decomposition of $d\mu$ into these three contributions comes with a global mean residual of 0.009 and -0.002 d^{-1} for small and large phytoplankton in ESM2M-LE and of -0.007 and 0.002 d^{-1} for small and large phytoplankton in CESM2-LE.

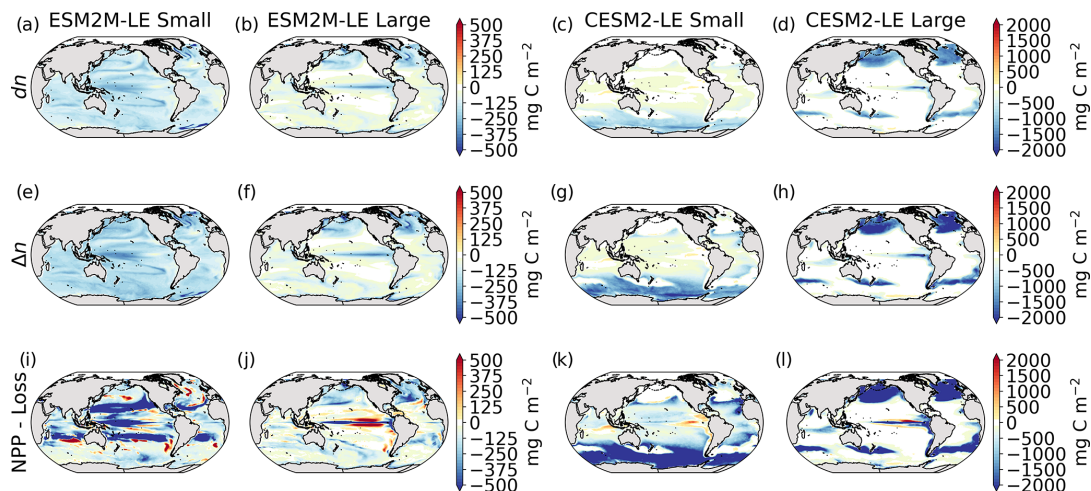


Figure 5. Biomass anomaly dn (mg C m^{-2}) of small and large phytoplankton during compound MHW–NPPX events in ESM2M-LE (a, b) and in CESM2-LE (c, d). Integrated biomass change Δn (mg C m^{-2}) leading to the maximum anomaly reached during a compound MHW–NPPX event (e–h). Contribution of biological processes (NPP – Loss, i–l) to Δn .

(Sect. 2.5). Even though dn and Δn differ by definition, they have almost identical spatial patterns (Fig. 5a–d compared to Fig. 5e–h), signifying it is indeed possible to understand dn from Δn .

Δn is driven by changes in the difference between phytoplankton NPP and Loss (NPP – Loss; Fig. 5i–l) and by changes in ocean circulation (see Eq. 8). The residual presented in Fig. B10 includes both the unknown contribution of ocean circulation and all errors inherent to our decomposition at low temporal resolution and vertical integration.

The role of biological processes in driving dn can be apprehended by the sign of the integrated NPP – Loss term over the period over which dn builds up. Although the individually integrated NPP and Loss terms seem almost equivalent (Fig. B9), phytoplankton loss actually exceeds phytoplankton NPP over most of the global ocean (Fig. 5i–l), which might contribute to decreasing the biomass over time (Fig. 5e–h) and thus to driving the negative biomass anomaly dn (Fig. 5a–d).

In ESM2M-LE, integrated NPP – Loss is particularly negative ($< -150 \text{ mg C m}^{-2}$) for small phytoplankton in the low to middle latitudes between 35° S and 35° N and for large phytoplankton in the northern high latitudes and in a narrow band along the Equator (Fig. 5i, j). In CESM2-LE, the negative NPP – Loss contribution to Δn seems especially strong ($< -200 \text{ mg C m}^{-2}$) for small phytoplankton in the low to middle latitudes between 35° S and 35° N and in the Southern Ocean and for large phytoplankton along the Equator and in the high latitudes (Fig. 5k, l).

Note that integrated NPP – Loss generally exceeds the integrated biomass changes (Fig. 5e–l), with some exceptions, e.g., in the high latitudes for small phytoplankton in ESM2M-LE. Δn , NPP, and Loss terms include an error term when computed from 5 d mean, 10 m vertically integrated biomass. Further studies at higher temporal and vertical resolution are needed to remove errors in all terms in Eq. (8) so as to quantify the exact NPP – Loss contribution to Δn .

Overall in both models, the negative biomass anomaly dn (Fig. 5a–d) can be explained by negative biomass changes (Δn , Fig. 5e–h) over time, which seem to be driven by negative contributions from NPP – Loss (Fig. 5m–p). Loss terms include grazing of phytoplankton by zooplankton in TOPAZv2 and by grazing, mortality, and aggregation in MARBL. During MHWs, not only do higher temperatures enhance NPP via their positive effect on the growth rate but they also directly enhance phytoplankton loss via their similarly positive effect on phytoplankton grazing and mortality (see Sect. A1.5 and A2.5). However, other factors such as nutrient and light limitation moderate phytoplankton growth during compound MHW–NPPX events, as we have seen in the previous section. In turn, nutrient and/or light limitation might moderate NPP sufficiently for it to be exceeded by phytoplankton loss, allowing a decrease in phytoplankton biomass over time.

3.3.3 Summary of driving processes

Figure 6 summarizes the drivers of NPPX during MHWs in ESM2M-LE and in CESM2-LE. We distinguish between four regions of rather homogeneous drivers: the northern high latitudes north of 35° N ; the low latitudes between 35° S and 35° N , except for the eastern equatorial Pacific (as defined by Fay and Mckinley, 2014); and lastly the southern high latitudes south of 35° S . Small- and large-phytoplankton contributions to dNPP are represented in Fig. 6 by dark and light colors, respectively. Here, we compare the drivers of NPPX in the two models and choose not to focus on the magnitude of their NPP anomalies (note the different y axes in Fig. 6). Small and large phytoplankton both contribute to driving NPPX during compound MHW–NPPX events. In the two models, small phytoplankton is responsible for the majority ($> 70\%$) of dNPP in the low latitudes and in the southern high latitudes. In ESM2M, large phytoplankton accounts for a larger part (44%) of dNPP in the northern high latitudes and about half of dNPP over the cold tongue, whereas in CESM2-LE, large phytoplankton dominates ($> 84\%$) dNPP in the northern high latitudes and over the cold tongue.

We further decomposed dNPP into the contributions from a change in the temperature function T_f (red bars in Fig. 6), in the light limitation L_{lim} (yellow bars), and in the nutrient limitation N_{lim} (blue bars) by multiplying their contributions to the growth rate anomaly $d\mu$ (Sect. 3.3.1) with the climatological mean biomass n . We also assessed the contribution of the biomass anomaly dn (green bar) to dNPP by multiplying dn with the climatological mean growth rate μ (Sect. 3.3.2). In Fig. 6, we did not decompose the biomass anomaly contribution to dNPP into the further contribution of a change in NPP – Loss, since this decomposition might be associated with substantial errors when performed at 5 d mean resolution and when integrating over the top 100 m layer (see Sect. 2.5), resulting in a slightly inaccurate estimation of the NPP – Loss contribution. The decomposition in Sect. 3.3.2 is not intended to quantify the exact NPP – Loss contribution to dn but rather to apprehend the sign of the biomass anomaly.

Over all four regions and in both models, high temperatures during MHWs have a positive effect on the growth rate and thus positively contribute to dNPP. This positive effect can be supported or counteracted by the light and nutrient contributions to dNPP.

On average, in the low latitudes, changes in the light limitation hardly contribute to dNPP. In the high latitudes and in the equatorial Pacific, the models disagree on the sign of the light contribution. Although in CESM2-LE, reduced light limitation during MHW–NPPX events has for the most part a positive effect on dNPP except on large phytoplankton in the equatorial Pacific (Fig. 6b, f, h), in ESM2M-LE, strong light limitation on phytoplankton growth contributes to reducing dNPP and thus to driving NPPX in the high latitudes (Fig. 6a, g).

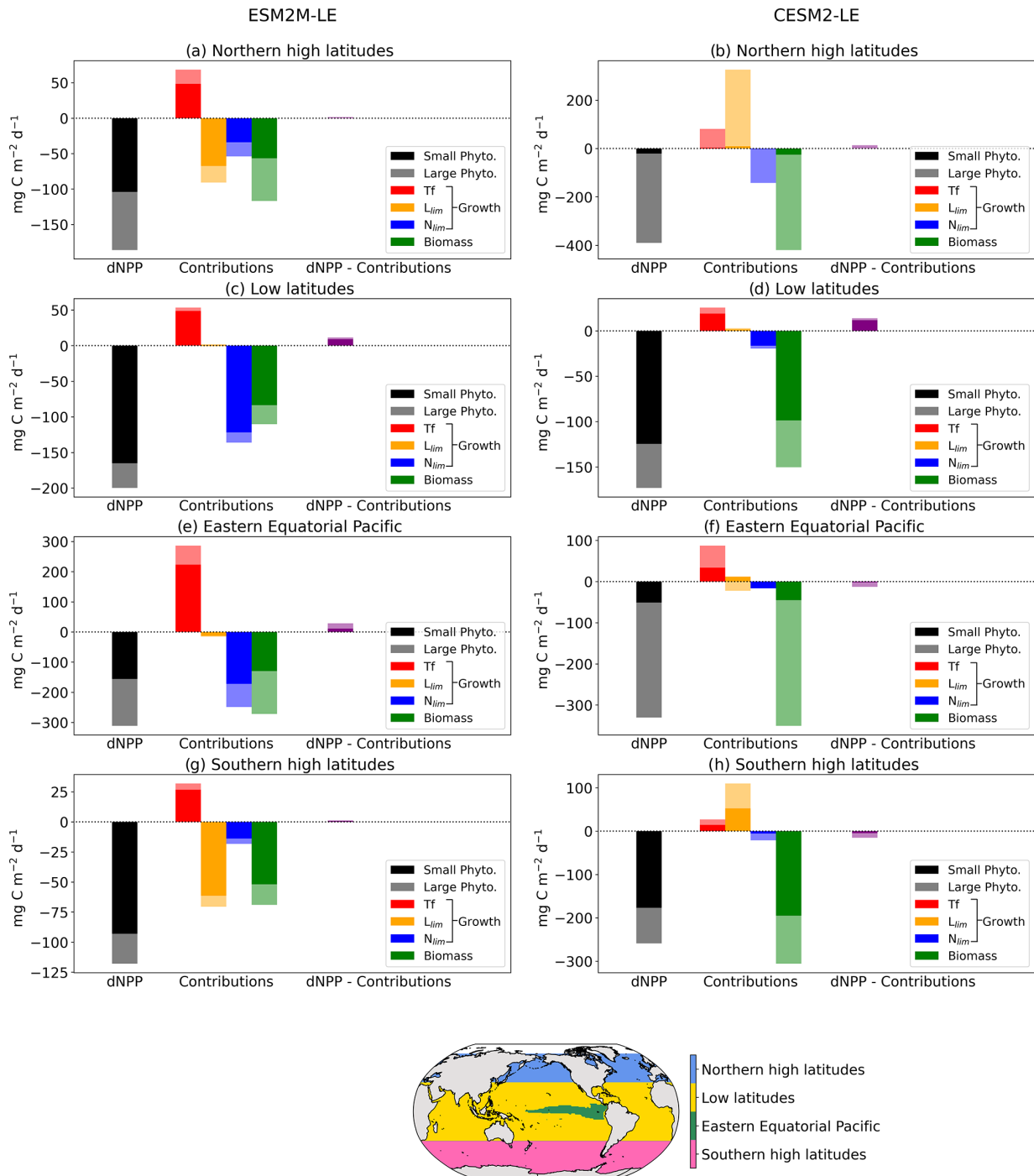


Figure 6. Regional mean NPP anomaly ($\text{mg C m}^{-2} \text{d}^{-1}$) during compound MHW–NPPX events in ESM2M-LE and in CESM2-LE over the northern latitudes (a, b), the low latitudes (c, d), the eastern equatorial region (e, f), and the southern latitudes (g, h). Contributions of the small- and large-phytoplankton dNPP to the total NPP anomaly are represented in black and gray, respectively. The indirect contributions to dNPP of changes in each phytoplankton growth limiting factor (the temperature function T_f , in red; the light limitation L_{lim} , in orange; and the nutrient limitation N_{lim} , in blue) and of changes in phytoplankton biomass, in green, during compound MHW–NPPX events are indicated in dark and light colors for small and large phytoplankton, respectively. Remaining changes in NPP that could not be explained by the decomposition of dNPP are represented in purple.

The models agree that lower nutrient levels limit phytoplankton growth during compound MHW–NPPX events. However, the models disagree on the strength of the nutrient limitation changes. In ESM2M-LE, the nutrient limitation on phytoplankton growth is strong enough (in combination with the light limitation in the high latitudes) to reduce the growth rate, which directly contributes to reducing NPP and thus to driving NPPX events (Fig. 6a, c, e, g). On the other hand, in CESM2-LE, the nutrient limitation is not sufficient to counterbalance the positive effects of temperature and light on the growth rate during MHWs in the high latitudes and over the cold tongue (Fig. 6b, d, h) and only slightly contributes to reducing dNPP in the low latitudes (Fig. 6f) along with enhanced light limitation.

Both models agree on low phytoplankton biomass during compound events, which contributes to driving low NPP over all four biomes. The negative biomass anomaly might be explained by a relative increase in phytoplankton loss compared to phytoplankton NPP during compound events, as discussed in Sect. 3.3.2. It might also be explained or counteracted by changes in ocean circulation, which this study does not address. Low biomass contributes to driving NPPX by about 50 % in ESM2M-LE and > 100 % in CESM2-LE.

Overall, the models agree on the effect of high temperatures, which tend to increase NPP during MHWs. They disagree on the sign of the light limitation in the high latitudes, potentially due to reduced light levels in ESM2M-LE and higher light levels in CESM2-LE during compound MHW–NPPX events. Lastly, the models agree on increased nutrient limitation during compound MHW–NPPX events, which contributes to driving NPPX. The main difference between ESM2M-LE and CESM2-LE is the strength of the nutrient limitation effect on phytoplankton growth during MHW–NPPX events. In ESM2M-LE, the nutrient limitation is strong enough to reduce the growth rate and directly drive NPPX. In CESM2-LE, weaker nutrient limitation simply moderates the temperature effect on the growth rate and thus on NPP, thereby potentially allowing NPP to be exceeded by phytoplankton loss, which might decrease the biomass over time and eventually drive NPPX. Divergent responses of the nutrient limitation in the two models can be explained by a stronger reduction in nutrient levels during MHW–NPPX events in ESM2M-LE compared to CESM2-LE and by higher background nutrient limitation in ESM2M-LE, which implies higher sensitivity of the nutrient limitation to changes in nutrient levels.

4 Discussion and conclusion

We had three primary goals in setting out with this study: (i) identify hotspots of compound marine heatwaves and low-NPP (MHW–NPPX) events, (ii) assess the fidelity of state-of-the-art Earth system models (ESMs) in representing MHW–NPPX events, and (iii) apply the models to develop

mechanistic insights into the underlying drivers of these potentially harmful compound MHW–NPPX events.

The analysis revealed that compound MHW–NPPX events occur relatively frequently in the low latitudes, especially in the center of the equatorial Pacific and in the subtropical Indian Ocean, and less frequently in the northern high latitudes (Fig. 2a, d; first goal). Both models agree with observations in the low latitudes (second goal). However, CESM2-LE overestimates the frequency of compound MHW–NPPX events in the northern high latitudes. In the southern high latitudes, elevated uncertainty in the observation-based products renders it difficult to determine which of the two models better simulates compound events. Overall, our results agree with previous studies that reported suppressed NPP during MHWs in regions with relatively low surface nutrient levels, such as the subtropical gyres (Hayashida et al., 2020; Gupta et al., 2020; Le Grix et al., 2021). Gupta et al. (2020), for example, reported low chlorophyll during an MHW in the Indian Ocean, where background nitrate concentrations are especially low. Le Grix et al. (2021) described frequent co-occurrence of MHWs and low-chlorophyll events in the center of the equatorial Pacific and in the Indian Ocean. These correspond to the regions where we found especially frequent MHW–NPPX events in the observation-based estimates and in the two models. In addition, previous studies reported elevated chlorophyll concentrations during MHWs over regions with high nutrient concentrations, such as in the northern reaches of the Southern Ocean (Hayashida et al., 2020; Gupta et al., 2020). These are regions where we also found compound events to be rare.

We then investigated the drivers of compound MHW–NPPX events and the reasons why ESM2M-LE and CESM2-LE have similar compound-event likelihoods in the low latitudes and divergent likelihoods in the high latitudes (third goal). We found that the models represent NPPX events of different magnitude and duration, which is suggestive of different drivers for NPPX events during MHWs. In both models, higher temperatures have a positive effect on NPP during MHW–NPPX events. In ESM2M-LE, this temperature effect is counteracted by enhanced nutrient limitation in the low latitudes and by enhanced light limitation in the high latitudes, which contribute to driving approximately half of the negative NPP anomaly by directly limiting phytoplankton growth. Although higher temperatures have the same enhancing effect on phytoplankton NPP and loss, nutrient and light limitation during MHW–NPPX events might decrease NPP sufficiently for it to be exceeded by phytoplankton loss over the global ocean. This relative increase in phytoplankton loss compared to NPP possibly explains the buildup of a negative biomass anomaly that contributes to driving the other half of the negative NPP anomaly during MHW–NPPX events. In CESM2-LE, nutrient limitation over the global ocean is too weak to counterbalance the positive temperature effect on phytoplankton growth, though it may moderate the growth sufficiently for NPP to be exceeded by phy-

toplankton loss, resulting in a biomass decrease over time. Lower biomass is the main driver of NPPX events over the global ocean in CESM2-LE. These divergent drivers of NPPX events in ESM2M-LE and CESM2-LE reflect the low degree of agreement in how ESMs represent phytoplankton growth and loss (Laufkötter et al., 2015), with this constituting a major source of uncertainties in global projections of NPP under global warming (Laufkötter et al., 2015; Frölicher et al., 2016; Kwiatkowski et al., 2020; Tagliabue et al., 2021). We expect ESMs to differ not only in their projection of NPP but also in how they simulate future changes in NPPX events and compound MHW–NPPX events, depending on how the drivers of NPPX events evolve under global warming.

These NPPX drivers may well also be responsible for the differences in the likelihood of compound MHW–NPPX events between the models. We expect MHWs to be frequently associated with increases in vertical stratification that inhibit the upward mixing of deep nutrients (Holbrook et al., 2019; Hayashida et al., 2020); therefore, in regions where nutrient limitation is the dominant NPPX driver, we would expect NPPX events to frequently co-occur with MHWs. That is indeed the case in the low latitudes, where nutrient limitation drives NPPX events in the two models via its direct effect on the growth rate (in ESM2M) and its indirect effect on NPP – Loss, which reduces the biomass (in ESM2M-LE and CESM2-LE). Previous studies have identified nutrient limitation as the main driver of negative NPP anomalies during MHWs. For example, Whitney (2015) and Le et al. (2019) found that decreased westerly winds and southward Ekman transport over the eastern part of the North Pacific transition zone reduced nutrient concentrations during the Blob and thus inhibited NPP. Compound MHW–NPPX events are also relatively frequent in CESM2-LE in the high latitudes, where nutrient limitation contributes to driving NPPX events. On the other hand, it has been shown that MHWs are associated with enhanced incident shortwave radiation in the high latitudes (Vogt et al., 2022). Therefore, in regions where light limitation drives NPPX events, we expect rare compound events, which is indeed the case in the high latitudes in ESM2M-LE.

Our analysis revealed that compound MHW–NPPX events are accompanied by shifts in phytoplankton species. The models suggest a general shift towards larger phytoplankton over most of the global ocean during MHW–NPPX events, except in the eastern equatorial Pacific in ESM2M-LE and in CESM2-LE, as well as north of 35° N and between 35 and 50° S in CESM2-LE, where the contribution of smaller-phytoplankton NPP increases during MHW–NPPX events. In general, the shift towards larger phytoplankton occurs over regions where small phytoplankton are dominant and vice versa. Other studies have previously documented phytoplankton shifts during MHWs (Yang et al., 2018; Wyatt et al., 2022). Wyatt et al. (2022), for example, described a relative shift towards small phytoplankton in the north-east Pacific during the 2014–2015 Blob due to a stronger

response of large phytoplankton to reduced nutrient levels and a stronger response of small phytoplankton to increased light availability driven by shallower mixed layers. Small phytoplankton even increased during the Blob over the Gulf of Alaska (Wyatt et al., 2022), in agreement with CESM2-LE, which simulates increased small-phytoplankton NPP during MHW–NPPX events in the northern high latitudes (Fig. 3c). Peña et al. (2019) also found a shift towards cyanobacteria, i.e., small phytoplankton, in the north-eastern Pacific during the Blob. Their results are consistent with modeling studies showing that a surface ocean with lower nutrient concentrations and increased light availability favors smaller phytoplankton species (Litchman et al., 2006; Acevedo-Trejos et al., 2014). These phytoplankton shifts might lead to cascading impacts on marine ecosystems depending on which phytoplankton type marine species preferentially graze on (Cavole et al., 2016; Bindoff et al., 2019; Cheung and Frölicher, 2020). They might also impact the biological carbon pump because larger and heavier phytoplankton sink faster to the deep ocean (Boyd and Harrison, 1999). To better predict phytoplankton shifts and their impacts on marine ecosystems and the carbon pump during MHW–NPPX events, we need models to accurately simulate these events and their associated changes in small- and large-phytoplankton NPP. Yet models such as ESM2M and CESM2 still disagree, especially in the high latitudes.

One important aspect of our study is the use of large-ensemble simulations (LES) with high-frequency ocean output, encompassing not only SST and NPP but also diagnostic variables used for driver attribution. The large sample size mandated by the study of compound extreme events is even larger than that required for extreme events with single variables (Deser et al., 2020; Burger et al., 2022; Zscheischler and Lehner, 2022). This is particularly important under non-stationary conditions, where relatively short time series need to be analyzed to obtain a picture of quasi-stationary conditions. The application of two different Earth system models facilitated an exploration of how uncertainties in the formulation of NPP manifest themselves in the occurrence (pattern and frequency) of compound events. This should complement work by Kwiatkowski et al. (2020) and Bopp et al. (2022) in underscoring the challenges faced by the Earth system modeling community given pervasive NPP uncertainty.

One challenging aspect of our study is the lack of agreement between observation-based estimates of the frequency of compound MHW–NPPX events in the middle to high southern latitudes, which makes it difficult to determine whether the ESMs well represent compound MHW–NPPX events and their drivers over this region. NPP estimates produced by models assimilating satellite data are still uncertain and highly sensitive to their respective model configurations (e.g., Behrenfeld et al., 2005; J. S. Long et al., 2021), especially in sea-ice-covered regions. We decided to include five observation-based NPP products in this study to take into account the high uncertainty in NPP estimates, which affects

the observation-based estimates of MHW–NPPX event frequency. Direct NPP measurements would be needed to better constrain the NPP estimated by ESMs in the future.

To conclude, the combination of an MHW and an NPPX event constitutes a compound hazard which potentially leads to severe impacts on marine organisms and ecosystems. Here, we assessed whether LES from two ESMs can be used to understand compound MHW–NPPX events in the ocean and to project them into the future. Our analysis reveals that the likelihood of compound MHW–NPPX events depends on how ESMs represent the factors limiting phytoplankton growth and loss. These factors are similar in ESM2M and CESM2 in the low latitudes but differ in the high latitudes. This identifies an important need for improved process understanding in the models used for predicting and projecting the potentially harmful compound MHW–NPPX events in the ocean.

Appendix A: Ecosystem model description

A1 GFDL ESM2M: TOPAZv2

TOPAZv2 stands for Tracers of Ocean Phytoplankton with Allometric Zooplankton version 2.0. It is the biogeochemical and ecological module used in GFDL's ESM2M (Dunne et al., 2013). Three phytoplankton types are represented: nano-phytoplankton (or small phytoplankton), large phytoplankton, and diazotrophs. Nitrogen in each phytoplankton type i is a prognostic variable.

$$\partial_t n_i = \text{NPP}_i - \text{Loss}_i + \text{Circ}_i, \quad (\text{A1})$$

where NPP is the nitrogen-specific NPP, Loss is the nitrogen-specific decay, and Circ corresponds to the physical advection and mixing of phytoplankton nitrogen n by ocean circulation. The NPP of each phytoplankton type is the product of its growth rate μ and its biomass n :

$$\text{NPP}_i = \mu_i n_i. \quad (\text{A2})$$

A1.1 Phytoplankton growth

In TOPAZv2, the nitrogen-specific growth rate is defined for all phytoplankton types as follows:

$$\mu_i = \frac{\mu_{\max} N_{\text{lim}_i} T_f + \varepsilon}{1 + \zeta} L_{\text{lim}_i} \approx \mu_{\max} N_{\text{lim}_i} L_{\text{lim}_i} T_f, \quad (\text{A3})$$

where N_{lim} is the nutrient limitation, L_{lim} is the light limitation, and T_f is an Eppley function of the temperature.

A1.2 Nutrient limitation

N_{lim} is computed using Liebig's law of the minimum, where N_{Fe} , $N_{\text{Si(OH)}_4}$, N_{PO_4} , N_{NH_4} , and N_{NO_3} correspond to the nu-

trient limitation specific to iron, silicon, phosphate, ammonia, and nitrate.

$$N_{\text{lim}_i} = \min \left(N_{\text{Fe}_i}, N_{\text{Si(OH)}_4}, N_{\text{PO}_4}, N_{\text{NH}_4} + N_{\text{NO}_3} \right)$$

Nutrient limitation is represented according to Michaelis–Menten kinetics, where K_{Fe} , $K_{\text{Si(OH)}_4}$, K_{PO_4} , K_{NH_4} , and K_{NO_3} are the half-saturation constants of each nutrient.

$$N_{\text{Fe}_i} = \frac{\text{Fe}}{\text{Fe} + K_{\text{Fe}_i}} \quad (\text{A4})$$

$$N_{\text{PO}_4} = \frac{\text{PO}_4}{\text{PO}_4 + K_{\text{PO}_4}} \quad (\text{A5})$$

$$N_{\text{Si(OH)}_4} = \frac{\text{Si(OH)}_4}{\text{Si(OH)}_4 + K_{\text{Si(OH)}_4}} \quad (\text{A6})$$

$$N_{\text{NH}_4} = \frac{\text{NH}_4}{\text{NH}_4 + K_{\text{NH}_4}} \quad (\text{A7})$$

Nitrate limitation with ammonia inhibition is represented after Frost and Franzen (1992).

$$N_{\text{NO}_3} = \frac{\text{NO}_3}{\text{NO}_3 + K_{\text{NO}_3}} \cdot \left(1 + \frac{\text{NH}_4}{K_{\text{NH}_4}} \right) \quad (\text{A8})$$

A1.3 Light limitation

Light limitation is calculated as

$$L_{\text{lim}_i} = 1 - e^{-\frac{\alpha_i \theta_i \text{Irr}}{N_{\text{lim}_i} T_f \mu_{\max} + \varepsilon}}, \quad (\text{A9})$$

where α is the light harvest coefficient, θ is the chlorophyll-to-carbon ratio, and Irr corresponds to the mean light level (W m^{-2}) of a depth layer. μ_{\max} is the maximal growth rate and ε a constant for numerical stability. More details on how to compute θ , N_{Fe} , N_{PO_4} , and the limitation terms specific to iron and phosphate when Fe : N or P : N varies in phytoplankton are given in Dunne et al. (2013).

A1.4 Temperature function

The temperature function is given as

$$T_f = e^{K_{\text{epp}} T}, \quad (\text{A10})$$

where T is the temperature and K_{epp} is the constant temperature coefficient for growth.

A1.5 Phytoplankton grazing

In TOPAZ, phytoplankton decays through grazing only. Grazing is computed separately for small and large phyto-

Table A1. Parameter values used in TOPAZv2 to compute the production and grazing of both small and large phytoplankton.

Parameter	Value	Unit	Name
K_{epp}	0.063	$^{\circ}\text{C}^{-1}$	temperature coefficient for growth
μ_{max}	1.296	d^{-1}	maximal growth rate at 0°C
ζ	0.1	–	photosynthetic respiration loss
ε	8.64×10^{-26}	d^{-1}	constant for numerical stability
α	9.2×10^{-5}	$\text{g C (g Chl)}^{-1} \text{ m}^2 \text{ W}^{-1} \text{ s}^{-1}$	light harvest coefficient
n_{\star}	$1.9 \times 10^{-6} \times 16.0 / 106.0$	mol N kg^{-1}	pivot phytoplankton concentration
$k_{\text{graz}_{\text{max}}}$	6	d^{-1}	maximum phytoplankton grazing rate
λ_0	0.19	d^{-1}	phytoplankton grazing rate
n_{min}	1×10^{-6}	mol N m^{-3}	minimum phytoplankton concentration for grazing
τ	0.01	d^{-1}	temperature-dependent response timescale for grazers

Table A2. Parameter values used in TOPAZv2 to compute the production and grazing of small phytoplankton.

Parameter	Value	Unit	Name
K_{Fe}	3×10^{-3}	$\text{mmol dissolved Fe m}^{-3}$	half-saturation coefficient
K_{PO_4}	0.2	$\text{mmol PO}_4 \text{ m}^{-3}$	half-saturation coefficient
K_{NH_4}	0.2	$\text{mmol NH}_4 \text{ m}^{-3}$	half-saturation coefficient
K_{NO_3}	2	$\text{mmol NO}_3 \text{ m}^{-3}$	half-saturation coefficient

Table A3. Parameter values used in TOPAZv2 to compute the production and grazing of large phytoplankton.

Parameter	Value	Unit	Name
K_{Fe}	9×10^{-3}	$\text{mmol dissolved Fe m}^{-3}$	half-saturation coefficient
K_{PO_4}	0.6	$\text{mmol PO}_4 \text{ m}^{-3}$	half-saturation coefficient
K_{NH_4}	0.6	$\text{mmol NH}_4 \text{ m}^{-3}$	half-saturation coefficient
K_{NO_3}	6	$\text{mmol NO}_3 \text{ m}^{-3}$	half-saturation coefficient
$K_{\text{Si(OH)}_4}$	1	$\text{mmol Si(OH)}_4 \text{ m}^{-3}$	half-saturation coefficient

plankton.

$$G_{\text{small}} = \min\left(k_{\text{graz}_{\text{max}}}, \lambda_0 T_f \frac{n_{\text{small}}}{n_{\star}}\right) \frac{n_{\text{small}}^2}{n_{\text{small}} + n_{\text{min}}}, \quad (\text{A11})$$

$$G_{\text{large}} = \min\left(k_{\text{graz}_{\text{max}}}, \lambda_0 T_f \left(\frac{n^{\text{graz}_{\text{large}}}}{n_{\star}}\right)^{1/3}\right) \frac{n^{\text{graz}_{\text{large}}}}{n_{\text{large}} + n_{\text{min}}} n_{\text{large}}, \quad (\text{A12})$$

where $k_{\text{graz}_{\text{max}}}$ is the maximum grazing rate, λ_0 is another grazing rate, and n_{\star} is the pivot phytoplankton concentration for grazing-based variations in ecosystem structure. $n^{\text{graz}_{\text{large}}}$ is an implicit phytoplankton concentration after incorporation of a temperature-dependent time lag:

$$n^{\text{graz}_{\text{large}}} = \left(n^{\text{graz}_{\text{large}}}\right)_{\text{old}} \cdot e^{\frac{n_{\text{large}} - \left(n^{\text{graz}_{\text{large}}}\right)_{\text{old}}}{n_{\text{large}} + \left(n^{\text{graz}_{\text{large}}}\right)_{\text{old}}} \cdot 2 \cdot \min\left(1, T_f \frac{\Delta t}{\tau}\right)}, \quad (\text{A13})$$

where $\left(n^{\text{graz}_{\text{large}}}\right)_{\text{old}}$ corresponds to $n^{\text{graz}_{\text{large}}}$ of the previous time step Δt and τ is the temperature-dependent response timescale for grazers, which is set to a very small number to simulate instantaneous response. More explanations are given in Dunne et al. (2013). Parameter values used in TOPAZv2 to compute phytoplankton production and grazing are provided in Tables A1, A2, and A3.

A2 CESM2: MARBL

The Marine Biogeochemistry Library (MARBL) is the biogeochemical component of CESM2. It is a prognostic ocean biogeochemistry model that simulates marine-ecosystem dynamics and the coupled cycles of carbon, nitrogen, phosphorus, iron, silicon, and oxygen (M. C. Long et al., 2021). Three phytoplankton types are represented: small phytoplankton, diatoms, and diazotrophs. The concentration P_i of each phytoplankton type i is a prognostic variable.

$$\partial_t P_i = \text{NPP}_i - \text{Loss}_i + \text{Circ}_i, \quad (\text{A14})$$

where Loss corresponds to phytoplankton decay and Circ corresponds to the physical advection and mixing of phytoplankton by ocean circulation. The NPP of each phytoplankton type is the product of its growth rate μ and its biomass n :

$$\text{NPP}_i = \mu_i P_i. \quad (\text{A15})$$

Table A4. Parameter values used in MARBL to compute the production and loss of small and large phytoplankton.

Parameter	Value	Unit	Name
μ_{ref}	5	d^{-1}	resource-unlimited growth rate
α_{small}	0.39	$\text{mol C (g Chl)}^{-1} \text{ m}^2 \text{ W}^{-1} \text{ d}^{-1}$	light harvest coefficient
α_{large}	0.28	$\text{mol C (g Chl)}^{-1} \text{ m}^2 \text{ W}^{-1} \text{ d}^{-1}$	light harvest coefficient
K^{P}	1.2	mmol m^{-3}	half-saturation coefficient for grazing
m	0.1	d^{-1}	linear mortality rate

Table A5. Parameter values used in MARBL to compute the production and loss of small phytoplankton.

Parameter	Value	Unit	Name
K_{Fe}	3×10^{-5}	$\text{mmol dissolved Fe kg}^{-1}$	half-saturation coefficient
K_{PO_4}	0.01	$\text{mmol PO}_4 \text{ m}^{-3}$	half-saturation coefficient
K_{NH_4}	0.01	$\text{mmol NH}_4 \text{ m}^{-3}$	half-saturation coefficient
K_{NO_3}	0.25	$\text{mmol NO}_3 \text{ m}^{-3}$	half-saturation coefficient
g_{max}	3.3	d^{-1}	maximum grazing rate

Table A6. Parameter values used in MARBL to compute the production and loss of large phytoplankton.

Parameter	Value	Unit	Name
K_{Fe}	7×10^{-5}	$\text{mmol dissolved Fe kg}^{-1}$	half-saturation coefficient
K_{PO_4}	0.05	$\text{mmol PO}_4 \text{ m}^{-3}$	half-saturation coefficient
K_{NH_4}	0.05	$\text{mmol NH}_4 \text{ m}^{-3}$	half-saturation coefficient
K_{NO_3}	0.5	$\text{mmol NO}_3 \text{ m}^{-3}$	half-saturation coefficient
K_{SiO_3}	0.7	$\text{mmol SiO}_3 \text{ m}^{-3}$	half-saturation coefficient
g_{max}	3.15	d^{-1}	maximum grazing rate

A2.1 Phytoplankton growth

In MARBL, the carbon-specific growth rate of phytoplankton is defined as

$$\mu_i = \mu_{\text{ref}} N_{\text{lim}_i} L_{\text{lim}_i} T_f, \quad (\text{A16})$$

where μ_{ref} is a constant accounting for the maximum growth rate at the reference temperature of 30 °C. N_{lim} is the nutrient limitation; L_{lim} is the light limitation; T_f is the temperature function.

A2.2 Nutrient limitation

N_{lim} is computed using Liebig's law of the minimum, where N_{Fe} , N_{SiO_3} , N_{P} , N_{NH_4} , and N_{NO_3} correspond to the nutrient limitation specific to iron, silicon, phosphate, ammonia, and nitrate.

$$N_{\text{lim}_i} = \min \left(N_{\text{Fe}_i}, N_{\text{SiO}_3_i}, N_{\text{P}_i}, N_{\text{NH}_4_i} + N_{\text{NO}_3_i} \right) \quad (\text{A17})$$

$$N_{\text{Fe}_i} = \frac{\text{Fe}}{\text{Fe} + K_{\text{Fe}_i}} \quad (\text{A18})$$

$$N_{\text{SiO}_3} = \frac{\text{SiO}_3}{\text{SiO}_3 + K_{\text{SiO}_3}} \quad (\text{A19})$$

Phytoplankton can alternatively assimilate nitrate and ammonium following O'Neill et al. (1989), such that

$$N_{\text{NH}_4} = \frac{\frac{\text{NH}_4}{K_{\text{NH}_4}}}{1 + \frac{\text{NO}_3}{K_{\text{NO}_3}} + \frac{\text{NH}_4}{K_{\text{NH}_4}}}, \quad (\text{A20})$$

$$N_{\text{NO}_3} = \frac{\frac{\text{NO}_3}{K_{\text{NO}_3}}}{1 + \frac{\text{NO}_3}{K_{\text{NO}_3}} + \frac{\text{NH}_4}{K_{\text{NH}_4}}}. \quad (\text{A21})$$

Phytoplankton is able to assimilate phosphorus in the form of phosphate (PO_4) and semi-labile dissolved organic phosphate (DOP); a similar approach is used to compute N_p .

A2.3 Light limitation

The light limitation is given as

$$L_{\text{lim}_i} = 1 - e^{-\frac{\alpha_i \theta_i \text{Irr}}{N_{\text{lim}_i} T_f^{\mu_{\text{ref}}}}}, \quad (\text{A22})$$

where α is the light harvest coefficient; θ is the chlorophyll-to-carbon ratio; and Irr corresponds to the photosynthetically available radiation, defined as 45 % of incoming shortwave radiation (W m^{-2}). In the high latitudes, CESM2 simulates a subgrid-scale sea-ice thickness distribution and computes shortwave penetration independently in each sub-column. MARBL then takes an area-weighted average across sub-columns to compute the grid cell mean light level. For more details on how to compute θ and N_p , see M. C. Long et al. (2021).

A2.4 Temperature function

The temperature function is given as

$$T_f = 1.7 \frac{T - 30^\circ\text{C}}{10^\circ\text{C}}, \quad (\text{A23})$$

where T is the temperature.

A2.5 Phytoplankton loss

In MARBL, phytoplankton decays through grazing G , mortality M , and aggregation A , which refers to the process by which dying phytoplankton form aggregates that sink through the water column. The three loss terms depend on P' , the phytoplankton concentration in excess of a temperature- and depth-dependent threshold (M. C. Long et al., 2021).

$$P'_i = \max(P_i - P_{\text{threshold}_i}, 0) \quad (\text{A24})$$

$$\text{Loss}_i = G(P'_i)_i + M(P'_i) + A_i(P'_i) \quad (\text{A25})$$

Grazing by zooplankton is given as

$$G_i(P'_i) = g_{\text{max}_i} T_f \frac{P'_i}{K^P + P'_i} z, \quad (\text{A26})$$

where g_{max} is the maximum grazing rate, K^P is the half-saturation constant for phytoplankton grazing, and z is the zooplankton biomass.

Mortality is given as

$$M(P'_i) = m T_f P'_i, \quad (\text{A27})$$

where m is the linear mortality rate.

Finally, aggregation is parameterized as

$$A_i(P'_i) = a_i \times (P'_i)^{1.75}, \quad (\text{A28})$$

where a is the aggregation rate (see M. C. Long et al., 2021, for more details). Parameter values used in MARBL to compute phytoplankton production and loss are provided in Tables A4, A5, and A6.

Appendix B: Additional figures

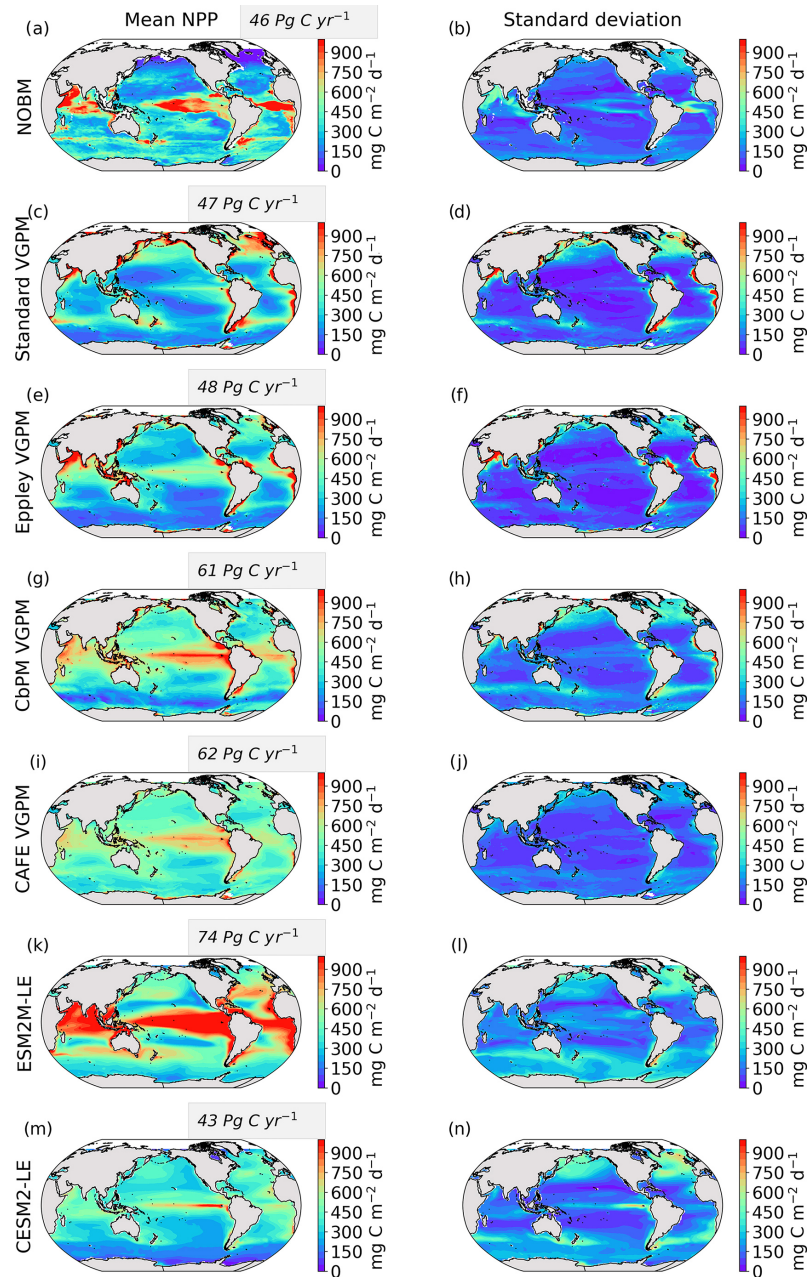


Figure B1. Climatological mean and standard deviation of the observation-based NPP estimates ($\text{mg C m}^{-2} \text{d}^{-1}$) calculated from NOBM (a, b), Standard VGPM (c, d), Eppley-VGPM (e, f), CbPM (g, h), and CAFE (i, j) and simulated by ESM2M-LE (k, l) and CESM2-LE (m, n) over 1998–2018. Gray boxes indicate the globally integrated mean NPP (Pg C yr^{-1}). We use 5 d mean NPP output for all products except for the VGPM-based products (c–j).

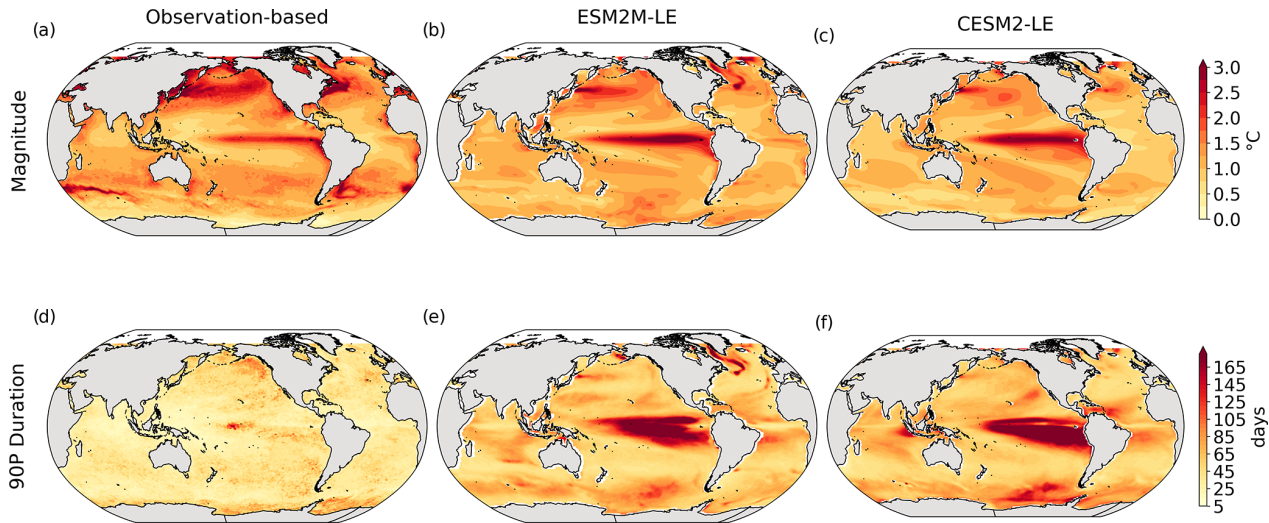


Figure B2. Simulated mean magnitude and duration of MHWs over 1998–2018. Mean SST anomaly relative to the seasonal cycle ($^{\circ}\text{C}$) during MHWs in (a) the observation-based estimate, (b) ESM2M-LE, and (c) CESM2-LE. Simulated 90th percentile of the MHW durations (days) in (d) the observation-based estimate, (e) ESM2M-LE, and (f) CESM2-LE. The global mean magnitude equals 1.3, 1.2, and 1.2°C , while the global mean 90th percentile of the duration equals 36, 69, and 75 d in the observations, ESM2M-LE, and CESM2-LE, respectively.

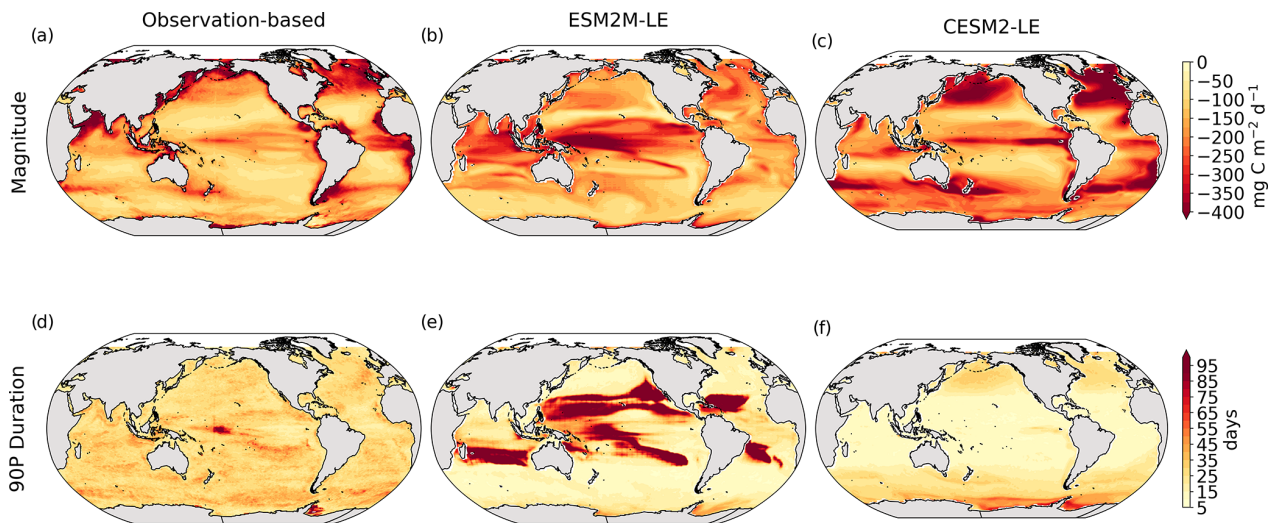


Figure B3. Simulated mean magnitude and duration of NPPX events over 1998–2018. Mean NPP anomaly relative to the seasonal cycle ($\text{mg C m}^{-2} \text{d}^{-1}$) during NPPX events in (a) observation-based estimates, (b) ESM2M-LE, and (c) CESM2-LE. The 90th percentile of the NPPX events duration (days) in (d) observation-based estimates, (e) ESM2M-LE, and (f) CESM2-LE. The global mean magnitude equals -209 , -182 and $-223 \text{ mg C m}^{-2} \text{d}^{-1}$, while the global mean 90th percentile of the duration equals 29, 34, and 18 d in the observations, ESM2M-LE, and CESM2-LE, respectively.

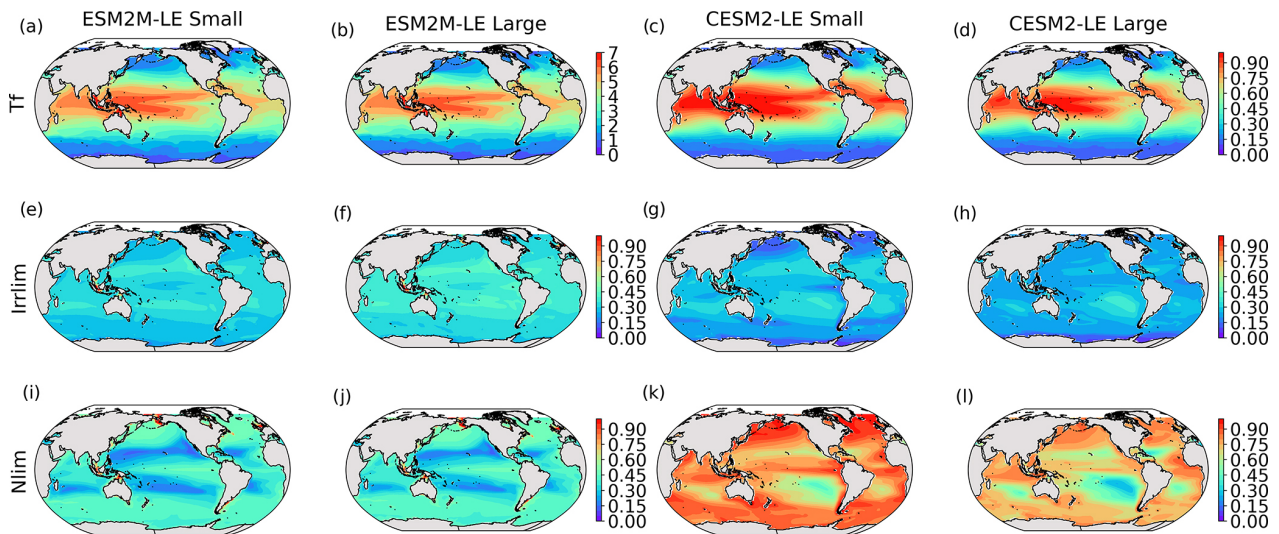


Figure B4. Simulated mean states of the temperature (a–d, T_f), light (e–h, Irr_{lim}), and nutrient (i–l, N_{lim}) limitations on the small- and large-phytoplankton growth rates in ESM2M-LE and CESM2-LE over 1998–2018.

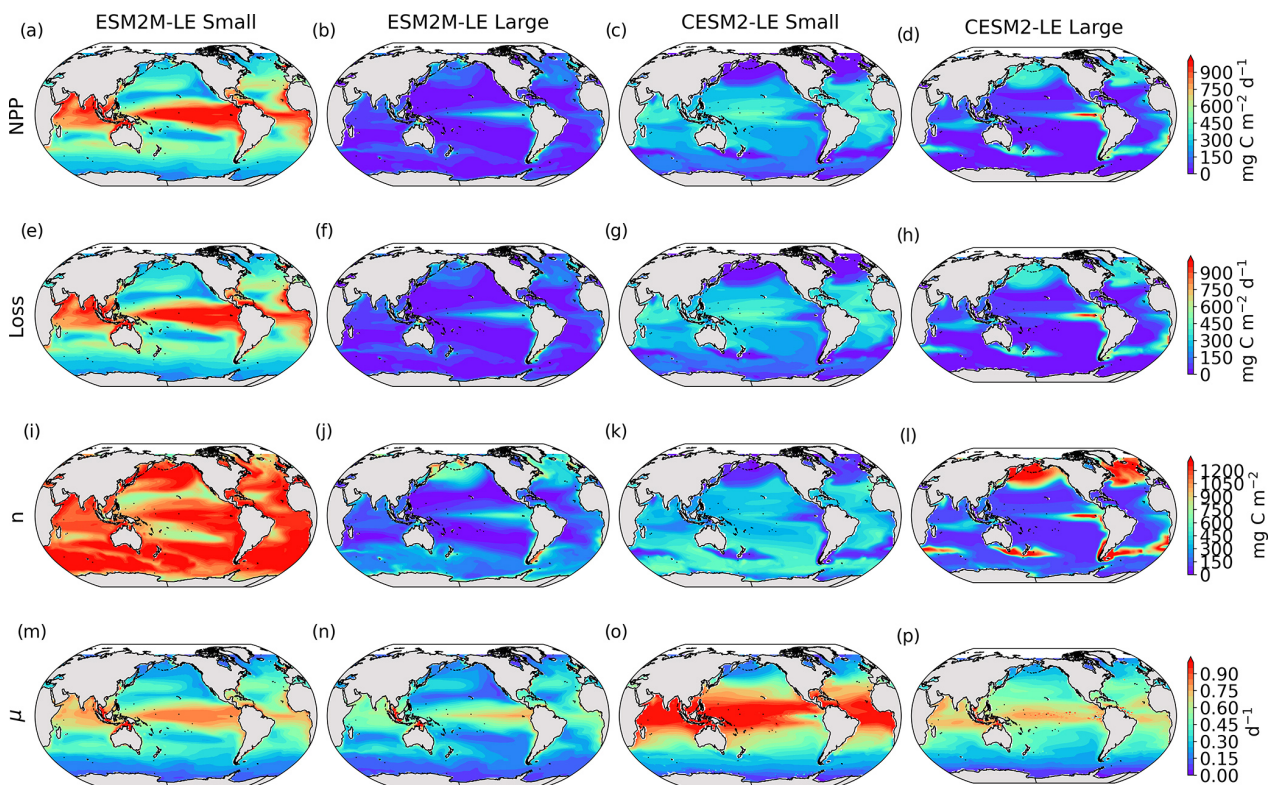


Figure B5. Simulated mean states of small- and large-phytoplankton NPP (a–d, $\text{mg C m}^{-2} \text{d}^{-1}$), loss (e–h, $\text{mg C m}^{-2} \text{d}^{-1}$), biomass (i–l, mg C m^{-2}), and growth rates (m–p, d^{-1}) in ESM2M-LE and CESM2-LE over 1998–2018.

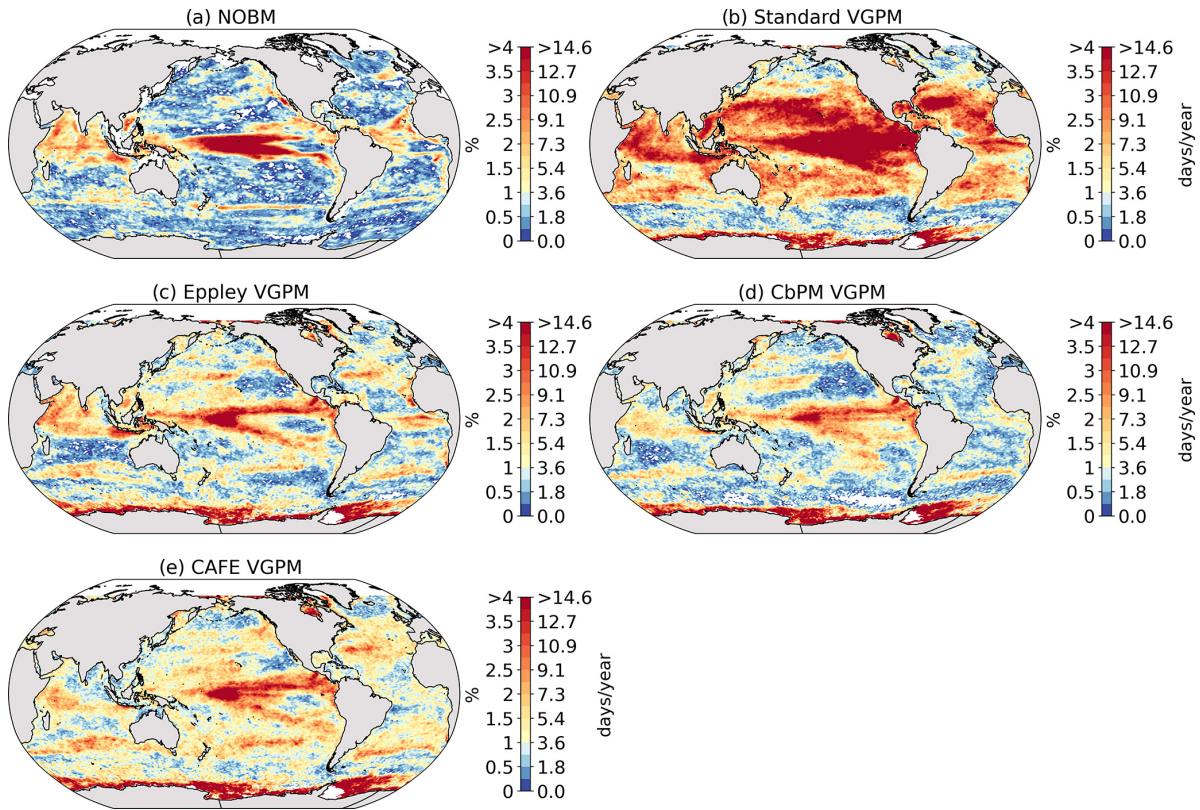


Figure B6. Likelihood (%) of compound MHW–NPPX events estimated using the observation-based NPP product of (a) NOBM, (b) Standard VGPM, (c) Eppley-VGPM, (d) CbPM-VGPM, and (e) CAFE-VGPM.

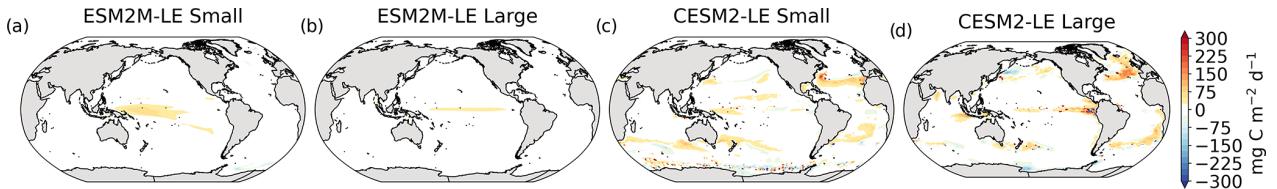


Figure B7. Difference between the NPP anomaly $dNPP$ during compound MHW–NPPX events and its decomposition into a contribution of the growth rate anomaly $nd\mu$ and of the biomass anomaly μdn ($mg\ C\ m^{-2}\ d^{-1}$) during compound MHW–NPPX events for small and large phytoplankton in ESM2M-LE (a, b) and in CESM2-LE (c, d).

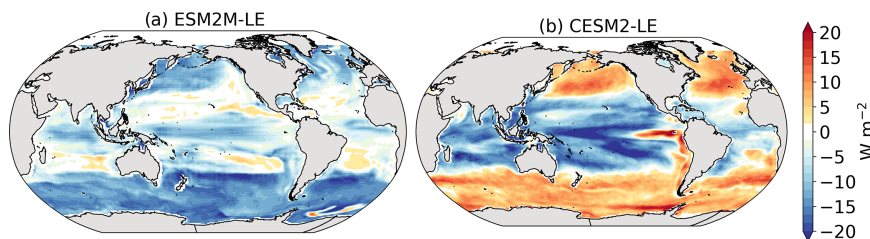


Figure B8. Surface photosynthesis available radiation anomaly ($W\ m^{-2}$) during MHW–NPPX events relative to the seasonal cycle in ESM2M-LE (a) and in CESM2-LE (b).

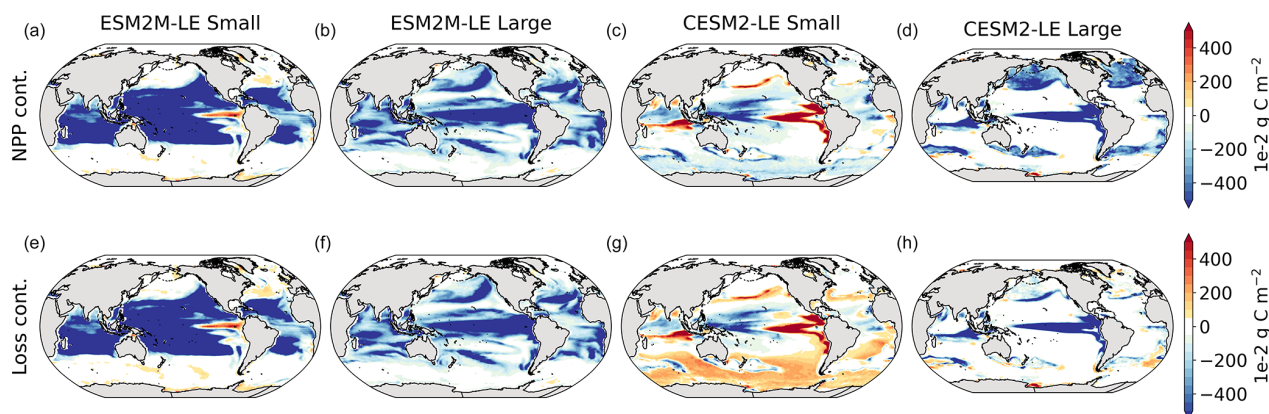


Figure B9. Contributions ($1 \times 10^{-2} \text{ g C m}^{-2} \text{ d}^{-1}$) of small- and large-phytoplankton NPP and Loss to the buildup of the maximum biomass anomaly ($\text{mg C m}^{-2} \text{ d}^{-1}$) in ESM2M-LE (a, b, e, f) and in CESM2-LE (c, d, g, h).

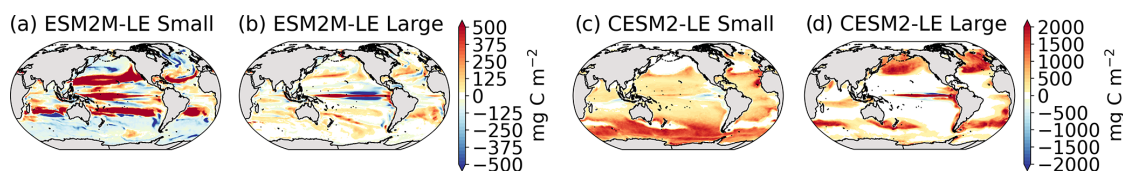


Figure B10. Difference between the integrated biomass change Δn (Fig. 5e–h) and the NPP – Loss contribution to Δn (Fig. 5i–l). This residual term includes the circulation contribution to Δn and all errors inherent to the decomposition in Eq. (8).

Code and data availability. The satellite SST data are available under <https://psl.noaa.gov/data/gridded/data.noaa.oisst.v2.highres.html> (last access: 21 October 2021; Reynolds et al., 2007). The NPP data assimilated by the NASA Ocean Biogeochemical Model are publicly available from 1998 to 2015 under <https://doi.org/10.5067/PT6TXZKSHBW9> (Watson and Rousseaux, 2017). Cécile Rousseaux provided a pre-release of the chlorophyll data from 2016 to 2018, and these data are available upon request. The NPP data assimilated by the VGPM-based models are publicly available under http://orca.science.oregonstate.edu/npp_products.php (last access: 30 November 2021; Standard-VGPM and Eppley-VGPM: <https://doi.org/10.4319/lo.1997.42.1.0001>, Behrenfeld and Falkowski, 1997; CbPM: <https://doi.org/10.1029/2007GB003078>, Westberry et al., 2008; CAFE: <https://doi.org/10.1002/2016GB005521>, Silsbe et al., 2016). The data and the code to generate the figures in this study have been deposited in a Zenodo repository under <https://doi.org/10.5281/zenodo.7330443> (Le Grix, 2022).

Author contributions. NLG, JZ, and TLF designed the study. KBR and RY provided the CESM2 output. NLG performed the analysis and wrote the initial draft of the manuscript. All authors discussed the analysis and results and contributed to the writing of the paper.

Competing interests. The contact author has declared that none of the authors has any competing interests.

Disclaimer. The work reflects only the authors' view; the European Commission and their executive agency are not responsible for any use that may be made of the information the work contains.

Publisher's note: Copernicus Publications remains neutral with regard to jurisdictional claims in published maps and institutional affiliations.

Acknowledgements. The GFDL ESM2M simulations were conducted at the Swiss National Supercomputing Centre, and CESM2-LE was run on the IBS/ICCP supercomputer "Aleph" in South Korea. The authors thank Friedrich Burger for help with setting up the simulations, Cecile Rousseaux for providing the NASA Ocean Biogeochemical Model dataset for net primary production, and Charlotte Laufkötter for initial discussions.

Financial support. This research has been supported by the Schweizerischer National Fonds zur Förderung der Wissenschaftlichen Forschung (grant no. PP00P2-198897), the Institute for Basic Science (grant no. IBS-R028-D1), and the European Union's Horizon 2020 research and innovation programme under grant agreement no. 820989 (project COMFORT) and no. 862923 (project AtlantECO).

Review statement. This paper was edited by Julia Uitz and reviewed by Lester Kwiatkowski and Matthieu Lengaigne.

References

- Acevedo-Trejos, E., Brandt, G., Steinacher, M., and Merico, A.: A glimpse into the future composition of marine phytoplankton communities, *Frontiers in Marine Science*, 1, 15, <https://doi.org/10.3389/fmars.2014.00015>, 2014.
- Banzon, V., Smith, T. M., Chin, T. M., Liu, C., and Hankins, W.: A long-term record of blended satellite and in situ sea-surface temperature for climate monitoring, modeling and environmental studies, *Earth Syst. Sci. Data*, 8, 165–176, <https://doi.org/10.5194/essd-8-165-2016>, 2016.
- Behrenfeld, M. J. and Falkowski, P. G.: Photosynthetic rates derived from satellite-based chlorophyll concentration, *Limnol. Oceanogr.*, 42, 1–20, <https://doi.org/10.4319/lo.1997.42.1.0001>, 1997 (data available at: http://orca.science.oregonstate.edu/npp_products.php, last access: 30 November 2021).
- Behrenfeld, M. J., Boss, E., Siegel, D. A., and Shea, D. M.: Carbon-based ocean productivity, phytoplankton physiology from space, *Global Biogeochem. Cy.*, 19, GB1006, <https://doi.org/10.1029/2004GB002299>, 2005.
- Bindoff, N., Cheung, W., Kairo, J., Aristegui, J., Guinder, V., Hallberg, R., Hilmi, N., Jiao, N., Karim, M., Levin, L., O'Donoghue, S., Cuicapusa, S. P., Rinkevich, B., Suga, T., Tagliabue, A., and Williamson, P.: Changing Ocean, Marine Ecosystems, and Dependent Communities, in: IPCC Special Report on the Ocean, Cryosphere in a Changing Climate, Cambridge University Press, <https://doi.org/10.1017/9781009157964>, 2019.
- Bond, N. A., Cronin, M. F., Freeland, H., and Mantua, N.: Causes, impacts of the 2014 warm anomaly in the NE Pacific, *Geophys. Res. Lett.*, 42, 3414–3420, <https://doi.org/10.1002/2015GL063306>, 2015.
- Bopp, L., Resplandy, L., Orr, J. C., Doney, S. C., Dunne, J. P., Gehlen, M., Halloran, P., Heinze, C., Ilyina, T., Séférian, R., Tjiputra, J., and Vichi, M.: Multiple stressors of ocean ecosystems in the 21st century: projections with CMIP5 models, *Biogeosciences*, 10, 6225–6245, <https://doi.org/10.5194/bg-10-6225-2013>, 2013.
- Bopp, L., Aumont, O., Kwiatkowski, L., Clerc, C., Dupont, L., Ethé, C., Gorgues, T., Séférian, R., and Tagliabue, A.: Diazotrophy as a key driver of the response of marine net primary productivity to climate change, *Biogeosciences*, 19, 4267–4285, <https://doi.org/10.5194/bg-19-4267-2022>, 2022.
- Boyce, D. G., Lewis, M. R., and Worm, B.: Global phytoplankton decline over the past century, *Nature*, 466, 591–596, <https://doi.org/10.1038/nature09268>, 2010.
- Boyd, P. and Harrison, P.: Phytoplankton dynamics in the NE subarctic Pacific, *Deep-Sea Res. Pt. II*, 46, 2405–2432, [https://doi.org/10.1016/S0967-0645\(99\)00069-7](https://doi.org/10.1016/S0967-0645(99)00069-7), 1999.
- Boyd, P. W. and Brown, C. J.: Modes of interactions between environmental drivers, marine biota, *Frontiers in Marine Science*, 2, 9, <https://doi.org/10.3389/fmars.2015.00009>, 2015.
- Burger, F., Terhaar, J., and Frölicher, T. L.: Compound marine heatwaves and ocean acidity extremes, *Nat. Commun.*, 13, 4722, <https://doi.org/10.1038/s41467-022-32120-7>, 2022.
- Burger, F. A., John, J. G., and Frölicher, T. L.: Increase in ocean acidity variability and extremes under increasing atmospheric CO₂, *Biogeosciences*, 17, 4633–4662, <https://doi.org/10.5194/bg-17-4633-2020>, 2020.
- Cavole, L., Demko, A., Diner, R., Giddings, A., Koester, I., Pagniello, C., Paulsen, M.-L., Ramírez-Valdez, A., Schwenck, S., Zill, M., and Franks, P.: Biological Impacts of the 2013–2015 Warm-Water Anomaly in the Northeast Pacific: Winners, Losers, and the Future, *Oceanography*, 29, 273–285, <https://doi.org/10.5670/oceanog.2016.32>, 2016.
- Cheng, L., Trenberth, K. E., Fasullo, J., Boyer, T., Abraham, J., and Zhu, J.: Improved estimates of ocean heat content from 1960 to 2015, *Sci. Adv.*, 3, e1601545, <https://doi.org/10.1126/sciadv.1601545>, 2017.
- Cheung, W. W. L. and Frölicher, T. L.: Marine heatwaves exacerbate climate change impacts for fisheries in the northeast Pacific, *Sci. Rep.*, 10, 6678, <https://doi.org/10.1038/s41598-020-63650-z>, 2020.
- Danabasoglu, G., Lamarque, J.-F., Bacmeister, J., Bailey, D. A., DuVivier, A. K., Edwards, J., Emmons, L. K., Fasullo, J., Garcia, R., Gettelman, A., Hannay, C., Holland, M. M., Large, W. G., Lauritzen, P. H., Lawrence, D. M., Lenaerts, J. T. M., Lindsay, K., Lipscomb, W. H., Mills, M. J., Neale, R., Oleson, K. W., Otto-Bliesner, B., Phillips, A. S., Sacks, W., Tilmes, S., van Kampenhou, L., Vertenstein, M., Bertini, A., Dennis, J., Deser, C., Fischer, C., Fox-Kemper, B., Kay, J. E., Kinnison, D., Kushner, P. J., Larson, V. E., Long, M. C., Mickelson, S., Moore, J. K., Nienhouse, E., Polvani, L., Rasch, P. J., and Strand, W. G.: The Community Earth System Model Version 2 (CESM2), *J. Adv. Model. Earth Syst.*, 12, e2019MS001916, <https://doi.org/10.1029/2019MS001916>, 2020.
- Deser, C., Lehner, F., Rodgers, K., Ault, T., Delworth, T., DiNezio, P., Fiore, A., Frankignoul, C., Fyfe, J., Horton, D., Kay, J., Knutti, R., Lovenduski, N., Marotzke, J., McKinnon, K., Minobe, S., Randerson, J., Screen, J., Simpson, I., and Ting, M.: Insights from Earth system model initial-condition large ensembles and future prospects, *Nat. Clim. Change*, 10, 277–286, <https://doi.org/10.1038/s41558-020-0731-2>, 2020.
- Di Lorenzo, E. and Mantua, N.: Multi-year persistence of the 2014/15 North Pacific marine heatwave, *Nat. Clim. Change*, 6, 1042–1047, <https://doi.org/10.1038/nclimate3082>, 2016.
- Doney, S. C., Ruckelshaus, M., Emmett Duffy, J., Barry, J. P., Chan, F., English, C. A., Galindo, H. M., Grebmeier, J. M., Hollowed, A. B., Knowlton, N., Polovina, J., Rabalais, N. N., Sydeman, W. J., and Talley, L. D.: Climate Change Impacts on Marine Ecosystems, *Annu. Rev. Mar. Sci.*, 4, 11–37, <https://doi.org/10.1146/annurev-marine-041911-111611>, 2012.
- Dunne, J. P., John, J. G., Adcroft, A. J., Griffies, S. M., Hallberg, R. W., Shevliakova, E., Stouffer, R. J., Cooke, W., Dunne, K. A., Harrison, M. J., Krasting, J. P., Malyshev, S. L., Milly, P.

N. Le Grix et al.: Drivers of compound marine heatwaves and low NPP extremes

5833

- C. D., Philipps, P. J., Sentman, L. T., Samuels, B. L., Spelman, M. J., Winton, M., Wittenberg, A. T., and Zadeh, N.: GFDL's ESM2 Global Coupled Climate–Carbon Earth System Models. Part I: Physical Formulation, Baseline Simulation Characteristics, *J. Climate*, 25, 6646–6665, <https://doi.org/10.1175/JCLI-D-11-00560.1>, 2012.
- Dunne, J. P., John, J. G., Shevliakova, E., Stouffer, R. J., Krasting, J. P., Malyshev, S. L., Milly, P. C. D., Sentman, L. T., Adcroft, A. J., Cooke, W., Dunne, K. A., Griffies, S. M., Hallberg, R. W., Harrison, M. J., Levy, H., Wittenberg, A. T., Phillips, P. J., and Zadeh, N.: GFDL's ESM2 Global Coupled Climate–Carbon Earth System Models. Part II: Carbon System Formulation, Baseline Simulation Characteristics, *J. Climate*, 26, 2247–2267, <https://doi.org/10.1175/JCLI-D-12-00150.1>, 2013.
- Eppley, R. W.: Temperature, phytoplankton growth in the sea, *Fish. Bull.*, 70, 1063–1085, 1972.
- Eyring, V., Bony, S., Meehl, G. A., Senior, C. A., Stevens, B., Stouffer, R. J., and Taylor, K. E.: Overview of the Coupled Model Intercomparison Project Phase 6 (CMIP6) experimental design and organization, *Geosci. Model Dev.*, 9, 1937–1958, <https://doi.org/10.5194/gmd-9-1937-2016>, 2016.
- Fay, A. R. and McKinley, G. A.: Global open-ocean biomes: mean and temporal variability, *Earth Syst. Sci. Data*, 6, 273–284, <https://doi.org/10.5194/essd-6-273-2014>, 2014.
- Frost, B. W. and Franzen, N. C.: Grazing, iron limitation in the control of phytoplankton stock, nutrient concentration: a chemostat analogue of the Pacific equatorial upwelling zone, *Mar. Ecol. Prog. Ser.*, 83, 291–303, 1992.
- Frölicher, T. L. and Laufkötter, C.: Emerging risks from marine heat waves, *Nat. Commun.*, 9, 650, <https://doi.org/10.1038/s41467-018-03163-6>, 2018.
- Frölicher, T. L., Joos, F., Plattner, G.-K., Steinacher, M., and Doney, S. C.: Natural variability and anthropogenic trends in oceanic oxygen in a coupled carbon cycle–climate model ensemble, *Global Biogeochem. Cy.*, 23, GB1003, <https://doi.org/10.1029/2008GB003316>, 2009.
- Frölicher, T. L., Rodgers, K. B., Stock, C. A., and Cheung, W. W. L.: Sources of uncertainties in 21st century projections of potential ocean ecosystem stressors, *Global Biogeochem. Cy.*, 30, 1224–1243, <https://doi.org/10.1002/2015GB005338>, 2016.
- Frölicher, T. L., Fischer, E. M., and Gruber, N.: Marine heatwaves under global warming, *Nature*, 560, 360–364, <https://doi.org/10.1038/s41586-018-0383-9>, 2018.
- Gelaro, R., McCarty, W., Suárez, M., Todling, R., Molod, A., Takacs, L., Randles, C., Darmenov, A., Bosilovich, M., Reichle, R., Wargan, K., Coy, L., Cullather, R., Draper, C., Akella, S., Buchard, V., Conaty, A., Da Silva, A., Gu, W., and Zhao, B.: The Modern-Era Retrospective Analysis for Research, Applications, Version 2 (MERRA-2), *J. Climate*, 30, 5419–5454, <https://doi.org/10.1175/JCLI-D-16-0758.1>, 2017.
- Gittings, J., Raitos, D., Krokos, G., and Hoteit, I.: Impacts of warming on phytoplankton abundance, phenology in a typical tropical marine ecosystem, *Sci. Rep.*, 8, 2240, <https://doi.org/10.1038/s41598-018-20560-5>, 2018.
- Gregg, W. and Rousseaux, C. (Eds.): NASA Ocean Biogeochemical Model assimilating satellite chlorophyll data global daily VR2017, Goddard Earth Sciences Data and Information Services Center (GES DISC) [data set], Greenbelt, MD, USA, <https://doi.org/10.5067/PT6TXZKSHBW9>, 2017.
- Gregg, W. W. and Casey, N. W.: Sampling biases in MODIS, SeaWiFS ocean chlorophyll data, *Remote Sens. Environ.*, 111, 25–35, <https://doi.org/10.1016/j.rse.2007.03.008>, 2007.
- Griffies, S. M.: Elements of the modular ocean model (MOM), GFDL Ocean Group Tech. Rep. 7, 1–633, https://mom-ocean.github.io/assets/pdfs/MOM5_manual.pdf (last access: 1 January 2022), 2012.
- Gruber, N.: Warming up, turning sour, losing breath: ocean biogeochemistry under global change, *Philos. T. Roy. Soc. A*, 369, 1980–1996, <https://doi.org/10.1098/rsta.2011.0003>, 2011.
- Gruber, N., Boyd, P. W., Frölicher, T. L., and Vogt, M.: Ocean biogeochemical extremes, compound events, *Nature*, 600, 395–407, <https://doi.org/10.1038/s41586-021-03981-7>, 2021.
- Gupta, A., Thomsen, M., Benthuyzen, J., Hobday, A., Oliver, E., Alexander, L., Burrows, M., Donat, M., Feng, M., Holbrook, N., Perkins-Kirkpatrick, S., Moore, P., Rodrigues, R., Scannell, H., Taschetto, A., Ummenhofer, C., Wernberg, T., and Smale, D.: Drivers and impacts of the most extreme marine heatwave events, *Sci. Rep.*, 10, 19359, <https://doi.org/10.1038/s41598-020-75445-3>, 2020.
- Hayashida, H., Matear, R. J., and Strutton, P. G.: Background nutrient concentration determines phytoplankton bloom response to marine heatwaves, *Glob. Change Biol.*, 26, 4800–4811, <https://doi.org/10.1111/gcb.15255>, 2020.
- Hobday, A. J., Alexander, L. V., Perkins, S. E., Smale, D. A., Straub, S. C., Oliver, E. C., Benthuyzen, J. A., Burrows, M. T., Donat, M. G., Feng, M., Holbrook, N. J., Moore, P. J., Scannell, H. A., Sen Gupta, A., and Wernberg, T.: A hierarchical approach to defining marine heatwaves, *Prog. Oceanogr.*, 141, 227–238, <https://doi.org/10.1016/j.pocean.2015.12.014>, 2016.
- Holbrook, N. J., Scannell, H. A., Gupta, A. S., Benthuyzen, J. A., Feng, M., Oliver, E. C. J., Alexander, L. V., Burrows, M. T., Donat, M. G., Hobday, A. J., Moore, P. J., Perkins-Kirkpatrick, S. E., Smale, D. A., Thomas, S. C. S., and Thomas, W.: A global assessment of marine heatwaves and their drivers, *Nat. Commun.*, 10, 2624, <https://doi.org/10.1038/s41467-019-10206-z>, 2019.
- Jones, T., Parrish, J. K., Peterson, W. T., Bjorkstedt, E. P., Bond, N. A., Ballance, L. T., Bowes, V., Hipfner, J. M., Burgess, H. K., Dolliver, J. E., Lindquist, K., Lindsey, J., Nevins, H. M., Robertson, R. R., Roletto, J., Wilson, L., Joyce, T., and Harvey, J.: Massive Mortality of a Planktivorous Seabird in Response to a Marine Heatwave, *Geophys. Res. Lett.*, 45, 3193–3202, <https://doi.org/10.1002/2017GL076164>, 2018.
- Kwiatkowski, L., Torres, O., Bopp, L., Aumont, O., Chamberlain, M., Christian, J. R., Dunne, J. P., Gehlen, M., Ilyina, T., John, J. G., Lenton, A., Li, H., Lovenduski, N. S., Orr, J. C., Palmieri, J., Santana-Falcón, Y., Schwinger, J., Séférian, R., Stock, C. A., Tagliabue, A., Takano, Y., Tjiputra, J., Toyama, K., Tsujino, H., Watanabe, M., Yamamoto, A., Yool, A., and Ziehn, T.: Twenty-first century ocean warming, acidification, deoxygenation, and upper-ocean nutrient and primary production decline from CMIP6 model projections, *Biogeosciences*, 17, 3439–3470, <https://doi.org/10.5194/bg-17-3439-2020>, 2020.
- Laufkötter, C., Vogt, M., Gruber, N., Aita-Noguchi, M., Aumont, O., Bopp, L., Buitenhuis, E., Doney, S. C., Dunne, J., Hashioka, T., Hauck, J., Hirata, T., John, J., Le Quéré, C., Lima, I. D., Nakano, H., Seferian, R., Totterdell, I., Vichi, M., and Völker, C.: Drivers and uncertainties of future global marine primary pro-

- duction in marine ecosystem models, *Biogeosciences*, 12, 6955–6984, <https://doi.org/10.5194/bg-12-6955-2015>, 2015.
- Laufkötter, C., Zscheischler, J., and Frölicher, T. L.: High-impact marine heatwaves attributable to human-induced global warming, *Science*, 369, 1621–1625, <https://doi.org/10.1126/science.aba0690>, 2020.
- Le, C., Wu, S., Hu, C., Beck, M. W., and Yang, X.: Phytoplankton decline in the eastern North Pacific transition zone associated with atmospheric blocking, *Glob. Change Biol.*, 25, 3485–3493, <https://doi.org/10.1111/gcb.14737>, 2019.
- Le Grix, N.: Data and code for “Hotspots and drivers of compound marine heatwave and low net primary production extremes” (1.0), Zenodo [data set and code], <https://doi.org/10.5281/zenodo.7330443>, 2022.
- Le Grix, N., Zscheischler, J., Laufkötter, C., Rousseaux, C. S., and Frölicher, T. L.: Compound high-temperature and low-chlorophyll extremes in the ocean over the satellite period, *Biogeosciences*, 18, 2119–2137, <https://doi.org/10.5194/bg-18-2119-2021>, 2021.
- Leonard, M., Westra, S., Phatak, A., Lambert, M., van den Hurk, B., McInnes, K., Risbey, J., Schuster, S., Jakob, D., and Stafford-Smith, M.: A compound event framework for understanding extreme impacts, *WIREs Climate Change*, 5, 113–128, <https://doi.org/10.1002/wcc.252>, 2014.
- Litchman, E., Klausmeier, C. A., Miller, J. R., Schofield, O. M., and Falkowski, P. G.: Multi-nutrient, multi-group model of present and future oceanic phytoplankton communities, *Biogeosciences*, 3, 585–606, <https://doi.org/10.5194/bg-3-585-2006>, 2006.
- Long, J. S., Fassbender, A. J., and Estapa, M. L.: Depth-Resolved Net Primary Production in the Northeast Pacific Ocean: A Comparison of Satellite, Profiling Float Estimates in the Context of Two Marine Heatwaves, *Geophys. Res. Lett.*, 48, e2021GL093462, <https://doi.org/10.1029/2021GL093462>, 2021.
- Long, M. C., Moore, J. K., Lindsay, K., Levy, M., Doney, S. C., Luo, J. Y., Krumhardt, K. M., Letscher, R. T., Grover, M., and Sylvester, Z. T.: Simulations With the Marine Biogeochemistry Library (MARBL), *J. Adv. Model. Earth Syst.*, 13, e2021MS002647, <https://doi.org/10.1029/2021MS002647>, 2021.
- Mogen, S. C., Lovenduski, N. S., Dallmann, A. R., Gregor, L., Sutton, A. J., Bograd, S. J., Quiros, N. C., Di Lorenzo, E., Hazen, E. L., Jacox, M. G., Buil, M. P., and Yeager, S.: Ocean Biogeochemical Signatures of the North Pacific Blob, *Geophys. Res. Lett.*, 49, e2021GL096938, <https://doi.org/10.1029/2021GL096938>, 2022.
- Oliver, E. C., Benthuisen, J. A., Darmaraki, S., Donat, M. G., Hobday, A. J., Holbrook, N. J., Schlegel, R. W., and Sen Gupta, A.: Marine Heatwaves, *Annu. Rev. Mar. Sci.*, 13, 313–342, <https://doi.org/10.1146/annurev-marine-032720-095144>, 2021.
- Oliver, E. C. J., Donat, M. G., Burrows, M. T., Moore, P. J., Smale, D. A., Alexander, L. V., Benthuisen, J. A., Feng, M., Sen Gupta, A., Hobday, A. J., Holbrook, N. J., Perkins-Kirkpatrick, S. E., Scannell, H. A., Straub, S. C., and Wernberg, T.: Longer, more frequent marine heatwaves over the past century, *Nat. Commun.*, 9, 1324, <https://doi.org/10.1038/s41467-018-03732-9>, 2018.
- O’Neill, R., DeAngelis, D., Pastor, J., Jackson, B., and Post, W.: Multiple nutrient limitations in ecological models, *Ecol. Model.*, 46, 147–163, [https://doi.org/10.1016/0304-3800\(89\)90015-X](https://doi.org/10.1016/0304-3800(89)90015-X), 1989.
- Peña, M. A., Nemcek, N., and Robert, M.: Phytoplankton responses to the 2014–2016 warming anomaly in the northeast subarctic Pacific Ocean, *Limnol. Oceanogr.*, 64, 515–525, <https://doi.org/10.1002/lno.11056>, 2019.
- Piatt, J. F., Parrish, J. K., Renner, H. M., Schoen, S. K., Jones, T., Arimitsu, M. L., Kuletz, K. J., Bodenstein, B. L., García-Reyes, M., Duerr, R. S., Corcoran, R. M., Kaler, R. S. A., McChesney, G. J., Golightly, R. T., Coletti, H. A., Suryan, R. M., Burgess, H. K., Lindsey, J., Lindquist, K., Warzybok, P. M., Jahncke, J., Roletto, J., and Sydeman, W. J.: Extreme mortality, reproductive failure of common murrelets resulting from the northeast Pacific marine heatwave of 2014–2016, *PLoS ONE*, 15, e0226087, <https://doi.org/10.1371/journal.pone.0226087>, 2020.
- Pilo, G. S., Holbrook, N. J., Kiss, A. E., and Hogg, A. M.: Sensitivity of Marine Heatwave Metrics to Ocean Model Resolution, *Geophys. Res. Lett.*, 46, 14604–14612, <https://doi.org/10.1029/2019GL084928>, 2019.
- Reynolds, R. W., Smith, T. M., Liu, C., Chelton, D. B., Casey, K. S., and Schlax, M. G.: Daily High-Resolution-Blended Analyses for Sea Surface Temperature, *J. Climate*, 20, 5473–5496, 2007 (data available at: <https://psl.noaa.gov/data/gridded/data.noaa.oisst.v2.highres.html>, last access: 30 November 2021).
- Riahi, K., Rao, S., Krey, V., Cho, C., Chirkov, V., Fischer, G., Kindermann, G., Nakicenovic, N., and Rafaj, P.: RCP 8.5 – A scenario of comparatively high greenhouse gas emissions, *Climatic Change*, 109, 33–57, <https://doi.org/10.1007/s10584-011-0149-y>, 2011.
- Riahi, K., van Vuuren, D. P., Kriegler, E., Edmonds, J., O’Neill, B. C., Fujimori, S., Bauer, N., Calvin, K., Dellink, R., Fricko, O., Lutz, W., Popp, A., Cuaresma, J. C., KC, S., Leimbach, M., Jiang, L., Kram, T., Rao, S., Emmerling, J., Ebi, K., Hasegawa, T., Havlik, P., Humenöder, F., Da Silva, L. A., Smith, S., Stehfest, E., Bosetti, V., Eom, J., Gernaat, D., Masui, T., Rogelj, J., Strefler, J., Drouet, L., Krey, V., Luderer, G., Harmsen, M., Takahashi, K., Baumstark, L., Doelman, J. C., Kainuma, M., Klimont, Z., Marangoni, G., Lotze-Campen, H., Obersteiner, M., Tabeau, A., and Tavoni, M.: The Shared Socioeconomic Pathways, their energy, land use, and greenhouse gas emissions implications: An overview, *Global Environ. Chang.*, 42, 153–168, <https://doi.org/10.1016/j.gloenvcha.2016.05.009>, 2017.
- Ridder, N., Pitman, A., Westra, S., Do, H., Bador, Margot, H., Annette, E., Jason, Di Luca, A., and Zscheischler, J.: Global hotspots for the occurrence of compound events, *Nat. Commun.*, 11, 5956, <https://doi.org/10.1038/s41467-020-19639-3>, 2020.
- Ridder, N., Ukkola, A., Pitman, A., and Perkins-Kirkpatrick, S.: Increased occurrence of high impact compound events under climate change, *npj Climate, Atmospheric Science*, 5, 3, <https://doi.org/10.1038/s41612-021-00224-4>, 2022.
- Rodgers, K. B., Lee, S.-S., Rosenbloom, N., Timmermann, A., Danabasoglu, G., Deser, C., Edwards, J., Kim, J.-E., Simpson, I. R., Stein, K., Stuecker, M. F., Yamaguchi, R., Bóday, T., Chung, E.-S., Huang, L., Kim, W. M., Lamarque, J.-F., Lombardozzi, D. L., Wieder, W. R., and Yeager, S. G.: Ubiquity of human-induced changes in climate variability, *Earth Syst. Dynam.*, 12, 1393–1411, <https://doi.org/10.5194/esd-12-1393-2021>, 2021.
- Rousseaux, C. S. and Gregg, W. W.: Interannual Variation in Phytoplankton Primary Production at A Global Scale, *Remote Sens.*, 6, 1–19, <https://doi.org/10.3390/rs6010001>, 2014.

N. Le Grix et al.: Drivers of compound marine heatwaves and low NPP extremes

5835

- Sherman, E., Moore, J. K., Primeau, F., and Tanouye, D.: Temperature influence on phytoplankton community growth rates, *Global Biogeochem. Cy.*, 30, 550–559, <https://doi.org/10.1002/2015GB005272>, 2016.
- Shi, H., García-Reyes, M., Jacox, M. G., Rykaczewski, R. R., Black, B. A., Bograd, S. J., and Sydeman, W. J.: Co-occurrence of California Drought and Northeast Pacific Marine Heatwaves Under Climate Change, *Geophys. Res. Lett.*, 48, e2021GL092765, <https://doi.org/10.1029/2021GL092765>, 2021.
- Silsbe, G. M., Behrenfeld, M. J., Halsey, K. H., Milligan, A. J., and Westberry, T. K.: The CAFE model: A net production model for global ocean phytoplankton, *Global Biogeochem. Cy.*, 30, 1756–1777, <https://doi.org/10.1002/2016GB005521>, 2016 (data available at: http://orca.science.oregonstate.edu/npp_products.php, last access: 30 November 2021).
- Smith, R. and Gent, P.: The Parallel Ocean Program (POP) reference manual, Los Alamos Unclassified Report LA-UR-02-2484, 2010.
- Tagliabue, A., Kwiatkowski, L., Bopp, L., Butenschön, M., Cheung, W., Lengaigne, M., and Vialard, J.: Persistent Uncertainties in Ocean Net Primary Production Climate Change Projections at Regional Scales Raise Challenges for Assessing Impacts on Ecosystem Services, *Frontiers in Climate*, 3, 738224, <https://doi.org/10.3389/fclim.2021.738224>, 2021.
- The GFDL Global Atmospheric Model Development Team: The New GFDL Global Atmosphere and Land Model AM2–LM2: Evaluation with Prescribed SST Simulations, *J. Climate*, 17, 4641–4673, <http://www.jstor.org/stable/26251977> (last access: 1 January 2022), 2004.
- Vogt, L., Burger, F. A., Griffies, S. M., and Frölicher, T. L.: Local Drivers of Marine Heatwaves: A Global Analysis With an Earth System Model, *Frontiers in Climate*, 4, 847995, <https://doi.org/10.3389/fclim.2022.847995>, 2022.
- Watson G. and Rousseaux, C. (Eds.): NASA Ocean Biogeochemical Model assimilating satellite chlorophyll data global daily VR2017, Goddard Earth Sciences Data and Information Services Center (GES DISC) [data set], Greenbelt, MD, USA, <https://doi.org/10.5067/PT6TXZKSHBW9>, 2017.
- Wernberg, T., Smale, D., Thomsen, M., Langlois, T., de Bettignies, T., Bennett, S., and Rousseaux, C.: An extreme climatic event alters marine ecosystem structure in a global biodiversity hotspot, *Nat. Clim. Change*, 3, 78–82, <https://doi.org/10.1038/nclimate1627>, 2013.
- Westberry, T., Behrenfeld, M. J., Siegel, D. A., and Boss, E.: Carbon-based primary productivity modeling with vertically resolved photoacclimation, *Global Biogeochem. Cy.*, 22, GB2024, <https://doi.org/10.1029/2007GB003078>, 2008 (data available at: http://orca.science.oregonstate.edu/npp_products.php, last access: 30 November 2021).
- Whitney, F. A.: Anomalous winter winds decrease 2014 transition zone productivity in the NE Pacific, *Geophys. Res. Lett.*, 42, 428–431, <https://doi.org/10.1002/2014GL062634>, 2015.
- Woolway, R. I., Kraemer, B. M., Zscheischler, J., and Albergel, C.: Compound hot temperature, high chlorophyll extreme events in global lakes, *Environ. Res. Lett.*, 16, 124066, <https://doi.org/10.1088/1748-9326/ac3d5a>, 2021.
- Wyatt, A., Resplandy, L., and Marchetti, A.: Ecosystem impacts of marine heat waves in the Northeast Pacific, *EGU sphere* [preprint], <https://doi.org/10.5194/egusphere-2022-17>, 2022.
- Yang, B., Emerson, S. R., and Peña, M. A.: The effect of the 2013–2016 high temperature anomaly in the subarctic Northeast Pacific (the “Blob”) on net community production, *Biogeosciences*, 15, 6747–6759, <https://doi.org/10.5194/bg-15-6747-2018>, 2018.
- Zscheischler, J. and Lehner, F.: Attributing Compound Events to Anthropogenic Climate Change, *B. Am. Meteorol. Soc.*, 103, E936–E953, <https://doi.org/10.1175/BAMS-D-21-0116.1>, 2022.
- Zscheischler, J. and Seneviratne, S. I.: Dependence of drivers affects risks associated with compound events, *Sci. Adv.*, 3, e1700263, <https://doi.org/10.1126/sciadv.1700263>, 2017.
- Zscheischler, J., Westra, S., van den Hurk, B. J. J. M., Seneviratne, S. I., Ward, P. J., Pitman, A., AghaKouchak, A., Bresch, D. N., Leonard, M., Wahl, T., and Zhang, X.: Future climate risk from compound events, *Nat. Clim. Change*, 8, 469–477, <https://doi.org/10.1038/s41558-018-0156-3>, 2018.
- Zscheischler, J., Martius, O., Westra, S., Bevacqua, E., Raymond, C., Horton, R., Hurk, B., AghaKouchak, A., Jézéquel, A., Mahecha, M., Maraun, D., Ramos, A., Ridder, N., Thiery, W., and Vignotto, E.: A typology of compound weather, climate events, *Nature Reviews Earth, Environment*, 1, 333–347, <https://doi.org/10.1038/s43017-020-0060-z>, 2020.

Chapter 5

Extreme and compound ocean events are key drivers of projected low pelagic fish biomass

Natacha Le Grix, William Cheung, Gabriel Reygondeau, Jakob Zscheischler, and Thomas L. Frölicher

Submitted to *Global Change Biology*. This chapter includes an Appendix and Bibliography

Extreme and compound ocean events are key drivers of projected low pelagic fish biomass

Natacha Le Grix^{1,2}, William Cheung³, Gabriel Reygondeau³, Jakob Zscheischler^{4,5}, and Thomas L. Frölicher^{1,2}

¹Climate and Environmental Physics, Physics Institute, University of Bern, Bern, Switzerland

²Oeschger Centre for Climate Change Research, University of Bern, Bern, Switzerland

³Changing Ocean Research Unit, Nippon Foundation-Nereus Program, Institute for the Oceans and Fisheries, University of British Columbia, Vancouver, BC, Canada

⁴Department of Computational Hydrosystems, Helmholtz Centre for Environmental Research – UFZ, Leipzig, Germany

⁵Technische Universität Dresden, Dresden, Germany

Correspondence: Natacha Le Grix (natacha.legrix@unibe.ch)

Abstract. Ocean extreme events, such as marine heatwaves, can have harmful impacts on marine ecosystems. Understanding the risks posed by such extreme events is key to develop strategies to predict and mitigate their effects. However, the underlying ocean conditions driving severe impacts on marine ecosystems are complex and often unknown as risks to marine ecosystems arise not only from hazards, but from the interactions between hazards, exposure and vulnerability. Marine ecosystems may not be impacted by extreme events in single drivers but rather by the compounding effects of moderate ocean anomalies instead. Here, we employ an ensemble climate-impact modelling approach that combines a global marine fish model with output from a large ensemble simulation of an Earth system model, to identify the key ocean ecosystem drivers associated with the most severe impacts on the total biomass of 326 pelagic fish species. We show that low net primary productivity is the most influential driver of extremely low fish biomass over 68% of the ocean area, especially in the subtropics and the mid-latitudes, followed by high temperature and low oxygen in the eastern equatorial Pacific and the high latitudes. Severe biomass loss is generally driven by extreme anomalies in at least one ocean ecosystem driver, except in the tropics, where a combination of moderate ocean anomalies is sufficient to drive extreme impacts. Single moderate anomalies never drive extremely low fish biomass. Compound events with either moderate or extreme ocean conditions are a necessary condition for extremely low fish biomass over 78% of the global ocean, and compound events with at least one extreme variable are a necessary condition over 61% of the global ocean. Overall, our model results highlight the crucial role of extreme and compound events in driving severe impacts on pelagic marine ecosystems.

1 Introduction

Extreme events, such as marine heatwaves (Hobday et al., 2016) or low net primary production (NPP) events (Le Grix et al., 2021, 2022) have been linked to a range of negative impacts on marine organisms and ecosystems (Wernberg et al., 2013; Cavole et al., 2016; Smale et al., 2019; Wernberg et al., 2016; Smith et al., 2023), including the collapse of entire ecosystems (e.g., Wernberg (2021)). Of particular concern are compound events, which occur when conditions are anomalous for multiple

ocean ecosystem drivers (Zscheischler et al., 2018; Gruber et al., 2021; Le Grix et al., 2021, 2022; Burger et al., 2022). The 'Blob', a prolonged and extensive marine heatwave that occurred from 2013 to 2015 in the Northeast Pacific, illustrates the potential threat posed by marine compound events on ecosystems. This marine heatwave coincided with anomalously low oxygen, low pH, and large negative anomalies in phytoplankton NPP (Whitney, 2015; Le Grix et al., 2021; Gruber et al., 2021; Mogen et al., 2022; Wyatt et al., 2022), leading to severe impacts on marine life (Cavole et al., 2016), including mortality and reproductive failure of sea birds (Jones et al., 2018; Piatt et al., 2020), mass strandings of sea lions in California and of whales in the western Gulf of Alaska (Cavole et al., 2016), as well as shifts in species distribution towards warm-water species, with repercussions on fisheries (Cavole et al., 2016; Cheung and Frölicher, 2020). Previous research has shown that marine heatwaves and compound extreme events have become more frequent over the past century (Oliver et al., 2018; Gruber et al., 2021) and that this trend is projected to continue as global warming persists (e.g., Frölicher et al. (2018); Burger et al. (2022)). If extreme events and compound events regularly induce collapses in animal biomass and community reorganization, the consequences of an increase in their frequency could be catastrophic for ecosystems, fisheries and human coastal communities. However, the extent to which ocean extreme events and compound events have negative impacts on marine ecosystems remains unclear.

Risks to marine ecosystems arise not only from hazards, such as marine heatwaves or compound events, but from the interactions between hazards, exposure and vulnerability (e.g., Bindoff et al. (2019); Magnan et al. (2021)). Marine ecosystems may not be exposed nor vulnerable to certain extreme or compound extreme events. For example, Fredston, A. L. et al. (2023) (submitted) uses a collection of bottom trawl data from Atlantic and Pacific marine ecosystems to show that historical marine heatwaves did not substantially impact the community composition and biomass of these ecosystems. Certain marine species may even benefit from extreme events. Cavole et al. (2016) reported increased recruitment of rockfish in California and northward expansion of tropical and subtropical copepods during the 'Blob'. These findings highlight the complexity in the relationship between hazards and impacts on marine ecosystems, and suggest that compound events with moderate anomalous ocean conditions may also drive or contribute to severe impacts (Zscheischler et al., 2018). To effectively predict and mitigate future impacts on marine ecosystems, a better understanding of the ocean conditions leading to extreme impacts on marine ecosystems is needed.

The limited understanding of the drivers of extreme impacts on marine ecosystems is partly a result of a lack of sufficient observations (Gruber et al., 2021). One approach that circumvents this lack of observations is the use of *ensemble climate-impact modelling* simulations (van der Wiel et al., 2020; Tschumi et al., 2022). These simulations couple a climate model with an impact model, in our case a global marine fish model. Ensemble climate simulations are produced with the same single climate model under identical external forcing but starting from different initial conditions (Frölicher et al., 2009; Deser et al., 2020). These simulations are then used to force the marine fish model, resulting in a large dataset from which to analyze rare events (e.g., Poschlod et al. (2020); Maher et al. (2021); Bevacqua et al. (2022); Cheung et al. (2021); Le Grix et al. (2021)). The ensemble climate-impact modelling simulations are used for two different purposes. The first and most common purpose is forward modelling, which samples oceanic events, such as marine heatwaves, and quantifies their associated impacts on marine ecosystems (Cheung and Frölicher, 2020; Cheung et al., 2021). However, this approach requires prior knowledge of

potentially harmful hazards and typically only considers extreme events and ignores other moderate drivers of extreme impacts. Here, we employ a backward approach (e.g., Zscheischler et al. (2014b, c); Ben-Ari et al. (2018); van der Wiel et al. (2020); Vogel et al. (2021)), which starts by sampling events of extreme impacts and then looks back at the ocean conditions potentially causing these events. This "impact-driven" approach allows for the discovery of unexpected drivers (van der Wiel et al., 2020) of extreme impacts on fish biomass.

The goal of this study is to identify the ocean conditions associated with the most severe impacts on pelagic fish species, especially those associated with extremely low fish biomass. To achieve this, we employ the global marine fish model DBEM, driven by output of a large ensemble simulation of the comprehensive Earth system model GFDL ESM2M. By considering the total biomass of 326 pelagic fish species, we aim to gain a deeper understanding of the drivers of extreme impacts on the entire pelagic community, rather than focusing on individual species. While this study focuses on a specific climate-fish impact model that is associated with particular assumptions and uncertainties, we aim to obtain generalizable insights that would form the foundation for future studies.

2 Methods

70 2.1 Ensemble climate-impact modelling

We apply an ensemble climate-impact modelling (van der Wiel et al., 2020; Vogel et al., 2021) approach to identify the environmental drivers that lead to projected low pelagic fish biomass events. The approach consists of three steps: 1. Forward modelling; 2. Identification of low biomass events; 3. Backward assessment of the drivers of low fish biomass events. These three steps are illustrated in Fig. 1 and described in detail in the following.

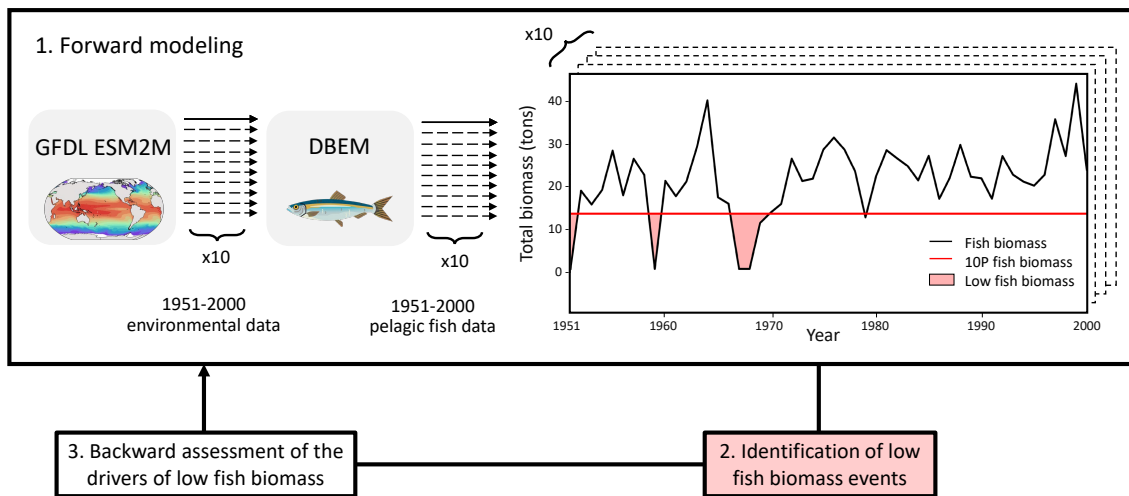


Figure 1. Schematic of the *ensemble climate-impact modelling* approach used in this study. In a first step ("forward modelling"), changes in fish biomass for 326 pelagic species were simulated over the period 1951-2000 by the Dynamic Bioclimatic Envelope Model (DBEM) forced with environmental data from a 10-member large ensemble simulation of the Earth System Model GFDL ESM2M. In a second step ("Identification of low fish biomass events"), low fish biomass events were identified using the 10th percentile threshold (red areas in the bottom figure). In a final step ("backward assessment of the drivers of low fish biomass"), the environmental conditions driving low fish biomass events are assessed. The right panel illustrates low fish biomass events sampled at a grid cell in the northern Pacific (at 71°N; 167°W) for one ensemble member, when the pelagic fish biomass is lower than its local 10th percentile computed from 1951 to 2000 over the entire 10-member simulation.

75 1. Step: Forward modelling

We use annual mean fish biomass data of 326 pelagic fish species simulated by the species-based Dynamic Bioclimatic Envelope Model (DBEM, Cheung et al. (2008, 2016)) (Fig. 1). Pelagic fish represent a large proportion of the marine fish biomass relevant to fisheries (Pauly D. and Palomares M.L.D., 2020). The DBEM uses a species distribution modeling algorithm (Close et al., 2006) to estimate the species initial distribution based on its maximum and minimum depth limits, northern and southern latitudinal range limits, habitat type and known occurrence boundaries (Cheung et al., 2008). These input parameters are mainly provided by two online databases: FishBase (www.fishbase.org) and SeaLifeBase (www.sealifebase.org). Once the DBEM has determined the species distribution, it then simulates their growth, population dynamics and net migrations, depending on ocean temperature, oxygen, and advection, as well as a set of species-specific growth parameters. Movement and dispersal of adults and larvae are modeled through advection-diffusion reaction equations. Environmental preferences are identified for each species by overlaying environmental data from the Earth system model GFDL ESM2M (see below) with maps of the species relative abundance. When environmental conditions deviate from a species environmental preferences, habitat suitability decreases, resulting in a decrease in the species abundance. Biomass is calculated from the population mean body weight and abundance.

The DBEM projects shifts in marine species biomass and distribution under changes in ocean conditions (e.g., Cheung et al. (2013, 2016)) including changes in ocean extreme conditions, such as marine heatwaves, that are consistent with alternative species distribution models and empirical evidence, where data exists (e.g., Cheung et al. (2021)). The horizontal resolution of the DBEM is 0.5° longitude x 0.5° latitude. The model was spun-up for a thousand years using climatological average ocean conditions from 1971 to 2000, allowing the population to reach an equilibrium before it was perturbed with environmental changes from 1951 to 2000.

95 The DBEM was driven by environmental data from a 10-member large ensemble simulation (LES) of an Earth system model, the GFDL ESM2M, covering the time period 1951-2000 (Fig. 1). The GFDL ESM2M, developed at NOAA's Geophysical Fluid Dynamics Laboratory (GFDL), is a fully coupled carbon cycle–climate Earth system model (Dunne et al., 2012, 2013). It couples an atmospheric circulation model to an oceanic circulation model, and includes representations of land, sea ice, and iceberg dynamics, as well as interactive biogeochemistry. The ocean biogeochemical module, TOPAZv2
100 (Dunne et al., 2013), simulates 30 tracers, including three phytoplankton groups (small and large phytoplankton, diazotrophs) and implicit zooplankton activity. The horizontal resolution of the ocean model MOM4p1 (Griffies, 2012) is nominally 1° with increasing meridional resolution of up to $1/3^\circ$ towards the equator. The 10-member large ensemble simulation is forced with prescribed historical concentrations of atmospheric CO_2 and non- CO_2 radiative forcing agents over the historical period (Burger et al., 2020, 2022). The GFDL ESM2M data was regridded to a horizontal resolution of 0.5° for use in the DBEM.
105 Input GFDL ESM2M data into the DBEM includes annual mean horizontal velocities, temperature, dissolved O_2 and salinity at the surface of the ocean, vertically integrated NPP (sum of small and large phytoplankton and diazotrophs), and sea-ice extent. These DBEM simulations do not take into account changes in acidity (e.g., Tai et al. (2021)) or fisheries pressure (e.g., Cheung et al. (2018)).

110 2. Step: Identification of low fish biomass events

Next, we identify low fish biomass (LFB) events over the period 1951 to 2000 (Fig. 1). We chose that time period as it represents the historical oceanic state and is short enough to not contain too large long-term trends in ocean variables. At each grid cell, we define LFB events as years when the annual mean total biomass of pelagic fish is lower than its local 10th percentile (Fig. A1) computed from all ensemble members over 1951-2000. Therefore these events correspond to 1-in-10 year events.

115 From the 10 realizations of the 50-year period, we thus identify $10 \times 5 = 50$ LFB events per grid cell.

3. Step: Backward assessment of the drivers of low fish biomass events

In a third step, we investigate the drivers of extreme reductions in simulated pelagic fish biomass over the 1951-2000 historical period. To do this, we perform a backward assessment of the environmental drivers of LFB events (e.g., Zscheischler et al. (2014b, c); Ben-Ari et al. (2018); van der Wiel et al. (2020); Gagné et al. (2020); Vogel et al. (2021)). Changes in pelagic fish
120 biomass in the DBEM can be driven by changes in depth-integrated net primary production (NPP), surface temperature (T), surface dissolved oxygen levels (O_2), surface salinity (S), and sea-ice extent (Ice). We standardize these ocean variables so

as to best compare their contributions to driving LFB events, by removing the mean and dividing by the standard deviation computed over 1951-2000.

125 To identify drivers of LFB events, we employ a LASSO (least absolute shrinkage and selection operator) logistic regression (Tibshirani, 1996; Vogel et al., 2021). This statistical model allows for classifying years into LFB events and non-LFB events depending on ocean conditions. We consider ocean conditions up to two years before the event, to account for possible lagged effects. The probability of an LFB event to occur is given as:

$$P(LFB) = \frac{1}{1 + e^{-y}} \quad (1)$$

130 with

$$y = \beta_0 + \beta_i X_i \quad (2)$$

where $X_i \in [\text{NPP}, \text{T}, \text{O}_2, \text{S}, \text{and Ice}]$ at the year of the event, one year prior to the event (indicated with -1y) and two years prior to the event (indicated with -2y). An LFB event is predicted when $P(LFB) > 0.5$.

The regression coefficient β_i accounts for the link between an ocean variable X_i and the probability of LFB. A positive β_i 135 signifies that an increase in X_i raises the probability of LFB, and vice versa. However, high correlation between NPP, T, O_2 , S, and Ice implies a high variability of the coefficients β_i (Vogel et al., 2021). For example, T and O_2 are often negatively correlated in the surface ocean, where the main driver of oxygen changes is oxygen solubility, which decreases with increasing temperature (Garcia and Gordon, 1992). The information brought by a high absolute value of T and a low absolute value of O_2 could alternatively be conveyed by a low absolute value of T and a high absolute value of O_2 . To address the high correlation 140 between variables, we specifically employ a LASSO logistic regression (Tibshirani, 1996), which prevents high variability in the coefficients by applying a penalty term on the norm of the coefficients $\|\beta\|$. The regression coefficients are determined by minimizing a cost function $\text{Cost}(\beta)$ with regularization on $\|\beta\|$:

$$\min_{\beta} (\text{Cost}(\beta) + \lambda \|\beta\|) \quad (3)$$

The parameter λ controls the strength of the regularization. Through 5-fold cross validation, we obtained $\lambda_{optimal}$, the value 145 of λ associated with the highest mean cross-validated performance of the model. We then selected $\lambda = \lambda_{SE}$, the value of λ that gives the most regularized model (i.e. the highest lambda) such that its cross-validated performance is within one standard deviation of that of $\lambda_{optimal}$ (Friedman et al., 2010; Krstajic et al., 2014). The penalty term $\lambda \|\beta\|$ tends to produce some regression coefficients β_i that are exactly 0. The LASSO logistic regression therefore performs an automatic selection of the variables that are statistically linked to LFB. As a result, certain grid cells might have just one predictor, like NPP, while others 150 might have up to fifteen predictors.

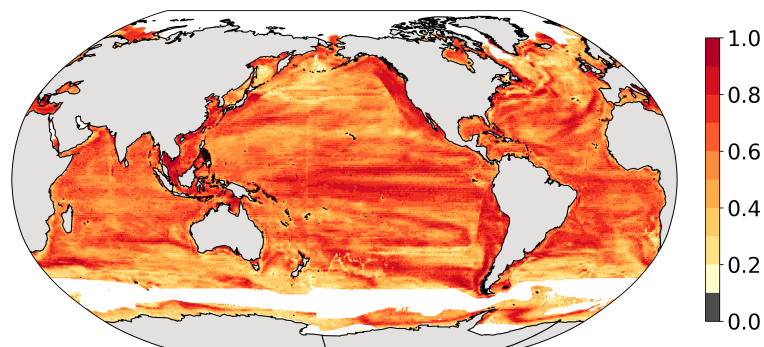


Figure 2. Area under the precision-recall curve (AUC PR) of the LASSO logistic regression. Model performance is satisfactory over areas where AUC PR > 0.1. White areas correspond to regions without fish biomass data.

Model performance is assessed by the area under the precision-recall curve (AUC PR), a metric commonly used to summarize the performance of a binary classification model when the sets are unbalanced (here, 10% of years are LFB events, 90% are not) (Saito and Rehmsmeier, 2015; Cook and Ramadas, 2020). More than 99.99% of the ocean surface area has an AUC PR value greater than 0.1 (Fig. 2), the rate of LFB events in the time series (Saito and Rehmsmeier, 2015), which indicates that the logistic regression performs well at predicting LFB events. Note that we allowed for the inclusion of lagged-effects. Namely, variables one year (-1 year NPP, -1 year T, -1 year O₂, -1 year S, -1 year Ice) and two years (-2 years NPP, -2 years T, -2 years O₂, -2 years S, -2 years Ice) before the event can also be selected as predictors. Allowing for lagged effects increases model performance by 35% compared to a model based on concurrent predictors only.

2.2 Categorizing the drivers of low fish biomass events

We use the coefficients from the LASSO logistic regression to assess whether *extreme*, *compound*, or *compound and extreme* drivers are necessary conditions for LFB events. An LFB is predicted when $P(LFB) > 0.5$, which is equivalent to $y > 0$ in equation 2. For a given location and given the regression coefficients β_i , we test whether y can be positive with all predictors between their 10th and 90th percentile. If not, moderate events cannot drive LFB events, and extreme events are necessary to drive LFB events. Similarly, we test whether drivers can be univariate by testing whether y can be positive with only one predictor being non-zero (and the rest are zero). If not, compounding drivers are a necessary condition for LFB events.

3 Results

Low fish biomass events are associated with shifts in ocean conditions, as demonstrated by the red and blue distributions presented in Fig. 3. On a global scale and on average, NPP is decreased by 0.8 standard deviation (SD) during LFB events compared to normal conditions. Temperature is increased by 0.5 SD, dissolved oxygen decreased by 0.5 SD, and salinity is 0.1

170 SD lower than usual. Furthermore, sea ice extent variability is also enhanced during LFB events. In the following subsections, we further discuss these changes in ocean conditions and show how they can be used to predict LFB events.

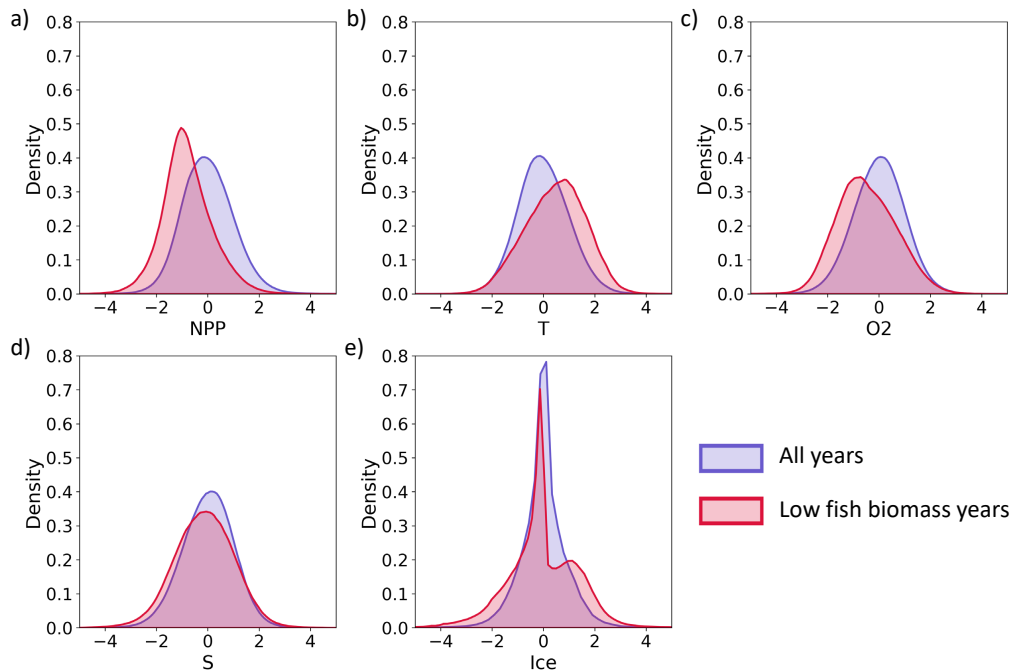


Figure 3. Global distribution of the annual mean standardized NPP, T, O₂, S, and sea ice extent over all years (in blue) and low fish biomass years (in red) over 1951-2000. On the y-axis, density accounts for the probability density function, whose area under the curve is equal to 1. On the x-axis, a shift of the distribution towards -1 corresponds to a reduction in annual mean values of one standard deviation.

3.1 Drivers of low fish biomass events

Using LASSO logistic regression, the probability of an LFB event to occur is modeled as a function of NPP, T, O₂, S, and Ice conditions up to two years prior to the event. Fig. 4a presents the global mean regression coefficients associated with each predictor. A positive coefficient indicates that any increase in the associated predictor increases the probability of an LFB event, while a negative coefficient indicates that any decrease in the associated predictor increases the probability. We first describe the regression coefficients associated with NPP, T, O₂, S, and Ice conditions in the year of the event.

175

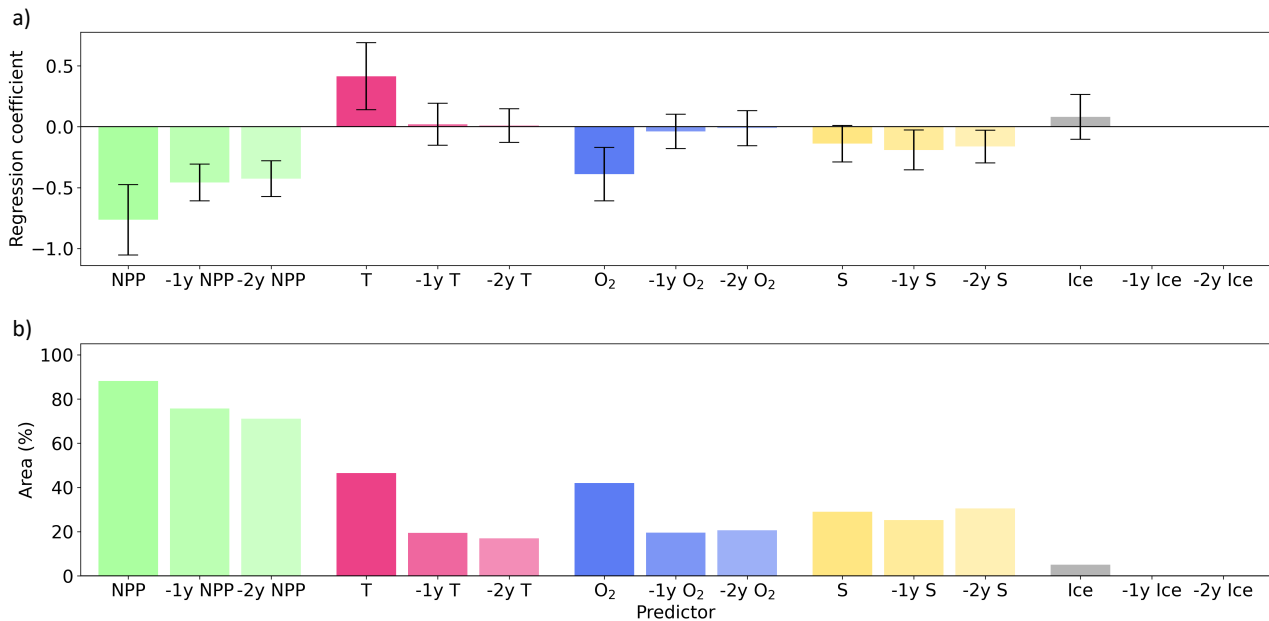


Figure 4. (a) Global mean logistic regression coefficient associated with T, O₂, S, NPP, Ice, -1 year T (one year prior of the event), -1 year O₂, -1 year S, -1 year NPP, -1 year Ice, -2 years T, -2 years O₂, -2 years S, -2 years NPP, -2 years Ice. Error bars indicate the standard deviation of each regression coefficient across space. (b) Fraction of the global ocean (%) over which each variable is selected as a predictor of LFB events in the regression.

Globally, the LASSO logistic regression coefficients indicate that LFB events are more likely to occur when NPP, O₂, and S are anomalously low, and when T and Ice are anomalously high (Fig. 4a). This is consistent with the shift in these ocean variables' distribution during LFB events (Fig. 3). NPP is selected over 88% of the global ocean (Fig. 4b), due to its negative impacts on the biomass of fish species in the DBEM (Cheung et al., 2011). On the other hand, T, O₂, S are selected over 47%, 42%, and 29% of the global ocean, respectively (Fig. 4b). The effect of changes in T on fish biomass varies depending on the species' temperature preference, which may result in poor prediction of LFB events when considering the total biomass of all pelagic fish species. Changes in salinity are usually too subtle in the open ocean to directly affect osmotic processes in fish and ultimately limit fish biomass. However, salinity changes may be correlated with changes in other ocean conditions that directly influence fish biomass and thus serve as a proxy for LFB events in certain regions. Ice is only selected as a predictor in and around sea-ice covered regions (5% of the global ocean, Fig. 4b).

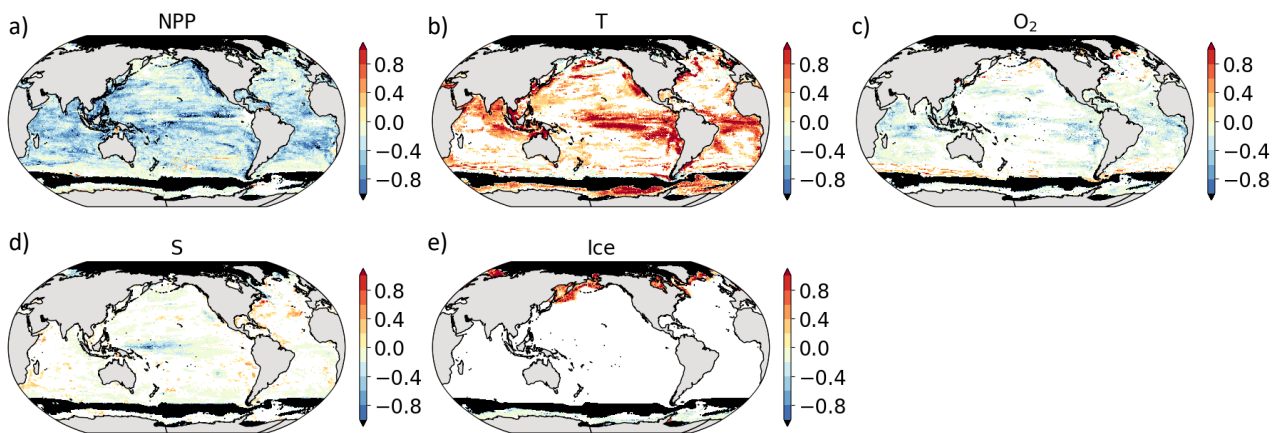


Figure 5. Regression coefficient associated with NPP (a), T (b), O₂ (c), S (d) and Ice (e) conditions in the year of the event in the logistic regression. Black areas correspond to regions without fish biomass data, in contrast to white areas, which correspond to regions where a given ocean variable was not selected as a predictor in the logistic regression.

There is substantial degree of spatial variability, as indicated by the standard deviation of each regression coefficient over the area over which it is selected (Fig. 4a). The regression coefficient for NPP (Fig. 5a) is negative over most of the global ocean, which means that low NPP is related to LFB. The more negative the regression coefficient, the more a reduction in NPP increases the likelihood of LFB. For example, in the northeastern Pacific, where the regression coefficient for NPP is particularly negative, even a relatively weak reduction in NPP might be sufficient to drive LFB events. In contrast, in the center of the northern Pacific, a stronger reduction in NPP might be necessary, as indicated by the less negative regression coefficient. LFB events are associated with high temperatures over most of the area over which T is a predictor (positive coefficient on Fig. 5b), yet they are also associated with low temperatures over a few regions in the northern high latitudes and in the northern part of the Southern Ocean. The regression coefficient for O₂ varies in sign over the global ocean (Fig. 5c). Over most of the low to mid-latitudes, LFB events are associated with low O₂. Low oxygen levels limit metabolism, growth performance and body size, and therefore limit total population biomass (Pauly and Cheung, 2017; Cheung et al., 2011, 2013; Clarke et al., 2021), potentially driving LFB events. In isolated grid cells in the high northern latitudes and in the northern part of the Southern Ocean, LFB events are, however, associated with high O₂. There, high O₂ is usually driven by increased solubility associated with lower T (Fig. A3), a potential driver of LFB for which high O₂ would simply be a proxy. Low salinity is an indicator of LFB especially in the equatorial Pacific, whereas high salinity is an indicator of LFB in the western South Indian Ocean and the North Atlantic (Fig. 5d). LFB events are also favored by high Ice in the northern high latitudes and low Ice in the southern high latitudes (Fig. 5e). This hemispheric divergence might be explained by the species composition. In the Arctic, although larger sea-ice extent provides more favorable conditions for polar species, it reduces the suitable habitat for sub-Arctic species. In the Antarctic, marine species are highly endemic (Eastman, 2005) and sub-polar species are less connected with the Antarctic compared to Arctic marine species. Thus, the relationship between reduced sea-ice extent and LFB in the Antarctic is

largely driven by species that are better adapted to polar conditions, namely to cold and light-limited conditions under sea-ice (Eastman, 2005).

210 3.2 The role of lagged effects in driving low fish biomass events

Anomalous ocean conditions may have lagged effects on fish biomass, which potentially drive LFB events a few years later. To account for these lagged effects, ocean conditions one to two years prior to an LFB event were also selected as predictors in our analysis.

We found that NPP from one and two years prior to an LFB event was selected as a predictor over about 70% of the global ocean (Fig. 4b). The associated regression coefficients are still relatively high (on the order of -0.3; Fig. 4a). This lagged effect might be explained by NPP having large negative impacts on fish population biomass (Chassot et al., 2010), leading to a reduction in reproductive capacity that would take multiple years to recover particularly for longer-lived, later-matured species (i.e., with lower intrinsic population growth rate). Negative impacts from low NPP propagate over time through the population, potentially driving a decline in overall fish biomass. The lagged effect is most pronounced in the low latitudes (Fig. A4), where time variability in NPP is also especially low in the ESM2M (Le Grix et al., 2022). Low NPP may therefore be associated with low NPP in the following years, and thus indirectly with LFB in the following years. A time lag of 1 year or 2 years for T and O₂ is rarely selected as a predictor (over less than 21% of the global ocean, Fig. 4b). Moreover, the regression coefficients associated with lagged T and O₂ are of much lower absolute value compared to the regression coefficients associated with concurrent T and O₂ (Fig. 4a). T and O₂ appear better suited at predicting concurrent LFB events than future LFB events. Compared to concurrent salinity, one-year and two-year lagged S were selected as a predictor over a similar area (30% of the global ocean). This suggests persistent low salinity conditions which indicate negative impacts on fish biomass over time. In contrast, one-year and two-year lagged Ice are never selected as a predictor, potentially reflecting high interannual variability in sea-ice extent. Maps of the regression coefficient associated with one-year and two-year lagged predictors are shown in Fig. A4.

Our results highlight the important role of lagged effects in driving LFB events. They might include “direct” lagged effects, by which anomalous ocean conditions drive LFB on their own after one or two years, as well as “indirect” lagged effects. Anomalous ocean conditions may indirectly drive LFB by playing the role of a preconditioning event or by temporally compounding with other events (Zscheischler et al., 2020). Preconditioning events correspond to anomalous ocean conditions rendering an ecosystem more vulnerable to subsequent ocean events, which might end up driving LFB. Temporally compounding events correspond to a repetition of the same kind of ocean event, like a marine heatwave, whose impacts accumulate over time and end up driving LFB.

3.3 Most influential predictor of low fish biomass events

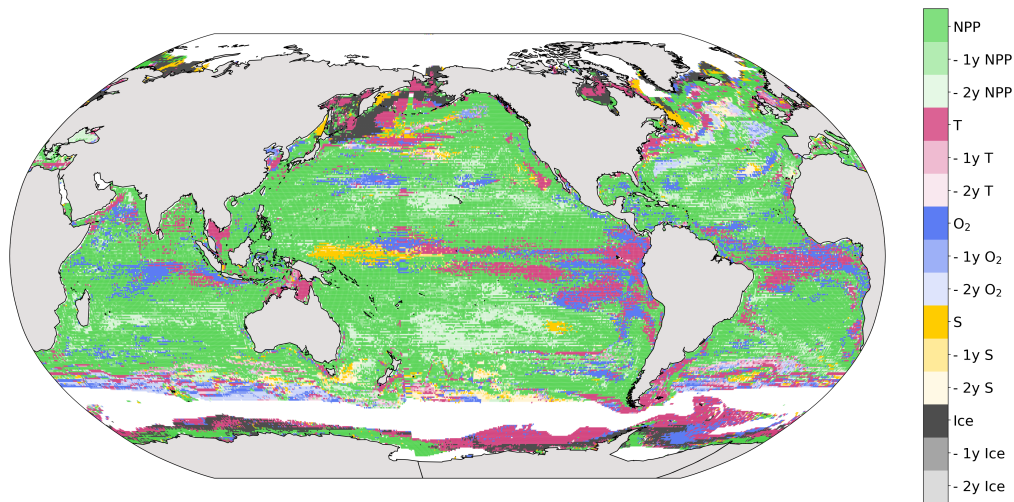


Figure 6. Most influential predictor of LFB events, defined as the predictor with highest absolute regression coefficient in the logistic regression.

We identified at each grid cell the most influential predictor of LFB events, i.e., the predictor associated with the highest absolute regression coefficient (Fig. 6). NPP is the main predictor over most of the global ocean (52% of the area). -1 year and
 240 -2 year-lagged NPP are the main predictors over 16% of the global ocean, mostly located in the subtropical gyres, where NPP variability is low. T is the main predictor in the eastern equatorial Pacific, in the equatorial Atlantic and locally over the Gulf Stream region and in the high latitudes. O₂ is the main predictor over a few regions, e.g., locally in the eastern equatorial Pacific and Atlantic. S is the main predictor in the western equatorial Pacific. Lastly, Ice is the main predictor over certain regions in the high latitudes, such as in the Arctic Ocean. Overall, our results highlight the dominance of NPP, as a useful indicator of
 245 potential extreme declines in pelagic fish biomass over most of the global ocean (Fig. 6).

3.4 Categorizing the drivers of low fish biomass events into moderate, extreme, univariate, and compound drivers

We use LASSO logistic regression with lagged effects to classify the drivers of LFB events into four categories: univariate, compound, moderate and extreme. Our methodology utilizes the regression coefficients from the previously-built logistic regression to determine whether an LFB event can be driven by univariate or moderate anomalies in ocean conditions or if
 250 compound or extreme anomalies are necessary (see Methods).

Our analysis shows that moderate oceanic events can drive LFB events over only 30% of the global ocean (in grey in Fig. 7a), primarily in the low latitudes, particularly in the central equatorial Pacific, and in the California Current System. These regions have a high number of predictors in the logistic regression and moderate anomalies in multiple variables may compound to

drive LFB events. Extreme oceanic events are necessary to experience LFB events over 70% of the global ocean, primarily in the mid to high latitudes (yellow area in Fig. 7a). This is further supported by the co-occurrence of LFB events with extreme conditions, such as extremely high SST, low O₂ and low NPP in the mid latitudes, as well as with extremely high Ice and low Ice in the northern and southern high latitudes, respectively (Fig. A5).

Next, we analyze whether univariate events alone can drive LFB events or if compound events are necessary. Our results show that univariate events can drive LFB events over 22% of the global ocean, primarily in the eastern equatorial Pacific (in grey on Fig. 7b), where high absolute regression coefficient for O₂ and T suggest that even univariate O₂ and T events may be sufficient to drive LFB events. Over the remaining 78% of the global ocean (in blue on Fig. 7b), compound events are necessary to experience LFB events. In the Appendix, we further differentiate between *temporally compounding* events, where one single ocean variable is anomalous over multiple years, and *multivariate* compound events, where multiple ocean variables are anomalous (Fig. A6). Temporally compounding events are necessary for the occurrence of LFB events over 36% of the global ocean (in light blue on Fig. A6), mostly located in the subtropics, where NPP, -1 year NPP and -2 year NPP are LFB predictors. There, low NPP could persist over multiple years and drive LFB. In contrast, multivariate compound events are necessary for LFB events over the remaining 42% of the global ocean (in dark blue on Fig. A6), where multiple events such as high T, low O₂, and low NPP events may compound to drive LFB.

Lastly, we overlapped Fig. 7a and Fig. 7b to identify regions where the LFB drivers must be both an extreme and a compound event (Fig. 7c). The fraction of the global ocean where extreme and compound events are necessary to experience LFB events overlap in the mid to high latitudes (61% of the ocean, in green on Fig. 7c). There, a compound extreme event with an extreme in at least one variable is required to drive extreme impacts on pelagic fish. Note that although compound extreme events are necessary to experience LFB events over 61% of the global ocean, this area comprises only 37% of the total pelagic fish biomass, as fish species are heterogeneously distributed over the global ocean (Fig. A1a). Over the remaining 13% of the global ocean (in grey on Fig. 7c), LFB events can be driven by a univariate event as long as it is extreme or, interchangeably, by a moderate event as long as it is a compound moderate event (i.e. a combination of moderate anomalies in multiple ocean variables). A univariate *and* moderate anomaly in one ocean variable is not sufficient to drive LFB anywhere (in black on the legend of Fig. 7c).

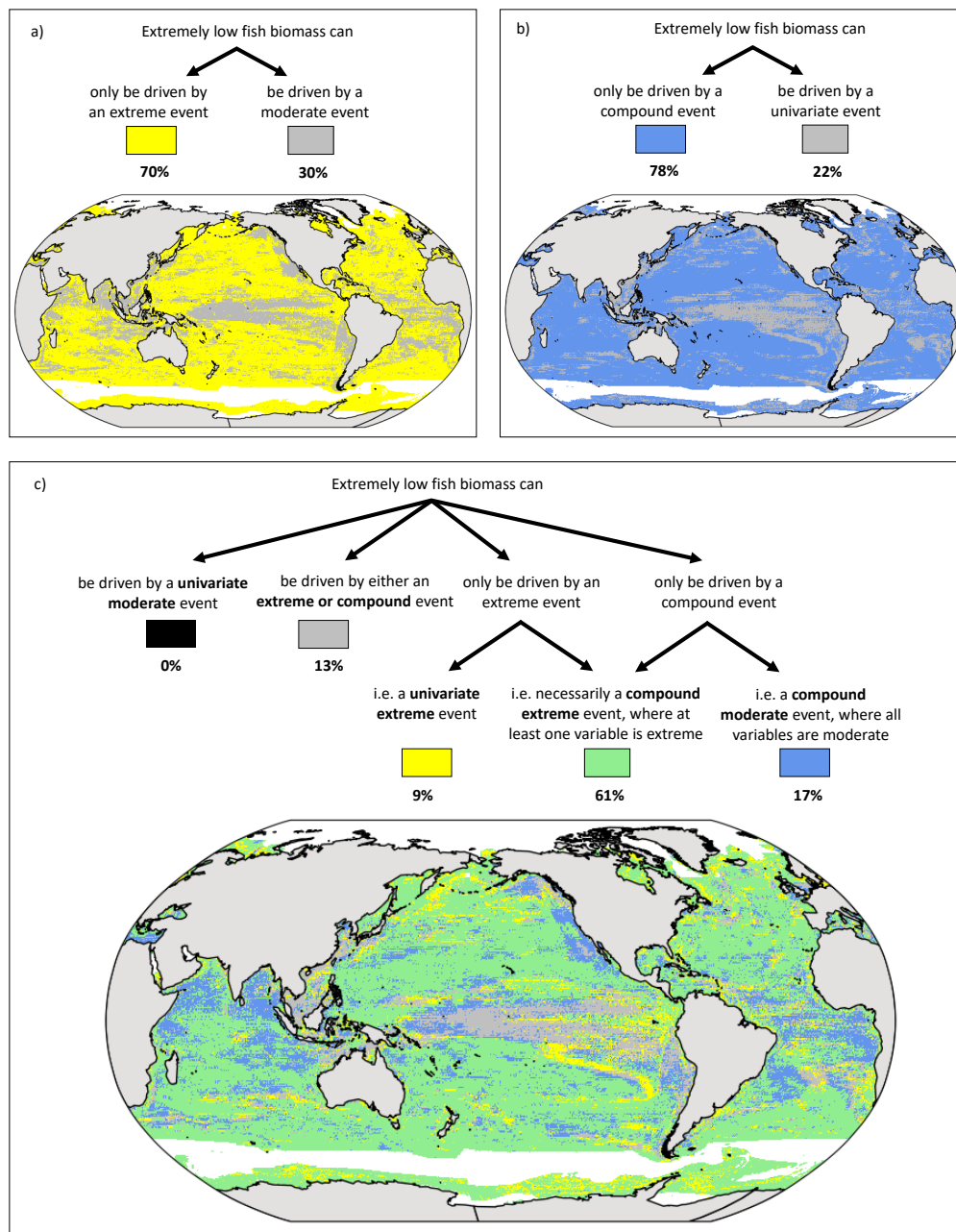


Figure 7. Spatial distribution of each category of LFB drivers. The legend indicates the fraction of the global ocean occupied by each category. (a) Extreme events are necessary to experience LFB events. (b) Compound events are necessary to experience LFB events. Both upper panels are superposed to create the bottom panel (c), which shows where compound extreme events are necessary to experience LFB events.

4 Discussion and Conclusion

280 We investigated the drivers of extremely low pelagic fish biomass (LFB) events by applying a LASSO logistic regression to
output of a global marine fish model. We found that low net primary productivity is the most influential predictor of LFB events
over the majority (68%) of the surface ocean. The prediction of such LFB events is substantially improved by considering net
primary production one to two years before the event. We also found that a moderate and univariate anomaly in one ocean
variable is not sufficient to drive LFB events, and that over 61% of the surface ocean, anomalies in multiple ocean variables
285 – which must be extreme in at least one variable – are required to cause LFB events. Our findings highlight the key role of
extreme and compound events for severe impacts on pelagic fish biomass.

This study takes the original approach of investigating the drivers of extreme impacts on pelagic fish biomass using a
backward assessment method. Contrary to previous studies that apply a forward approach to investigate the impacts of extreme
hazards, such as marine heatwaves, on ecosystems (e.g., Smale et al. (2019); Cheung and Frölicher (2020); Cheung et al.
290 (2021); Smith et al. (2023)), the focus here is rather on extreme impacts on fish and what drives such impacts. Such backward
approaches have become more common in recent years, for instance to identify drivers of extremely low vegetation activity and
carbon uptake (Zscheischler et al., 2013, 2014a), floods (Jiang et al., 2022), and crop failure events (Vogel et al., 2021). The
backward approach allows for the identification of potentially unexpected drivers (van der Wiel et al., 2020), such as low NPP,
and for the distinction between univariate, compound, moderate, and extreme drivers. The dominant role of low NPP, and not
295 of marine heatwaves (e.g., Cheung and Frölicher (2020)), in driving extremely low fish biomass, was particularly unexpected.
Our findings may explain why some recent studies did not find substantial impacts of marine heatwaves on ecosystems, e.g., on
the biomass and community composition of coastal Atlantic and Pacific demersal fish communities over the last three decades
(Fredston, A. L. et al. (2023) submitted). Additionally, we found that combinations of moderate ocean anomalies might be
sufficient to drive extreme impacts on pelagic fish biomass over 22% of the global ocean. Therefore, monitoring multiple
300 ocean ecosystem drivers in addition to marine heatwaves (e.g., Jacox et al. (2022)) may help to improve predictions of high
impacts on the pelagic fish ecosystem.

An important aspect of this study is that it considers the perspective of the entire pelagic fish community, as opposed to
focusing on individual species. Each species has its own unique response to anomalous ocean conditions, based on its natural
habitat and range of tolerance (Pörtner, 2002; Pörtner and Peck, 2010). For instance, some species that are already at the upper
305 limit of their thermal tolerance might be negatively affected by elevated temperatures, while others may benefit from the same
warming event. However, the overall response of the pelagic fish ecosystem to changes in ocean conditions is not yet well
understood. This study offers an initial evaluation of the drivers of extreme declines in the biomass of pelagic fishes.

A compound event combines individual ocean events, whose effects may act synergistically to drive LFB events (Boyd
and Brown, 2015; Gruber et al., 2021). We employed a logistic regression to analyze these effects, assuming an additive
310 relationship between them. However, it is important to note that these effects may not be linear, as demonstrated by previous
research (Zscheischler and Seneviratne, 2017). For example, the combined effect of increased temperature and reduced net
primary production on fish may be different from the sum of their isolated effects. To further investigate this, we conducted a

sensitivity analysis (not shown) that considered mixed effects in the logistic regression. Specifically, we allowed the product of two ocean variables to be selected as a predictor of LFB events under the condition that it improved the prediction. However, accounting for mixed effects did not substantially improve the prediction of LFB events in our study.

The robustness of the results presented here depends on the fidelity of the DBEM in simulating the ocean ecosystem drivers of changes in pelagic fish biomass. The DBEM has been shown to reproduce observed shifts in the biomass and distribution of hundreds of fish species under moderate (e.g., Cheung et al. (2013, 2016)) and extreme (Cheung et al., 2021) changes in ocean conditions. However, as with any model, the DBEM is an incomplete representation of the pelagic ecosystems (Cheung et al., 2011) and certain limitations require further discussion. One limitation of the DBEM is that it does not account for vertical heterogeneity in ocean ecosystem drivers and assumes surface ocean conditions to be the primary drivers of pelagic fish biomass. In reality, subsurface ocean conditions may also play a significant role in driving extreme declines in pelagic fish biomass. Additionally, the DBEM simulations that we used in this study do not consider the effects of ocean acidification or fishing pressure on fish biomass. Ocean acidification can cause physiological stress and perturb fish olfactory ability to detect suitable habitat, potentially leading to population declines (Melzner et al., 2009; Munday et al., 2009; Cheung et al., 2011; Branch et al., 2013; Tai et al., 2021). These effects may be particularly pronounced when combined with other ocean stressors such as low oxygen (Gobler and Baumann, 2016) or high temperature (Cornwall et al., 2021; Burger et al., 2022). Fishing pressure also impacts fish biomass (e.g. Watson et al. (2013)), and may be a primary reason for the recent marine biodiversity decline (Jaureguiberry et al., 2022). Further DBEM simulations representing the impacts of fishing pressure on fish biomass would help to assess the role of human activities in driving extreme changes in fish biomass (Cheung et al., 2011; Tai et al., 2018; Cheung et al., 2022).

The conclusions of this study are not only dependent on the global fish model used, but also on the ocean ecosystem drivers as simulated by the GFDL ESM2M. For example, the dependencies between ocean variables, such as the correlation between net primary production and temperature, may differ between the GFDL ESM2M and other Earth system models. Dependencies between ocean variables are reflected in the logistic regression coefficients and may impact our results. In particular, the negative correlation between net primary production and temperature in GFDL ESM2M is overestimated in the tropics and strongly underestimated around Antarctica when compared to observation-based data (Le Grix et al., 2022). Therefore, the role of compound high temperature and low net primary productivity events in driving low fish biomass events may be overestimated in the tropics and underestimated around Antarctica. To further validate the robustness of our results, different Earth system models with potentially divergent dependencies between ocean variables should be used, following similar sensitivity experiments as over land (Tschumi et al., 2023). New simulations from global fish models forced by different Earth system models, that have now become available under the Inter-Sectoral Impact Model Intercomparison Project (ISIMIP) framework (Tittensor et al., 2021), might be used for an intermodel comparison study in the future. In this study, the selection of the GFDL ESM2M was motivated by the availability of a large ensemble simulation, which provides the necessary large dataset from which to study rare extreme events over a time period sufficiently short to be assumed quasi-stationary. At present, there are only a few large ensemble simulations available with fully coupled Earth system models that simulate ocean ecosystem drivers (e.g., Rodgers et al. (2015); Deser et al. (2020)).

This study provides insights into potential environmental drivers of high impacts on pelagic fish biomass. We highlight the key role played by univariate extreme events, compound moderate events and compound extreme events in driving severe impacts on fish. Our results motivate further work on ocean extreme and compound events, as well as the monitoring of multiple ocean ecosystem drivers including net primary productivity as a means to predict impacts on pelagic fish.

Appendix A: Additional figures

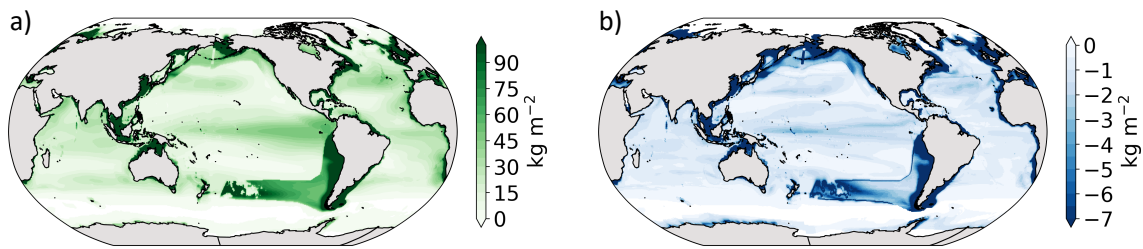


Figure A1. (a) Mean pelagic fish biomass (kg m^{-2}) over 1951-2000. (b) Difference between the 10th percentile of the annual mean pelagic fish biomass and the mean pelagic fish biomass (kg m^{-2}) over 1951-2000.

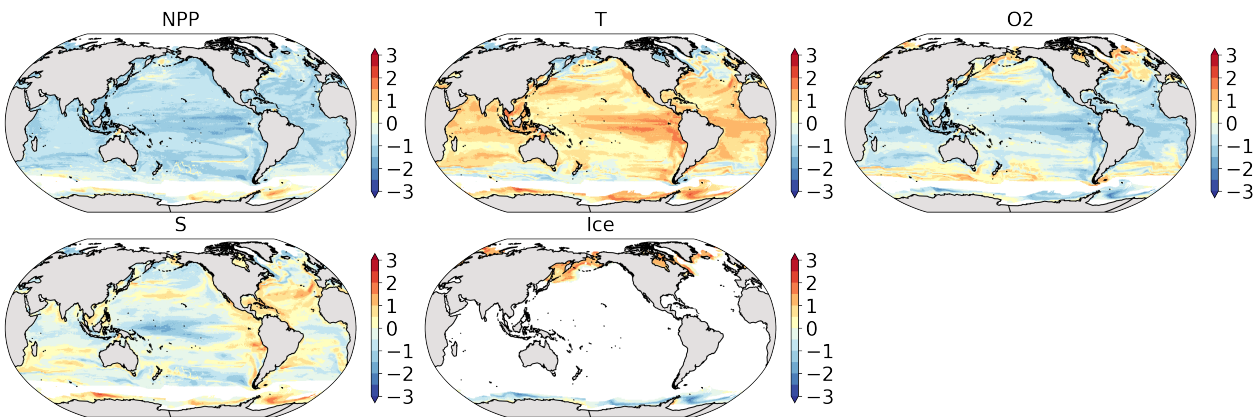


Figure A2. Mean standardized NPP, T, O₂, S, and sea ice extent during the LFB years. Ocean variables are standardized by removing their mean and dividing by their standard deviation at each grid cell.

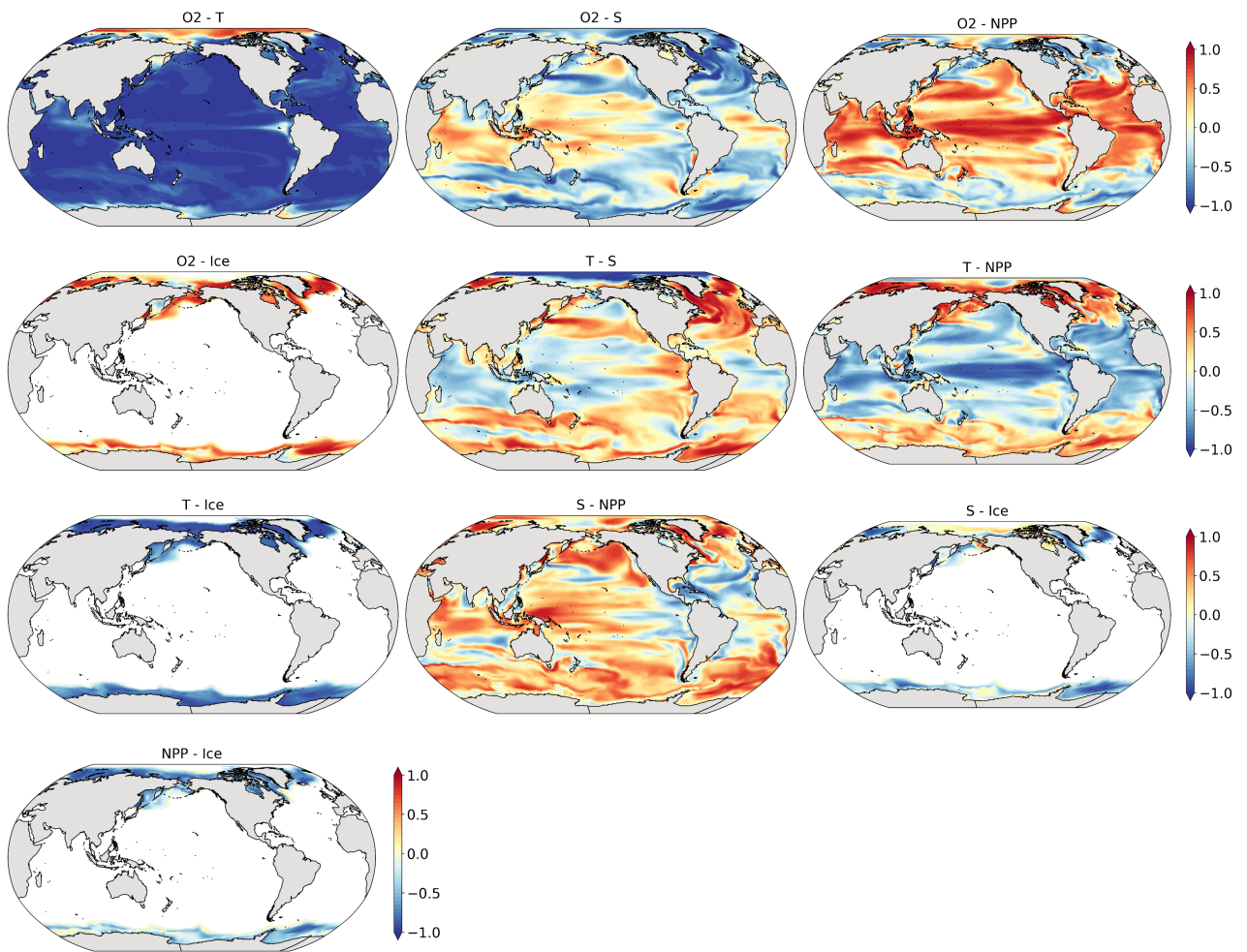


Figure A3. Pearson's correlation coefficient between each pair of ocean variables.

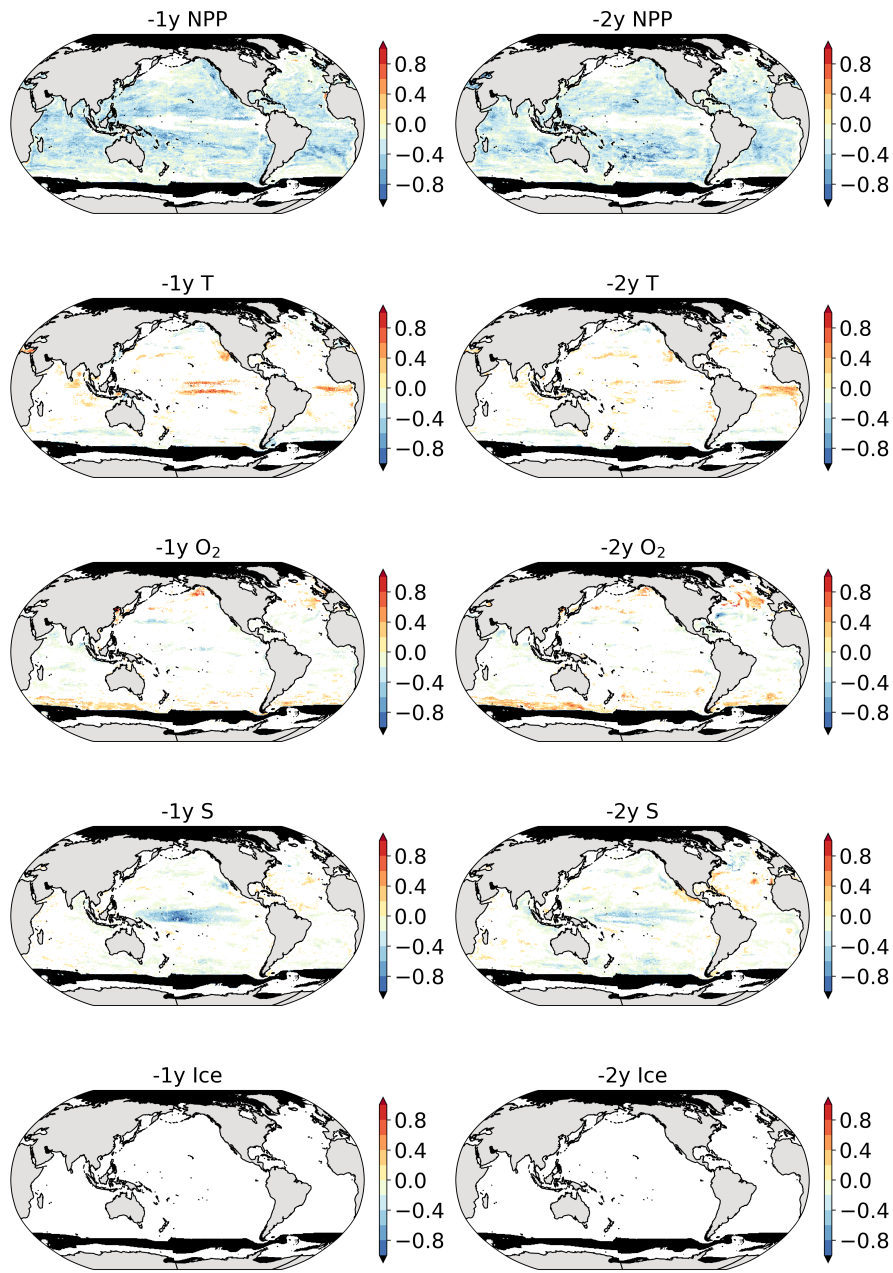


Figure A4. Regression coefficients associated with NPP, T, O₂, S, Ice, -1 year NPP, -1 year T, -1 year O₂, -1 year S, -1 year Ice, -2 years NPP, -2 years T, -2 years O₂, -2 years S, and -2 years Ice. Black areas correspond to regions without fish biomass data, in contrast to white areas, which correspond to regions where a given ocean variable was not selected as a predictor in the logistic regression.

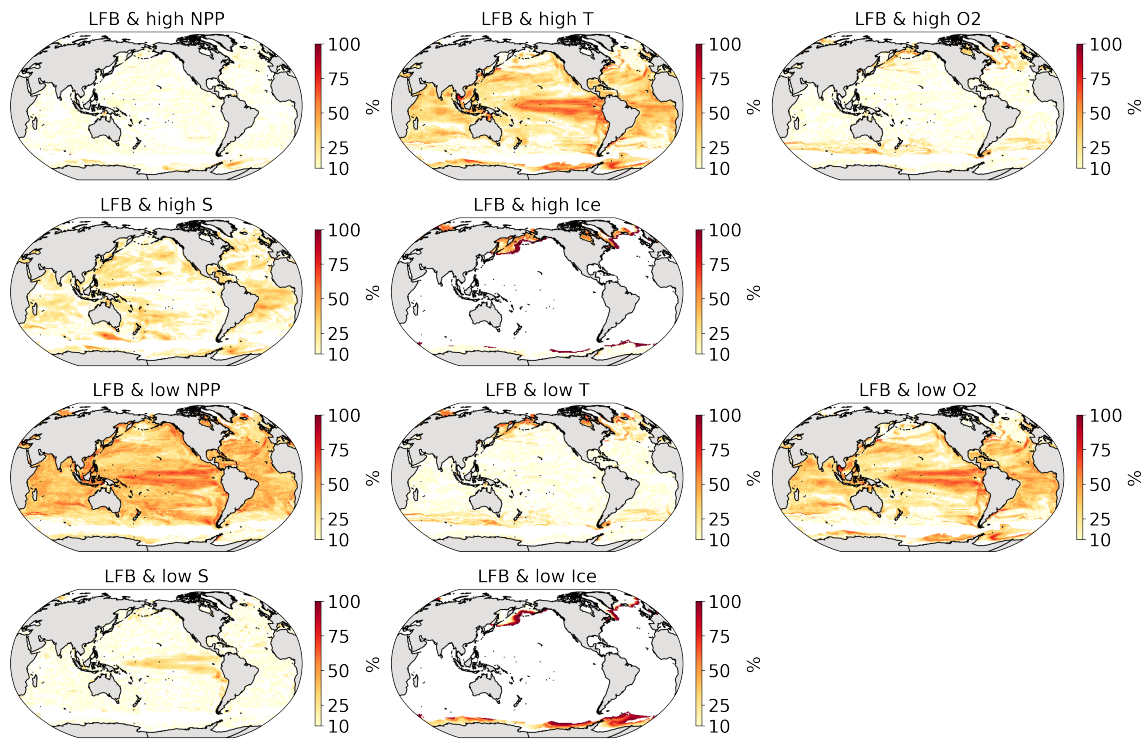


Figure A5. Percentage of LFB events co-occurring with extreme ocean conditions. High and low NPP, T, O₂, S, and Ice events are defined as years when the annual mean NPP, T, O₂, S, and Ice is higher or lower than their 10th or 90th percentiles, respectively. Grid cells where the co-occurrence is not significantly high remain white. Statistical relevance is assessed by artificially shuffling the time series of ocean variables and counting the co-occurrence days. We proceed to a thousand shuffle tests and consider LFB events to frequently co-occur with extreme events when co-occurrence in the initial time series is higher than in at least 95% of shuffle tests.

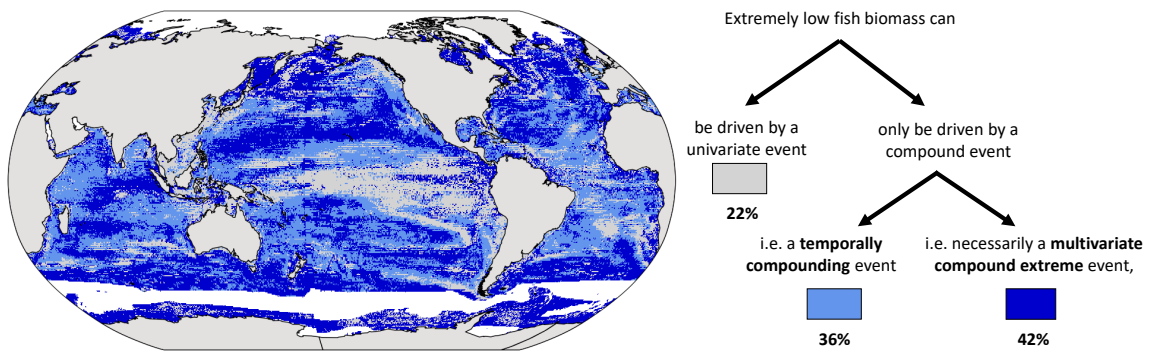


Figure A6. Spatial distribution of univariate and compound LFB drivers. LFB can be driven by a univariate event over regions in grey. It must be driven by a compound event over the regions in blue. A temporally compounding event is sufficient to drive LFB over the regions in light blue, whereas a multivariate compound event is necessary to drive LFB over the regions in dark blue.

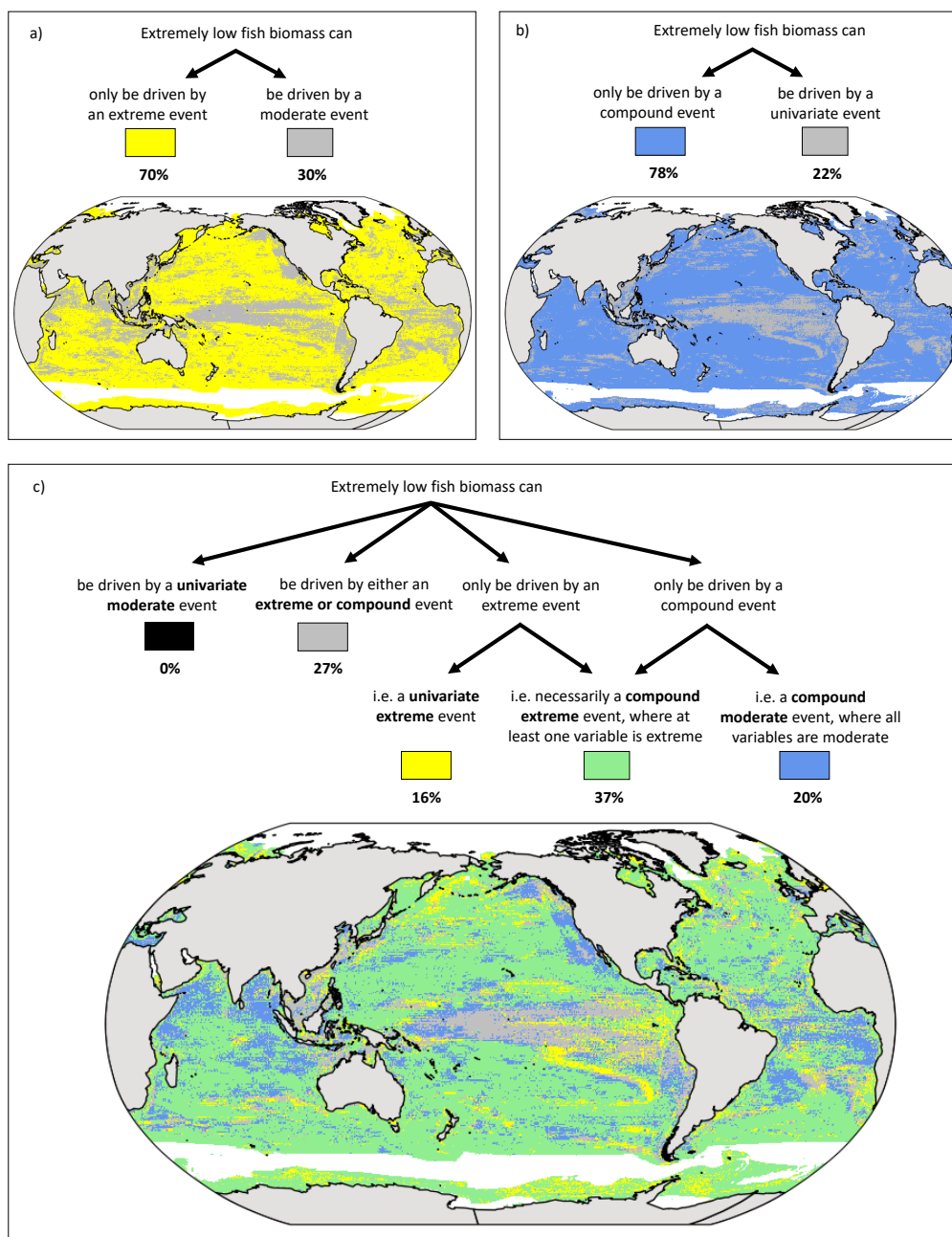


Figure A7. Spatial distribution of each category of LFB drivers. The legend indicates the fraction of global mean fish biomass (%) comprised within the area occupied by each category.

Author contributions. NLG, TLF, GR, and WC designed the study. TLF provided the GFDL ESM2M output. WC provided the DBEM output. JZ helped with the lasso regression analysis. NLG performed the analysis and wrote the initial draft of the manuscript. All authors
355 discussed the analysis and results, and contributed to the writing of the paper.

Data availability.

Competing interests. All authors declare no competing interests.

Disclaimer. The work reflects only the authors' view; the European Commission and their executive agency are not responsible for any use that may be made of the information the work contains.

360 *Acknowledgements.* The GFDL ESM2M simulations were conducted at the Swiss National Supercomputing Centre. This research has been supported by the Swiss National Science Foundation (grant no. PP00P2-198897), the Bretscher Foundation, and the European Union's Horizon 2020 research and innovation programme under grant agreement no. 820989 (project COMFORT) and no. 862923 (project AtlantECO).

References

- Ben-Ari, T., Boé, J., Ciais, P., Lecerf, R., Van der Velde, M., and Makowski, D.: Causes and Implications of the Unforeseen 2016 Extreme Yield Loss in the Breadbasket of France, *Nature Communications*, 9, 1627, <https://doi.org/10.1038/s41467-018-04087-x>, 2018.
- 365 Bevacqua, E., Jézéquel, A., Suarez-Gutierrez, L., Lehner, F., Vrac, M., Yiou, P., and Zscheischler, J.: Advancing Our Understanding of Compound Weather and Climate Events via Large Ensemble Model Simulations, <https://doi.org/10.21203/rs.3.rs-1791760/v1>, 2022.
- Bindoff, N., Cheung, W., Kairo, J., Arístegui, J., Guinder, V., Hallberg, R., Hilmi, N., Jiao, N., Karim, M., Levin, L., O'Donoghue, S., Cuicapusa, S. P., Rinkevich, B., Suga, T., Tagliabue, A., and Williamson, P.: Changing Ocean, Marine Ecosystems, and Dependent Communities, in: IPCC Special Report on the Ocean, Cryosphere in a Changing Climate, edited by Pörtner, H.-O., Roberts, D., Masson-Delmotte, V., Zhai, P., Tignor, M., Poloczanska, E., Mintenbeck, K., Alegría, A., Nicolai, M., Okem, A., Petzold, J., Rama, B., and Weyer, N., Cambridge University Press, 2019.
- 370 Boyd, P. W. and Brown, C. J.: Modes of Interactions between Environmental Drivers, Marine Biota, *Frontiers in Marine Science*, 2, 9, <https://doi.org/10.3389/fmars.2015.00009>, 2015.
- 375 Branch, T. A., DeJoseph, B. M., Ray, L. J., and Wagner, C. A.: Impacts of Ocean Acidification on Marine Seafood, *Trends in Ecology & Evolution*, 28, 178–186, <https://doi.org/10.1016/j.tree.2012.10.001>, 2013.
- Burger, F. A., John, J. G., and Frölicher, T. L.: Increase in Ocean Acidity Variability, Extremes under Increasing Atmospheric CO₂, *Biogeosciences (Online)*, 17, 4633–4662, <https://doi.org/10.5194/bg-17-4633-2020>, 2020.
- Burger, F. A., Terhaar, J., and Frölicher, T. L.: Compound Marine Heatwaves and Ocean Acidity Extremes, *Nature Communications*, 13, 4722, <https://doi.org/10.1038/s41467-022-32120-7>, 2022.
- 380 Cavole, L., Demko, A., Diner, R., Giddings, A., Koester, I., Pagniello, C., Paulsen, M.-L., Ramirez-Valdez, A., Schwenck, S., Yen, N., Zill, M., and Franks, P.: Biological Impacts of the 2013–2015 Warm-Water Anomaly in the Northeast Pacific: Winners, Losers, and the Future, *Oceanography*, 29, <https://doi.org/10.5670/oceanog.2016.32>, 2016.
- Chassot, E., Bonhommeau, S., Dulvy, N. K., Mélin, F., Watson, R., Gascuel, D., and Le Pape, O.: Global Marine Primary Production Constrains Fisheries Catches, *Ecology Letters*, 13, 495–505, <https://doi.org/10.1111/j.1461-0248.2010.01443.x>, 2010.
- Cheung, W., Lam, V., and Pauly, D.: Dynamic Bioclimate Envelope Model to Predict Climate-Induced Changes in Distribution of Marine Fishes and Invertebrates, *Modelling Present and Climate-shifted Distributions of Marine Fishes and Invertebrates*, 16, 5–50, 2008.
- Cheung, W. W. L. and Frölicher, T. L.: Marine Heatwaves Exacerbate Climate Change Impacts for Fisheries in the Northeast Pacific, *Scientific Reports*, 10, 6678, <https://doi.org/10.1038/s41598-020-63650-z>, 2020.
- 390 Cheung, W. W. L., Dunne, J., Sarmiento, J. L., and Pauly, D.: Integrating Ecophysiology and Plankton Dynamics into Projected Maximum Fisheries Catch Potential under Climate Change in the Northeast Atlantic, *ICES Journal of Marine Science*, 68, 1008–1018, <https://doi.org/10.1093/icesjms/fsr012>, 2011.
- Cheung, W. W. L., Watson, R., and Pauly, D.: Signature of Ocean Warming in Global Fisheries Catch, *Nature*, 497, 365–368, <https://doi.org/10.1038/nature12156>, 2013.
- 395 Cheung, W. W. L., Jones, M. C., Reygondeau, G., Stock, C. A., Lam, V. W. Y., and Frölicher, T. L.: Structural Uncertainty in Projecting Global Fisheries Catches under Climate Change, *Ecological Modelling*, 325, 57–66, <https://doi.org/10.1016/j.ecolmodel.2015.12.018>, 2016.
- Cheung, W. W. L., Jones, M. C., Reygondeau, G., and Frölicher, T. L.: Opportunities for Climate-Risk Reduction through Effective Fisheries Management, *Global Change Biology*, 24, 5149–5163, <https://doi.org/10.1111/gcb.14390>, 2018.

- 400 Cheung, W. W. L., Frölicher, T. L., Lam, V. W. Y., Oyinlola, M. A., Reygondeau, G., Sumaila, U. R., Tai, T. C., Teh, L. C. L., and Wabnitz, C. C. C.: Marine High Temperature Extremes Amplify the Impacts of Climate Change on Fish and Fisheries, *Science Advances*, 7, eabh0895, <https://doi.org/10.1126/sciadv.abh0895>, 2021.
- Cheung, W. W. L., Palacios-Abrantes, J., Frölicher, T. L., Palomares, M. L., Clarke, T., Lam, V. W. Y., Oyinlola, M. A., Pauly, D., Reygondeau, G., Sumaila, U. R., Teh, L. C. L., and Wabnitz, C. C. C.: Rebuilding Fish Biomass for the World’s Marine Ecoregions under Climate
405 Change, *Global Change Biology*, 28, 6254–6267, <https://doi.org/10.1111/gcb.16368>, 2022.
- Clarke, T. M., Wabnitz, C. C. C., Striegel, S., Frölicher, T. L., Reygondeau, G., and Cheung, W. W. L.: Aerobic Growth Index (AGI): An Index to Understand the Impacts of Ocean Warming and Deoxygenation on Global Marine Fisheries Resources, *Progress in Oceanography*, 195, 102588, <https://doi.org/10.1016/j.pocean.2021.102588>, 2021.
- Close, C., Cheung, W., Hodgson, S., Lam, V., Watson, R., and Pauly, D.: Distribution Ranges of Commercial Fishes and Invertebrates,
410 vol. 14, 2006.
- Cook, J. and Ramadas, V.: When to Consult Precision-Recall Curves, *The Stata Journal*, 20, 131–148, <https://doi.org/10.1177/1536867X20909693>, 2020.
- Cornwall, C. E., Comeau, S., Kornder, N. A., Perry, C. T., van Hooedonk, R., DeCarlo, T. M., Pratchett, M. S., Anderson, K. D., Browne, N., Carpenter, R., Diaz-Pulido, G., D’Olivo, J. P., Doo, S. S., Figueiredo, J., Fortunato, S. A. V., Kennedy, E., Lantz, C. A., Mc-
415 Culloch, M. T., González-Rivero, M., Schoepf, V., Smithers, S. G., and Lowe, R. J.: Global Declines in Coral Reef Calcium Carbonate Production under Ocean Acidification and Warming, *Proceedings of the National Academy of Sciences*, 118, e2015265118, <https://doi.org/10.1073/pnas.2015265118>, 2021.
- Deser, C., Lehner, F., Rodgers, K. B., Ault, T., Delworth, T. L., DiNezio, P. N., Fiore, A., Frankignoul, C., Fyfe, J. C., Horton, D. E., Kay, J. E., Knutti, R., Lovenduski, N. S., Marotzke, J., McKinnon, K. A., Minobe, S., Randerson, J., Screen, J. A., Simpson, I. R., and Ting,
420 M.: Insights from Earth System Model Initial-Condition Large Ensembles and Future Prospects, *Nature Climate Change*, 10, 277–286, <https://doi.org/10.1038/s41558-020-0731-2>, 2020.
- Dunne, J. P., John, J. G., Adcroft, A. J., Griffies, S. M., Hallberg, R. W., Shevliakova, E., Stouffer, R. J., Cooke, W., Dunne, K. A., Harrison, M. J., Krasting, J. P., Malyshev, S. L., Milly, P. C. D., Phillipps, P. J., Sentman, L. T., Samuels, B. L., Spelman, M. J., Winton, M., Wittenberg, A. T., and Zadeh, N.: GFDL’s ESM2 Global Coupled Climate–Carbon Earth System Models. Part I: Physical Formulation
425 and Baseline Simulation Characteristics, *Journal of Climate*, 25, 6646–6665, <https://doi.org/10.1175/JCLI-D-11-00560.1>, 2012.
- Dunne, J. P., John, J. G., Shevliakova, E., Stouffer, R. J., Krasting, J. P., Malyshev, S. L., Milly, P. C. D., Sentman, L. T., Adcroft, A. J., Cooke, W., Dunne, K. A., Griffies, S. M., Hallberg, R. W., Harrison, M. J., Levy, H., Wittenberg, A. T., Phillips, P. J., and Zadeh, N.: GFDL’s ESM2 Global Coupled Climate–Carbon Earth System Models. Part II: Carbon System Formulation and Baseline Simulation Characteristics*, *Journal of Climate*, 26, 2247–2267, <https://doi.org/10.1175/JCLI-D-12-00150.1>, 2013.
- 430 Eastman, J. T.: The Nature of the Diversity of Antarctic Fishes, *Polar Biology*, 28, 93–107, <https://doi.org/10.1007/s00300-004-0667-4>, 2005.
- Fredston, A. L., Cheung, W. W. L., Frölicher, T. L., Kitchel, Z., A. A. Maureaud, J. T. Thorson, A. Auber, B. Mérigot, J. Palacios-Abrantes, Lourdes D. Palomares, L. Pecuchet, N. Shackell, and M. L. Pinsky: Marine Heatwaves Have Not Emerged as a Dominant Driver of Ecological Change., *Nature* (in review), 2023.
- Friedman, J. H., Hastie, T., and Tibshirani, R.: Regularization Paths for Generalized Linear Models via Coordinate Descent, *Journal of*
435 *Statistical Software*, 33, 1–22, <https://doi.org/10.18637/jss.v033.i01>, 2010.
- Frölicher, T. L., Joos, F., Plattner, G.-K., Steinacher, M., and Doney, S. C.: Natural Variability and Anthropogenic Trends in Oceanic Oxygen in a Coupled Carbon Cycle–Climate Model Ensemble, *Global Biogeochemical Cycles*, 23, <https://doi.org/10.1029/2008GB003316>, 2009.

- Frölicher, T. L., Fischer, E. M., and Gruber, N.: Marine Heatwaves under Global Warming, *Nature*, 560, 360–364, <https://doi.org/10.1038/s41586-018-0383-9>, 2018.
- 440 Gagné, T. O., Reygondeau, G., Jenkins, C. N., Sexton, J. O., Bograd, S. J., Hazen, E. L., and Houtan, K. S. V.: Towards a Global Understanding of the Drivers of Marine and Terrestrial Biodiversity, *PLOS ONE*, 15, e0228065, <https://doi.org/10.1371/journal.pone.0228065>, 2020.
- Garcia, H. E. and Gordon, L. I.: Oxygen Solubility in Seawater: Better Fitting Equations, *Limnology and Oceanography*, 37, 1307–1312, <https://doi.org/10.4319/lo.1992.37.6.1307>, 1992.
- 445 Gobler, C. J. and Baumann, H.: Hypoxia and Acidification in Ocean Ecosystems: Coupled Dynamics and Effects on Marine Life, *Biology Letters*, 12, <https://doi.org/10.1098/rsbl.2015.0976>, 2016.
- Griffies, S.: Elements of the Modular Ocean Model (MOM), pp. 1–633, 2012.
- Gruber, N., Boyd, P. W., Frölicher, T. L., and Vogt, M.: Biogeochemical Extremes and Compound Events in the Ocean, *Nature*, 600, 395–407, <https://doi.org/10.1038/s41586-021-03981-7>, 2021.
- 450 Hobday, A. J., Alexander, L. V., Perkins, S. E., Smale, D. A., Straub, S. C., Oliver, E. C., Benthuysen, J. A., Burrows, M. T., Donat, M. G., Feng, M., Holbrook, N. J., Moore, P. J., Scannell, H. A., Sen Gupta, A., and Wernberg, T.: A Hierarchical Approach to Defining Marine Heatwaves, *Progress in Oceanography*, 141, 227–238, <https://doi.org/10.1016/j.pocean.2015.12.014>, 2016.
- Jacox, M. G., Alexander, M. A., Amaya, D., Becker, E., Bograd, S. J., Brodie, S., Hazen, E. L., Pozo Buil, M., and Tommasi, D.: Global Seasonal Forecasts of Marine Heatwaves, *Nature*, 604, 486–490, <https://doi.org/10.1038/s41586-022-04573-9>, 2022.
- 455 Jaureguiberry, P., Titeux, N., Wiemers, M., Bowler, D. E., Coscieme, L., Golden, A. S., Guerra, C. A., Jacob, U., Takahashi, Y., Settele, J., Díaz, S., Molnár, Z., and Purvis, A.: The Direct Drivers of Recent Global Anthropogenic Biodiversity Loss, *Science Advances*, 8, eabm9982, <https://doi.org/10.1126/sciadv.abm9982>, 2022.
- Jiang, S., Bevacqua, E., and Zscheischler, J.: River Flooding Mechanisms and Their Changes in Europe Revealed by Explainable Machine Learning, *Hydrology and Earth System Sciences*, 26, 6339–6359, <https://doi.org/10.5194/hess-26-6339-2022>, 2022.
- 460 Jones, T., Parrish, J. K., Peterson, W. T., Bjorkstedt, E. P., Bond, N. A., Ballance, L. T., Bowes, V., Hipfner, J. M., Burgess, H. K., Dolliver, J. E., Lindquist, K., Lindsey, J., Nevins, H. M., Robertson, R. R., Roletto, J., Wilson, L., Joyce, T., and Harvey, J.: Massive Mortality of a Planktivorous Seabird in Response to a Marine Heatwave, *Geophysical Research Letters*, 45, 3193–3202, <https://doi.org/10.1002/2017GL076164>, 2018.
- Krstajic, D., Buturovic, L. J., Leahy, D. E., and Thomas, S.: Cross-Validation Pitfalls When Selecting and Assessing Regression and Classification Models, *Journal of Cheminformatics*, 6, 10, <https://doi.org/10.1186/1758-2946-6-10>, 2014.
- 465 Le Grix, N., Zscheischler, J., Laufkötter, C., Rousseaux, C. S., and Frölicher, T. L.: Compound High-Temperature and Low-Chlorophyll Extremes in the Ocean over the Satellite Period, *Biogeosciences*, 18, 2119–2137, <https://doi.org/10.5194/bg-18-2119-2021>, 2021.
- Le Grix, N., Zscheischler, J., Rodgers, K. B., Yamaguchi, R., and Frölicher, T. L.: Hotspots and Drivers of Compound Marine Heatwaves and Low Net Primary Production Extremes, *Biogeosciences*, 19, 5807–5835, <https://doi.org/10.5194/bg-19-5807-2022>, 2022.
- 470 Magnan, A. K., Pörtner, H.-O., Duvat, V. K. E., Garschagen, M., Guinder, V. A., Zommers, Z., Hoegh-Guldberg, O., and Gattuso, J.-P.: Estimating the Global Risk of Anthropogenic Climate Change, *Nature Climate Change*, 11, 879–885, <https://doi.org/10.1038/s41558-021-01156-w>, 2021.
- Maher, N., Milinski, S., and Ludwig, R.: Large Ensemble Climate Model Simulations: Introduction, Overview, and Future Prospects for Utilising Multiple Types of Large Ensemble, *Earth System Dynamics*, 12, 401–418, <https://doi.org/10.5194/esd-12-401-2021>, 2021.

- 475 Melzner, F., Gutowska, M. A., Langenbuch, M., Dupont, S., Lucassen, M., Thorndyke, M. C., Bleich, M., and Pörtner, H.-O.: Physiological Basis for High CO₂ Tolerance in Marine Ectothermic Animals: Pre-Adaptation through Lifestyle and Ontogeny?, *Biogeosciences*, 6, 2313–2331, <https://doi.org/10.5194/bg-6-2313-2009>, 2009.
- Mogen, S. C., Lovenduski, N. S., Dallmann, A. R., Gregor, L., Sutton, A. J., Bograd, S. J., Quiros, N. C., Di Lorenzo, E., Hazen, E. L., Jacox, M. G., Buil, M. P., and Yeager, S.: Ocean Biogeochemical Signatures of the North Pacific Blob, *Geophysical Research Letters*, 49, e2021GL096938, <https://doi.org/10.1029/2021GL096938>, 2022.
- 480 Munday, P. L., Dixon, D. L., Donelson, J. M., Jones, G. P., Pratchett, M. S., Devitsina, G. V., and Døving, K. B.: Ocean Acidification Impairs Olfactory Discrimination and Homing Ability of a Marine Fish, *Proceedings of the National Academy of Sciences*, 106, 1848–1852, <https://doi.org/10.1073/pnas.0809996106>, 2009.
- Oliver, E. C. J., Donat, M. G., Burrows, M. T., Moore, P. J., Smale, D. A., Alexander, L. V., Benthuisen, J. A., Feng, M., Sen Gupta, A., Hobday, A. J., Holbrook, N. J., Perkins-Kirkpatrick, S. E., Scannell, H. A., Straub, S. C., and Wernberg, T.: Longer and More Frequent Marine Heatwaves over the Past Century, *Nature Communications*, 9, 1324, <https://doi.org/10.1038/s41467-018-03732-9>, 2018.
- Pauly, D. and Cheung, W.: Sound Physiological Knowledge and Principles in Modeling Shrinking of Fishes under Climate Change, *Global Change Biology*, 24, <https://doi.org/10.1111/gcb.13831>, 2017.
- Pauly D. and Palomares M.L.D.: *Searoundus*, <https://www.searoundus.org/>, 2020.
- 490 Piatt, J. F., Parrish, J. K., Renner, H. M., Schoen, S. K., Jones, T. T., Arimitsu, M. L., Kuletz, K. J., Bodenstein, B., García-Reyes, M., Duerr, R. S., Corcoran, R. M., Kaler, R. S. A., McChesney, G. J., Golightly, R. T., Coletti, H. A., Suryan, R. M., Burgess, H. K., Lindsey, J., Lindquist, K., Warzybok, P. M., Jahncke, J., Roletto, J., and Sydeman, W. J.: Extreme Mortality and Reproductive Failure of Common Murres Resulting from the Northeast Pacific Marine Heatwave of 2014-2016, *PLOS ONE*, 15, e0226087, <https://doi.org/10.1371/journal.pone.0226087>, 2020.
- 495 Pörtner, H. O.: Climate Variations and the Physiological Basis of Temperature Dependent Biogeography: Systemic to Molecular Hierarchy of Thermal Tolerance in Animals, *Comparative Biochemistry and Physiology. Part A, Molecular & Integrative Physiology*, 132, 739–761, [https://doi.org/10.1016/s1095-6433\(02\)00045-4](https://doi.org/10.1016/s1095-6433(02)00045-4), 2002.
- Pörtner, H. O. and Peck, M. A.: Climate Change Effects on Fishes and Fisheries: Towards a Cause-and-Effect Understanding, *Journal of Fish Biology*, 77, 1745–1779, <https://doi.org/10.1111/j.1095-8649.2010.02783.x>, 2010.
- 500 Poschlod, B., Zscheischler, J., Sillmann, J., Wood, R. R., and Ludwig, R.: Climate Change Effects on Hydrometeorological Compound Events over Southern Norway, *Weather and Climate Extremes*, 28, 100253, <https://doi.org/10.1016/j.wace.2020.100253>, 2020.
- Rodgers, K. B., Lin, J., and Frölicher, T. L.: Emergence of Multiple Ocean Ecosystem Drivers in a Large Ensemble Suite with an Earth System Model, *Biogeosciences (Online)*, 12, 3301–3320, <https://doi.org/10.5194/bg-12-3301-2015>, 2015.
- Saito, T. and Rehmsmeier, M.: The Precision-Recall Plot Is More Informative than the ROC Plot When Evaluating Binary Classifiers on Imbalanced Datasets, *PLOS ONE*, 10, e0118432, <https://doi.org/10.1371/journal.pone.0118432>, 2015.
- 505 Smale, D. A., Wernberg, T., Oliver, E. C. J., Thomsen, M., Harvey, B. P., Straub, S. C., Burrows, M. T., Alexander, L. V., Benthuisen, J. A., Donat, M. G., Feng, M., Hobday, A. J., Holbrook, N. J., Perkins-Kirkpatrick, S. E., Scannell, H. A., Sen Gupta, A., Payne, B. L., and Moore, P. J.: Marine Heatwaves Threaten Global Biodiversity and the Provision of Ecosystem Services, *Nature Climate Change*, 9, 306–312, <https://doi.org/10.1038/s41558-019-0412-1>, 2019.
- 510 Smith, K. E., Burrows, M. T., Hobday, A. J., King, N. G., Moore, P. J., Sen Gupta, A., Thomsen, M. S., Wernberg, T., and Smale, D. A.: Biological Impacts of Marine Heatwaves, *Annual Review of Marine Science*, 15, 119–145, <https://doi.org/10.1146/annurev-marine-032122-121437>, 2023.

- Tai, T. C., Harley, C. D. G., and Cheung, W. W. L.: Comparing Model Parameterizations of the Biophysical Impacts of Ocean Acidification to Identify Limitations and Uncertainties, *Ecological Modelling*, 385, 1–11, <https://doi.org/10.1016/j.ecolmodel.2018.07.007>, 2018.
- 515 Tai, T. C., Sumaila, U. R., and Cheung, W. W. L.: Ocean Acidification Amplifies Multi-Stressor Impacts on Global Marine Invertebrate Fisheries, *Frontiers in Marine Science*, 8, 2021.
- Tibshirani, R.: Regression Shrinkage and Selection via the Lasso, *Journal of the Royal Statistical Society. Series B (Methodological)*, 58, 267–288, 1996.
- Tittensor, D. P., Novaglio, C., Harrison, C. S., Heneghan, R. F., Barrier, N., Bianchi, D., Bopp, L., Bryndum-Buchholz, A., Britten, G. L.,
520 Büchner, M., Cheung, W. W. L., Christensen, V., Coll, M., Dunne, J. P., Eddy, T. D., Everett, J. D., Fernandes-Salvador, J. A., Fulton, E. A., Galbraith, E. D., Gascuel, D., Guiet, J., John, J. G., Link, J. S., Lotze, H. K., Maury, O., Ortega-Cisneros, K., Palacios-Abrantes, J., Petrik, C. M., du Pontavice, H., Rault, J., Richardson, A. J., Shannon, L., Shin, Y.-J., Steenbeek, J., Stock, C. A., and Blanchard, J. L.: Next-Generation Ensemble Projections Reveal Higher Climate Risks for Marine Ecosystems, *Nature Climate Change*, 11, 973–981, <https://doi.org/10.1038/s41558-021-01173-9>, 2021.
- 525 Tschumi, E., Lienert, S., van der Wiel, K., Joos, F., and Zscheischler, J.: The Effects of Varying Drought-Heat Signatures on Terrestrial Carbon Dynamics and Vegetation Composition, *Biogeosciences*, 19, 1979–1993, <https://doi.org/10.5194/bg-19-1979-2022>, 2022.
- Tschumi, E., Lienert, S., Bastos, A., Ciais, P., Gregor, K., Joos, F., Knauer, J., Papastefanou, P., Rammig, A., van der Wiel, K., Williams, K., Xu, Y., Zaehle, S., and Zscheischler, J.: Large variability in simulated response of vegetation composition and carbon dynamics to variations in drought-heat occurrence, *Journal of Geophysical Research: Biogeosciences*, 128, e2022JG007332, <https://doi.org/10.1029/2022JG007332>, 2023.
- 530 van der Wiel, K., Selten, F. M., Bintanja, R., Blackport, R., and Screen, J. A.: Ensemble Climate-Impact Modelling: Extreme Impacts from Moderate Meteorological Conditions, *Environmental Research Letters*, 15, 034050, <https://doi.org/10.1088/1748-9326/ab7668>, 2020.
- Vogel, J., Rivoire, P., Deidda, C., Rahimi, L., Sauter, C. A., Tschumi, E., van der Wiel, K., Zhang, T., and Zscheischler, J.: Identifying Meteorological Drivers of Extreme Impacts: An Application to Simulated Crop Yields, *Earth System Dynamics*, 12, 151–172, <https://doi.org/10.5194/esd-12-151-2021>, 2021.
- 535 Watson, R. A., Cheung, W. W. L., Anticamara, J. A., Sumaila, R. U., Zeller, D., and Pauly, D.: Global Marine Yield Halved as Fishing Intensity Redoubles, *Fish and Fisheries*, 14, 493–503, <https://doi.org/10.1111/j.1467-2979.2012.00483.x>, 2013.
- Wernberg, T.: Marine Heatwave Drives Collapse of Kelp Forests in Western Australia, in: *Ecosystem Collapse and Climate Change*, edited by Jackson, R.B. and Canadell, J.G., *Ecological Studies-Analysis and Synthesis*, pp. 325–343, Springer Heidelberg, https://doi.org/10.1007/978-3-030-71330-0_12, 2021.
- 540 Wernberg, T., Smale, D., Thomsen, M., Langlois, T., de Bettignies, T., Bennett, S., and Rousseaux, C.: An Extreme Climatic Event Alters Marine Ecosystem Structure in a Global Biodiversity Hotspot, *Nature Climate Change*, 3, 78–82, <https://doi.org/10.1038/nclimate1627>, 2013.
- Wernberg, T., Bennett, S., Babcock, R. C., de Bettignies, T., Cure, K., Depczynski, M., Dufois, F., Fromont, J., Fulton, C. J., Hovey, R. K.,
545 Harvey, E. S., Holmes, T. H., Kendrick, G. A., Radford, B., Santana-Garcon, J., Saunders, B. J., Smale, D. A., Thomsen, M. S., Tuckett, C. A., Tuya, F., Vanderklift, M. A., and Wilson, S.: Climate-Driven Regime Shift of a Temperate Marine Ecosystem, *Science*, 353, 169–172, <https://doi.org/10.1126/science.aad8745>, 2016.
- Whitney, F. A.: Anomalous Winter Winds Decrease 2014 Transition Zone Productivity in the NE Pacific, *Geophysical Research Letters*, 42, 428–431, <https://doi.org/10.1002/2014GL062634>, 2015.

- 550 Wyatt, A., Resplandy, L., and Marchetti, A.: Ecosystem Impacts of Marine Heat Waves in the Northeast Pacific, *EGUsphere Discussions*, 2022, 1–24, <https://doi.org/10.5194/egusphere-2022-17>, 2022.
- Zscheischler, J. and Seneviratne, S. I.: Dependence of Drivers Affects Risks Associated with Compound Events, *Science Advances*, 3, e1700263, <https://doi.org/10.1126/sciadv.1700263>, 2017.
- Zscheischler, J., Mahecha, M. D., Harmeling, S., and Reichstein, M.: Detection and Attribution of Large Spatiotemporal Extreme Events in
555 Earth Observation Data, *Ecological Informatics*, 15, 66–73, <https://doi.org/10.1016/j.ecoinf.2013.03.004>, 2013.
- Zscheischler, J., Mahecha, M. D., von Buttlar, J., Harmeling, S., Jung, M., Rammig, A., Randerson, J. T., Schölkopf, B., Seneviratne, S. I., Tomelleri, E., Zaehle, S., and Reichstein, M.: A Few Extreme Events Dominate Global Interannual Variability in Gross Primary Production, *Environmental Research Letters*, 9, 035001, <https://doi.org/10.1088/1748-9326/9/3/035001>, 2014a.
- Zscheischler, J., Michalak, A. M., Schwalm, C., Mahecha, M. D., Huntzinger, D. N., Reichstein, M., Berthier, G., Ciais, P., Cook, R. B.,
560 El-Masri, B., Huang, M., Ito, A., Jain, A., King, A., Lei, H., Lu, C., Mao, J., Peng, S., Poulter, B., Ricciuto, D., Shi, X., Tao, B., Tian, H., Viovy, N., Wang, W., Wei, Y., Yang, J., and Zeng, N.: Impact of Large-Scale Climate Extremes on Biospheric Carbon Fluxes: An Intercomparison Based on MsTMIP Data, *Global Biogeochemical Cycles*, 28, 585–600, <https://doi.org/10.1002/2014GB004826>, 2014b.
- Zscheischler, J., Reichstein, M., von Buttlar, J., Mu, M., Randerson, J. T., and Mahecha, M. D.: Carbon Cycle Extremes during the 21st Century in CMIP5 Models: Future Evolution and Attribution to Climatic Drivers, *Geophysical Research Letters*, 41, 8853–8861,
565 <https://doi.org/10.1002/2014GL062409>, 2014c.
- Zscheischler, J., Westra, S., van den Hurk, B. J. J. M., Seneviratne, S. I., Ward, P. J., Pitman, A., AghaKouchak, A., Bresch, D. N., Leonard, M., Wahl, T., and Zhang, X.: Future Climate Risk from Compound Events, *Nature Climate Change*, 8, 469–477, <https://doi.org/10.1038/s41558-018-0156-3>, 2018.
- Zscheischler, J., Martius, O., Westra, S., Bevacqua, E., Raymond, C., Horton, R. M., van den Hurk, B., AghaKouchak, A., Jézéquel, A.,
570 Mahecha, M. D., Maraun, D., Ramos, A. M., Ridder, N. N., Thiery, W., and Vignotto, E.: A Typology of Compound Weather and Climate Events, *Nature Reviews Earth & Environment*, 1, 333–347, <https://doi.org/10.1038/s43017-020-0060-z>, 2020.

Chapter 6

Discussion

6.1 Summary and discussion of the main results

The principal objectives of this thesis were (1) to characterize compound marine heatwave (MHW) and low net productivity (NPPX) events over the satellite period, (2) to assess the ability of Earth system models (ESMs) to correctly represent these compound events and (3) to identify their physical and biogeochemical drivers, and finally, (4) to assess the risk posed by these compound events on marine ecosystems.

(1) Distribution of compound MHW-NPPX events over the satellite period

We characterized the distribution of compound MHW-NPPX events over the satellite period using satellite-based sea surface temperature, chlorophyll concentration as a proxy for NPP, as well as five different satellite-derived NPP products. From 1998 to 2018, we found compound events to be frequent in the low latitudes, especially in the center of the equatorial Pacific, in the Arabian Sea and along the borders of the subtropical gyres. These are nutrient-limited regions (Hayashida et al., 2020a), where SST and NPP are negatively correlated (Chapter 5), and where chlorophyll concentration and NPP are typically low during MHWs (Sen Gupta et al., 2020). These regions are particularly exposed to compound MHW-NPPX events. In contrast, compound MHW-NPPX events are rare in the high northern latitudes and in the northern part of the Southern Ocean, where MHWs rarely co-occur with NPPX events. Along Antarctica, there is low agreement across satellite-derived estimates of compound MHW-NPPX event frequency (Le Grix et al., 2022). Disagreement arises from divergent satellite-derived estimates of NPP. NPP is estimated as a function of various ocean variables available from satellite observations, such as chlorophyll concentration and carbon biomass, using various algorithms (Behrenfeld & Falkowski, 1997; Behrenfeld et al., 2005; Westberry et al., 2008; Silsbe et al., 2016; Gregg & Rousseaux, 2014). These different algorithms yield divergent NPP estimates. In addition to structural uncertainty in satellite-derived NPP estimates, uncertainties are also inherent to the satellite observations these estimates are based on. Sea-ice and clouds cause gaps in satellite observations, which are artificially filled in by interpolation and entail biases. Biases can be corrected using in-situ NPP measurements, yet they are relatively rare in the sea-ice-covered waters of the high latitudes (Del Castillo et al., 2019). Increased sampling of in-situ NPP measurements in recent years in the high latitudes (Boutin & Merlivat, 2009; Roemmich et al., 2009; McMahon et al., 2021; Su et al., 2022) may help to constrain satellite-based NPP estimates and to gain confidence in satellite-derived estimates of compound MHW-NPPX event frequency along Antarctica.

The frequency of compound MHW-NPPX events varies on seasonal to interannual timescales. At the seasonal timescale, most compound events occur in spring in the mid latitudes and in

summer in both hemispheres. These are the seasons with highest SST and NPP variability, resulting in most exceedances of the MHW and NPPX event threshold. Note that the use of a seasonally-varying percentile threshold for the definition of MHWs and NPPX events would, however, yield to uniform MHW, NPPX event, and compound MHW-NPPX event frequency throughout the year (Chapter 2). At the interannual timescale, the frequency is strongly modulated by large-scale modes of climate variability such as the El Niño–Southern Oscillation (ENSO). During the positive phase of ENSO, i.e., during El Niño events, compound MHW and low chlorophyll event frequency is multiplied by a factor ≥ 5 in the eastern equatorial Pacific and in the Indian Ocean, whereas during the reverse phase, i.e. during La Niña events, compound MHW and low chlorophyll event occurrence is suppressed over these regions. This is consistent with the results of Holbrook et al. (2019), who assessed statistical links between climate modes and MHW frequency. Previous studies also linked NPP variability to climate modes (Barber & Chavez, 1983; Behrenfeld et al., 2001, 2006; Saba et al., 2010; Racault et al., 2017). For example, Saba et al. (2010) reported positive correlation between the North Pacific Gyre Oscillation (NPGO) index and in-situ NPP measurements at the Hawaii Ocean Time series (HOT) station. There, we would expect NPP to be generally low during the negative phase of NPGO. Holbrook et al. (2019) also found enhanced MHW frequency during the negative phase of NPGO around Hawaii. These results are consistent with increased compound event frequency during the negative phase of NPGO (Chapter 3). The phase of such climate modes may ultimately be used to predict the likelihood of compound MHW-NPPX events (see section 6.3.5).

(2) Representation of compound MHW-NPPX events in ESMs

We evaluated the representation of compound MHW-NPPX events in large ensemble simulations (LES) by two ESMs: the GFDL ESM2M and the CESM2. LES provide a large dataset from which to sample and analyse rare compound MHW-NPPX events. We removed uncertainties arising from internal climate variability by averaging our results over all ensemble members of each LES. Thereby, differences between the ensemble mean results of each LES only account for structural differences between the GFDL ESM2M and CESM2 (Bevacqua et al., 2023). This method enables to identify similarities and divergences in how the models simulate compound events.

We found that compared to satellite-derived observations, both models correctly simulate frequent compound MHW-NPPX events in the low latitudes. However, in the high latitudes, the GFDL ESM2M and CESM2 simulate divergent compound MHW-NPPX event frequency. There, low agreement across satellite-derived estimates of compound MHW-NPPX event frequency prevents knowing which of the two models better simulates compound events. Recent deployment of a multitude of sensors, including gliders (Henson et al., 2023) and Argo floats (Boutin & Merlivat, 2009; Roemmich et al., 2009; Su et al., 2022), collects valuable NPP data, which could help to constrain satellite-derived NPP estimates, improve our understanding of NPP variability and thus model representation of NPP. Improved representation of NPP in ESMs is necessary before they can be used in the high latitudes to simulate NPPX events and their combination with MHWs.

(3) Drivers of compound MHW-NPPX events

In the low latitudes, the GFDL ESM2M and CESM2 correctly simulate frequent compound MHW-NPPX events and may be used to identify their physical and biogeochemical drivers. Previous studies already identified the drivers of MHWs, specifically Holbrook et al. (2019), Amaya et al. (2020), Sen Gupta et al. (2020), and Vogt et al. (2022). Most subtropical MHWs

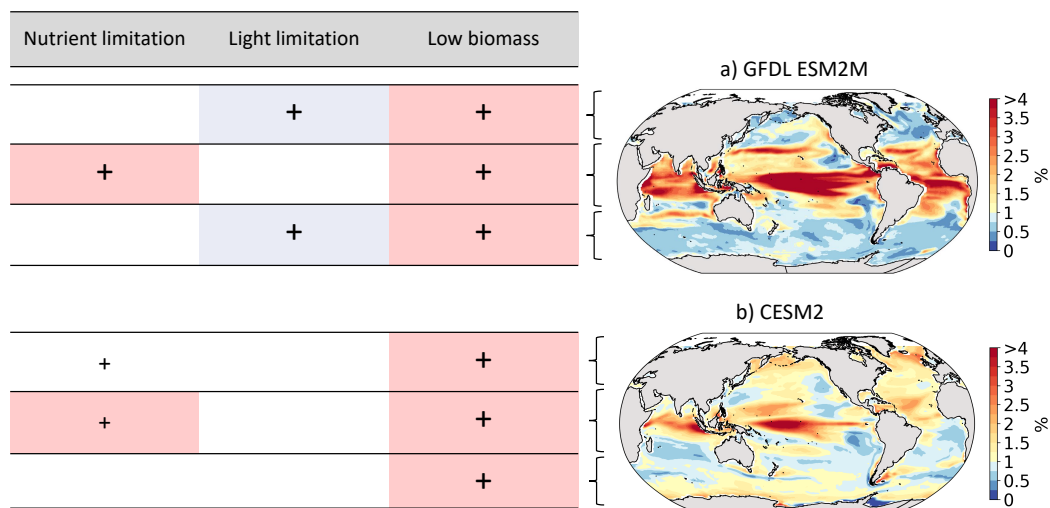


Figure 6.1: Summary of NPPX drivers during compound MHW-NPPX events (a) in the GFDL ESM2M and (b) in the CESM2 in the high northern, low, and high southern latitudes. NPPX can be driven by (1st column) nutrient limitation on phytoplankton growth, (2nd column) light limitation on phytoplankton growth, or (3rd column) low phytoplankton biomass. A cross indicates that a process contributes to driving NPPX during compound MHW-NPPX events. Larger cross size indicates dominant NPPX drivers per region. Red box colour indicates that nutrient limitation in the low latitudes, as well as low biomass, are expected to co-occur with surface warming. Blue box colour indicates that light limitation in the high latitudes is not expected to co-occur with surface warming. The maps show the compound MHW-NPPX event frequency (%) over 1998-2018. The more/less likely NPPX drivers are to co-occur with surface warming and thus with a MHW (in red/blue), the higher/lower the compound MHW-NPPX event frequency.

are triggered by persistent atmospheric high-pressure systems and anomalously weak wind speeds, associated with increased insolation, driving reduced ocean heat losses towards the atmosphere (e.g., Sen Gupta et al. (2020)). Tropical MHWs are associated with locally reduced vertical mixing and enhanced heat diffusion (Vogt et al., 2022). In this thesis, we rather investigated the drivers of an extreme reduction in NPP, which associated with a MHW, would drive a compound MHW-NPPX event. Fig. 6.1 summarizes these drivers. We found that in both the GFDL ESM2M and CESM2, nutrient limitation on phytoplankton growth increases during MHW-NPPX events, especially in the low latitudes in the GFDL ESM2M, which contributes to driving low NPP (Fig. 6.1, first column). In addition, phytoplankton biomass is low due to a relative increase in phytoplankton loss compared to phytoplankton production. As grazing, mortality, and aggregation are all enhanced by high temperatures (Dunne et al., 2013; Long et al., 2021b), a MHW may itself enhance phytoplankton loss and contribute to driving low NPP during compound MHW-NPPX events in the two models.

In the high latitudes, high nutrient levels (Hayashida et al., 2020a; Le Grix et al., 2022) imply that phytoplankton growth is limited by light and temperature rather than by the nutrient supply. During MHWs, temperature is high and light may be the only limiting factor of phytoplankton growth. In the GFDL ESM2M, enhanced light limitation on phytoplankton growth is a dominant driver of reduced NPP during compound MHW-NPPX events (Fig. 6.1a). This result may be counter-intuitive, as in the high latitudes, MHWs are mainly driven by radiative heating due to reduced cloud cover (Vogt et al., 2022). Namely, MHWs are expected to co-occur with relieved light limitation, yet for an NPPX event to occur, it must generally be driven by enhanced light limitation. Therefore, compound MHW-NPPX events are rare in the GFDL

ESM2M in the high latitudes (Fig. 6.1a), and when they do occur, they uncharacteristically combine a MHW with enhanced light limitation. In contrast, in the CESM2, compound MHW-NPPX events are associated with relieved light limitation, and mostly driven by a relative increase in phytoplankton loss compared to its production, resulting in low phytoplankton biomass (Fig. 6.1b).

Overall, the likelihood of compound MHW-NPPX events in each model depends on how likely a MHW is to co-occur with these NPPX event drivers. A MHW is expected to co-occur with nutrient limitation in the low latitudes as well as with low phytoplankton biomass (red boxes on Fig. 6.1), which may explain frequent MHW-NPPX events in the low latitudes in both models and relatively frequent MHW-NPPX events in the high latitudes in the CESM2. In contrast, a MHW is not expected to co-occur with light limitation in the high latitudes (blue boxes on Fig. 6.1), which may explain the rare compound MHW-NPPX events in the high latitudes in the GFDL ESM2M. Divergent NPPX drivers and therefore divergent likelihood of compound MHW-NPPX events in the GFDL ESM2M and CESM2 imply the need to improve model representation of NPP – and therefore of the processes driving NPPX – before the models can adequately represent compound MHW-NPPX events, especially in the high latitudes. As discussed in subsection 6.1, the rise in NPP measurements, as well as zooplankton grazing activity measurements, would help improve our understanding of the factors controlling NPP and thus NPP representation by ESMs.

(4) Impacts of compound MHW-NPPX events

We assessed the severity of the threat posed by compound MHW-NPPX events on pelagic ecosystems (Chapter 5). Enhanced surface temperature and reduced NPP are both drivers of extreme impacts on pelagic fish biomass in the equatorial Atlantic, the central and eastern equatorial Pacific, in the northern part of the Indian Ocean, and in the northeastern Pacific. There, pelagic ecosystems may be particularly vulnerable to compound MHW-NPPX events.

In the following, we present several biological mechanisms through which compound MHW-NPPX events may drive impacts on pelagic organisms and ecosystems.

(4.1) Shifts in plankton community structure:

Small phytoplankton are characterized by a high surface-to-volume ratio and a thin cell boundary layer compared to large phytoplankton (Raven, 1998). Their small size supports efficient nutrient and light absorption and offers an advantage in nutrient or light limited waters. As MHWs tend to be associated with surface stratification and low nutrient levels (e.g., Wyatt et al. (2022)), they favor small phytoplankton such as cyanobacteria (Mousing et al., 2014; Fu et al., 2016; Peña et al., 2019; Schmidt et al., 2020) (Fig. 6.2b compared to Fig. 6.2a). In particular, low levels of silica during MHWs have been associated with a decline in diatoms and a shift towards smaller phytoplankton in the Gulf of Alaska (Arteaga & Rousseaux, 2023). NPPX events may also be associated with light limitation in the high latitudes (Le Grix et al., 2022), and thus favor small phytoplankton. Reduced phytoplankton size during MHW-NPPX events affects the amount of energy transferred to higher trophic levels (Brander & Kiørboe, 2020), as small phytoplankton are sometimes too small to be grazed by the larger zooplankton (Cheung et al., 2011) and lack essential biomolecules such as omega-3 polyunsaturated fatty acids and sterols (Schmidt et al., 2020). Fig. 6.2b illustrates the poor food supply provided by small phytoplankton to its grazers, with negative repercussions on the marine food web.

(4.2) Too little food supply:

In addition to poor food quality during MHW-NPPX events, synergistic effects between the MHW and NPPX event may also reduce food quantity. Indeed, high temperatures enhance

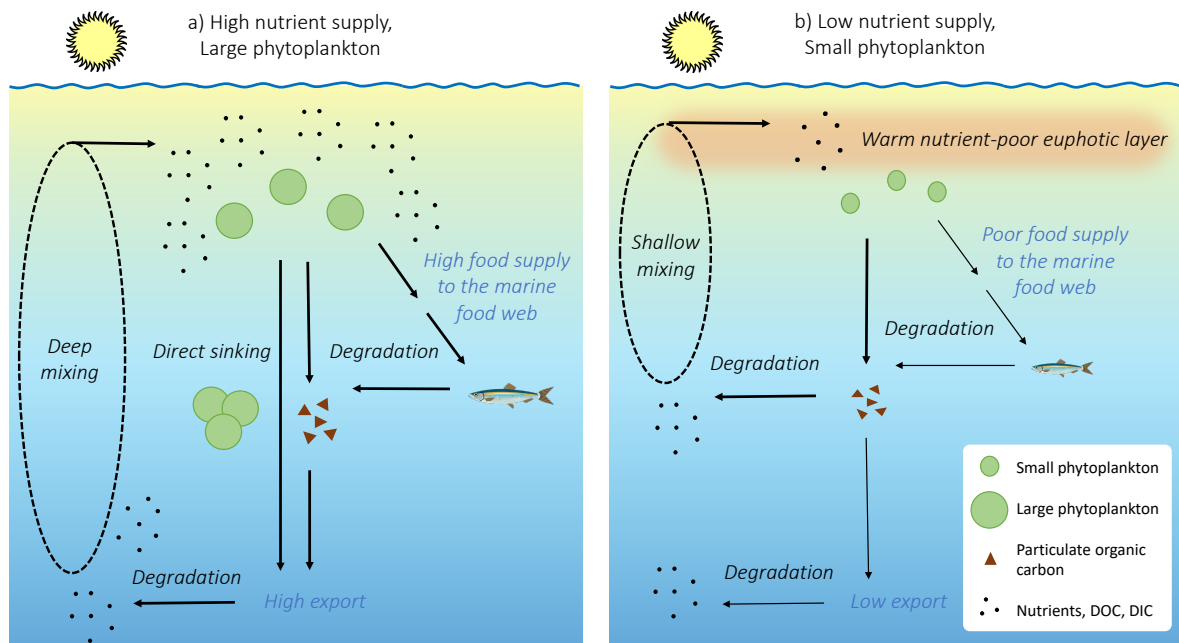


Figure 6.2: Phytoplankton community structure impacts the transfer of organic carbon through the marine food web, as well carbon export efficiency. (a) High nutrient levels, e.g. due to intense vertical mixing, are associated with a high proportion of large phytoplankton. Large phytoplankton provide quality food to grazers, with positive repercussions on higher trophic levels. They also favor downward carbon export by forming aggregates that are heavy enough to sink, and through production of particulate organic carbon. (b) Low nutrient levels due to stratification and weak vertical mixing – e.g., during MHWs – are associated with a high proportion of small phytoplankton. Small phytoplankton provide less quality food to grazers, and tend to remain in the surface ocean, where they are degraded.

metabolic growth costs (Barneche et al., 2021) and thus food demand, whereas low phytoplankton production impairs the transfer of energy through the food chain, which ultimately limits food supply (Pauly & Christensen, 1995; Chassot et al., 2010; Blanchard et al., 2012; Marshak & Link, 2021). High food demand combined with low food supply may negatively impact the growth, reproductive success, and survival rate of certain species (e.g., Piatt et al. (2020)).

(4.3) Deoxygenation:

High temperature and low NPP are both correlated with low oxygen levels in the surface waters of the low and mid latitudes (e.g., Chapter 5). Most compound MHW-NPPX events are therefore combined with extremely low oxygen in these regions (Fig. 6.3). Low oxygen during compound MHW-NPPX events negatively impacts marine organisms, e.g., by limiting their growth and maximum body size (Pauly, 1980), with repercussions at the ecosystem level (Wu, 2002).

(4.4) Species migration and changes in species interaction:

Changes in ocean conditions cause the dispersion of species looking for more suitable habitats (e.g., Cavole et al. (2016)). For example, ocean warming triggers the northward migration of warm-water copepods in the northern Atlantic (Beaugrand et al., 2002) and in the northeastern Pacific (Cavole et al., 2016). Warm-water copepods are smaller and contain lower quantities of fatty acids and wax esters than their cold-water counterparts, whose diversity and abundance decrease in response to warm-water copepod invasion, with negative implications for the ecosystem (Leising et al., 2015; Cavole et al., 2016). Compound MHW-NPPX events, such as

the ‘Blob’ (Chapter 1, section 1.4), were also associated with the migration of numerous marine species toward higher latitudes, where they disrupted species interactions (Cavole et al., 2016).

Overall, altered phytoplankton community structure, enhanced competition for food, additional stressors such as deoxygenation, and changes in species interactions during compound MHW-NPPX events may have compounding effects on pelagic ecosystems, resulting in decreased pelagic fish biomass over certain regions.

6.2 Limitations

In the following section, we discuss the caveats and limitations of this thesis.

6.2.1 Low confidence in NPP estimates

First we discuss our limited confidence in satellite-derived NPP estimates. We used chlorophyll concentration as a proxy for NPP in Chapter 3, as chlorophyll is more directly available from satellite ocean colour than NPP. However, chlorophyll variability alone is insufficient to explain the complete NPP variability over time and space (Behrenfeld & Falkowski (1997); Chapter 2). Chlorophyll would be a proxy for phytoplankton carbon biomass only if the chlorophyll to carbon ratio in phytoplankton was constant, yet it varies with light and nutrient conditions (Geider et al., 1997). Changes in phytoplankton community structure, e.g. from diatoms to dinoflagellates, also affect chlorophyll concentration (Arteaga & Rousseaux, 2023), as certain phytoplankton types are more concentrated in chlorophyll than others. Besides, changes in phytoplankton biomass do not exactly mirror changes in phytoplankton NPP, namely the rate of new biomass production. Low phytoplankton biomass may co-occur with high NPP simply due to low phytoplankton grazing, and vice-versa.

In Chapter 4, instead of using chlorophyll as an imperfect proxy for NPP, we used NPP estimates derived from satellite observations using various algorithms. Nevertheless, uncertainties remain, due to structural and parametric uncertainty in these algorithms and to uncertainties in the satellite observations themselves (see Section 2.1.3).

Another limitation of satellite-derived chlorophyll and NPP estimates is their reliance on satellite ocean color measurements which only survey the upper layer of the ocean, i.e. about 10 meter deep (Brewin et al., 2016; Groom et al., 2019), although the euphotic layer can extend up to about 200 meters (Encyclopedia Britannica, 1998; Lee et al., 2007). As nutrients tend to be more concentrated at subsurface than at the surface, NPP is highest at the base of the euphotic layer in nutrient-depleted regions (Smith, 1981). Therefore, satellite observations tend to underestimate chlorophyll and NPP in the nutrient-depleted subtropical gyres (Sigman, D & Hain, M, 2012). Long et al. (2021a) also highlighted discrepancies between float and satellite-based NPP data caused by various depth resolutions.

6.2.2 2D perspective

The 2D perspective from which we approached ocean biogeochemical extremes in this thesis neglects their 3D structure (Gruber et al., 2021). Following the common and widely-used definition of MHWs as surface MHWs (Hobday et al., 2016), we conveniently identified MHWs using the sea surface temperature estimated by satellites or extracted from the upper depth level of ESM outputs. Holbrook et al. (2019) justify the restriction of MHW studies to the surface ocean by stating that subsurface temperature data are sparse and that MHWs are

most likely to cause ecological impacts in the upper ocean where biological productivity is highest. Nevertheless, MHWs can extend to depth, and even remain there long after they have dissipated at the surface (Scannell et al., 2020; Koehn et al., 2022), with potential repercussions on marine organisms that dwell below the uppermost layer of the ocean. Similarly, we neglected the vertical structure of NPP by integrating it over the top 100-meter layer before defining NPPX events. However, depending on the vertical structure of its NPP anomaly, an NPPX event may be more or less likely to co-occur with a MHW, it may be driven by different physical and biogeochemical processes, and it may have different impacts on marine life. Lastly, in Chapter 5, we only considered surface ocean conditions as potential drivers of extreme impacts on pelagic fish biomass, although pelagic fish are not restricted to the surface ocean and can also be impacted by anomalous ocean conditions at subsurface.

6.2.3 Imperfect representation of ocean biogeochemical extremes in ESMs

Like any model, the GFDL ESM2M and the CESM2 are an incomplete representation of the Earth's climate. For example, their relatively low resolution does not allow them to resolve mesoscale eddies and submesoscale fronts, and their significant impacts on nutrient levels, phytoplankton diversity and productivity (Lévy et al., 2015; Couespel et al., 2021). NPPX events may be driven by mesoscale and submesoscale processes unresolved by the GFDL ESM2M and by the CESM2. Similarly, low resolution models tend to underestimate SST variability and thus the intensity of MHWs, as well as the severity of their biological impacts in western boundary current regions (Pilo et al., 2019; Hayashida et al., 2020b; Guo et al., 2022).

As discussed in Chapter 4, model representation of NPP is subject to large uncertainties, especially in the high latitudes, where the GFDL ESM2M and the CESM2 disagree on the factors controlling phytoplankton NPP. Phytoplankton growth and decay are represented using a set of equations associated with both structural and parametric uncertainties (Balaji et al., 2022). Moreover, the GFDL ESM2M and the CESM2 simplify the high diversity of phytoplankton species and functions by representing three phytoplankton types only (small phytoplankton; large phytoplankton; and diazotrophs, which we omitted from our analysis due to their negligible contribution to NPPX events) (Dunne et al., 2013; Long et al., 2021b). Still, ocean biogeochemical modules in ESMs are valuable tools to apprehend NPP variability and its drivers. Improved understanding of phytoplankton processes gained from observations and in-situ studies would help improve ESMs representation of NPP, so they could be used to study NPPX and compound MHW-NPPX events also in the high latitudes.

ESMs do not represent all components of the Earth's climate. For example, the GFDL ESM2M omits the role of ice sheets in providing fresh water to the surface ocean (Dunne et al., 2012). It has been shown that warming induces ice sheet melting, which may enhance stratification (Madsen et al., 2022) and therefore nutrient limitation on phytoplankton growth (Sarmiento & Gruber, 2006), potentially driving low NPP (Le Grix et al., 2022). Locally, the calving of ice sheets into icebergs may also interact with ocean productivity by providing iron from aeolian dust to the marine environment and promoting NPP (Wu & Hou, 2017). Although the GFDL ESM2M and CESM2 fail to represent numerous processes that may affect the likelihood of compound MHW-NPPX events, sacrificing accuracy in one part of the climate system, such as ice sheets, allows them to remain of relatively low complexity (Balaji et al., 2022), so computation costs are reasonable. Indeed, the study of ocean compound events requires a large sample size (Deser et al., 2020; Zscheischler & Lehner, 2022), and large ensemble simulations by the GFDL ESM2M and CESM2 can be run in a reasonable amount of time given realistic computing resources.

6.2.4 Imperfect representation of the drivers of extreme impact on fish in global marine fish models

The DBEM is also an imperfect representation of pelagic ecosystems' response to changes in ocean conditions (Chapter 5). The discussion of Chapter 5 lists the main caveats of this model. We mentioned that the DBEM only considers surface ocean conditions as ecosystem stressors of pelagic species, although pelagic species also dwell at subsurface. Besides, the DBEM simulations that we use in Chapter 5 omit the impact of acidity changes on marine organisms (Melzner et al., 2009; Munday et al., 2009; Cheung et al., 2011), as well as the additional impact of human activities (Watson et al., 2013; Cheung et al., 2018).

Our results are highly dependent on the DBEM's representation of pelagic species. An intermodel comparison study would allow us to determine whether the drivers of extreme impacts on pelagic fish, which we identified in Chapter 5, are robust across models (Tebaldi & Knutti, 2007; van der Wiel et al., 2020).

6.3 Outlook

6.3.1 Describe the spatio-temporal structure of compound MHW-NPPX events

In this thesis, we limited the study of compound MHW-NPPX events to the surface ocean, where satellite observations are available (Le Traon et al., 2015). However, outputs from the GFDL ESM2M and CESM2 also include information about the vertical structure of compound MHW-NPPX events. Sea water temperature and NPP fields are available up to at least 100-meter depth, at a vertical resolution of about 10m. These model outputs could be evaluated using in-situ data collected by ships, Argo floats, or moorings, which all provide measurements at depth.

Depending on their vertical extent, one might expect compound MHW-NPPX events to be more or less persistent over time (Koehn et al., 2022), with implications for marine ecosystems' resilience (Gruber et al., 2021). Impacts from ocean extremes also depend on their vertical and horizontal extent as ocean extremes compress the habitat of marine organisms into a smaller volume (Gruber et al., 2021). Habitat compression can disrupt species interactions, increase food competition, and fisheries pressure (e.g., Santora et al. (2020)). Therefore, I would suggest considering the 4D structure of compound MHW-NPPX events across the horizontal, vertical, and time axes when investigating compound MHW-NPPX events impacts on marine ecosystems.

Compound MHW-NPPX events are also bound to evolve under climate change as the ocean is getting warmer (Frölicher & Laufkötter, 2018; Oliver et al., 2018; Gruber et al., 2021). In the low latitudes, ESMs successfully represent present-day compound MHW-NPPX events (Le Grix et al., 2022) and could be used to project them into the future, just as Burger et al. (2022) projected future compound MHW and high acidity extremes. In the high latitudes, however, ESMs are not yet ready to project compound MHW-NPPX events into the future.

6.3.2 Further investigate the impacts of compound MHW-NPPX events

In Chapter 5, we differentiated the drivers of extreme impacts across oceanic regions (Chapter 5). However, a certain driver, such as a compound MHW-NPPX event, may drive more or less severe impacts depending on its duration, depth and horizontal extent. In addition, impacts may also correlate with the timing, intensity and recurrence rate of compound MHW-NPPX events (Gruber et al., 2021). Lastly, impacts depend on the resilience and resistance strategies of an

ecosystem (Gruber et al., 2021). Improved understanding of all factors controlling the severity of impacts from compound MHW-NPPX events is a necessary step towards better prediction of their future impacts.

In this thesis, we assessed impacts on the total biomass of pelagic fishes. We could also assess impacts on singular species, including demersal fishes which account for a large proportion of the marine fish biomass relevant to fisheries (Pauly D. & Palomares M.L.D., 2020), as well as on the species composition of an ecosystem. Species react differently to changes in ocean conditions, depending on their habitat preferences (Cheung et al., 2008) and adaptive ability (Gruber et al., 2021). The response of an entire ecosystem to compound MHW-NPPX events likely depends on its species composition and on their interactions. In turn, compound MHW-NPPX events may alter the structure and functioning of an ecosystem, just as previous MHWs triggered profound ecosystem reconfiguration (Smith et al., 2021), thereby rendering that ecosystem more vulnerable to subsequent events and to climate change in general (Urban et al., 2012; Gruber et al., 2021). We could therefore quantify the impacts of compound MHW-NPPX events on ecosystem composition and structure using various complementary metrics, such as species richness and Simpson's evenness (Supp & Ernest, 2014; Elahi et al., 2015; Henson et al., 2021). We could also investigate the impacts of compound MHW-NPPX events on species distribution. Indeed, extreme events trigger species migration (e.g., Cavole et al. (2016); Santora et al. (2020); Smith et al. (2021)) and maybe also redistribution across depth (as under climate change; e.g., Santana-Falcón & Séférian (2022)), with implications for fisheries (Cavole et al., 2016; Smith et al., 2021). Lastly, impacts on human societies could also be considered, as MHWs and NPPX events both limit fisheries performance (Cavole et al., 2016; Smith et al., 2021; Marshak & Link, 2021), and may trigger biodiversity loss (Gruber et al., 2021), impairing ocean ecosystem services (Worm et al., 2006).

6.3.3 Implications for the carbon pump

In the Introduction of this thesis, we introduced phytoplankton NPP and its role in the biological carbon pump. Any reduction in NPP may reduce the amount of carbon transferred to depth (Bopp et al., 2001; Moore et al., 2013). However, there is no direct relationship between NPP and the associated carbon export (e.g., Henson et al. (2019); Fan et al. (2020); Lacour et al. (2023)). Carbon export depends for example on phytoplankton community structure (Dunne et al., 2005; Moore et al., 2013; Fan et al., 2020), i.e. on the type of phytoplankton responsible for NPP. The larger the phytoplankton, the more efficient the carbon export generally is (Dunne et al., 2005) (Fig. 6.2a compared to Fig. 6.2b). Indeed, large phytoplankton produce abundant sinking material and are grazed by multicellular zooplankton which also produce sinking material such as fecal pellets (Sigman, D & Hain, M, 2012). In contrast, small phytoplankton are directly grazed by unicellular zooplankton, which lack a digestive tract and do not produce fecal pellets (Sigman, D & Hain, M, 2012). The shift towards smaller phytoplankton during compound MHW-NPPX events (e.g., in the high northern latitudes; Le Grix et al. (2022)) mirrors the long-term shift in phytoplankton communities under climate change, which results in a less efficient carbon export (Bopp et al., 2005; Fu et al., 2016). In addition, MHWs have also been associated with reduced carbon sequestration (Arias-Ortiz et al., 2018; Smith et al., 2021). Compound extreme events such as compound MHW-NPPX events are thus likely to impact carbon uptake by the ocean.

Although compound MHW-NPPX events are typically short (Le Grix et al., 2021), they provide a window into a potential future and could inform changes in oceanic carbon uptake under climate change.

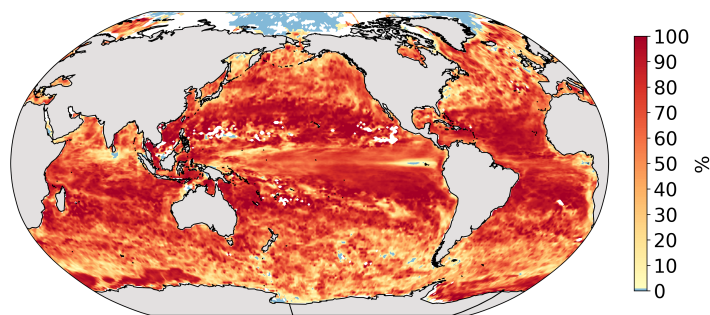


Figure 6.3: Percentage of compound MHW-NPPX events co-occurring with a low O_2 event over the preindustrial period in the GFDL ESM2M. Here, compound MHW-NPPX events correspond to days when the SST is higher than its 99th percentile and the vertically-integrated NPP is lower than its 1st percentile, relative to their respective preindustrial climatology. Low O_2 events correspond to days when surface O_2 is lower than its 1st percentile relative to the preindustrial climatology. Compound MHW-NPPX and low O_2 events are sampled from a 500-year-long preindustrial simulation, where atmospheric CO_2 concentrations are set to 286 ppm.

6.3.4 Other types of ocean compound events

In this thesis, we focused on one type of ocean compound event: a multivariate compound event consisting of two co-occurring extreme events, i.e. a marine heatwave and an extremely low NPP event. However, in Chapter 5, we found that extreme impacts on pelagic ecosystems might also be driven by compound moderate events, which consist of moderate anomalies in multiple variables. Moreover, temporally compounding events, such as persistent low NPP over multiple years, may also drive extreme impacts in the subtropics (Chapter 5). Therefore, I would suggest extending the study of ocean compound events to other types of compound events.

The increase in extreme event frequency under climate change (e.g., Frölicher et al. (2018); Oliver et al. (2018); Guo et al. (2022)) implies higher likelihood that marine ecosystems will experience multiple extreme events in short succession. Temporally compounding events may alter the ecosystems' resistance and resilience over time, and aggravate impacts (Gruber et al., 2021). For example, as corals need a recovery window in between bleaching events (Hughes et al., 2018), successive MHWs would impair successful recovery. Marine ecosystems' vulnerability to oceanic events also depends on their preconditioning; e.g., exposure to warm temperatures alters the response of diatoms and macrophytes to subsequent MHWs (Saha et al., 2020; Samuels et al., 2021). Spatially compounding events may also be worth investigating, as multiple events combined over an extended region may compound and aggravate impacts on marine life (Zscheischler et al., 2020). Finally, multivariate compound events combining more than two ocean ecosystem stressors potentially aggravate impacts on marine life and therefore warrant investigation. For example, compound MHW-NPPX events may often be associated with low O_2 levels, e.g., due to reduced O_2 solubility (Garcia & Gordon, 1992) and reduced mixing with subsurface waters (Sarmiento et al., 1998) during MHWs. Indeed, we find that over the preindustrial period, more than 80% of the compound MHW-NPPX events simulated by the GFDL ESM2M in the mid latitudes co-occur with extremely low O_2 (Fig. 6.3). Deoxygenation puts marine ecosystems under additional stress (Wu, 2002). Future work could therefore describe the distribution and impacts of such trivariate MHW-NPPX and low O_2 events.

6.3.5 Impact prediction and mitigation

This thesis provides insights into strategies to predict, prevent or moderate future impacts from ocean compound events.

First, Chapter 5 revealed the key role of compound events in driving severe declines in pelagic fish biomass. We identified potentially harmful combinations of ocean conditions, such as high temperature and low NPP in the low latitudes. These findings motivate the monitoring of multiple ocean ecosystem stressors, including temperature and NPP, as a means to predict impacts on pelagic ecosystems. Operational forecast systems, such as those developed by the Copernicus Marine Center (<https://marine.copernicus.eu/>), the Copernicus Climate Change Service (<https://climate.copernicus.eu/seasonal-forecasts>), or the NOAA Center for Weather and Climate Prediction (<https://www.weather.gov/ncep/>), provide readily available ocean analysis and forecast data. These data could be used to detect or forecast compound ocean events and to send an early warning to ocean stakeholders who could act to mitigate potential impacts on ecosystems. For example, over regions where compound MHW-NPPX events negatively impact marine ecosystems, measures could be implemented whenever SST and NPP forecasts jointly exceed a certain variable-specific threshold. Thresholds would be defined as a trade-off between the risk of inaction and the risk of unnecessary action (Jacox et al., 2022). In addition, we investigated in this thesis the physical and biological drivers of compound MHW-NPPX events. For example, in the low latitudes, surface warming is associated with nutrient limitation which contributes to driving compound MHW-NPPX events (Chapter 4). SST and nutrient levels could inform the prediction of compound MHW-NPPX events, similarly as to how Jacox et al. (2022) use SST forecasts to forecast MHWs. Alternatively, the state of large-scale climate modes of variability, which modulate compound MHW-NPPX event likelihood (Chapter 3), could also be used to inform their prediction. Jacox et al. (2022) show that MHW forecast skill is improved by considering the state of large-scale climate modes such as ENSO at the time when forecasts are initialized. Similarly, the observed and predicted state of ENSO could well be used to predict compound MHW-NPPX events, e.g. in the eastern equatorial Pacific and Indian Ocean, where El Niño events are associated with increased compound MHW-NPPX event likelihood.

Early prediction of harmful compound events allows mitigating measures to be quickly implemented to prevent impacts. In particular, measures could alleviate additional pressure from fisheries (Smith et al., 2021; Jacox et al., 2022), e.g., by applying fishing quotas, which might be especially low for forage species (Pikitch et al., 2012; Watters et al., 2020), or by forbidding harmful fishing practices (e.g., bottom trawling ; Hiddink et al. (2011)) and access to certain regions.

Marine protected areas are designated reserves that exclude fishing and have been shown to promote abundance, size, and diversity of marine species (Gaines et al., 2010; Brito-Morales et al., 2022). Promoting biodiversity within an ecosystem generally increases its resistance to perturbations (Worm et al., 2006) such as compound MHW-NPPX events. Marine protected areas could also be designed after harmful oceanic events as a means to restore biodiversity and ecosystem functioning (Sala et al., 2021).

Critically, anthropogenic emissions must be curbed to prevent increasing impacts from compound MHW-NPPX events on marine ecosystems. Climate change has been associated with long-term changes in ocean conditions, which cause a rise in extreme event frequency, intensity, duration and extent (Frölicher et al., 2018; Oliver et al., 2018). A low emissions pathway moderates climate change and ensures a moderate rise in extreme and compound extreme events (Seneviratne et al., 2012; Burger et al., 2022) such as compound MHW-NPPX events.

6.4 Conclusion

This thesis provides a first understanding of the distribution, drivers, and impacts of compound marine heatwave and low net primary productivity events in the ocean. Our results highlight the need to further study these impactful compound events, and to extend compound event research to other types of oceanic compound events. They also inform potential strategies to predict, prevent and moderate impacts. Finally, compound MHW-NPPX events provide a window into a potentially warmer and less productive ocean from which to investigate the response of marine ecosystems to climate change.

Bibliography

- Amaya, D. J., Miller, A. J., Xie, S.-P., & Kosaka, Y., 2020. Physical drivers of the summer 2019 North Pacific marine heatwave, *Nature Communications*, 11(1), 1903.
- Arias-Ortiz, A., Serrano, O., Masqué, P., Lavery, P. S., Mueller, U., Kendrick, G. A., Rozaimi, M., Esteban, A., Fourqurean, J. W., Marbà, N., Mateo, M. A., Murray, K., Rule, M. J., & Duarte, C. M., 2018. A marine heatwave drives massive losses from the world's largest seagrass carbon stocks, *Nature Climate Change*, 8(4), 338–344.
- Arteaga, L. A. & Rousseaux, C. S., 2023. Impact of Pacific Ocean heatwaves on phytoplankton community composition, *Communications Biology*, 6(1), 1–13.
- Balaji, V., Couvreur, F., Deshayes, J., Gautrais, J., Hourdin, F., & Rio, C., 2022. Are general circulation models obsolete?, *Proceedings of the National Academy of Sciences*, 119(47), e2202075119.
- Barber, R. T. & Chavez, F. P., 1983. Biological Consequences of El Niño, *Science*, 222(4629), 1203–1210.
- Barneche, D. R., Hulatt, C. J., Dossena, M., Padfield, D., Woodward, G., Trimmer, M., & Yvon-Durocher, G., 2021. Warming impairs trophic transfer efficiency in a long-term field experiment, *Nature*, 592(7852), 76–79.
- Beaugrand, G., Reid, P. C., Ibañez, F., Lindley, J. A., & Edwards, M., 2002. Reorganization of North Atlantic Marine Copepod Biodiversity and Climate, *Science*, 296(5573), 1692–1694.
- Behrenfeld, M. J. & Falkowski, P. G., 1997. Photosynthetic rates derived from satellite-based chlorophyll concentration, *Limnology, Oceanography*, 42, 1–20.
- Behrenfeld, M. J., Randerson, J. T., McClain, C. R., Feldman, G. C., Los, S. O., Tucker, C. J., Falkowski, P. G., Field, C. B., Frouin, R., Esaias, W. E., Kolber, D. D., & Pollack, N. H., 2001. Biospheric Primary Production During an ENSO Transition, *Science (New York, N. Y.)*, 291(5513), 2594.
- Behrenfeld, M. J., Boss, E., Siegel, D. A., & Shea, D. M., 2005. Carbon-based ocean productivity, phytoplankton physiology from space, *Global Biogeochemical Cycles*, 19(1).
- Behrenfeld, M. J., O'Malley, R. T., Siegel, D. A., McClain, C. R., Sarmiento, J. L., Feldman, G. C., Milligan, A. J., Falkowski, P. G., Letelier, R. M., & Boss, E. S., 2006. Climate-driven trends in contemporary ocean productivity, *Nature*, 444(7120), 752–755.
- Bevacqua, E., Suarez-Gutierrez, L., Jézéquel, A., Lehner, F., Vrac, M., Yiou, P., & Zscheischler, J., 2023. Advancing research on compound weather and climate events via large ensemble model simulations, *Nature Communications*, 14(1), 2145.
- Blanchard, J. L., Jennings, S., Holmes, R., Harle, J., Merino, G., Allen, J. I., Holt, J., Dulvy, N. K., & Barange, M., 2012. Potential consequences of climate change for primary production and fish production in large marine ecosystems, *Philosophical Transactions of the Royal Society B: Biological Sciences*, 367(1605), 2979–2989.
- Bopp, L., Monfray, P., Aumont, O., Dufresne, J.-L., Le Treut, H., Madec, G., Terray, L., & Orr, J. C., 2001. Potential impact of climate change on marine export production, *Global Biogeochemical Cycles*, 15(1), 81–99.
- Bopp, L., Aumont, O., Cadule, P., Alvain, S., & Gehlen, M., 2005. Response of diatoms distribution to global warming and potential implications: A global model study, *Geophysical Research Letters*, 32(19).
- Boutin, J. & Merlivat, L., 2009. New in situ estimates of carbon biological production rates in the Southern Ocean from CARIOCA drifter measurements, *Geophysical Research Letters*, 36(13).
- Brander, K. & Kiørboe, T., 2020. Decreasing phytoplankton size adversely affects ocean food chains, *Global Change Biology*, 26(10), 5356–5357.
- Brewin, R. J. W., Dall'Olmo, G., Pardo, S., van Dongen-Vogels, V., & Boss, E. S., 2016. Underway spectrophotometry along the Atlantic Meridional Transect reveals high performance in satellite chlorophyll retrievals, *Remote Sensing of Environment*, 183, 82–97.
- Brito-Morales, I., Schoeman, D. S., Everett, J. D., Klein, C. J., Dunn, D. C., García Molinos, J., Burrows, M. T., Buenafe, K. C. V., Dominguez, R. M., Possingham, H. P., & Richardson, A. J., 2022. Towards climate-smart, three-dimensional protected areas for biodiversity conservation in the high seas, *Nature Climate Change*, 12(4), 402–407.

- Burger, F. A., Terhaar, J., & Frölicher, T. L., 2022. Compound marine heatwaves and ocean acidity extremes, *Nature Communications*, 13(1), 4722.
- Cavole, L., Demko, A., Diner, R., Giddings, A., Koester, I., Pagniello, C., Paulsen, M.-L., Ramírez-Valdez, A., Schwenck, S., Zill, M., & Franks, P., 2016. Biological impacts of the 2013–2015 warm-water anomaly in the northeast pacific: Winners, losers, and the future, *Oceanography (Washington D.C.)*, 29.
- Chassot, E., Bonhommeau, S., Dulvy, N. K., Mélin, F., Watson, R., Gascuel, D., & Le Pape, O., 2010. Global marine primary production constrains fisheries catches, *Ecology Letters*, 13(4), 495–505.
- Cheung, W., Lam, V., & Pauly, D., 2008. Dynamic bioclimate envelope model to predict climate-induced changes in distribution of marine fishes and invertebrates, *Modelling Present and Climate-shifted Distributions of Marine Fishes and Invertebrates*, 16, 5–50.
- Cheung, W. W. L., Dunne, J., Sarmiento, J. L., & Pauly, D., 2011. Integrating ecophysiology and plankton dynamics into projected maximum fisheries catch potential under climate change in the Northeast Atlantic, *ICES Journal of Marine Science*, 68(6), 1008–1018.
- Cheung, W. W. L., Jones, M. C., Reygondeau, G., & Frölicher, T. L., 2018. Opportunities for climate-risk reduction through effective fisheries management, *Global Change Biology*, 24(11), 5149–5163.
- Couespel, D., Lévy, M., & Bopp, L., 2021. Oceanic primary production decline halved in eddy-resolving simulations of global warming, *Biogeosciences*, 18(14), 4321–4349.
- Del Castillo, C. E., Signorini, S. R., Karaköylü, E. M., & Rivero-Calle, S., 2019. Is the Southern Ocean Getting Greener?, *Geophysical Research Letters*, 46(11), 6034–6040.
- Deser, C., Lehner, F., Rodgers, K., Ault, T., Delworth, T., DiNezio, P., Fiore, A., Frankignoul, C., Fyfe, J., Horton, D., Kay, J., Knutti, R., Lovenduski, N., Marotzke, J., McKinnon, K., Minobe, S., Randerson, J., Screen, J., Simpson, I., & Ting, M., 2020. Insights from Earth system model initial-condition large ensembles and future prospects, *Nature Climate Change*, 10, 277–286.
- Dunne, J. P., Armstrong, R. A., Gnanadesikan, A., & Sarmiento, J. L., 2005. Empirical and mechanistic models for the particle export ratio, *Global Biogeochemical Cycles*, 19(4).
- Dunne, J. P., John, J. G., Adcroft, A. J., Griffies, S. M., Hallberg, R. W., Shevliakova, E., Stouffer, R. J., Cooke, W., Dunne, K. A., Harrison, M. J., Krasting, J. P., Malyshev, S. L., Milly, P. C. D., Philipps, P. J., Sentman, L. T., Samuels, B. L., Spelman, M. J., Winton, M., Wittenberg, A. T., & Zadeh, N., 2012. GFDL’s ESM2 global coupled Climate–Carbon earth system models. Part I: Physical formulation, baseline simulation characteristics, *Journal of Climate*, 25(19), 6646–6665.
- Dunne, J. P., John, J. G., Shevliakova, E., Stouffer, R. J., Krasting, J. P., Malyshev, S. L., Milly, P. C. D., Sentman, L. T., Adcroft, A. J., Cooke, W., Dunne, K. A., Griffies, S. M., Hallberg, R. W., Harrison, M. J., Levy, H., Wittenberg, A. T., Phillips, P. J., & Zadeh, N., 2013. GFDL’s ESM2 global coupled Climate–Carbon earth system models. Part II: Carbon system formulation, baseline simulation characteristics, *Journal of Climate*, 26(7), 2247–2267.
- Elahi, R., O’Connor, M. I., Byrnes, J. E. K., Dunic, J., Eriksson, B. K., Hensel, M. J. S., & Kearns, P. J., 2015. Recent Trends in Local-Scale Marine Biodiversity Reflect Community Structure and Human Impacts, *Current biology: CB*, 25(14), 1938–1943.
- Encyclopedia Britannica, 1998. "photic zone", <https://www.britannica.com/science/photic-zone>.
- Fan, G., Han, Z., Ma, W., Chen, S., Chai, F., Mazloff, M. R., Pan, J., & Zhang, H., 2020. Southern Ocean carbon export efficiency in relation to temperature and primary productivity, *Scientific Reports*, 10(1), 13494.
- Frölicher, T. L. & Laufkötter, C., 2018. Emerging risks from marine heat waves, *Nature Communications*, 9(1), 650.
- Frölicher, T. L., Fischer, E. M., & Gruber, N., 2018. Marine heatwaves under global warming, *Nature*, 560(7718), 360–364.
- Fu, W., Randerson, J. T., & Moore, J. K., 2016. Climate change impacts on net primary production (NPP) and export production (EP) regulated by increasing stratification and phytoplankton community structure in the CMIP5 models, *Biogeosciences*, 13(18), 5151–5170.

- Gaines, S. D., White, C., Carr, M. H., & Palumbi, S. R., 2010. Designing marine reserve networks for both conservation and fisheries management, *Proceedings of the National Academy of Sciences*, 107(43), 18286–18293.
- Garcia, H. E. & Gordon, L. I., 1992. Oxygen solubility in seawater: Better fitting equations, *Limnology and Oceanography*, 37(6), 1307–1312.
- Geider, R., Macintyre, H., & Kana, T., 1997. Dynamic model of phytoplankton growth and acclimation: Responses of the balanced growth rate and the chlorophyll a:carbon ratio to light, nutrient-limitation and temperature, *Marine Ecology Progress Series*, 148, 187–200.
- Gregg, W. W. & Rousseaux, C. S., 2014. Decadal trends in global pelagic ocean chlorophyll: A new assessment integrating multiple satellites, in situ data, and models, *Journal of Geophysical Research: Oceans*, 119(9), 5921–5933.
- Groom, S., Sathyendranath, S., Ban, Y., Bernard, S., Brewin, R., Brotas, V., Brockmann, C., Chauhan, P., Choi, J.-k., Chuprin, A., Ciavatta, S., Cipollini, P., Donlon, C., Franz, B., He, X., Hirata, T., Jackson, T., Kampel, M., Krasemann, H., Lavender, S., Pardo-Martinez, S., Mélin, F., Platt, T., Santoleri, R., Skakala, J., Schaeffer, B., Smith, M., Steinmetz, F., Valente, A., & Wang, M., 2019. Satellite Ocean Colour: Current Status and Future Perspective, *Frontiers in Marine Science*, 6.
- Gruber, N., Boyd, P. W., Frölicher, T. L., & Vogt, M., 2021. Biogeochemical extremes and compound events in the ocean, *Nature*, 600(7889), 395–407.
- Guo, X., Gao, Y., Zhang, S., Wu, L., Chang, P., Cai, W., Zscheischler, J., Leung, L. R., Small, J., Danabasoglu, G., Thompson, L., & Gao, H., 2022. Threat by marine heatwaves to adaptive large marine ecosystems in an eddy-resolving model, *Nature Climate Change*, 12(2), 179–186.
- Hayashida, H., Matear, R. J., & Strutton, P. G., 2020a. Background nutrient concentration determines phytoplankton bloom response to marine heatwaves, *Global Change Biology*, 26(9), 4800–4811.
- Hayashida, H., Matear, R. J., Strutton, P. G., & Zhang, X., 2020b. Insights into projected changes in marine heatwaves from a high-resolution ocean circulation model, *Nature Communications*, 11(1), 4352.
- Henson, S., Le Moigne, F., & Giering, S., 2019. Drivers of Carbon Export Efficiency in the Global Ocean, *Global Biogeochemical Cycles*, 33(7), 891–903.
- Henson, S. A., Cael, B. B., Allen, S. R., & Dutkiewicz, S., 2021. Future phytoplankton diversity in a changing climate, *Nature Communications*, 12(1), 5372.
- Henson, S. A., Briggs, N., Carvalho, F., Manno, C., Mignot, A., & Thomalla, S., 2023. A seasonal transition in biological carbon pump efficiency in the northern Scotia Sea, Southern Ocean, *Deep Sea Research Part II: Topical Studies in Oceanography*, 208, 105274.
- Hiddink, J. G., Johnson, A. F., Kingham, R., & Hinz, H., 2011. Could our fisheries be more productive? Indirect negative effects of bottom trawl fisheries on fish condition, *Journal of Applied Ecology*, 48(6), 1441–1449.
- Hobday, A. J., Alexander, L. V., Perkins, S. E., Smale, D. A., Straub, S. C., Oliver, E. C., Benthuyesen, J. A., Burrows, M. T., Donat, M. G., Feng, M., Holbrook, N. J., Moore, P. J., Scannell, H. A., Sen Gupta, A., & Wernberg, T., 2016. A hierarchical approach to defining marine heatwaves, *Progress in Oceanography*, 141, 227–238.
- Holbrook, N. J., Scannell, H. A., Gupta, A. S., Benthuyesen, J. A., Feng, M., Oliver, E. C. J., Alexander, L. V., Burrows, M. T., Donat, M. G., Hobday, A. J., Moore, P. J., Perkins-Kirkpatrick, S. E., Smale, D. A., Thomas, S. C. S., & Thomas, W., 2019. A global assessment of marine heatwaves and their drivers, *Nature Communications*, 10(1), 2624.
- Hughes, T. P., Anderson, K. D., Connolly, S. R., Heron, S. F., Kerry, J. T., Lough, J. M., Baird, A. H., Baum, J. K., Berumen, M. L., Bridge, T. C., Claar, D. C., Eakin, C. M., Gilmour, J. P., Graham, N. A. J., Harrison, H., Hobbs, J.-P. A., Hoey, A. S., Hoogenboom, M., Lowe, R. J., McCulloch, M. T., Pandolfi, J. M., Pratchett, M., Schoepf, V., Torda, G., & Wilson, S. K., 2018. Spatial and temporal patterns of mass bleaching of corals in the Anthropocene, *Science (New York, N. Y.)*, 359(6371), 80–83.
- Jacox, M. G., Alexander, M. A., Amaya, D., Becker, E., Bograd, S. J., Brodie, S., Hazen, E. L., Pozo Buil, M., & Tommasi, D., 2022. Global seasonal forecasts of marine heatwaves, *Nature*, 604(7906), 486–490.
- Koehn, E., Gruber, N., Münnich, M., Desmet, F., & Vogt, M., 2022. On the vertical structure and propagation of marine heatwaves in the Eastern Pacific, in *Ocean Sciences Meeting 2022*.

- Lacour, L., Llorc, J., Briggs, N., Strutton, P. G., & Boyd, P. W., 2023. Seasonality of downward carbon export in the Pacific Southern Ocean revealed by multi-year robotic observations, *Nature Communications*, 14(1), 1278.
- Le Grix, N., Zscheischler, J., Laufkötter, C., Rousseaux, C. S., & Frölicher, T. L., 2021. Compound high-temperature and low-chlorophyll extremes in the ocean over the satellite period, *Biogeosciences*, 18(6), 2119–2137.
- Le Grix, N., Zscheischler, J., Rodgers, K. B., Yamaguchi, R., & Frölicher, T. L., 2022. Hotspots and drivers of compound marine heatwaves and low net primary production extremes, *Biogeosciences*, 19(24), 5807–5835.
- Le Traon, P.-Y., Antoine, D., Bentamy, A., Bonekamp, H., Breivik, L., Chapron, B., Corlett, G., Dibarboure, G., DiGiacomo, P., Donlon, C., Faugère, Y., Font, J., Girard-Ardhuin, F., Gohin, F., Johannessen, J., Kamachi, M., Lagerloef, G., Lambin, J., Larnicol, G., Le Borgne, P., Leuliette, E., Lindstrom, E., Martin, M., Maturi, E., Miller, L., Mingsen, L., Morrow, R., Reul, N., Rio, M., Roquet, H., Santoleri, R., & Wilkin, J., 2015. Use of satellite observations for operational oceanography: Recent achievements and future prospects, *Journal of Operational Oceanography*, 8(sup1), s12–s27.
- Lee, Z., Weidemann, A., Kindle, J., Arnone, R., Carder, K. L., & Davis, C., 2007. Euphotic zone depth: Its derivation and implication to ocean-color remote sensing, *Journal of Geophysical Research: Oceans*, 112(C3).
- Leising, A., Schroeder, I., Bograd, S., Abell, J., Durazo, R., Gaxiola-Castro, G., CICESE, Bjorkstedt, E., Field, J., Sakuma, K., Robertson, R., Goericke, R., Peterson, W., Brodeur, R., Barceló, C., Auth, T., Daly, E., Suryan, R., Gladics, A., & Warzybok, P., 2015. State of the California Current 2014–15: Impacts of the warm-water “Blob”, *CalCOFI Report*, 56, 31–68.
- Lévy, M., Jahn, O., Dutkiewicz, S., Follows, M. J., & d’Ovidio, F., 2015. The dynamical landscape of marine phytoplankton diversity, *Journal of the Royal Society Interface*, 12(111), 20150481.
- Long, J. S., Fassbender, A. J., & Estapa, M. L., 2021a. Depth-resolved net primary production in the northeast Pacific ocean: A comparison of satellite, profiling float estimates in the context of two marine heatwaves, *Geophysical Research Letters*, 48(19), e2021GL093462.
- Long, M. C., Moore, J. K., Lindsay, K., Levy, M., Doney, S. C., Luo, J. Y., Krumhardt, K. M., Letscher, R. T., Grover, M., & Sylvester, Z. T., 2021b. Simulations with the marine biogeochemistry library (MARBL), *Journal of Advances in Modeling Earth Systems*, 13(12), e2021MS002647.
- Madsen, M. S., Yang, S., Aalgeirsdóttir, G., Svendsen, S. H., Rodehacke, C. B., & Ringgaard, I. M., 2022. The role of an interactive Greenland ice sheet in the coupled climate-ice sheet model EC-Earth-PISM, *Climate Dynamics*, 59(3), 1189–1211.
- Marshak, A. R. & Link, J. S., 2021. Primary production ultimately limits fisheries economic performance, *Scientific Reports*, 11(1), 12154.
- McMahon, C. R., Roquet, F., Baudel, S., Belbeoch, M., Bestley, S., Blight, C., Boehme, L., Carse, F., Costa, D. P., Fedak, M. A., Guinet, C., Harcourt, R., Heslop, E., Hindell, M. A., Hoenner, X., Holland, K., Holland, M., Jaime, F. R. A., Jeanniard du Dot, T., Jonsen, I., Keates, T. R., Kovacs, K. M., Labrousse, S., Lovell, P., Lydersen, C., March, D., Mazloff, M., McKinzie, M. K., Muelbert, M. M. C., O’Brien, K., Phillips, L., Portela, E., Pye, J., Rintoul, S., Sato, K., Sequeira, A. M. M., Simmons, S. E., Tsontos, V. M., Turpin, V., van Wijk, E., Vo, D., Wege, M., Whoriskey, F. G., Wilson, K., & Woodward, B., 2021. Animal Borne Ocean Sensors – AniBOS – An Essential Component of the Global Ocean Observing System, *Frontiers in Marine Science*, 8.
- Melzner, F., Gutowska, M. A., Langenbuch, M., Dupont, S., Lucassen, M., Thorndyke, M. C., Bleich, M., & Pörtner, H.-O., 2009. Physiological basis for high CO₂ tolerance in marine ectothermic animals: Pre-adaptation through lifestyle and ontogeny?, *Biogeosciences*, 6(10), 2313–2331.
- Moore, J. K., Lindsay, K., Doney, S. C., Long, M. C., & Misumi, K., 2013. Marine Ecosystem Dynamics and Biogeochemical Cycling in the Community Earth System Model [CESM1(BGC)]: Comparison of the 1990s with the 2000s under the RCP4.5 and RCP8.5 Scenarios, *Journal of Climate*, 26(23), 9291–9312.
- Mousing, E. A., Ellegaard, M., & Richardson, K., 2014. Global patterns in phytoplankton community size structure—evidence for a direct temperature effect, *Marine Ecology Progress Series*, 497, 25–38.
- Munday, P. L., Dixson, D. L., Donelson, J. M., Jones, G. P., Pratchett, M. S., Devitsina, G. V., & Døving, K. B., 2009. Ocean acidification impairs olfactory discrimination and homing ability of a marine fish, *Proceedings of the National Academy of Sciences*, 106(6), 1848–1852.

- Oliver, E. C. J., Donat, M. G., Burrows, M. T., Moore, P. J., Smale, D. A., Alexander, L. V., Benthuisen, J. A., Feng, M., Sen Gupta, A., Hobday, A. J., Holbrook, N. J., Perkins-Kirkpatrick, S. E., Scannell, H. A., Straub, S. C., & Wernberg, T., 2018. Longer and more frequent marine heatwaves over the past century, *Nature Communications*, 9(1), 1324.
- Pauly, D., 1980. On the interrelationships between natural mortality, growth parameters, and mean environmental temperature in 175 fish stocks, *ICES Journal of Marine Science*, 39(2), 175–192.
- Pauly, D. & Christensen, V., 1995. Primary production required to sustain global fisheries, *Nature*, 374(6519), 255–257.
- Pauly D. & Palomares M.L.D., 2020. Seaaroundus, <https://www.seaaroundus.org/>.
- Peña, M. A., Nemcek, N., & Robert, M., 2019. Phytoplankton responses to the 2014–2016 warming anomaly in the northeast subarctic Pacific Ocean, *Limnology and Oceanography*, 64(2), 515–525.
- Piatt, J. F., Parrish, J. K., Renner, H. M., Schoen, S. K., Jones, T. T., Arimitsu, M. L., Kuletz, K. J., Bodenstein, B., García-Reyes, M., Duerr, R. S., Corcoran, R. M., Kaler, R. S. A., McChesney, G. J., Golightly, R. T., Coletti, H. A., Suryan, R. M., Burgess, H. K., Lindsey, J., Lindquist, K., Warzybok, P. M., Jahncke, J., Roletto, J., & Sydeman, W. J., 2020. Extreme mortality and reproductive failure of common murrelets resulting from the northeast Pacific marine heatwave of 2014–2016, *PLOS ONE*, 15(1), e0226087.
- Pikitch, E., Boersma, P., Boyd, I., Conover, D., Cury, P., Essington, T., & Heppell, S., 2012. Little Fish, Big Impact: Managing a Crucial Link in Ocean Food Webs, *Lenfest Ocean Program*.
- Pilo, G. S., Holbrook, N. J., Kiss, A. E., & Hogg, A. M., 2019. Sensitivity of marine heatwave metrics to ocean model resolution, *Geophysical Research Letters*, 46(24), 14604–14612.
- Racault, M.-F., Sathyendranath, S., Brewin, R. J. W., Raitsos, D. E., Jackson, T., & Platt, T., 2017. Impact of el niño variability on oceanic phytoplankton, *Frontiers in Marine Science*, 4, 133.
- Raven, J. A., 1998. The Twelfth Tansley Lecture, Small is Beautiful: The Picophytoplankton, *Functional Ecology*, 12(4), 503–513.
- Roemmich, D., Johnson, G. C., Riser, S., Davis, R., Gilson, J., Owens, W. B., Garzoli, S. L., Schmid, C., & Ignaszewski, M., 2009. The Argo Program: Observing the Global Ocean with Profiling Floats, *Oceanography*, 22(2), 34–43.
- Saba, V. S., Friedrichs, M. A. M., Carr, M.-E., Antoine, D., Armstrong, R. A., Asanuma, I., Aumont, O., Bates, N. R., Behrenfeld, M. J., Bennington, V., Bopp, L., Bruggeman, J., Buitenhuis, E. T., Church, M. J., Ciotti, A. M., Doney, S. C., Dowell, M., Dunne, J., Dutkiewicz, S., Gregg, W., Hoepffner, N., Hyde, K. J. W., Ishizaka, J., Kameda, T., Karl, D. M., Lima, I., Lomas, M. W., Marra, J., McKinley, G. A., Mélin, F., Moore, J. K., Morel, A., O'Reilly, J., Salihoglu, B., Scardi, M., Smyth, T. J., Tang, S., Tjiputra, J., Uitz, J., Vichi, M., Waters, K., Westberry, T. K., & Yool, A., 2010. Challenges of modeling depth-integrated marine primary productivity over multiple decades: A case study at BATS and HOT: MODELING MARINE PRIMARY PRODUCTIVITY, *Global Biogeochemical Cycles*, 24(3).
- Saha, M., Barboza, F. R., Somerfield, P. J., Al-Janabi, B., Beck, M., Brakel, J., Ito, M., Pansch, C., Nascimento-Schulze, J. C., Jakobsson Thor, S., Weinberger, F., & Sawall, Y., 2020. Response of foundation macrophytes to near-natural simulated marine heatwaves, *Global Change Biology*, 26(2), 417–430.
- Sala, E., Mayorga, J., Bradley, D., Cabral, R. B., Atwood, T. B., Auber, A., Cheung, W., Costello, C., Ferretti, F., Friedlander, A. M., Gaines, S. D., Garilao, C., Goodell, W., Halpern, B. S., Hinson, A., Kaschner, K., Kesner-Reyes, K., Leprieur, F., McGowan, J., Morgan, L. E., Mouillot, D., Palacios-Abrantes, J., Possingham, H. P., Rechberger, K. D., Worm, B., & Lubchenco, J., 2021. Protecting the global ocean for biodiversity, food and climate, *Nature*, 592(7854), 397–402.
- Samuels, T., Rynearson, T. A., & Collins, S., 2021. Surviving Heatwaves: Thermal Experience Predicts Life and Death in a Southern Ocean Diatom, *Frontiers in Marine Science*, 8.
- Santana-Falcón, Y. & Séférian, R., 2022. Climate change impacts the vertical structure of marine ecosystem thermal ranges, *Nature Climate Change*, 12(10), 935–942.
- Santora, J. A., Mantua, N. J., Schroeder, I. D., Field, J. C., Hazen, E. L., Bograd, S. J., Sydeman, W. J., Wells, B. K., Calambokidis, J., Saez, L., Lawson, D., & Forney, K. A., 2020. Habitat compression and ecosystem shifts as potential links between marine heatwave and record whale entanglements, *Nature Communications*, 11(1), 536.

- Sarmiento, J. L. & Gruber, N., 2006. *Ocean Biogeochemical Dynamics*, Princeton University Press.
- Sarmiento, J. L., Hughes, T. M. C., Stouffer, R. J., & Manabe, S., 1998. Simulated response of the ocean carbon cycle to anthropogenic climate warming, *Nature*, 393(6682), 245–249.
- Scannell, H. A., Johnson, G. C., Thompson, L., Lyman, J. M., & Riser, S. C., 2020. Subsurface Evolution and Persistence of Marine Heatwaves in the Northeast Pacific, *Geophysical Research Letters*, 47(23), e2020GL090548.
- Schmidt, K., Birchill, A. J., Atkinson, A., Brewin, R. J. W., Clark, J. R., Hickman, A. E., Johns, D. G., Lohan, M. C., Milne, A., Pardo, S., Polimene, L., Smyth, T. J., Tarran, G. A., Widdicombe, C. E., Woodward, E. M. S., & Ussher, S. J., 2020. Increasing picocyanobacteria success in shelf waters contributes to long-term food web degradation, *Global Change Biology*, 26(10), 5574–5587.
- Sen Gupta, A., Thomsen, M., Benthuisen, J. A., Hobday, A. J., Oliver, E., Alexander, L. V., Burrows, M. T., Donat, M. G., Feng, M., Holbrook, N. J., Perkins-Kirkpatrick, S., Moore, P. J., Rodrigues, R. R., Scannell, H. A., Taschetto, A. S., Ummenhofer, C. C., Wernberg, T., & Smale, D. A., 2020. Drivers and impacts of the most extreme marine heatwave events, *Scientific Reports*, 10(1), 19359.
- Seneviratne, S. I., Nicholls, N., Easterling, D., Goodess, C. M., Kanae, S., Kossin, J., Luo, Y., Marengo, J., McInnes, K., Rahimi, M., Reichstein, M., Sorteberg, A., Vera, C., & Zhang, X., 2012. Changes in climate extremes and their impacts on the natural physical environment, in *Managing the Risks of Extreme Events and Disasters to Advance Climate Change Adaptation. A Special Report of Working Groups I and II of the Intergovernmental Panel on Climate Change (IPCC)*, pp. 109–230, eds Field, C. B., Barros, V., Stocker, T. F., Qin, D., Dokken, D. J., Ebi, K. L., Mastrandrea, M. D., Mach, K. J., Plattner, G.-K., Allen, S. K., Tignor, M., & Midgley, P. M., Cambridge University Press, Cambridge, United Kingdom and New York, NY, USA.
- Sigman, D & Hain, M, 2012. The Biological Productivity of the Ocean. *Nature Education Knowledge* 3(10):21, <https://www.nature.com/scitable/knowledge/library/the-biological-productivity-of-the-ocean-70631104/>.
- Silsbe, G. M., Behrenfeld, M. J., Halsey, K. H., Milligan, A. J., & Westberry, T. K., 2016. The CAFE model: A net production model for global ocean phytoplankton, *Global Biogeochemical Cycles*, 30(12), 1756–1777.
- Smith, K. E., Burrows, M. T., Hobday, A. J., Sen Gupta, A., Moore, P. J., Thomsen, M., Wernberg, T., & Smale, D. A., 2021. Socioeconomic impacts of marine heatwaves: Global issues and opportunities, *Science*, 374(6566), eabj3593.
- Smith, R. C., 1981. Remote Sensing and Depth Distribution of Ocean Chlorophyll, *Marine Ecology Progress Series*, 5(3), 359–361.
- Su, J., Schallenberg, C., Rohr, T., Strutton, P. G., & Phillips, H. E., 2022. New Estimates of Southern Ocean Annual Net Community Production Revealed by BGC-Argo Floats, *Geophysical Research Letters*, 49(15), e2021GL097372.
- Supp, S. R. & Ernest, S. K. M., 2014. Species-level and community-level responses to disturbance: A cross-community analysis, *Ecology*, 95(7), 1717–1723.
- Tebaldi, C. & Knutti, R., 2007. The use of the multi-model ensemble in probabilistic climate projections, *Philosophical Transactions of the Royal Society A: Mathematical, Physical and Engineering Sciences*, 365(1857), 2053–2075.
- Urban, M. C., Tewksbury, J. J., & Sheldon, K. S., 2012. On a collision course: Competition and dispersal differences create no-analogue communities and cause extinctions during climate change, *Proceedings of the Royal Society B: Biological Sciences*, 279(1735), 2072–2080.
- van der Wiel, K., Selten, F. M., Bintanja, R., Blackport, R., & Screen, J. A., 2020. Ensemble climate-impact modelling: Extreme impacts from moderate meteorological conditions, *Environmental Research Letters*, 15(3), 034050.
- Vogt, L., Burger, F. A., Griffies, S. M., & Frölicher, T. L., 2022. Local drivers of marine heatwaves: A global analysis with an earth system model, *Frontiers in Climate*, 4.
- Watson, R. A., Cheung, W. W. L., Anticamara, J. A., Sumaila, R. U., Zeller, D., & Pauly, D., 2013. Global marine yield halved as fishing intensity redoubles, *Fish and Fisheries*, 14(4), 493–503.
- Watters, G. M., Hinke, J. T., & Reiss, C. S., 2020. Long-term observations from Antarctica demonstrate that mismatched scales of fisheries management and predator-prey interaction lead to erroneous conclusions about precaution, *Scientific Reports*, 10(1), 2314.

- Westberry, T., Behrenfeld, M. J., Siegel, D. A., & Boss, E., 2008. Carbon-based primary productivity modeling with vertically resolved photoacclimation, *Global Biogeochemical Cycles*, 22(2).
- Worm, B., Barbier, E. B., Beaumont, N., Duffy, J. E., Folke, C., Halpern, B. S., Jackson, J. B. C., Lotze, H. K., Micheli, F., Palumbi, S. R., Sala, E., Selkoe, K. A., Stachowicz, J. J., & Watson, R., 2006. Impacts of Biodiversity Loss on Ocean Ecosystem Services, *Science*, 314(5800), 787–790.
- Wu, R. S. S., 2002. Hypoxia: From molecular responses to ecosystem responses, *Marine Pollution Bulletin*, 45(1-12), 35–45.
- Wu, S.-Y. & Hou, S., 2017. Impact of icebergs on net primary productivity in the Southern Ocean, *The Cryosphere*, 11(2), 707–722.
- Wyatt, A., Resplandy, L., & Marchetti, A., 2022. Ecosystem impacts of marine heat waves in the Northeast Pacific, *EGUsphere Discussions*, 2022, 1–24.
- Zscheischler, J. & Lehner, F., 2022. Attributing compound events to anthropogenic climate change, *Bulletin of the American Meteorological Society*, 103(3), E936 – E953.
- Zscheischler, J., Martius, O., Westra, S., Bevacqua, E., Raymond, C., Horton, R. M., van den Hurk, B., AghaKouchak, A., Jézéquel, A., Mahecha, M. D., Maraun, D., Ramos, A. M., Ridder, N. N., Thiery, W., & Vignotto, E., 2020. A typology of compound weather and climate events, *Nature Reviews Earth & Environment*, 1(7), 333–347.

Appendix A

Simulating compound weather extremes responsible for critical crop failure with stochastic weather generators

Peter Pfeiderer, Aglaé Jézéquel, Juliette Legrand, **Natacha Legrix**, Iason Markantonis, Edoardo Vignotto, and Pascal Yiou

Published in *Earth System Dynamics*, Volume 12, 103–120, 2021. This study started as a group project during the training school on Statistical Modelling of Compound Events, which took place at the Lake Como School of Advanced Studies in 2019.



Simulating compound weather extremes responsible for critical crop failure with stochastic weather generators

Peter Pfliederer, Aglaé Jézéquel, Juliette Legrand, Natacha Legrix, Iason Markantonis, Edoardo Vignotto, Pascal Yiou

► To cite this version:

Peter Pfliederer, Aglaé Jézéquel, Juliette Legrand, Natacha Legrix, Iason Markantonis, et al.. Simulating compound weather extremes responsible for critical crop failure with stochastic weather generators. *Earth System Dynamics*, 2021, 12, pp.103-120. 10.5194/esd-12-103-2021 . hal-02902943

HAL Id: hal-02902943

<https://hal.science/hal-02902943>

Submitted on 19 May 2021

HAL is a multi-disciplinary open access archive for the deposit and dissemination of scientific research documents, whether they are published or not. The documents may come from teaching and research institutions in France or abroad, or from public or private research centers.

L'archive ouverte pluridisciplinaire **HAL**, est destinée au dépôt et à la diffusion de documents scientifiques de niveau recherche, publiés ou non, émanant des établissements d'enseignement et de recherche français ou étrangers, des laboratoires publics ou privés.



Simulating compound weather extremes responsible for critical crop failure with stochastic weather generators

Peter Pfleiderer^{1,2,3}, Aglaé Jézéquel^{4,5}, Juliette Legrand⁶, Natacha Legrix^{7,8}, Jason Markantonis¹⁰, Edoardo Vignotto⁹, and Pascal Yiou⁶

¹Climate Analytics, Berlin, Germany

²Department of Geography, Humboldt University, Berlin, Germany

³Earth System Analysis, Potsdam Institute for Climate Impact Research, Potsdam, Germany

⁴LMD/IPSL, ENS, PSL Université, École Polytechnique, Institut Polytechnique de Paris, Sorbonne Université, CNRS, 75005 Paris, France

⁵École des Ponts Paristech, 77420 Champs-sur-Marne, France

⁶Laboratoire des Sciences du Climat et de l'Environnement, UMR8212 CEA-CNRS-UVSQ, IPSL & U Paris-Saclay, 91191 Gif-sur-Yvette, France

⁷Climate and Environmental Physics, Physics Institute, University of Bern, Bern, 3012, Switzerland

⁸Oeschger Centre for Climate Change Research, University of Bern, Bern, 3012, Switzerland

⁹Research Center for Statistics, University of Geneva, Geneva, 1211, Switzerland

¹⁰INRASTES Department, National Centre of Scientific Research “Demokritos”, Aghia Paraskevi, Greece

Correspondence: Peter Pfleiderer (peter.pfleiderer@climateanalytics.org)

Received: 28 May 2020 – Discussion started: 10 June 2020

Revised: 13 November 2020 – Accepted: 16 December 2020 – Published: 2 February 2021

Abstract. In 2016, northern France experienced an unprecedented wheat crop loss. The cause of this event is not yet fully understood, and none of the most used crop forecast models were able to predict the event (Ben-Ari et al., 2018). However, this extreme event was likely due to a sequence of particular meteorological conditions, i.e. too few cold days in late autumn–winter and abnormally high precipitation during the spring season. Here we focus on a compound meteorological hazard (warm winter and wet spring) that could lead to a crop loss.

This work is motivated by the question of whether the 2016 meteorological conditions were the most extreme possible conditions under current climate, and what the worst-case meteorological scenario would be with respect to warm winters followed by wet springs. To answer these questions, instead of relying on computationally intensive climate model simulations, we use an analogue-based importance sampling algorithm that was recently introduced into this field of research (Yiou and Jézéquel, 2020). This algorithm is a modification of a stochastic weather generator (SWG) that gives more weight to trajectories with more extreme meteorological conditions (here temperature and precipitation). This approach is inspired by importance sampling of complex systems (Ragone et al., 2017). This data-driven technique constructs artificial weather events by combining daily observations in a dynamically realistic manner and in a relatively fast way.

This paper explains how an SWG for extreme winter temperature and spring precipitation can be constructed in order to generate large samples of such extremes. We show that with some adjustments both types of weather events can be adequately simulated with SWGs, highlighting the wide applicability of the method.

We find that the number of cold days in late autumn 2015 was close to the plausible minimum. However, our simulations of extreme spring precipitation show that considerably wetter springs than what was observed in 2016 are possible. Although the relation of crop loss in 2016 to climate variability is not yet fully understood, these results indicate that similar events with higher impacts could be possible in present-day climate conditions.

1 Introduction

France is one of the highest wheat producers and exporters in the world thanks to yields that are roughly twice as high as the world average (FAO, 2013). Given the prominent role of wheat production in France, crop failures can impact the national economy. When an unprecedented disastrous harvest was registered in 2016, especially in northern parts of France, with a loss in production of about 30 % with respect to 2015 (Ben-Ari et al., 2018), France registered heavy losses in farmer income and a loss of approximately USD 2.3 billion in the yearly trade balance (OEC, 2020).

Interestingly, the extreme crop failure of 2016 was not predicted by any forecasting model, which all strongly overestimated yields even just before the harvesting period (Ben-Ari et al., 2018). Thus, classical crop yield forecasting models, based on a combination of expert knowledge and data-driven methods (Müller et al., 2019; MacDonald and Hall, 1980), could not anticipate this unprecedented event because it was outside their training range. To overcome these limitations Ben-Ari et al. (2018) developed a logistic model that links the meteorological conditions in the year preceding the harvest with the probability of a crop failure.

In their study, Ben-Ari et al. (2018) attribute the crop loss to a combination of two meteorological events: an insufficient number of cold days in the December preceding the harvest and an abnormally high precipitation during spring. It was argued that this low wheat yield was a preconditioned event wherein a mild autumn and winter favoured the build-up of biomass and parasites, which in combination with excess precipitation in late spring resulted in favourable conditions for root asphyxiation and fungus spread (ARVALIS, 2016). There could also be a direct influence of the meteorological conditions on plant development. For both potential mechanisms it is crucial to study the meteorological conditions leading to the crop loss as a compound event, as only the combination of a warm winter and wet spring had this unprecedented impact on wheat yields (Zscheischler et al., 2020).

The research question we want to address is what a worst case meteorological scenario would be for this kind of crop loss event under the current climate with enhanced winter temperatures and spring precipitation? This question arises from the fact that we only experienced one possible realization of our climate. Even under unchanged climate conditions, unprecedented extreme events would occur as time goes on. Thus, to be able to put in place effective preventive measures, it is important to understand how severe an extreme event could be.

To estimate how extreme a crop loss similar to the 2016 event could be, we need tools that all come with their assumptions and caveats. A standard approach would be to use large ensemble simulations based on circulation models of

current climate conditions (Massey et al., 2015a). If the ensemble was large enough and physical mechanisms are adequately reproduced in the circulation model, one would find the most extreme possible version of the 2016 crop loss event and could even estimate its occurrence probability. This approach has two main drawbacks: the often huge computational cost associated with a large number of simulations and the possibly flawed representation of physical processes in climate models that could introduce a systematic uncertainty that cannot be overcome easily (Shepherd, 2019).

A second approach relies on the analysis of historical data. There are many statistical methods that could be used in this context. Specifically, copula-based techniques (Jaworski et al., 2010) can be used to study the dependence between two or more climate hazards, while models based on extreme value theory (Cooley, 2009) are suited for analysing particularly rare events. These methods have the merit of being computationally cheap and of relying only on observed data, but dealing with non-stationarity can be challenging with these methods.

As another data-driven alternative, the so-called storyline approach has emerged recently. The idea is to construct a physically plausible extreme event that one can relate to without necessarily focusing on the statistical likelihood of such an event (Hazeleger et al., 2015; Shepherd et al., 2018; Shepherd, 2019). Rather than asking what the most likely representation of the climate would be, one could ask how some extreme realizations of climate could be like. It has been argued that for adaptation planning the latter question could be more relevant (Hazeleger et al., 2015). This kind of “stress-testing” based on the use of scenarios has been standard practice in catastrophe analysis and emergency preparedness, even outside of the context of climate change (see, for example, de Bruijn et al., 2016).

In this paper, we construct a climate storyline of a warm winter followed by a wet spring that is likely to lead to extremely low wheat crop yield in France. This storyline is based on an ensemble of simulations of temperature and precipitation with a stochastic weather generator that we nudge towards extreme behaviour.

Here, we adapt analogue-based stochastic weather generators (SWGs) presented by Yiou (2014) and Yiou and Jézéquel (2020), which simulate spatially coherent time series of a climate variable, drawn from meteorological observations. Those SWGs were mainly tested on European surface temperatures. A version was developed to simulate extreme summer heatwaves (Yiou and Jézéquel, 2020). This paper optimizes the parameters of the SWG of Yiou and Jézéquel (2020) to simulate extreme warm winters (especially December) and extreme wet springs.

The goal is to construct a large sample of extreme climate conditions and assess the atmospheric circulation properties leading to those conditions of high temperatures and precipi-

tation. The rationale of ensemble simulations is to determine uncertainties in the range of values that can be obtained.

Section 2 details the data that is used in this paper and explains the methodology of importance sampling with analogue simulators. Section 3 describes the experimental results of the simulations of temperature and precipitation. Section 4 provides a discussion of the results.

2 Methods

2.1 Data

We use temperature and precipitation observations from the E-OBS database (Haylock et al., 2008). The data are available on a $0.1 \times 0.1^\circ$ grid from 1950 to 2018. As an estimate of temperature and precipitation in northern France we average these two fields over a rectangle spanning $45.5\text{--}51.5^\circ$ N and 1.5° W– 8.0° E (see Fig. 1). This region also includes parts of the UK, Germany, Belgium, and Switzerland and therefore does not exactly match the studied area of (Ben-Ari et al., 2018). The seasonal meteorological conditions we study here are related to large-scale events, and averaging over a larger rectangle therefore seems appropriate.

We use the reanalysis data of the National Centers for Environmental Prediction (NCEP) (Kistler et al., 2001) for the analysis of atmospheric circulation. We consider the geopotential height at 500 hPa ($Z500$) and mean sea level pressure (SLP) over the North Atlantic region for computation of circulation analogues and a posteriori diagnostics. We used the daily averages between 1 January 1950 and 31 December 2018. The horizontal resolution is 2.5° in longitude and latitude. The rationale of using this reanalysis is that it covers 70 years and is regularly updated.

One of the caveats of this reanalysis dataset is the lack of homogeneity of assimilated data, especially before the satellite era. This can lead to breaks in pressure-related variables, although such breaks are mostly detected in the Southern Hemisphere and the Arctic region (Sturaro, 2003) and marginally impact the eastern North Atlantic region.

$Z500$ patterns are well correlated with western European temperature and precipitation because those quantities and their extremes are related to the atmospheric circulation (Yiou and Nogaj, 2004; Cassou et al., 2005). Since $Z500$ values depend on temperature, we detrend the $Z500$ daily field by removing a seasonal average linear trend from each grid point. This preprocessing is performed to ensure that the analogue selection is not influenced by atmospheric trends.

2.2 Stochastic weather generators and importance sampling

The idea behind importance sampling is to simulate trajectories of a physical system that optimize a criterion in a computationally efficient way. Ragone et al. (2017) used such an

algorithm to simulate extreme heatwaves with an intermediate complexity climate model.

The procedure of importance sampling algorithms, say to simulate extreme heatwaves with a climate model, is to start from an ensemble of S initial conditions and compute trajectories of the climate model from those initial conditions.

An optimization “observable” is defined for the system. In this case, it can be the spatially averaged temperature or precipitation over France. The trajectories for which the observable (e.g. daily average temperature) is lowest during the first steps of simulation are deleted and replaced by small perturbations of remaining ones. In this way, each time increment of the simulations keeps the trajectories with the highest values of the observable. At the end of a simulation, one obtains S trajectories for which the observable (here average temperature over France) has been maximized. Since those trajectories are solutions of the equations of a climate model, they are necessarily physically consistent (given that the perturbations are small).

Ragone et al. (2017) argue that the probability of the simulated trajectories is controlled by a parameter that weighs the importance to the highest observable values: if one trajectory is deleted at each time step, the simulation of an ensemble of M -long trajectories has a probability of $(1 - 1/S)^M$. Hence, one obtains a set of S trajectories with very low probability after M time increments at the cost of the computation of S trajectories.

For comparison purposes, if one wants to obtain S trajectories that have a low probability (p) observable, then the number of necessary “unconstrained” simulations is of the order of M/p , so that most of those simulations are left out. Systems like weather@home (Massey et al., 2015b) that generate tens of thousands of climate simulations are just sufficient to obtain $S = 100$ centennial heatwaves, and the number of “wasted” simulations is very high. Therefore, importance sampling algorithms are very efficient ways to circumvent this difficulty. The major caveat of this approach is that one needs to know the equations that drive the system and be able to simulate them. We use an alternative method that does not require such knowledge of the system.

We use two SWG-based circulation analogues (Yiou and Jézéquel, 2020) to simulate events of either warm temperature in December or high precipitation in spring. These SWGs resample daily weather observations in a plausible manner to simulate new weather events (Yiou, 2014).

Circulation analogues are computed on SLP (or detrended $Z500$) from NCEP between 1950 and 2018. For each day in 1950–2018, $K = 20$ best analogues are determined by minimizing a spatial Euclidean distance between SLP (or $Z500$) maps.

As explained by Yiou and Jézéquel (2020), the SWG randomly samples analogues by weighting the analogue days with a criterion that favours high temperatures or high precipitation. Hence, the importance sampling is summarized by the procedure of giving more weight to analogues that

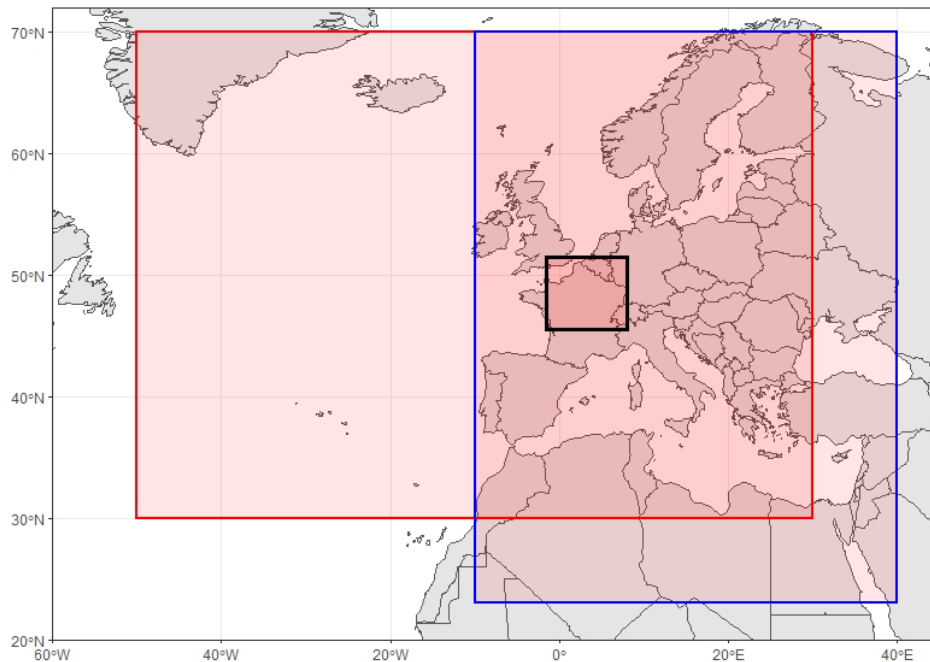


Figure 1. Regions used to identify circulation analogues for December temperatures (blue) and spring precipitation (red). The black rectangle indicates the region over which temperatures and precipitation are averaged in northern France.

yield temperature (or precipitation) properties. There are two types of importance sampling for the analogues, which are illustrated in Fig. 2.

The two main types of analogue SWGs described by Yiou (2014) and Yiou and Jézéquel (2020) are as follows:

1. A “static” weather generator replaces each day with one of its K circulation analogues or itself. With this type of SWG, simulated trajectories are perturbations (by analogues) of an observed trajectory.
2. A so-called “dynamic” weather generator has a similar random selection rule, but the “next” day to be simulated follows the selected analogue, rather than the observed actual calendar day. A probability weight ω_{cal} that is inversely proportional to the distance to the calendar day is introduced:

$$\omega_{\text{cal}} = A_{\text{cal}} e^{-\alpha_{\text{cal}} R_{\text{cal}}(k)}, \quad (1)$$

where A_{cal} is a normalizing constant, $\alpha_{\text{cal}} \geq 0$ is a weight, and $R_{\text{cal}}(k)$ is the number of days that separate the date of k th analogue from the calendar day of time t . This rule is important to prevent time from going “backward”. This type of SWG generates new trajectories by resampling already observed ones. They are not just perturbations of observed trajectories.

Those random selections of analogues are sequentially repeated until a lead time T .

An importance sampling is applied while selecting an analogue at each time step by weighing probabilities with the variable to be optimized (temperature or precipitation). The $K = 20$ best analogues and the day of interest are sorted by daily mean temperature or precipitation. The probability weights are determined by Yiou and Jézéquel (2020). If $R(k)$ is the rank (in terms of temperature or precipitation) of day k in decreasing order and ω_k the probability of day k to be selected, we set

$$\omega_k = A e^{-\alpha R(k)}, \quad (2)$$

where A is a normalizing constant so that the sum of weights over k is 1. The α parameter controls the strength of this importance sampling for temperature or precipitation.

The useful property of this formulation of weights is that the values of ω_k do not depend on time t because the rank values $R(k)$ are integers between 1 and $K + 1$. The weight values do not depend on the unit of the variable either, and thus this procedure is the same for temperature or precipitation. If $\alpha = 0$, this is equivalent to a stochastic weather generator described by Yiou (2014).

Combining the weights of the calendar day and the intensity of the climate variable, the probability of day k to be selected becomes

$$\omega'_k = A e^{-\alpha R(k)} e^{-\alpha_{\text{cal}} R_{\text{cal}}(k)}. \quad (3)$$

The generators thus give more weight to the warmest or wettest days when computing trajectories of December tem-

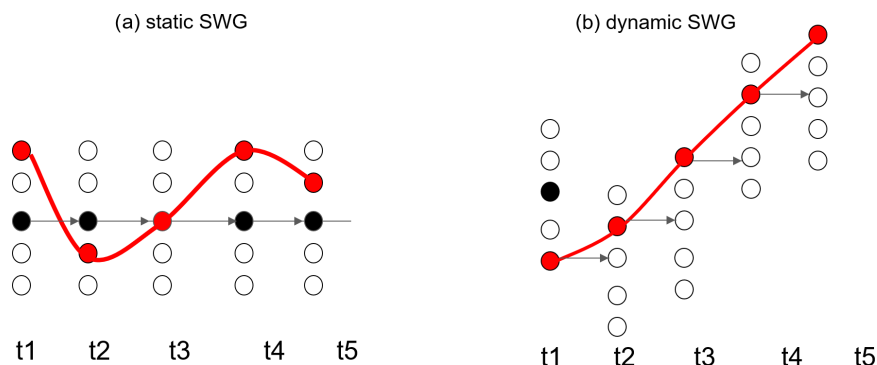


Figure 2. Illustration of the analogue-based importance sampling. **(a)** The static SWG replaces each day in the observed trajectory (black dots) with one of its analogues (red dots). **(b)** The dynamic SWG replaces the first day in the observations (black dot) with one of its analogues, reads the following day of this analogue, and repeats the procedure until creating a new trajectory (red dots).

perature or spring precipitation. We thereby simulate extreme events, e.g. warm Decembers and wet springs (May to July).

2.3 Experimental set-up

The parameters of the SWG depend on the variables and the seasons to be simulated. We determine those parameters experimentally and detail them hereafter. Table 1 lists all parameters used for the simulation of December temperature and spring precipitation. These parameters were set after performing a number of sensitivity tests that are going to be discussed in Sect. 3. Table 2 lists all values tested for α and α_{cal} . Most figures related to these tests can be found in the Appendix.

The procedure we follow is as follows.

- *Start and end day of simulations.* For each year from 1950 to 2018, 1000 simulations are started independently for temperature in December and precipitation in spring. The temperature simulations start on 1 December and end on 31 December. Precipitation simulations start on 1 April and end on 31 July. This results in 68 000 independent simulations of December temperatures and spring precipitation.
- *Identification of circulation analogues.* Weather analogues are identified by evaluating the similarity of weather patterns of an atmospheric variable in a chosen region. For December temperature, analogues are based on detrended geopotential height at 500 hPa (Z500) over a region covering most of Europe (70–23° N, 10° W–40° E) (see Fig. 1). Jézéquel et al. (2018) showed that Z500 is better suited to simulate temperature anomalies than SLP and that rather small domains lead to better reconstitutions. This result is supported by sensitivity tests we performed on the choice of variable for the computation of the circulation analogues used to simulate December temperature. For spring precipitation, we use analogues of SLP over a zone covering

30–70° N and 50° W–30° E, as shown in Fig. 1. This region includes large parts of the North Atlantic where rain-bringing storms usually come from.

- *Number of days before selecting a new analogue.* For the simulation of long-lasting precipitation events the consistency of day-to-day variability is important to ensure a plausible water vapour transport. We therefore adapt the stochastic weather generator (both static and dynamic). Instead of choosing a new analogue every day, we stay on an observed trajectory for a number of days (n_{days}) before choosing a new analogue (see Fig. 3). For the analogue selection we weight the analogues based on the accumulated precipitation of the analogue and the following n_{days} days, giving more weight to analogues that bring more precipitation in the following n_{days} days.
- *Selection of circulation analogues by the generators.* The α -parameter controls the strength of the importance sampling on either temperature or precipitation, while α_{cal} controls the influence of the calendar date when selecting an analogue. For temperature simulations, we use $\alpha = 0.75$ and $\alpha_{\text{cal}} = 6$. Note that we thus strongly condition the calendar day to restrict the SWGs to winter and late autumn days. For precipitation, we set both α and α_{cal} to 0.5.

3 Results

A lack of cold days in December 2015 and an exceptionally wet spring caused the 2016 crop loss in northern France. Although the interplay between these two meteorological events is crucial for the resulting crop loss, the two events (warm December and wet spring) seem to have happened independently from each other: the correlation between temperature in December and precipitation 4 months later is not

Table 1. Parameters used for the static and dynamic SWG to simulate warm Decembers (second column) and wet April–July periods (last column).

Parameter	Choice for warm Decembers	Choice for wet April–July periods
Start day	01/12	01/04
End day	31/12	31/07
Variable for analogues	Z500	SLP
Region for analogues	70–23° N, 10° W–40° E	30–70° N and –50° W–30° E 30–70° N
Weighting of temp. or precipitation (α)	0.75	0.5
Weighting of calendar day (α_{cal})	6	0.5
Number of days before selecting a new analogue (n_{days})	1	5

Table 2. Performed sensitivity tests for the parameters used to simulate warm Decembers (first three rows) and wet April–July periods (last three rows). The second column lists the parameters of which the sensitivity is assessed. The third column indicates at which levels all other parameters are fixed for the test. The fourth column lists all tested values and the last column indicates the figure where the results of the test are shown.

Experiment	Tested parameter	Fixed parameters	Tested values	Figure
December	variable for analogues	$\alpha = 0.5, \alpha_{\text{cal}} = 6, n_{\text{days}} = 1$	Z500, SLP	Fig. A1
December	α_{cal}	$\alpha = 0.5, n_{\text{days}} = 1$	0, 0.2, 0.5, 1, 2, 4, 6, 8, 10	Fig. A2
December	α	$\alpha_{\text{cal}} = 6, n_{\text{days}} = 1$	0, 0.1, 0.2, 0.5, 0.75, 1	Fig. A3
April–July	n_{days}	$\alpha = 0.5, \alpha_{\text{cal}} = 0.5$	1, 2, 3, 4, 5, 7, 9	Fig. A4
April–July	α	$\alpha_{\text{cal}} = 0.5, n_{\text{days}} = 5$	0, 0.1, 0.3, 0.5, 0.7, 0.9, 1	Fig. A5
April–July	α_{cal}	$\alpha = 0.5, n_{\text{days}} = 5$	0, 0.2, 0.5, 1, 2, 5, 10	Fig. A6

significantly different from zero and we cannot reject the hypothesis that both variables are not correlated (p value of the Pearson correlation > 0.6). In addition, from an energy point of view, the characteristic timescale of the atmosphere does not exceed 35 d (Peixoto and Oort, 1992, Sect. 14.6.2). This implies that it is unlikely to find links between climate variables in December and the following May. We therefore consider that it is reasonable to simulate warm Decembers and wet springs independently.

3.1 December temperature simulations

The winter preceding the 2016 crop loss was abnormally warm, with only a few cold days. Here, cold days are defined as days with daily maximal temperatures between 0 and 10 °C. This December was the hottest in the observational record and also the December with the fewest cold days.

Figure 4a shows the observed averages of daily maximal temperatures and the results from static and dynamic SWG simulations. The observed December temperatures fluctuate around 6 °C, with a small warming trend of 0.2 °C per decade over the whole time series (p value = 0.03). Simulations from the static SWG are consistently around 3.5 °C warmer and follow the year-to-year variability of the observations. With an average of 12 °C, the dynamic SWG simulations are significantly warmer than the static SWG simulations, and inter-annual variability is strongly reduced. This is to be expected as the dynamic SWG evolves freely from

the starting day and is therefore less bound to each year's circulation.

In years with higher December temperatures, the number of cold days with maximal temperatures between 0 and 10 °C is reduced (see Fig. 4b). Over the period 1950–2018 no trend in the number of cold days is observed and the number of cold days fluctuates around 25 d. As the SWG simulates warmer Decembers the number of cold days is on average 8 d lower in the static SWG and 16 d lower in the dynamic SWG. Nearly half of the simulations of the dynamic SWG thus have fewer cold days than what was observed in December 2015.

December 2015 was unprecedented in terms of missing cold days, and we simulate a number of warm Decembers with even fewer cold days. To estimate the probability of such an extreme December, we fit a beta-binomial distribution (Jézéquel et al., 2018) to the observations and find that 2015 was a 1-in-4000-year event and that 25 % of our dynamic SWG simulations are 1-in-1000-year events or even rarer (see Fig. A3).

As shown in Fig. 5, December 2015 was characterized by a persistent anticyclonic circulation with its centre over the Alps. The circulation in the coldest December (1969) was the opposite of 2015, with negative Z500 anomalies over Europe and positive anomalies over the Atlantic. In 2008, the December with most cold days in the observations, the data resemble 1969 but have less pronounced anomalies.

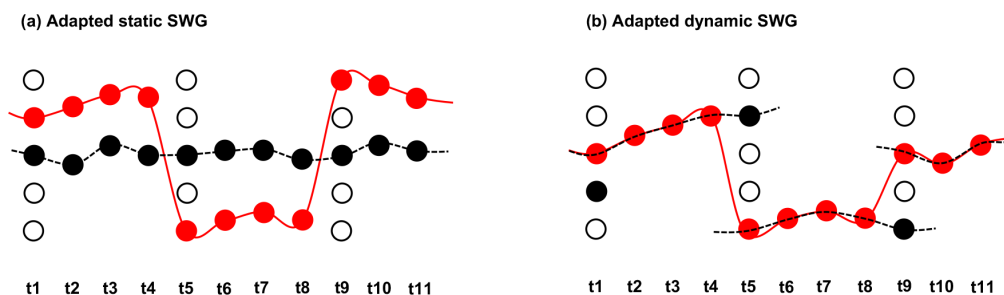


Figure 3. Adapted dynamic weather generators. **(a)** The adapted static SWG selects a new analogue every n th day (4 d in this illustration) and follows the observed trajectory (dotted black line) of that day for 3 d. The resulting simulation combines observed 4 d chunks into an artificial trajectory (red line). **(b)** The adapted dynamic SWG replaces the first day of the observations with one of its analogues and follows the observed trajectory of that analogue for 3 d. Following this, a new analogue of the following day in the observed trajectory is chosen.

For all example years, the circulation in the static SWG simulations exhibits the same features as the observed circulation. The dynamic SWG always simulates high-pressure anomalies over France irrespective of the starting conditions. These anomalies are, however, more pronounced in 2015 where the starting circulation favours the anticyclonic pattern over France.

The simulations of warm Decembers are most sensitive to the weighting of the calendar date. If this parameter is chosen too loosely, simulations would include days from other seasons, which are generally warmer. As shown in Fig. A2, for $\alpha_{\text{cal}} \geq 6$ over 70 % of all days in the simulations are sampled from the November–February period. Increasing the weighting of the calendar day further does not show a significant effect.

The simulations are also sensitive to the weighting of daily maximal temperatures α (Fig. A3). For $\alpha \geq 0.75$ we simulate a large number of Decembers that are more extreme than 2015.

Finally, the choice of geopotential height or mean sea level pressure to classify circulation analogues does not influence the simulations (see Fig. A1).

3.2 Spring precipitation

An extremely wet period from April to July 2016 followed the warm December in 2015, with an average precipitation of 2.7 mm per day and 332 mm for the whole period. This is more than the long-term 75th percentile, but it is topped by some years including 1983, 1987, and 2012.

Figure 6 shows the daily mean precipitation for April–July periods over 1950–2018. Accumulated April–July precipitation fluctuates around 256 mm with a strong year-to-year variability. Over the observed period no trend is detected.

Simulations from the static weather generator (blue boxplots in Fig. 6) also show a strong inter-annual variability but have significantly larger amounts of precipitation. The average seasonal precipitation for all simulations and all years is around 487 mm—190 % of the observed average. Single

simulations even reach daily mean precipitation of 6 mm for April–July, which is 3 times as high as the observed precipitation in 1983.

April–July periods simulated by the dynamic SWG are even wetter than the simulations of the static SWG, with an average seasonal precipitation of 590 mm. As expected, the inter-annual variations are smaller in the dynamic SWG simulations than in the static SWG simulations because the dynamic SWG evolves freely, with the starting conditions their only link to the observed circulation.

We estimate the return periods of our simulated events by fitting a normal distribution to the observed April–July precipitation events. As we average over a quite large region and over 4 months, a normal distribution represents the observations well (even though the analysed variable is precipitation). We find that the 2016 April–July period was a 1-in-17-year event, while the majority of our SWGs simulations are 1-in-10 000-year events.

In April–July 2016, the atmospheric circulation was characterized by a moderate low-pressure anomaly north of France and north of the Azores (Fig. 7a). The North Atlantic Oscillation (NAO) index switched from slightly positive to negative in May and remained negative until the end of June (NOAA, 2020).

We next analyse the large-scale atmospheric circulation patterns that characterize our SWG simulations by comparing them to a few examples of observed events. Figure 7a–d shows the mean sea level composites of 2016, the driest (1976), the median (1986), and the wettest (1983) April–July periods. The main feature in the median event (Fig. 7c) is a low pressure anomaly north-westward of the British Isles. The wettest event (Fig. 7d) is characterized by a strong dipole over the North Atlantic with low pressure in the east and high pressure in the west. In the driest event (Fig. 7b) this dipole is reversed and slightly shifted to the east.

For all four events, the static SWG tends to create events with stronger low pressure anomalies over northern France (Fig. 7e–h). Similarly, the simulations from the dynamic SWG all show a strong low-pressure anomaly over north-

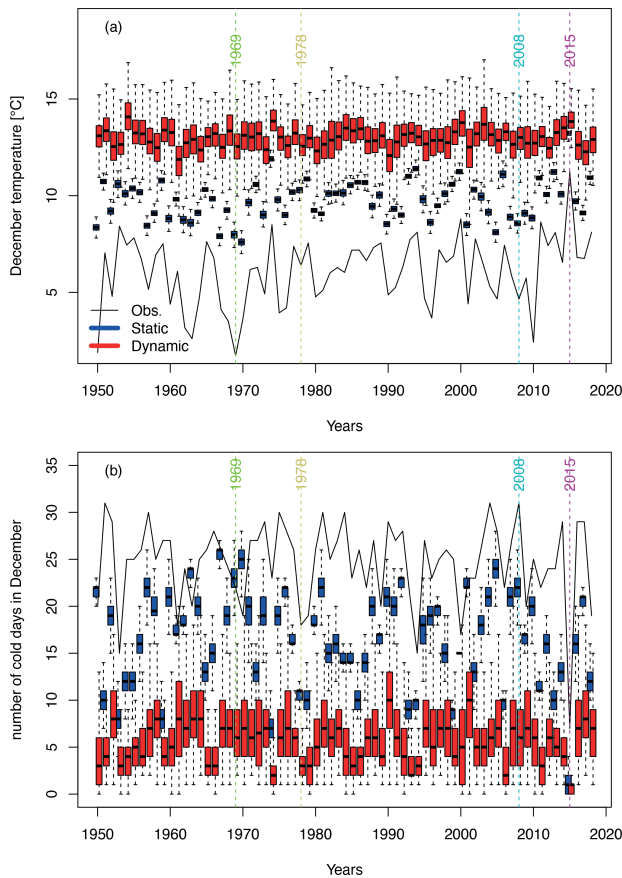


Figure 4. (a) Daily maximal temperature in December from 1950 to 2018. The black line shows E-OBS observations. The boxplots represent the ensemble variability of the simulations of the static (blue) and the dynamic (red) SWG for each year. The boxes of the boxplots indicate the median ($q50$) and lower ($q25$) and upper ($q75$) quartiles. The upper whiskers indicate $\min[\max(T), 1.5 \times (q75 - q25)]$. The lower whisker has a symmetrical formulation. The points are the simulated values that are above or below the defined whiskers. Panel (b) is the same as (a) but for the number of cold days. The coloured vertical lines indicate the coldest December (green), a median December (yellow), a December with 31 cold days (cyan) and the warmest December (purple).

ern France (Fig. 7i–l). For the dynamic SWG simulations, even in 1976, which was the driest April–July period, a low-pressure anomaly is simulated for northern France where a high-pressure system had been observed. In the static SWG, the high-pressure anomaly is relocated to the west, also leading to a low-pressure anomaly over northern France.

Besides a general tendency towards low-pressure anomalies over northern France, the 2016 April–July period was characterized by an increased daily pressure variability west of France (compare Figs. B1a and c). This indicates an enhanced storm track activity downstream of our region of interest and could explain the increased precipitation observed

in 2016. In contrast to the persistent anticyclonic anomaly that led to a continuously warm December in 2015, the wet April–July period was favoured by a number of storms passing over northern France.

Our simulations of April–July periods combine 5 d chunks of observed weather into one coherent time series. By using 5 d chunks instead of combining single-day observations, we constrain our simulations to observed day-to-day variations that appear to be crucially important for precipitation events. This ensures that in our simulations storms predominantly travel eastwards and that the moisture transport in the simulations is reasonable – at least during the 5 d in question (see the animated .gif files in the Supplement).

Sensitivity tests indeed show that simulations where a new analogue is chosen every day result in significantly higher precipitation, with 7 mm per day for the dynamic SWG simulations (see Fig. A4). The amount of precipitation steadily decreases with the length of the observed chunks that are assembled by the SWGs (n_{days}). This is to be expected, as with longer assembled chunks and fewer analogue choices the simulated weather events resemble the observations more and more. There is an especially strong decrease in simulated precipitation from 1 to 3 d, which suggests that when analogues are chosen more frequently than every third day potentially unreasonable weather events are created. Note that taking 5 d windows is a heuristic choice and that window sizes between 4 and 7 d give similar results.

The simulations are by definition sensitive to the weighting of the amount of precipitation α . As shown in Fig. A5, with a relatively small weight of 0.1 most dynamic simulations already bring more precipitation than what was observed in 2016. This could be due to the length of the simulations: it is rather unlikely that extreme weather endures over 4 months. However, with a weak weighting of wet weather simulations can already result in a long-lasting consistent wet periods. This increase in precipitation saturates after $\alpha \approx 0.5$, and increasing α further has no effect on the final results.

As for the other free parameters of the SWG, this sensitivity test does not directly justify the choice of the parameter α . It instead gives guidance on the values that would be appropriate choices for our application. In the end the parameter is heuristically chosen considering the trade-off between creating high-precipitation events and keeping as much randomness as possible in our simulations.

As shown in Fig. A6, the weighting of the calendar day has limited influence on the amount of precipitation in northern France simulated by our SWGs.

For precipitation in northern France the weighting of the calendar day is less relevant as there is no pronounced seasonal cycle in precipitation (see Fig. A6).

Finally, one feature in the simulations of April–July deserves some more attention: for both static and dynamic SWG simulations precipitation is exceptionally high in 1994 and 1998. Although observed precipitation in these years was relatively high, this cannot explain the amount of precipi-

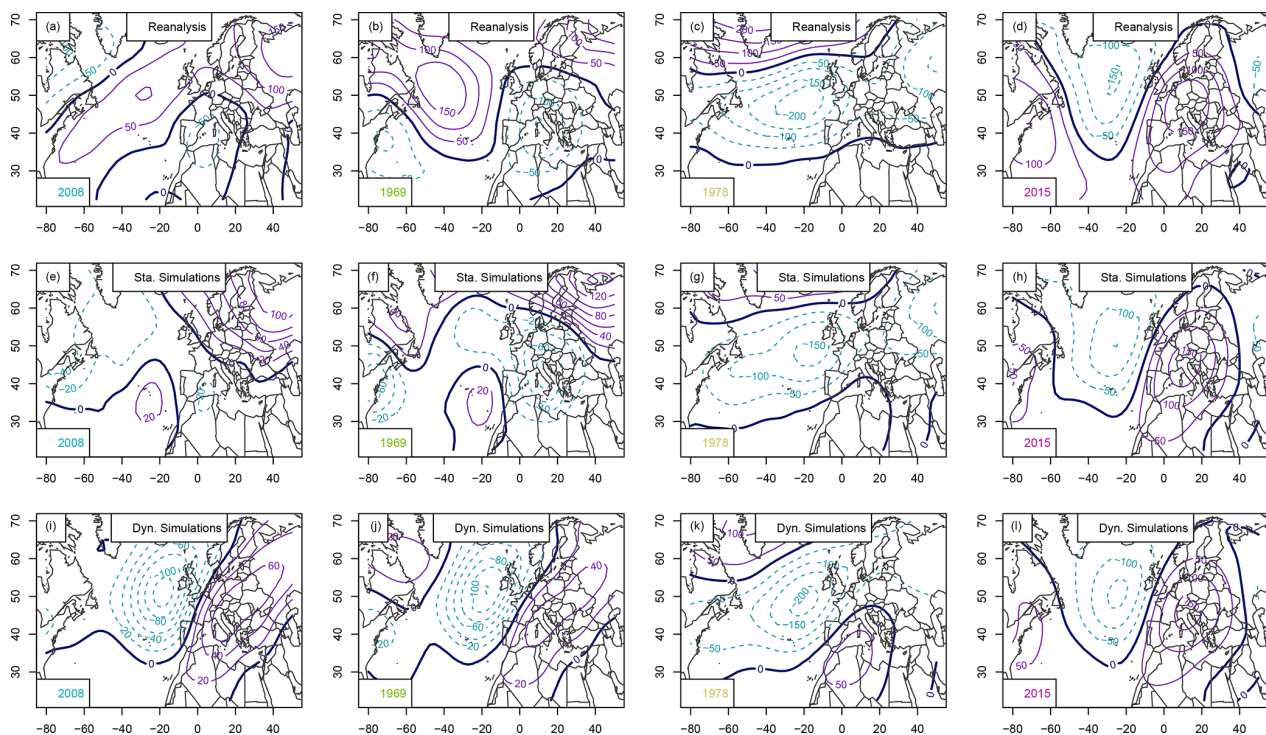


Figure 5. Geopotential height anomaly at 500 hPa (Z_{500}) composites for a year with 31 cold days (2008), the coldest December (1969), the median (1978), and the warmest December (2015): (a–c) mean Z_{500} from NCEP reanalyses, (d–f) static SWG simulations, (g–i) dynamic SWG simulations. Isolines are shown with 100 m increments. Positive Z_{500} anomalies are shown with continuous purple isolines, negative anomalies are shown with dashed cyan lines, and the 500 hPa isoline is shown with a continuous thick black line.

tation in the simulations. One explanation for these outlier years could be a loop in the simulations leading to an excessive repetition of the same (wet) sequence of days. As shown in Fig. A7, in 1998 one date is indeed repeated 10 times in both the static and dynamic weather generator. In most other years, repetitions of single dates are rare. As our results do not rely on simulations of single years, this feature does not affect the overall findings of the study.

These simulations show that there are many possible April–July periods that would be significantly wetter than what was observed in 2016 and also wetter than the observed record precipitation (1983).

4 Discussion

In 2016 northern France suffered an unprecedented crop loss that can be related to an abnormally warm December in 2015 and a following wet April–July period in 2016 (Ben-Ari et al., 2016). Here we investigated how extreme these meteorological precursors of the crop loss could be in the current climate. Using stochastic weather generators (SWG) we simulate warm Decembers and wet April–July periods independently.

The warm December in 2015 resulted in very few cold days with temperatures between 0 and 10 °C. Our simulations show that substantially warmer Decembers would be possible. However, in terms of cold days, which is a more relevant indicator for wheat phenology in that season (Ben-Ari et al., 2018), December 2015 was already extreme, and only a few simulations show lower numbers of cold days.

For April–July precipitation, we find that much wetter periods than what was observed in 2016 would be plausible. The simulated events bring more than twice as much precipitation than in 2016.

If crop yields responds to the number of cold days in winter and to the precipitation rate in spring, as shown in Ben-Ari et al. (2018), then we have shown here that in the current climate an even worse crop loss event would be possible. The April–July period in particular could be significantly wetter than what was observed in 2016.

We used stochastic weather generators to simulate extreme but plausible weather events. While the method is established for summer heat waves (Yiou and Jézéquel, 2020), the weather events we studied here brought new challenges: although the circulation pattern of the warm December 2015 was similar to a summer heat wave with an anticyclonic pattern over France, special care was required to assure that our

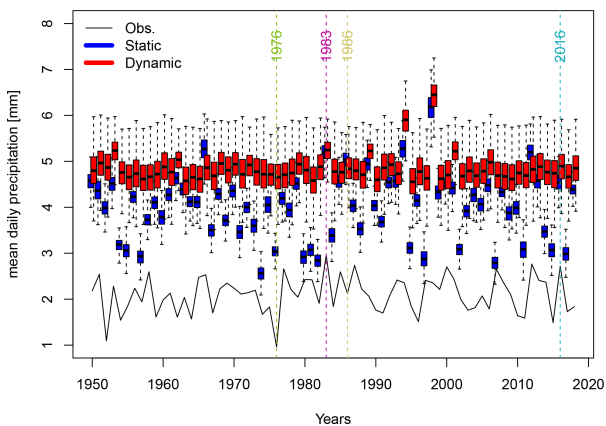


Figure 6. Daily precipitation averages for April–July from 1950 to 2018. The black line shows E-OBS observations. The boxplots represent the ensemble variability of the simulations of the static (blue) and the dynamic (red) SWG for each year. The boxes of boxplots indicate the median ($q50$), lower ($q25$), and upper ($q75$) quartiles. The upper whiskers indicate $\min[\max(T), 1.5 \times (q75 - q25)]$. The lower whisker has a symmetrical formulation. The points are the simulated values that are above or below the defined whiskers. The coloured vertical lines indicate the driest April–July period (1976), the wettest period (1983), a median period (1986), and 2016.

simulated events are actually realizations of winter weather. Here we assured for this by strongly weighting the calendar date when selecting analogues.

The wet April–July 2016 period was characterized by a series of passing storms that brought considerable amounts of precipitation. The main feature of this wet spring season was therefore not persistence and simulating plausible day-to-day variations with SWGs was a major challenge. SWGs that select a new analogue every day tend to simulate persistent rainfall events over spring, with little day-to-day variation.

As a first attempt to simulate plausible long lasting wet periods, we propose to reassemble 5 d windows of observed weather instead of single days. This ensures that low- and high-pressure systems predominantly travel eastward at a speed that is tightly linked to observations. An alternative approach could be to switch trajectories on dry days instead of switching after a fixed number of days. This would additionally avoid changing trajectories during precipitation events.

Evaluating the plausibility of our simulations remains a challenge: although sensitivity tests and an analysis of the simulated circulation patterns reveal the robust and clearly interpretable behaviour of SWGs, further tests would be required to assess whether all simulated events could really happen in our climate. It could, for instance, be interesting to analyse the simulated wet April–July periods with respect to more climate variables (e.g. relative humidity) to evaluate whether the water transport is physically plausible throughout the simulated period.

To further evaluate the plausibility of our simulations one could also compare them to extreme events simulated by large ensemble climate modelling experiments. In a study using a near-term climate prediction model, Thompson et al. (2017) found that for England there is a considerable chance of unprecedented winter rainfall. Replicating a similar study for northern France spring precipitation would not only provide an alternative estimate of extreme spring precipitation but would also allow us to further evaluate the circulation features of our weather simulations.

Finally, our simulated extremes could be used as input for the regression-based yield model of Ben-Ari et al. (2018). These results should, however, be interpreted cautiously as our simulated weather extremes lie outside of the observed range and therefore also the range within which the yield model was trained. They could also be used in process-based crop models as a worst-case meteorological scenario.

5 Conclusions

This paper is a proof of concept for the importance sampling for a simulation of a compound event (warm autumn–winter and wet spring) that would have an impact on crop yield. It relies on a data-resampling approach to maximize temperature and precipitation over extended periods of time.

The simulations are based on the a priori knowledge (from expertise on crop failures in northern France) that warm autumns and winters followed by wet springs have detrimental effects on crops.

The first application of SWGs to warm winter periods and wet springs is an important advance in this research field. It also shows that with only a few adaptations SWGs can be applied to new weather phenomena, highlighting the merits of the method. Moreover, the SWG parameters can be adapted to other types of crops (with other phenological parameters and key dates).

This approach is rather flexible and could be adapted to simulate compound extremes using climate model outputs based on different scenarios of climate change. This could lead to the first evaluation of the impact of climate change on worst-case scenarios of crop yields. This type of analysis has some limitations related to the uncertainty of models and scenarios, and it fails to take into account non-climatic drivers of crop yields such as pests, supply chains, or economical concerns. However, we believe it could be useful to estimate what could be plausible in terms of purely meteorological events in a changing climate.

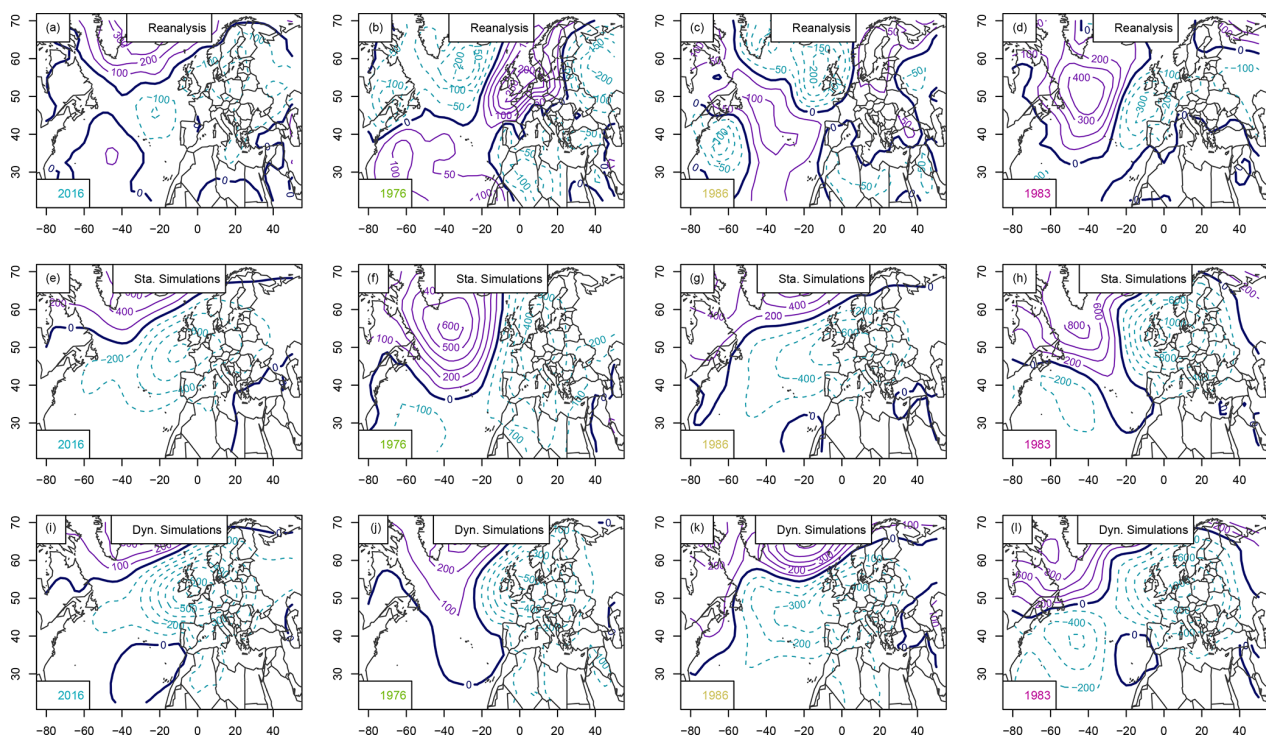


Figure 7. SLP anomaly composites (Pa) for April–July 2016, the driest period, the median (1986), and the wettest period (1983): (a–d) mean SLP from NCEP reanalyses, (e–h) static SWG simulations, (i–l) dynamic SWG simulations. Isolines are shown with 100 Pa increments. Positive SLP anomalies are shown with continuous purple isolines, negative anomalies are shown with dashed cyan lines, and the mean SLP isline is shown with a continuous thick black line.

Appendix A: Sensitivity tests

A1 December temperature

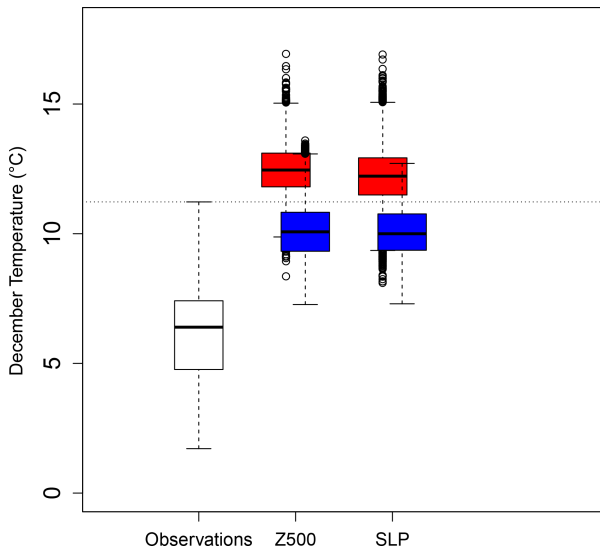


Figure A1. Distribution of the daily maximum temperature in December averaged in observations (white) and in simulations computed by the static (blue) and dynamic (red) generators using circulation analogues computed using the SLP or Z500. The horizontal dotted line corresponds to the daily maximum temperature observed in December 2015. The boxes of boxplots indicate the median (q_{50}), lower (q_{25}), and upper (q_{75}) quantiles. The upper whiskers indicate $\min[\max(T), 1.5 \times (q_{75} - q_{25})]$. The lower whisker has a symmetrical formulation. The points are the simulated values that are above or below the defined whiskers.

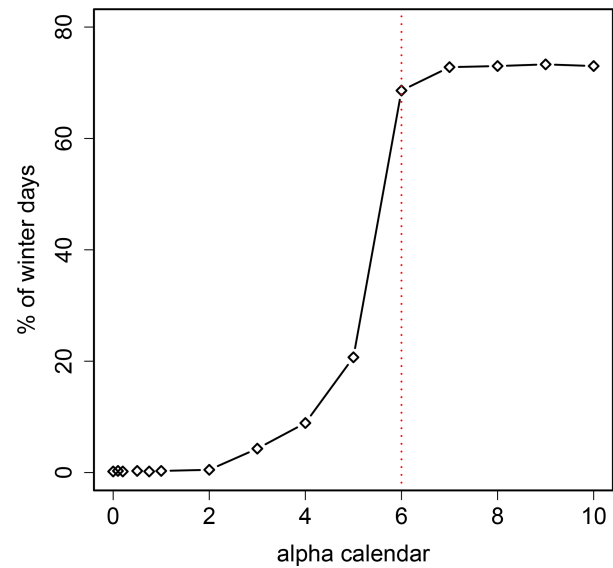


Figure A2. Percentage of days sampled between November and February by the dynamic generator when running 100 simulations of December temperatures as a function of the parameter α_{cal} . The dotted red line is for $\alpha_{\text{cal}} = 6$ (which is the value used in the analysis).

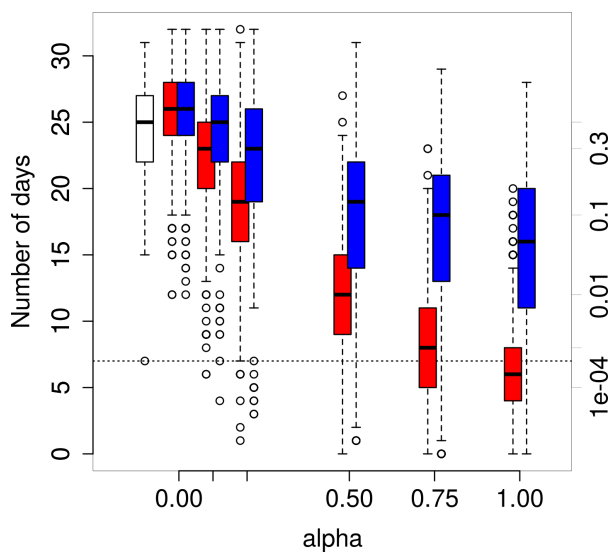


Figure A3. Distribution of the number of December days with maximal temperatures between 0 and 10 °C in observations (white) and in simulations computed by the static (blue) and dynamic (red) generators as a function of α . The axis on the right indicates the probability of occurrence, assuming a beta-binomial distribution of the number of winter days with parameters estimated from white boxplot. The horizontal dotted line corresponds to the observed number of days in December 2015. The boxes of boxplots indicate the median (q_{50}), lower (q_{25}), and upper (q_{75}) quartiles. The upper whiskers indicate $\min[\max(T), 1.5 \times (q_{75} - q_{25})]$. The lower whisker has a symmetrical formulation. The points are the simulated values that are above or below the defined whiskers.

A2 Spring precipitation

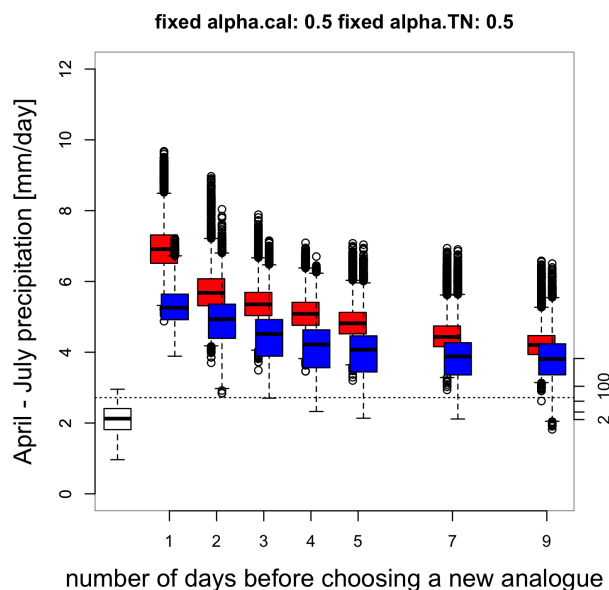


Figure A4. Distribution of April–July daily precipitation in observations (white) and in simulations computed by the static (blue) and dynamic (red) generators as a function of the number of days before selecting a new analogue n_{days} . The axis on the right indicates the probability of occurrence, assuming a normal distribution of daily precipitation with parameters estimated from white boxplot. The horizontal dotted line corresponds to the observed daily precipitation in April–July 2016. The boxes of boxplots indicate the median (q_{50}), lower (q_{25}), and upper (q_{75}) quartiles. The upper whiskers indicate $\min[\max(T), 1.5 \times (q_{75} - q_{25})]$. The lower whisker has a symmetrical formulation. The points are the simulated values that are above or below the defined whiskers.

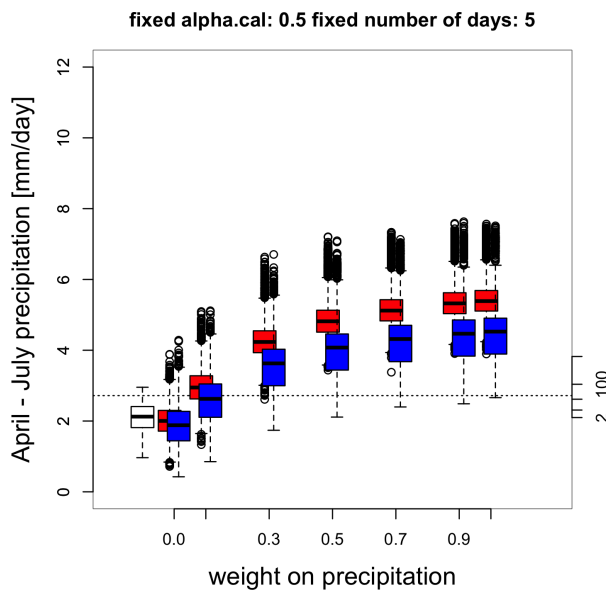


Figure A5. Distribution of April–July daily precipitation in observations (white) and in simulations computed by the static (blue) and dynamic (red) generators as a function of α . The axis on the right indicates the probability of occurrence, assuming a normal distribution of daily precipitation with parameters estimated from white boxplot. The horizontal dotted line corresponds to the observed daily precipitation in April–July 2016. The boxes of boxplots indicate the median (q_{50}), lower (q_{25}), and upper (q_{75}) quartiles. The upper whiskers indicate $\min[\max(T), 1.5 \times (q_{75} - q_{25})]$. The lower whisker has a symmetrical formulation. The points are the simulated values that are above or below the defined whiskers.

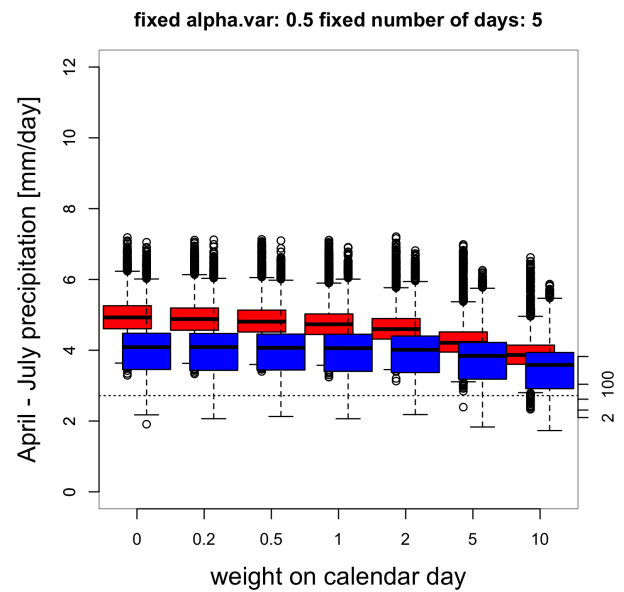


Figure A6. Distribution of April–July daily precipitation in observations (white) and in simulations computed by the static (blue) and dynamic (red) generators as a function of α_{cal} . The axis on the right indicates the probability of occurrence, assuming a normal distribution of daily precipitation with parameters estimated from the white boxplot. The horizontal dotted line corresponds to the observed daily precipitation in April–July 2016. The boxes of boxplots indicate the median (q_{50}), lower (q_{25}), and upper (q_{75}) quartiles. The upper whiskers indicate $\min[\max(T), 1.5 \times (q_{75} - q_{25})]$. The lower whisker has a symmetrical formulation. The points are the simulated values that are above or below the defined whiskers.

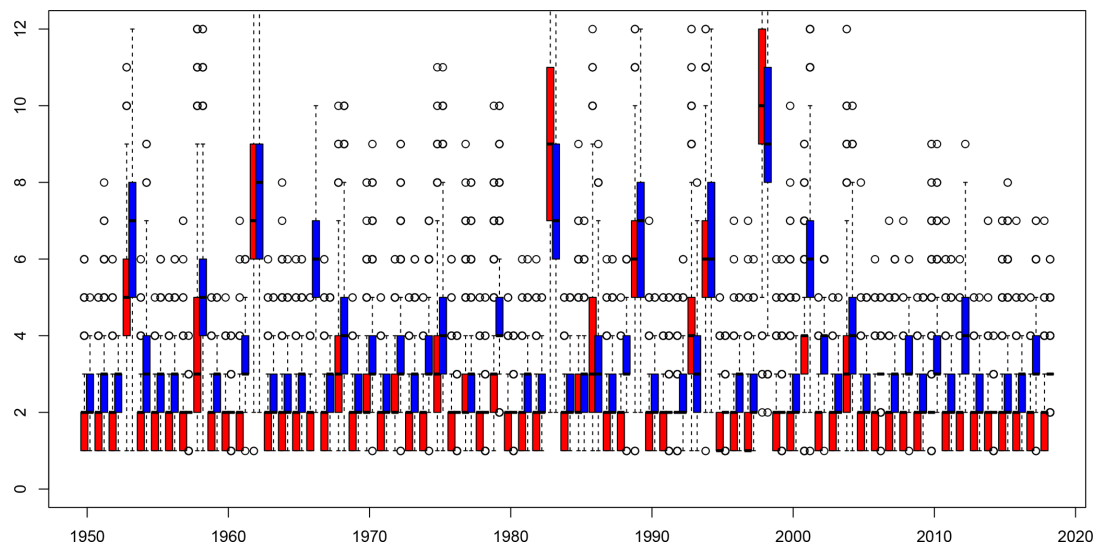


Figure A7. Maximal number of times a single date is repeated for each simulated year. The boxplots indicate the range of this maximal repetition number for the 1000 simulations for simulations of the static (blue) and dynamic (red) stochastic weather generator. The boxes of boxplots indicate the median ($q50$), lower ($q25$), and upper ($q75$) quartiles. The upper whiskers indicate $\min[\max(T), 1.5 \times (q75 - q25)]$. The lower whisker has a symmetrical formulation. The points are the simulated values that are above or below the defined whiskers.

Appendix B: Circulation details

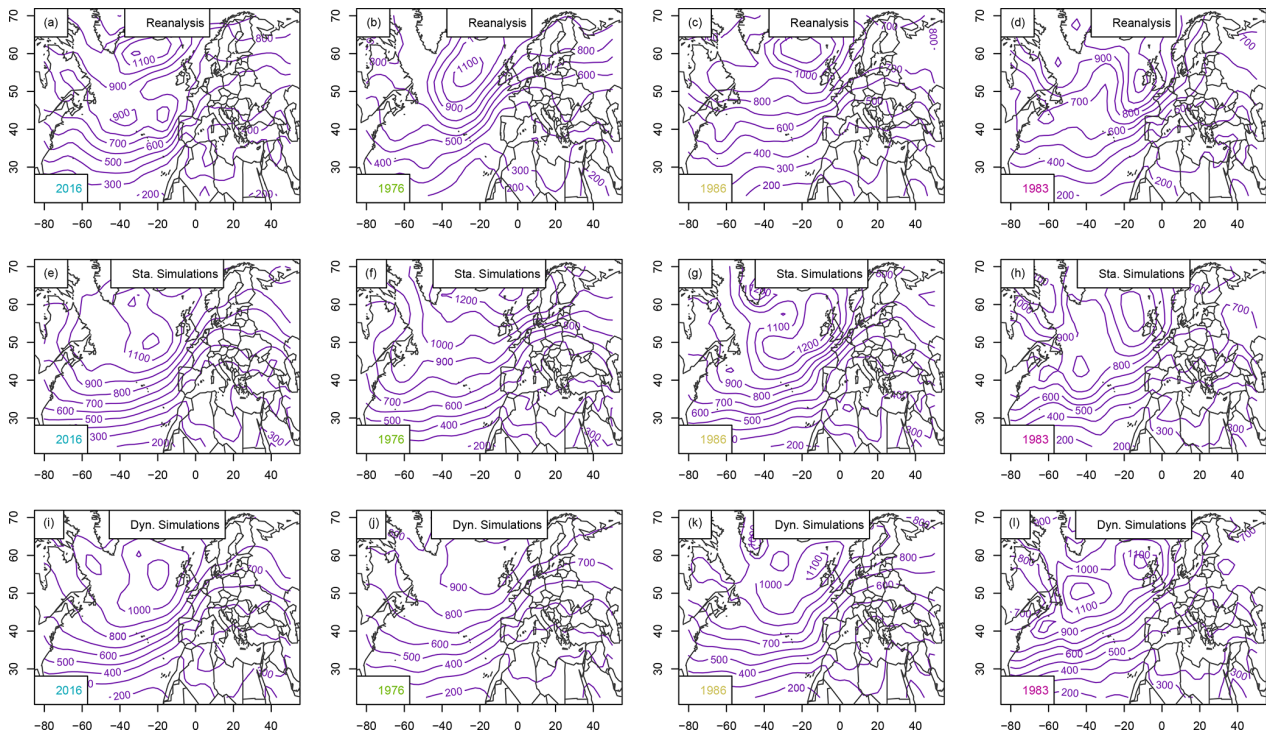


Figure B1. Standard deviation of daily SLP anomalies (Pa) for April–July 2016, the driest period, the median (1986), and 2018: (a–d) SLP from NCEP reanalyses, (e–h) static SWG simulations, (i–l) dynamic SWG simulations. For the SWG simulations the average of all 1000 runs for the given year is presented.

Code availability. All R scripts used for the analysis and the production of figures are openly available under <https://doi.org/10.5281/zenodo.4327671> (Pfeleiderer et al., 2020).

Supplement. The supplement related to this article is available online at: <https://doi.org/10.5194/esd-12-103-2021-supplement>.

Author contributions. PY and AJ conceived the study. NL, JL, IM, EV, and PP did the analysis and created all figures. PP wrote the manuscript with contributions from all authors.

Competing interests. The authors declare that they have no conflict of interest.

Special issue statement. This article is part of the special issue “Understanding compound weather and climate events and related impacts (BG/ESD/HESS/NHESS inter-journal SI)”. It is not associated with a conference.

Acknowledgements. We acknowledge the E-OBS dataset from the EU-FP6 project UERRA (<http://www.uerra.eu>, last access: 20 September 2019) and the Copernicus Climate Change Service and the data providers of the ECAD project (<https://www.ecad.eu>, last access: 20 September 2019). We also acknowledge the NCEP Reanalysis data provided by the NOAA/OAR/ESRL.

Financial support. This research has been supported by the DAMOCLES COST (grant no. CA17109). Peter Pfeleiderer was supported by the German Federal Ministry of Education and Research (grant no. 01LN1711A). Edoardo Vignotto was supported by the Swiss National Science Foundation (Doc.CE11 Mobility Grant no. 188229).

The publication of this article was funded by the Open Access Fund of the Leibniz Association.

Review statement. This paper was edited by Bart van den Hurk and reviewed by Daithi Stone and Henrique Moreno Dumont Goulart.

References

- ARVALIS: Rendements catastrophiques du blé en 2016: la pluie, seule responsable?, available at: <https://www.semencesdefrance.com/actualite-semences-de-france/rendements-catastrophiques-ble-2016-pluie-seule-responsable/> (last access: 23 October 2020), 2016 (in French).
- Ben-Ari, T., Adrian, J., Klein, T., Calanca, P., Van der Velde, M., and Makowski, D.: Identifying indicators for extreme wheat and maize yield losses, *Agr. Forest Meteorol.*, 220, 130–140, 2016.
- Ben-Ari, T., Boé, J., Ciais, P., Lecerf, R., Van der Velde, M., and Makowski, D.: Causes and implications of the unforeseen 2016 extreme yield loss in the breadbasket of France, *Nat. Commun.*, 9, 1627, <https://doi.org/10.1038/s41467-018-04087-x>, 2018.
- Cassou, C., Terray, L., and Phillips, A. S.: Tropical Atlantic influence on European heat waves, *J. Climate*, 18, 2805–2811, 2005.
- Cooley, D.: Extreme value analysis and the study of climate change, *Climatic Change*, 97, 77–83, 2009.
- de Bruijn, K. M., Lips, N., Gersonius, B., and Middelkoop, H.: The storyline approach: a new way to analyse and improve flood event management, *Nat. Hazards*, 81, 99–121, <https://doi.org/10.1007/s11069-015-2074-2>, 2016.
- FAO: Agricultural statistics database, Rome: World Agricultural, Information Center, available at: <http://faostat.fao.org/site/567/DesktopDefault.aspx> (last access: 22 May 2020), 2013.
- Haylock, M. R., Hofstra, N., Tank, A. M. G. K., Klok, E. J., Jones, P. D., and New, M.: A European daily high-resolution gridded data set of surface temperature and precipitation for 1950–2006, *J. Geophys. Res.-Atmos.*, 113, D20119, <https://doi.org/10.1029/2008JD010201>, 2008.
- Hazeleger, W., Van Den Hurk, B. J., Min, E., Van Oldenborgh, G. J., Petersen, A. C., Stainforth, D. A., Vasileiadou, E., and Smith, L. A.: Tales of future weather, *Nat. Clim. Change*, 5, 107–113, <https://doi.org/10.1038/nclimate2450>, 2015.
- Jaworski, P., Durante, F., Hardle, W. K., and Rychlik, T.: Copula theory and its applications, vol. 198, Springer, Berlin, Heidelberg, 2010.
- Jézéquel, A., Cattiaux, J., Naveau, P., Radanovics, S., Ribes, A., Vautard, R., Vrac, M., and Yiou, P.: Trends of atmospheric circulation during singular hot days in Europe, *Environ. Res. Lett.*, 13, 054007, <https://doi.org/10.1088/1748-9326/aab5da>, 2018.
- Kistler, R., Kalnay, E., Collins, W., Saha, S., White, G., Woollen, J., Chelliah, M., Ebisuzaki, W., Kanamitsu, M., Kousky, V., van den Dool, H., Jenne, R., and Fiorino, M.: The NCEP-NCAR 50-year reanalysis: Monthly means CD-ROM and documentation, *B. Am. Meteor. Soc.*, 82, 247–267, 2001.
- MacDonald, R. B. and Hall, F. G.: Global crop forecasting, *Science*, 208, 670–679, 1980.
- Massey, N., Jones, R., Otto, F., Aina, T., Wilson, S., Murphy, J., Hassell, D., Yamazaki, Y., and Allen, M.: weather@ home-development and validation of a very large ensemble modelling system for probabilistic event attribution, *Q. J. Roy. Meteor. Soc.*, 141, 1528–1545, 2015a.
- Massey, N., Jones, R., Otto, F. E. L., Aina, T., Wilson, S., Murphy, J. M., Hassell, D., Yamazaki, Y. H., and Allen, M. R.: weather@home-development and validation of a very large ensemble modelling system for probabilistic event attribution, *Q. J. Roy. Meteor. Soc.*, 141, 1528–1545, <https://doi.org/10.1002/qj.2455>, 2015b.
- Müller, C., Elliott, J., Kelly, D., Arneth, A., Balkovic, J., Ciais, P., Deryng, D., Folberth, C., Hoek, S., Izaurre, R. C., Jones, C. D., Khabarov, N., Lawrence, P., Liu, W., Olin, S., Pugh, T. A. M., Reddy, A., Rosenzweig, C., Ruane, A. C., Sakurai, G., Schmid, E., Skalsky, R., Wang, X., de Wit, A., and Yang, H.: The Global Gridded Crop Model Intercomparison phase 1 simulation dataset, *Scientific Data*, 6, 1–22, 2019.
- NOAA: North Atlantic Oscillation, available at: <https://www.cpc.ncep.noaa.gov/products/precip/CWlink/pna/nao.shtml>, last access: 10 January 2020.

- OEC: The Observatory of Economic Complexity, available at: <https://oec.world/en/>, last access: 23 April 2020.
- Peixoto, J. P. and Oort, A. H.: *Physics of Climate*: New York, American Institute of Physics, New York, United States, 520 pp., 1992.
- Pfleiderer, P., Jézéquel, A., Legrand, J., Legrix, N., Markantonis, I., Vignotto, E., and Yiou, P.: *analogues_of_2016_crop_failure_in_France*, Zenodo, <https://doi.org/10.5281/zenodo.4327671>, 2020.
- Ragone, F., Wouters, J., and Bouchet, F.: Computation of extreme heat waves in climate models using a large deviation algorithm, *P. Natl. Acad. Sci. USA*, 115, 24–29, 2017.
- Shepherd, T. G.: Storyline approach to the construction of regional climate change information, *P. Roy. Soc A-Math. Phys.*, 475, 20190013, <https://doi.org/10.1098/rspa.2019.0013>, 2019.
- Shepherd, T. G., Boyd, E., Calel, R. A., Chapman, S. C., Dessai, S., Dima-West, I. M., Fowler, H. J., James, R., Maraun, D., Martius, O., Senior, C. A., Sobel, A. H., Stainforth, D. A., Tett, S. F., Trenberth, K. E., van den Hurk, B. J., Watkins, N. W., Wilby, R. L., and Zenghelis, D. A.: Storylines: an alternative approach to representing uncertainty in physical aspects of climate change, *Climatic Change*, 151, 555–571, <https://doi.org/10.1007/s10584-018-2317-9>, 2018.
- Sturaro, G.: A closer look at the climatological discontinuities present in the NCEP/NCAR reanalysis temperature due to the introduction of satellite data, *Clim. Dynam.*, 21, 309–316, <https://doi.org/10.1007/s00382-003-0334-4>, 2003.
- Thompson, V., Dunstone, N. J., Scaife, A. A., Smith, D. M., Slingo, J. M., Brown, S., and Belcher, S. E.: High risk of unprecedented UK rainfall in the current climate, *Nat. Commun.*, 8, 1–6, <https://doi.org/10.1038/s41467-017-00275-3>, 2017.
- Yiou, P.: AnaWEGE: a weather generator based on analogues of atmospheric circulation, *Geosci. Model Dev.*, 7, 531–543, <https://doi.org/10.5194/gmd-7-531-2014>, 2014.
- Yiou, P. and Jézéquel, A.: Simulation of extreme heat waves with empirical importance sampling, *Geosci. Model Dev.*, 13, 763–781, <https://doi.org/10.5194/gmd-13-763-2020>, 2020.
- Yiou, P. and Nogaj, M.: Extreme climatic events and weather regimes over the North Atlantic: When and where?, *Geophys. Res. Lett.*, 31, L07202, <https://doi.org/10.1029/2003GL019119>, 2004.
- Zscheischler, J., Martius, O., Westra, S., Bevacqua, E., Raymond, C., Horton, R. M., van den Hurk, B., AghaKouchak, A., Jézéquel, A., Mahecha, M. D., Maraun, D., Ramos, A. M., Ridder, N. N., Thiery, W., and Vignotto, E.: A typology of compound weather and climate events, *Nat. Rev. Earth Environ.*, 1, 333–347, <https://doi.org/10.1038/s43017-020-0060-z>, 2020.

Acknowledgements

I would like to thank:

My supervisors, Thomas and Jakob, for their fantastic guidance throughout my PhD. They gave me the time and space to learn doing research at my own pace, and encouraged me to try out my own ideas, while always being available to discuss and making sure I stayed on track. They also challenged me at times, when I could have become lazy. They set the bar high, encouraged me to persevere until each study was on point and each paper polished. I admire them both as researchers and fully trust their scientific judgement, which helped me go through each study with confidence. I am also extremely grateful for they gave me the opportunity to attend many conferences as well as two exciting summer schools during my PhD, which allowed me to share my research, make precious connections - friends, and get inspired.

My colleagues at KUP, for creating such a welcoming atmosphere, for all the coffee and lunch breaks together, the laughter, the swimming, (the drinking) and playing cards. This relaxed and friendly environment made my PhD all the more enjoyable.

Special mention to the ocean group at KUP. Friedrich, who excels at everything and is always keen to help. You are surely too kind and generous for your own good! Anne, for being the best coach a PhD student could dream of. Catherine, who inspires me by her relaxed and easygoing attitude. Fabrice, for his contagious laughter. Yona, for acting as a social glue who instantly enhanced social cohesion at KUP upon her arrival, and for her precious friendship. Our times together will surely be among my fondest memories of Bern. Thanks also to the previous members of the ocean group: Sandra, Charlotte, Viktor, Mathias, Donat, Linus, and Jens. I learnt a lot from all the meetings together, the work they shared and their feedback on my own work.

William and Gabriel, for welcoming me at UBC. These two months in Vancouver have been a fantastic experience. I got extremely excited in the research project, made wonderful friends, and discovered a stunning rain forest.

Jakob's students in Leipzig, who included me online in their group meetings. Although mainly focused on compound events on land, these meetings unexpectedly taught me a lot, for example on how to read papers with a critical eye, and what novel methods could be used to analyze compound events. I loved meeting the group in Emmental, Leipzig, Lisbon, and Bern.

Pauline, Elisabeth, and Andreia, who accompanied me during the first part of my PhD. I had a lovely time traveling with them to conferences. Back in Bern, they helped me feel at home in this once-foreign city and colored my PhD with friendship.

My parents, for fostering my scientific curiosity at a young age and without whose support I would not have studied and received the diploma which allowed me to seek this PhD position in the first place. They never tried to influence my career choices and just believed I would do fine whatever I chose. Their trust gave me a pair of wings.

My PhD examiner, Stephanie Henson, who kindly accepted to examine my PhD thesis. Many thanks for taking the time to read and evaluate this entire thesis!

Sabrina Speich and Laurent Bopp, for convincing me to pursue research when I was close to giving up. Thanks also to all the teachers at the ENS for providing me with the best education I could ask for for a PhD.

Linus, for his precious proofreading skills and never-ending support.

And finally, for their continuous friendship and love, which got me where I am: les geosciences de l'ambience, Marine, Anna, Léa, Rimu, Caillou, Jacqui, Ambre, Vianney, Eleonore, Audrey, Raphaël, Valentine, Emma, la famille, Alexandre, Penny, et encore Linus.

Publications

Papers published:

- [1] P. Pfliegerer, A. Jézéquel, J. Legrand, N. Legrix, I. Markantonis, E. Vignotto, P. Yiou: Simulating compound weather extremes responsible for critical crop failure with stochastic weather generators, *Earth System Dynamics*, 12, 103–120

- [2] N. Le Grix, J. Zscheischler, K. Rodgers, R. Yamaguchi, T. L. Frölicher: Hotspots and drivers of compound marine heatwaves and low net primary production extremes, *Biogeosciences*, 18(6), 2119–2137

- [3] N. Le Grix, J. Zscheischler, K. Rodgers, R. Yamaguchi, T. L. Frölicher: Hotspots and drivers of compound marine heatwaves and low net primary production extremes, *Biogeosciences*, 19(24), 5807–5835

Papers submitted:

- [4] N. Le Grix, W. Cheung, G. Reygondeau, J. Zscheischler, T. L. Frölicher: Extreme and compound ocean events are key drivers of projected low pelagic fish biomass, *Global Change Biology*, (in review)

Erklärung gemäss Art. 18 PromR Phil.-nat. 2019

Name, Vorname: Legrix, Natacha

Matrikelnummer: 19-122-357

Studiengang: Climate Sciences
Dissertation

Titel der Arbeit: Distribution, drivers, and impacts of compound marine heatwave
and low net primary productivity extreme events in the ocean.

Leiter der Arbeit: Prof. Thomas Frölicher and Prof. Jakob Zschleischler

Ich erkläre hiermit, dass ich diese Arbeit selbständig verfasst und keine anderen als die angegebenen Quellen benutzt habe. Alle Stellen, die wörtlich oder sinngemäss aus Quellen entnommen wurden, habe ich als solche gekennzeichnet. Mir ist bekannt, dass andernfalls der Senat gemäss Artikel 36 Absatz 1 Buchstabe r des Gesetzes über die Universität vom 5. September 1996 und Artikel 69 des Universitätsstatuts vom 7. Juni 2011 zum Entzug des Dokortitels berechtigt ist. Für die Zwecke der Begutachtung und der Überprüfung der Einhaltung der Selbständigkeitserklärung bzw. der Reglemente betreffend Plagiate erteile ich der Universität Bern das Recht, die dazu erforderlichen Personendaten zu bearbeiten und Nutzungshandlungen vorzunehmen, insbesondere die Doktorarbeit zu vervielfältigen und dauerhaft in einer Datenbank zu speichern sowie diese zur Überprüfung von Arbeiten Dritter zu verwenden oder hierzu zur Verfügung zu stellen.

Bern, March 20, 2023

Unterschrift